RESPONSE OF SOLAR CELLS TO HIGH INTENSITY, CONCENTRATED RADIATION

A Thesis

submitted in partial fulfilment of the

requirements for the degree of

DOCTOR OF PHILOSOPHY

IN

PHYSICS

By

Amita Agarwala

BIRLA INSTITUTE OF TECHNOLOGY AND SCIENCE

PILANI (Rajasthan)

JULY, 1979

BIRLA INSTITUTE OF TECHNOLOGY AND SCIENCE

PILANI , RAJASTHAN

CERTIFICATE

This is to certify that the thesis entitled 'RESPONSE OF SOLAR CELLS TO HIGH INTENSITY, CONCENTRATED RADIATION' and submitted by (Km.) Amita Agarwala ID. No. 75S85001 for award of Ph.D. degree of the Institute, embodies original work done by her under my supervision.

Signature in full of the Supervisor: V. K. Tewary

Name in Capital block letters: V. K. TEWARY

Date 30 July, 1979

Designation: Professor and Dean-Research and Consultancy Division.

ACKNOWLEDGEMENTS

I am deeply indebted to my supervisor Dr. V.K. Tewary, Professor of Physics, B.I.T.S., Pilani (Rajasthan), for suggesting the problem and for his patient and valuable guidance through out the course of this work. I am indeed grateful to him for giving me his precious time inspite of his busy schedule.

I am especially grateful to Dr. Uma Jain for her valuable comments on the manuscript and her continued encouragement. My special thanks are also due to Drs. Aparna Gupta and S.Kumar for their help and support and to Dr. S.K. Agarwal for his timely sug estions.

I wish to express my gratitude to all the members of Solar Energy Group for helpful discussions during the seminar talks. In particular, I would like to mention Dr. A.P. Sathe, Dr. H.M. Ghule and Dr. S.K. Sharma.

Most of the experimental data reported in this thesis was obtained at the Solid State Physics Laboratory (SSPL), Ministry of Defence, Delhi. I am extremely grateful to Dr. S.C. Jain, Director, SSPL for granting permission to carry out these experiments at SSPL. In addition, I am also grateful to him for his kind help, valuable suggestions and keen interest in this work. I also wish to thank

the Solar Cell group at SSPL for their co-operation. In particular, I am grateful to Dr. S.K. Agarwal and Mr. R.Muralidharan for their generous help and for many illuminating discussions from which I have derived considerable benefit.

It is a great pleasure to express my gratitude to all the members of Physics group, and to all my colleagues and friends for the encouragement and support I received from them. My sincere thanks are due to Mr. S.K. Sharma for his help. I also wish to thank Dr. V.S. Kulhar, Mr. Lalit Kumar, Mr. Muralidhar, Mr. M.K. Madan, Mr. N.K.Swami, Mr. G.S. Tyagi, Mrs. S.Srivastava and Miss Anita Mishra.

Thanks are due to the staff of Information Processing Centre and Library for their help and co-operation.

I am grateful to Group Leader Physics, Dean Research and Consultancy, Dean Faculty Division-III and Director, B.I.T.S. for providing the necessary facilities.

I am grateful for the financial support received for this work which was provided by the University Grants Commission through a fellowship and the Department of Science and Technology, Government of India in the form of a sponsored project which supported a part of this work.

Last, but not in the least, I thank Mr. S.K.Sinha for his neat typing of the manuscript and to Mr. B.D. Sukheeja and Mr. K.N. Sharma for drawing work.

Above all, I am grateful to my parents for their patience and understanding during this seemingly endless task.

Amita Agarwala
(AMITA AGARWALA)

CONTENTS

Certificate		(i)
Acknowledgements		(ii)
List of Symbols		(xi)
INTRODUCTION		1
Chapter 1	SILICON p-n JUNCTION SOLAR CELLS - A BRIEF REVIEW.	7
1.1	Introduction.	7
1.2	Solar Spectrum	8
1.3	Photovoltaic effect in a p-n junction	11
1.4	Theory of p-n junction solar cells	13
	1.4.1 Transport equation for excess carriers.	13
	1.4.2 Charge neutrality assumption	16
	1.4.3 Ambipolar diffusion equation	17
	1.4.4 Dember field	19
	1.4.5 Limiting cases	21
	1.4.6 Solution of the Ambipolar equation in the low level limit	24
	1.4.7 Solar cell electrical characteristics.	28
	1.4.8 Efficiency	34
1.5	Solar cells for concentrated radiation	35
Chapter 2	RESPONSE OF SOLAR CELLS TO NONUNIFORM ILLUMINATION!	39
2.1	Introduction	39
2.2	Solution of the Ambipolar equation	42
2.3	Discussion.	50

Chapter 3	A THEORETICAL STUDY OF THE RESPONSE OF SOLAR CELLS TO DIFFERENT ILLUMINATION LEVELS, AT CONSTANT TEMPERATURE.	52
3.1	Introduction	52
3.2	Ambipolar equation and its analytical solution.	57
3.3	Numerical solution of the Ambipolar equation.	67
3.4	Electrical characteristics of solar cells.	76
	3.4.1 Current voltage relationship	76
	3.4.2 Maximum power output.	79
	3.4.3 Short circuit current.	79
	3.4.4 Open circuit voltage	80
	3.4.5 Fill factor.	81
	3.4.6 Efficiency.	81
3.5	Determination of the solar cell response for continuous spectrum.	81
3.6	Effect of the internal series resistance.	83
	3.6.1 I-V characteristics	83
	3.6.2 Short circuit current.	84
	3.6.3 Open circuit voltage.	85
	3.6.4 Maximum power output and fill factor.	85
3.7	Contribution of Dember effect.	86
3.8	Results and Discussions.	89
	3.8.1 Short circuit current.	91
	3.8.2 Open circuit voltage.	91

3.8.3 I-V characteristics. 94

3.8.4 Calculated cell response for different wavelengths. 94

3.8.5 Calculated cell response for AMO spectrum. 102

3.8.6 Effect of series resistance. 106

3.8.7 Infinitely high intensities. 108

Chapter 4 AN EXPERIMENTAL STUDY OF THE RESPONSE OF SOLAR CELLS TO DIFFERENT ILLUMINATION LEVELS, AT CONSTANT TEMPERATURE. 112

4.1 Introduction. 112

4.2 Experimental set up 113

4.3 Experimental results and discussions. 122

4.3.1 Photovoltaic I-V characteristics. 122

4.3.2 Open circuit voltage 126

4.3.3 Short circuit current. 128

4.3.4 Maximum power output. 129

4.3.5 Cell efficiency and fill factor. 133

4.4 Conclusions. 133

Chapter 5 EFFECT OF TEMPERATURE ON THE SOLAR CELL RESPONSE AT DIFFERENT LEVELS OF ILLUMINATION. 138

5.1 Introduction. 138

5.2 Temperature dependence of various cell parameters. 142

		5.2.1 Photon absorption coefficient	143
		5.2.2 Diffusion length.	149
		5.2.3 Generation rate.	154
		5.2.4 Intrinsic carrier concentration.	158
		5.2.5 Diffusion potential.	158
		5.2.6 Reverse saturation current.	159
	5.3	Results and Discussions.	159
Chapter 6		AN ANALYSIS OF THE VARIATION OF SPECTRAL RESPONSE OF SOLAR CELLS WITH TEMPERATURE.	173
	6.1	Introduction.	173
	6.2	Experimental arrangements.	176
	6.3	Experimental results.	179
	6.4	The role of various cell parameters in the temperature dependence of RSR.	180
		6.4.1 Absorption coefficient.	187
		6.4.2 Diffusion length.	191
		6.4.3 Band gap.	194
	6.5	Discussion of the experimental results and their theoretical interpretation.	194
		6.5.1 Variation of short circuit current with temperature under AM1, AMO spectra.	194
		6.5.2 Spectral response in the long wavelength region.	196
		6.5.3 Spectral response in the short wavelength region.	201

6.5.4 Peak position 205

6.5.5 Relative contribution of diffusion length and absorption coefficient at different temperatures. 206

6.6 Conclusions. 207

Chapter 7 MEASUREMENT OF SERIES RESISTANCE OF SOLAR CELLS . 209

7.1 Introduction. 209

7.2 Theory of different methods used for determining the series resistance. 213

7.2.1 Description of the various I-V characteristics of solar cells. 213

7.2.2 Various methods for determination of the cell internal series resistance. 217

7.3 Experimental set up. 218

7.3.1 Photovoltaic characteristics. 220

7.3.2 P-N junction characteristics 220

7.3.3 Dark forward characteristics. 222

7.4 Comparison of different methods of measuring the series resistance. 222

7.4.1 Comparison of the three conventional methods of measuring R_s 222

7.4.2 Description of the new method for measuring R_s 224

7.5 Experimental results and discussions. 226

7.5.1 Series resistance as measured by different methods. 226

7.5.2 Measurement of series resistance at high temperatures. 234

7.5.3 Series resistance of specially designed cells. 239

7.6 Conclusions 248

REFERENCES. 249

* * * *

LIST OF SYMBOLS

A	Diode quality factor in (exp(qV/AkT))
A_t	Total device area
b, b'	Ratio of electron to hole mobility
C	Concentration factor (In chapters 3 and 5 C =1 corresponds to one sun which is defined to be an illumination of 98 mW/cm^2 with an AMO spectrum).
C_B	Background concentration.
c	Velocity of light
D_n	Diffusion coefficient of electrons.
D_p	Diffusion coefficient of holes.
D^*	Ambipolar diffusion coefficient.
D_n^*	Ambipolar diffusion coefficient for electrons.
D_p^*	Ambipolar diffusion coefficient for holes.
d_1	Thickness of the diffused region.
d_2	Thickness of the base region.
E	Electric field
E_C	Conduction band edge energy.
E_F	Fermi level energy.
E_V	Valence band edge energy.
E_g	Band gap.
E_i	Intrinsic Fermi level energy.

E_t	Trap level energy.
E_g	Optical band gap.
E_{ex}	Exciton binding energy .
E_{int}	Internal electric field.
$F(\lambda)$	Photon flux in interval $\Delta\lambda$.
FF	Fill factor.
g'	Excess carrier generation rate.
h	Planck's constant.
I	Output current.
I_g	Photogenerated current.
I_T	Current at the terminals .
I_m	Current at maximum power point.
I_{sc}	Short circuit current.
I_o	Reverse saturation current.
J_B	Current from the base layer.
J_s	Current from the diffused layer.
J_n	Electron flux density.
J_p	Hole flux density
k	Boltzmann constant.
L	Diffusion length of excess carriers.
L_n	Diffusion length of electrons.
L_p	Diffusion length of holes.
L^*	Ambipolar diffusion length.
L_{Di}	Debye length.

m_n	Mass of electrons.
m_p	Mass of holes.
m_o	Free carrier mass.
m_{eff}	Effective mass of carriers.
N_A	Acceptor density.
N_D	Donor density.
N_C	Effective density of states in the conduction band.
N_V	Effective density of states in the valence band.
N_o	Total number of photons falling per cm^2 per sec. on the cell surface.
$N_o(\lambda)$	Number of Solar photons incident in the respective wave length interval $\Delta\lambda$
n	Electron concentration
n_i	Intrinsic carrier concentration.
n_n	Electron density in n-type material.
n_p	Electron density in p-type material.
n_o	Equilibrium electron concentration.
P_{in}	Input power falling on the cell.
P_{max}	Maximum output power.
P_{out}	Output power.
p	Hole concentration.
p_n	Hole density in n type material.
p_p	Hole density in p type material.
p_o	Equilibrium hole concentration.
q	Electronic charge.
R_L	Load resistance.

R_s	Series resistance.
s_1	Surface recombination velocity at the front surface which is exposed to light.
s_2	Surface recombination velocity at the back surface.
T	Temperature.
V	Output voltage.
V_B	Dember voltage.
V_D	Diffusion potential.
V_T	Terminal voltage.
V_j	Junction voltage.
V_m	Voltage at the maximum power point.
V_n	Voltage drop in the n region.
V_p	Voltage drop in the p region.
V_{oc}	Open circuit voltage.
W_T	Energy received per unit area per unit time.
W_λ	Spectral radiancy.
μ	Total carrier mobility.
μ_I	Impurity scattering mobility.
μ_n	Electron mobility.
μ_p	Hole mobility.
μ^*	Ambipolar mobility.
μ_{Ln}	Lattice scattering mobility
μ_{Lp}	Lattice scattering mobility for holes.

τ_n	Life time of excess electrons.
τ	Life time of excess holes.
τ_{no}	Life time of electrons in thermal equilibrium.
τ_{po}	Life time of holes in thermal equilibrium.
Δn	Excess electron concentration.
Δp	Excess hole concentration.
Δn_p	Excess electron concentration on p side.
Δp_n	Excess hole concentration on n side.
$(\Delta n_p)_o$	Excess electron density at the edge of the junction in p region.
$(\Delta p_n)_o$	Excess hole density at the edge of the junction in the n region.
$(\Delta n_p)_{-d_1}$	Excess electron density at the surface in p region.
ρ	Net charge density.
χ	Dielectric constant.
σ	Electrical conductivity.
α	Absorption coefficient.
η	Efficiency.
λ	Wavelength of light.
ν	Frequency of incident light.

INTRODUCTION

This thesis deals with the study of the response of solar cells to high intensity, concentrated radiation as obtained by using solar concentrators. Such concentrated radiation has certain special features such as nonuniformity in addition to high intensity illumination which has been included in the analysis.

Presently, there is a strong interest in the use of solar cells for the purpose of direct conversion of solar radiation into electrical energy. The response of a solar cell to solar radiation is generally studied through its three main parameters, the open circuit voltage, the short current, and the fill factor. These parameters determine the efficiency of the cell and the circuit conditions in which the cell should be used and give all the required information for most terrestrial applications. Although many different types of solar cells have been investigated and are being tried and used, the conventional p-n junction Silicon solar cell still seems to be the most useful from overall considerations. For terrestiral applications, use of solar concentrators, tracking as well as non-tracking types, is being tried to bring down the overall cost. Such concentrators provide high intensity (from a few suns to well over 1000 suns) illumination which, in general, is nonuniform over the surface of the cell. Though high intensity illumination enhances the cell efficiency, degradation effects due to rise in the temperature of the cell and due to its series resistance, also come in. A study of solar cell

response under high intensity, concentrated illumination must, therefore, include the study of all these effects. Such a study is not only of interest and importance from the point of view of applications, but also for understanding the various physical processes occurring during such illumination.

In this thesis, we present the results of theoretical as well as experimental studies on the response of p-n junction Silicon solar cells at high levels of illumination. The theoretical treatment given is, however, general in nature and is applicable to various kinds of p-n junction solar cells.

The main thesis consists of seven chapters as follows:

Chapter 1 contains a brief account of the physics of the p-n junction solar cell and the parameters which determine the solar cell response.

Chapter 2 deals with the effects of nonuniform illumination of the solar cell. The case of general non-uniformity under certain simplifying assumptions such as zero surface recombination velocity at the surface normal to the junction, has been studied using the technique of partial Fourier Transforms, to show its effect on the response of the solar cell.

In Chapter 3, a theoretical study of the response of a solar cell to all levels of illumination at constant cell temperature is presented. Numerical solution of the resulting nonlinear, steady-state, one-dimensional, ambipolar equation is obtained using a simple technique and taking into account the dependence of the ambipolar coefficients on the excess carrier concentration. Effects of surface recombination velocity and exponential absorption of light in the solar cell are also taken into account. The boundary conditions used at the junction of the solar cell are valid for all levels of injection. Appropriate boundary conditions are used at its top and bottom surfaces. The results obtained in this manner agree with these obtained by other workers for low and high injection limits. However, the present study also gives some useful results for intermediate levels of injection. The variation of the ambipolar diffusion coefficient and the life time of excess carriers with intensity, and hence, the variation of the diffusion length with intensity are discussed and presented in graphical form. Since the series and shunt resistances and the contact area loss are determined largly by technology, and since reflection of the incident light can be reduced by proper antireflection coatings, we have calculated the somewhat idealized efficiencies obtained by neglecting these technology oriented losses. Effect of internal series resistance on I-V characteristics

and cell response parameters is shown separately. Short-circuit current, open-circuit voltage, fill factor and efficiency have been calculated and shown as functions of the light level. All these results have been derived for monochromatic light of different wavelengths as well as for AMO spectrum. Although the calculations have been carried out up to infinite intensity levels, the results may not be valid for intensities above about 10^4 watts/cm^2 because certain factors like plasma reflection, exciton generation, Auger recombination etc., which may come in the picture, at such high intensities have not been considered.

In Chapter 4, experimental results on 2 x 2 cms, 10 ohm- cm solar cells under different intensity levels at constant cell temperature are reported and discussed.

Chapter 5 deals with the effect of temperature on the response of solar cells. The efficiency of a solar cell decreases with increasing temperature. A complete theoretical description of all the temperature dependent cell parameters is given. Changes in I-V characteristics, short-circuit current, open-circuit voltage, fill-factor and efficiency of the solar cell, with temperature are discussed. These results are obtained for different intensity levels by solving the steady-state, temperature dependent, one-dimensional ambipolar equation in the temperature range

$300^{o}K$ to $400^{o}K$. These could be useful in taking into account the effect of temperature rise on solar cell response under high intensity illumination.

In Chapter 6, an experimental study of the effect of temperature within the above range, on the spectral response of solar cells is presented. A detailed analysis of the observed change in spectral response with the rise in temperature is given, taking into account the temperature dependence of the various parameters. Diffusion length in the base region is calculated at different temperatures using the spectral response data. In addition, a relation between the junction depth, diffusion length of excess carriers and absorption coefficient at the peak of the spectral response curve is derived.

Response of a solar cell is also seriously affected due to the non-zero internal series resistance of the solar cell, and this effect is found to be pronounced at high intensities. Chapter 7 deals with the measurement of the series resistance by different methods. A new method of determining the series resistance of a solar cell is presented, in which the deviation from linearity of the short-circuit current, with increasing intensity, is used to estimate the series resistance. Results obtained by this

method are compared with those obtained by the conventional methods of measuring the series resistance of solar cells. Some interesting results on solar cells having different exposed areas are also presented.

Each chapter (Chapter 2 to 7) also contains discussion of the work reported therein.

To summarize, we present in this thesis a comprehensive theoretical treatment of the solar cell response under high intensity concentrated radiation. We have also carried out experimental work which confirm our theoretical predictions. We have also pointed out areas where further experimental and theoretical work is needed to provide better understanding of the subject.

CHAPTER-1.

SILICON p-n JUNCTION SOLAR CELLS-A BRIEF REVIEW

1.1 Introduction :

A solar cell is a photovoltaic device designed to convert sunlight into electrical power and to deliver this power into a suitable load in an efficient manner. The use of photovoltaic cells for direct energy conversion has been largely confined to space applications. However, the increasing need for alternate terrestrial energy sources, and ecological considerations have made solar energy and photovoltaic conversion an active area of research.

The early papers on Silicon p-n junction solar cells were by Rappaport (1954,1959), Cummerow (1954), Rittner (1954), Chapin et al (1954), Prince (1955) Rappaport et al (1956), Loferski (1956) and Wolf (1960). A great advancement has been made in the development of silicon solar cells in seventies and there are, now several review articles and books available in literature which deal with the design, fabrication, characteristics and physics of solar cells (see e.g. Wolf 1971, Hovel 1975, Rothwarf and Boer 1975, Meinel and Meinel 1976, Rouse 1977).

In this chapter, our purpose is to describe the under lying basic assumptions in the theory of p-n junction solar cells and to discuss the factors affecting the response

of solar cells. This will help in providing the necessary background for the development of later chapters in which we have presented the results of our studies on the response of p-n junction solar cells.

1.2 Solar Spectrum :

Since, the device under consideration is a solar energy converter and not a light converter in general, a study of the nature of the Sun's radiation and its spectral distribution is of prime importance in the design of solar cells.

Like any other radiant source, the sun emits photons of all wavelengths from 0 to ∞. More than 95 % of this energy is concentrated in the narrow span of 0.24 μm to 2.5 μm. The peak of the spectral radiancy curve occurs at 0.5 micron. About 30 % of the total energy emitted by the sun is reflected and 10 % is absorbed by the atmosphere.

In the outer atmosphere, the total energy received per unit area per unit second is

$$w_T = \int_0^\infty w_\lambda \, d\lambda = 135 \text{ mw/cm}^2$$

where w_λ is the spectral radiancy i.e. the amount of energy

radiated per unit area per second per unit wavelength interval.

The spectral distribution of the radiation reaching the earth from the sun can be approximated by a black body at a temperature of 5900°K. However, there is a sufficient departure from the idealized spectrum because of the absorption coefficients associated with atmospheric absorption by atmospheric gases, aqueous vapours and dust. All these absorption mechanisms tend to deplete the ultraviolet wavelengths preferentially. The effect can be described by means of the optical air mass m defined as the path length of radiation through the atmosphere considering the vertical path at sea level as unity and w which is defined as the perceptible water in a vertical column in the atmosphere measured in centemeters. Air mass zero (m = 0, written as AMO) is obviously the condition in space. The condition of air mass one (AM1) is the condition on the earth's surface when the sunlight is vertically overhead. Fig. 1.1 shows the AMO and AM1 spectra.

Energy density in AMO conditions is normally taken to be 0.135 W/cm^2 ($N_{ph} = 5.8 \times 10^{17}$ photons per cm^2 per sec.) and in AMI conditions 0.106 W/cm^2 ($N_{ph} = 5 \times 10^{17}$ photons/cm^2/sec).

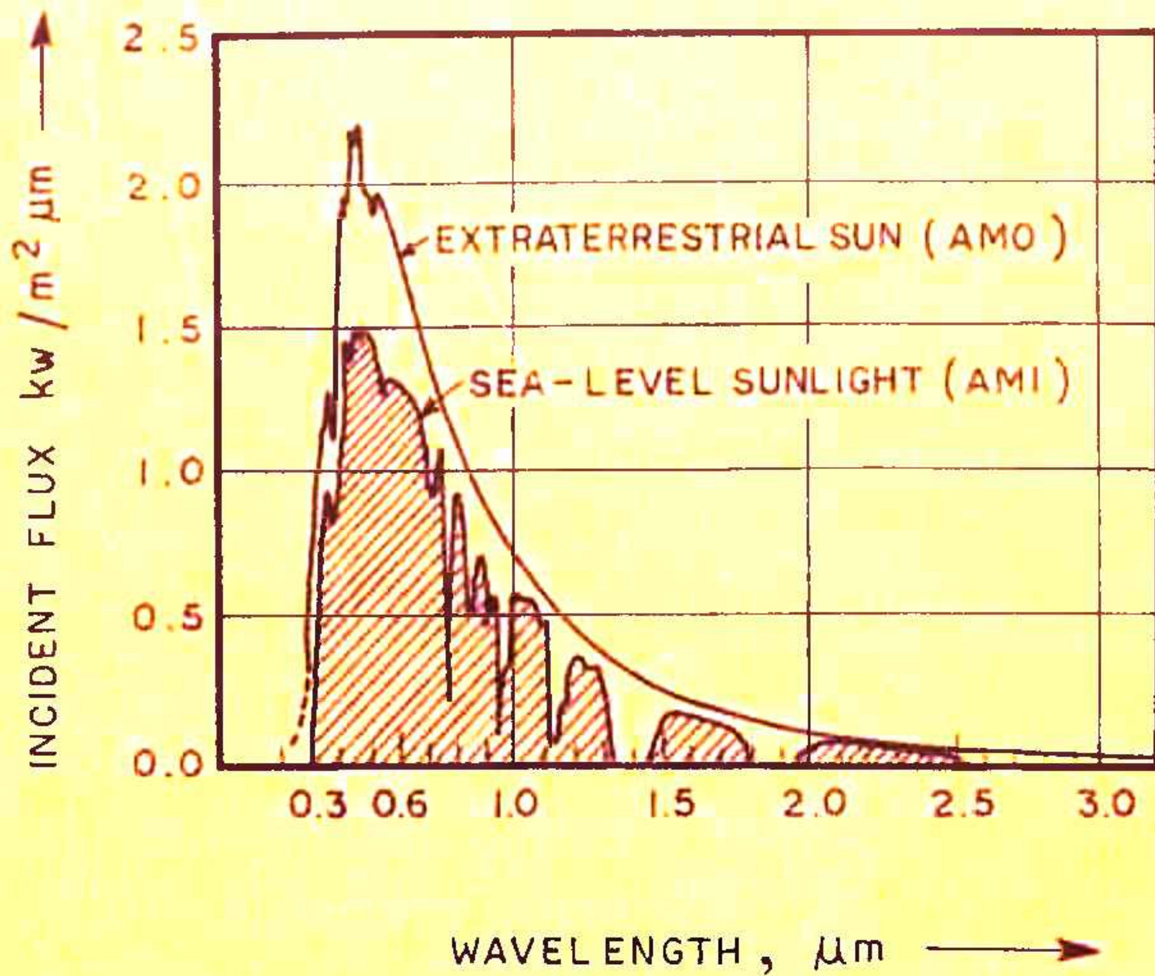

FIG. I.I SPECTRAL DISTRIBUTION OF ENERGY IN SUNLIGHT ABOVE ATMOSPHERE AND AFTER PASSAGE THROUGH ONE AIR MASS FOR AN ATMOSPHERE CONTAINING 20mm PRECIPITABLE WATER VAPOR. (TAKEN FROM MEINEL AND MEINEL 1977).

1.3 Photovoltaic effect in a p-n junction :

If the n and p type semiconductors are brought together, a p-n junction having a potential barrier is formed, because thermodynamics requires that the average energy of the carriers be the same in the two materials. The physics of silicon p-n junction diodes is well known. The operation of such a device as a solar cell is essentially different from that of a diode in that the deviation from thermal equilibrium necessary to produce a net conversion of energy by the device, is achieved by using incident radiation rather than by applying a voltage.

The photovoltaic effect in a p-n junction can be defined as the generation of a potential when the incident radiation ionizes the region in or near the built in potential barrier of a semiconductor. It is characterized by a self-generated emf and the ability to deliver power to a load, the primary power coming from the ionizing radiation.

Specifically, the light incident on a p-n junction have two effects:

a) the current of minority carriers crossing the junction (to become majority carriers) is increased.

b) the height of the potential barrier at the junction is reduced by this current, to an extent determined by the load resistance.

This reduction in barrier height is analogous with the effect of a forward bias on the cell, so the light is said to produce a photovoltage. However, the current of majority carriers which can cross the barrier because of its reduced height is not useful in photovoltaic generation because it opposes the flow of light generated minority carriers. A detailed description of this effect explained in terms of the energy band diagram is given by Mckelvey (1966).

The magnitude of the photovoltage V_o developed because of the incident radiation can be expressed in terms of the excess minority carrier concentrations at the boundaries of the junction space charge regions by the following equations

$$\left.\frac{n_p}{n_n}\right|_{\text{at the junction boundary on p side}} = e^{-q(V_D - V_o)/kT} \qquad (1.1)$$

and

$$\left.\frac{p_n}{p_p}\right|_{\text{at the junction boundary on n side}} = e^{-q(V_D - V_o)/kT} \qquad (1.2)$$

where n_p and p_n are the minority carrier concentrations on p and n sides respectively n_n denotes the concentration of electrons on n side and p_p gives the concentration of holes on p side.

1.4 Theory of p-n junction solar cells:

The theory of the p-n junction solar cell has its origin in the classical article by Shockley (1949) on semiconductor p-n junctions based upon a diffusion model. The first analytical treatment dealing explicitly with the solar cell case is that of Cummerow in 1954, who generalized Shockley's continuity equation by the addition of an optical generation term decreasing exponentially with distance. Numerical results were presented for both Germanium and Silicon solar cells. The next Milestone in the development of the theory is the calculation by Rittner, also in 1954, of the cell efficiency as a function of doping and semiconductor band gap. Wolf in 1960 have analytically evaluated the collection process under the appropriate boundary conditions including the effect of surface recombination. Mckelvey (1966) gives a good account of the physics of solar cells and has solved the minority carrier transport equation (described below) under generalized boundary conditions to derive expressions for the cell response.

1.4.1 Transport equation for excess carriers :

The continuity equations which describe the flow of carriers in a homogeneous semiconductor are (see e.g. Jonscher 1960, Mckelvey 1966):

$$D_p \nabla^2 p - \mu_p (\vec{E} . \vec{\nabla} p + p \vec{\nabla} . \vec{E}) + g'_p - (\frac{p}{\tau_p} - \frac{p_o}{\tau_{po}})$$

$$= \frac{\partial p}{\partial t} \quad .... \text{ for holes} \qquad (1.3)$$

and

$$D_n \nabla^2 n + \mu_n (\vec{E} . \vec{\nabla} n + n \vec{\nabla} . \vec{E}) + g'_n - (\frac{n}{\tau_n} - \frac{n_o}{\tau_{no}})$$

$$= \frac{\partial n}{\partial t} \quad .... \text{ for electrons} \qquad (1.4)$$

where g'_p and g'_n denote the excess carrier generation rate in the medium due to the absorption of incident photons. τ_n and τ_p are the life times of electrons and holes. Diffusion coefficients D_n, D_p are related to the mobilities μ_n, μ_p by the Einstein relations :

$$D_n = \frac{\mu_n kT}{q} \quad \text{for electrons ,} \qquad (1.5)$$

$$D_p = \frac{\mu_p kT}{q} \quad \text{for holes .} \qquad (1.6)$$

τ_{no}, τ_{po} denote the life times of electrons and holes in thermal equilibrium. n and p are the electron and hole concentrations respectively.

In the absence of an externally applied eläctric field, $\vec{E}$ denotes the internal $\vec{E}_{int}$ field arising because of

the difference in the mean free paths of electrons and holes. Different value of the electron and hole mobility in the medium gives rise to a separation of positive and negative charges and an internal electric field is set up. which is in a direction so as to oppose the charge separation. This internal field tends to retard the faster diffusing particles and to drag the slower ones on more rapidly. As a result, when this field becomes strong enough to counteract entirely any tendency for the electron and hole charge distributions to separate further, the positive and negative charge distributions start diffusing together. The effective diffusion coefficient in such a case is larger than that of the more slowly diffusing species, but smaller than that of the more rapidly diffusing type. This phenomenon is known as the ambipolar diffusion and the internal electric field responsible for it is called the Dember field.

A third equation relating the electric field and the net charge density ρ in the semiconductor is given by

$$\vec{\nabla} \cdot \vec{E}_{int} = \frac{4\pi \rho}{K} \tag{1.7}$$

where K is the dielectric constant. Eqns. 1.3, 1.4 and 1.7 form a set of 3 equations which can be used to determine the three unknowns n, p and $\vec{E}_{int}$.

1.4.2 Charge neutrality assumption :

Unfortunately, the above mentioned 3 equations cannot be solved analytically. Therefore, we must make some reasonable physical approximation which will allow us to arrive at a solution which, although not exact, will be adequate for most cases of practical importance. The approximation which is used for this purpose is the charge neutrality assumption. We shall assume in eqns. 1.3 and 1.4 that the excess hole density Δp is just balances by the excess electron density Δn :

$$\Delta p = p - p_o = n - n_o = \Delta n \qquad (1.8)$$

where p_o and n_o are equilibrium concentrations of the carriers.

It has been shown by Mckelvey (1966) that the charge neutrality assumption holds good when the following condition is satisfied:

$$\left| \frac{\Delta p - \Delta n}{\Delta p} \right| = \frac{L_{Di}^2}{L^2} \frac{(b-1)\, n_i}{nb + p} \ll 1 \,. \qquad (1.9)$$

It is clear from the above expression that the assumption of charge neutrality should be a good one when the characteristic distance L which is equal to the diffusion length

for purely diffusive systems is much larger than the intrinsic Debye length L_{Di}

$$L >> L_{Di} \qquad (1.10)$$

and where

$$nb + p >> (b - 1) n_i \qquad (1.11)$$

Here, b denotes the ratio of electron to hole mobility and n_i is the intrinsic carrier concentration. These conditions are almost always satisfied in the intrinsic and extrinsic samples of silicon (Mckelvey 1966). Therefore, it is a normal practice to assume eqn. 1.8 to be valid in the theory of silicon solar cells.

1.4.3 Ambipolar diffusion equation :

In a homogeneous sample, impurity density is uniform through out and therefore, n_o and p_o are constants. In such a case,

$$\frac{\partial n}{\partial t} = \frac{\partial \Delta n}{\partial t}$$

and $$\nabla n = \nabla(\Delta n) .$$

A similar relationship holds for holes. In eqns. 1.3 and 1.4 generation and recombinates rates for electrons and holes can be taken to be equal yielding :

$$\mathcal{G}'_p = \mathcal{G}'_n = \mathcal{G}' \tag{1.12}$$

and
$$\frac{p}{\tau_p} - \frac{p_o}{\tau_{po}} = \frac{n}{\tau_n} - \frac{n_o}{\tau_{no}} \quad . \tag{1.13}$$

Using the above described relationships in eqns. 1.3 and 1.4 and eliminating the term $\vec{\nabla} \cdot \vec{E}$ by multiplying eqn. 1.3 by $n\mu_n$, eqn. 1.4 by $p\mu_p$ and adding the two equations, we obtain

$$D^* \nabla^2 (\Delta p) - \mu^* \vec{E} \cdot (\Delta p) + g' - \frac{\Delta p}{\tau^*} = \frac{\partial(\Delta p)}{\partial t} \quad . \tag{1.14}$$

Eqn. 1.14 is the time dependent ambipolar transport equation obeyed by the the excess carrier concentration Δp . The excess carrier concentration of the other carrier species, Δn, is, of course, equal to Δp in accord with the charge neutrality assumption given in eqn. 1.8. D^*, μ^* are known as the ambipolar diffusion coefficient and ambipolar mobility respectively and are given by :

$$D^* = \frac{(n_o + p_o + 2\Delta p)\, D_n D_p}{(n_o + \Delta p)\, D_n + (p_o + \Delta p) D_p} , \tag{1.15}$$

$$\mu^* = \frac{(n_o - p_o)\, \mu_n \mu_p}{(n_o + \Delta p)\, \mu_n + (p_o + \Delta p)\, \mu_p} \quad . \tag{1.16}$$

τ^* is the excess carrier life time defined by

$$\frac{\Delta p}{\tau^*} = \frac{p_o + \Delta p}{\tau_p} - \frac{p_o}{\tau_{po}} = \frac{n_o + \Delta p}{\tau_n} - \frac{n_o}{\tau_{no}} \quad . \qquad (1.17)$$

τ^* as given by the Hall (1952), Shockley & Read (1952) is

$$\tau^* = \tau_{po} \frac{n_o + n_1 + \Delta p}{p_o + n_o + \Delta p} + \tau_{no} \frac{p_o + p_1 + \Delta p}{p_o + n_o + \Delta p} \qquad (1.18)$$

where n_o, p_o are the equilibrium carrier concentrations of holes and electrons respectively and

$$p_1 = N_v \exp\left(E_v - E_t \right) / kT \ , \qquad (1.18a)$$

$$n_1 = N_c \exp\left(E_t - E_c \right) / kT \ . \qquad (1.18b)$$

N_v, N_c are the effective densities of states in the valence and conduction bands, respectively. E_t is the trap level energy. E_c, E_v are the conduction band and valence band edge energies respectively.

1.4.4 Dember field :

An expression for the Dember field $\vec{E}_{int}$ appearing in eqn. 1.14 can be derived by noting that the total electrical current density I may be written as

$$\vec{I} = q \left(\vec{J}_p - \vec{J}_n \right) \qquad (1.19)$$

where $\vec{J}_p$ and $\vec{J}_n$ are the hole flux density and electron flux density respectively and q is the electronic charge. $\vec{J}_p$ and $\vec{J}_n$ are written as the sum of the diffusion flux density and a drift current density arising from the presence of an electric field $\vec{E}$ as :

$$\vec{J}_p = - D_p \nabla p + p \mu_p \vec{E} , \qquad (1.20)$$

$$\vec{J}_n = - D_n \nabla n + n \mu_n \vec{E} . \qquad (1.21)$$

Using these expressions $\vec{I}$ may be written as

$$\vec{I} = \sigma \vec{E} + q(D_n - D_p) \nabla (\Delta p) \qquad (1.22)$$

where σ is the electrical conductivity of the medium given by

$$\sigma = q (n \mu_n + p \mu_p) . \qquad (1.23)$$

In deriving eqn. 1.22 charge neutrality approximation is assumed to hold good. Solving for the field $\vec{E}$ in eqn. 1.22 and using eqns. 1.5 and 1.6 we obtain,

$$\vec{E} = \frac{\vec{I}}{\sigma} \quad \frac{kT}{q} \quad \frac{b - 1}{nb + p} \nabla (\Delta p). \qquad (1.24)$$

As first term above is clearly the field arising from the application of an external potential source; the second term represents the internal field:

$$\vec{E}_{int} = - \frac{kT}{q} \frac{b-1}{nb + p} \nabla (\Delta p). \qquad (1.25)$$

It is obvious that $\vec{E}_{int}$ vanishes if there is no gradient of carrier concentration, and also if the hole and electron mobilities are equal ($b = 1$).

For $b \neq 1$, $\vec{E}_{int}$ will have a small effect on the distribution of excess carriers which is neglected in general (Mckelvey 1966).

1.4.5 <u>Limiting cases</u> :

We consider the following two limiting cases:

(i) Low level limit:

We consider the case when the intensity of light falling on the semiconductor is low enough such that the density of excess carriers produced by light is much less than the equilibrium carrier concentration i.e. $\Delta p \ll$ larger of the two quantities n_o, p_o Under these conditions, D^* and μ^* are constants as discussed below:

For a strongly n type semiconductor, $n_o \gg p_o, \Delta p$. In general, it is observed that the life time of the minority carrier is essentially independent of the excess carrier concentration for the low level case whereas, the majority carrier life time is not. This is expected because the relative charge in the

minority carrier density is greater by several orders than the change in the majority carrier density due to photogeneration of electron-hole pairs. For a strongly n-type semiconductor, then,

$\tau_p = \tau_{po}$ for $\Delta p \ll n_o$.

The excess carrier life time τ^*, as defined by eqn. 1.18 reduces to

$$\tau^* = \tau_{po} \text{ (for a strongly n-type material) .} \quad (1.26)$$

Likewise, for a strongly extrinsic p-type crystal, it is readily seen that eqn. 1.18 gives

$$\tau^* = \tau_{no} \text{ (strongly p-type material) .} \quad (1.27)$$

Thus, for the low level case, the excess carrier lifetime τ^* simply reduces to the lifetime of the minority carrier.

From eqns. 1.15 and 1.16 it is readily seen that under low level conditions :

$$D^* = D_p \text{ , } \mu^* = \mu_p \text{ for a strongly n-type material ;} \quad (1.28)$$

$$D^* = D_n\text{, } \mu^* = -\mu_n \text{ for a strongly p-type material .} \quad (1.29)$$

Therefore, in the low level limit, ambipolar eqn. 1.14 has the same form as the minority carrier diffusion eqn. 1.3 for independently diffusing particles for the case when $\bar{E}$ is constant.

(ii) High level limit :

In this case when the excess carrier density is so high such that $\Delta n, \Delta p >> n_o, p_o$, eqns. 1.15, 1.16 and 1.18 give for D^*, μ^* and τ^* respectively the following values:

$$D^* \text{ goes to } \frac{2 D_n D_p}{D_n + D_p} , \quad (1.30a)$$

$$\mu^* \text{ goes to } 0 , \quad (1.30b)$$

$$\tau^* \text{ goes to } \tau_n + \tau_p . \quad (1.30c)$$

Thus, we see that in the above described two limiting cases the coefficients appearing in the ambipolar eqn. 1.14 become constants and a similar equation is obtained for both the low as well as high intensity limits. Since the effect of $\vec{E}_{int}$ is negligible for the low level case as discussed by Mckelvey(1966) and μ^* becomes very small for the high level case (eqn. 1.30b) , second term in eqn. 1.14 is generally neglected in these two limiting cases.

Solution of the eqn. 1.14 in the steady state has been obtained by Mckelvey (1966) in the n and p regions of the solar cell, under appropriate boundary conditions. However, they have considered the case of low level illu-

mination only and have also neglected the contribution of the second term in eqn. 1.14 . In the next section we will describe these results for the low level case. Solution for the high level case will be discussed in Chapter-3.

1.4.6 Solution of the ambipolar equation in the low level limit:

Let us consider a p-n junction solar cell illuminated uniformly by light. One dimensional model of the cell is shown in Fig. 1.2. Although here we will confine ourselves to the p on n type of solar cell, the same treatment is valid for n on p type of solar cells also. For the case of low level illumination D^*, μ^* and τ^* are constants, their values being equal to the minority carrier value as discussed in Sec. 1.4.5. Ambipolar transport equation in the p and n regions of the solar cell is solved under the following assumptions:

1. injection level is low,
2. generation and recombination of carriers in the space charge region is negligible,
3. thickness of the space charge region is negligible in comparison with the diffusion lengths of carriers,
4. the semiconductor is non-degenerate,

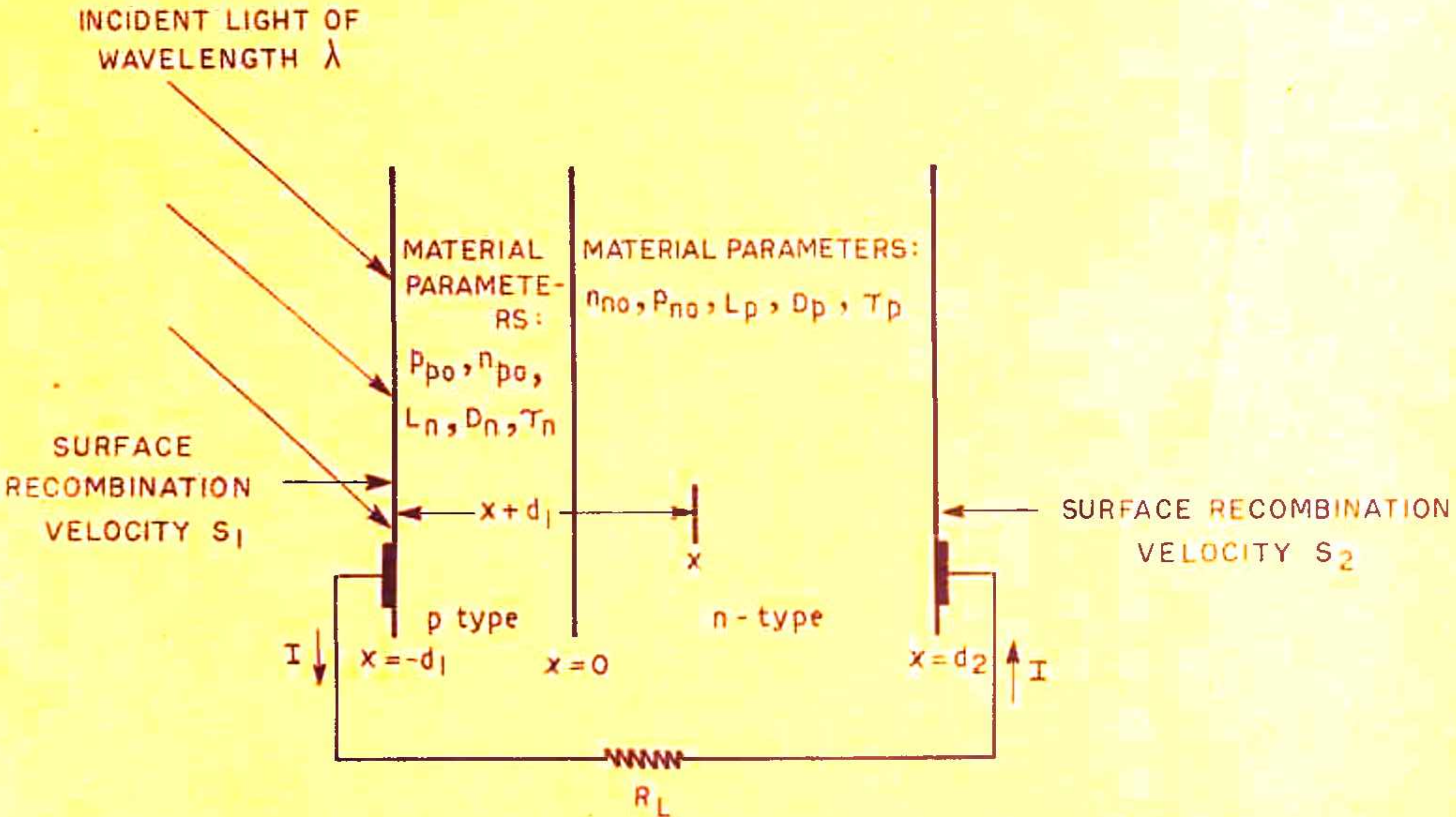

FIG. 1.2 GEOMETRY FOR THE p-n PHOTOVOLTAIC CELL.

5. the quasi- Fermi levels for electrons and holes are constant over the space charge regions,
6. the condition of quasi-neutrality holds elsewhere,
7. and the impurities are completely ionized at room temperature.

Light of a monochromatic wavelength λ is considered to be incident on the p surface of the cell. The absorption coefficient corresponding to that particular wavelength is taken to be α. The excess carrier generation rate is given by

$$g'(x) = \alpha N_o e^{-\alpha(x + d_1)} \qquad (1.31)$$

where d_1 is the thickness of the p region and N_o is number of photons incident per cm^2 per sec. on the cell surface. The continuity equation for excess electrons in the p region is given by

$$\frac{d^2 \Delta n}{dx^2} - \frac{(\Delta n)}{L_n^2} = \frac{-\alpha N_o e^{-\alpha(x+d_1)}}{D_n} \qquad (1.32)$$

where Δn is the excess carrier concentration and L_n is the diffusion length of electrons given by

$$L_n = \sqrt{D_n \times \tau_n} \quad . \qquad (1.32a)$$

A similar equation is written for the excess carrier concentration Δp on the n side as

$$\frac{d^2 \Delta p}{dx^2} - \frac{\Delta p}{L_p^2} = - \frac{\alpha N_o e^{-\alpha(x + d_1)}}{D_p} \qquad (1.33)$$

where $\quad L_p = \sqrt{D_p \times \tau_p}$. $\qquad$ (1.33a)

The general solution of eqn. 1.32 is given by

$$\Delta n(x) = A \cosh \frac{x}{L_n} + B \sinh \frac{x}{L_n} + \frac{\alpha N_o \tau_n}{1-\alpha^2 L_n^2} e^{-\alpha(x+d_1)} .$$

(1.34)

Similarly, in the n region, solution of eqn. 1.33 is given by

$$\Delta p (x) = C e^{x/L_p} + D e^{-x/L_p} + \frac{\alpha N_o \tau_p}{1- \alpha^2 L_p^2} e^{-\alpha(x+d_1)}$$

(1.35)

where A, B, C and D are constants.

If the cell is considered to be of infinite extent in the n region, i.e. $d_2 \to \infty$ constant C must be zero because $\Delta p(x)$ must decay to zero for large values of x. Constants A, B and D are evaluated by applying the folowing boundary conditions :

(i) At the top surface of the cell :

$$D_n \left(\frac{d (\Delta n)}{dx} \right) \Big|_{x = - d_1} = S_1 (\Delta n) \Big|_{x=-d_1}$$

(1.36).

where S_1 is the surface recombination velocity at the top surface

(ii) At the junction (x = 0) :

$$\frac{n_p(0)}{n_{po}} = \frac{p_n(0)}{p_{no}} = e^{qV_j/kT} \qquad (1.37)$$

where V_j denotes the junction voltage, The above boundary condition given by eqn. 1.37 is valid only for low levels of illumination when the excess carrier density everywhere is much smaller than the equilibrium majority carrier density.

1.4.7 Solar cell electrical characteristics:

The junction current is the sum of diffusion currents due to holes and electrons

$$I = q\left(J_p(0) - J_n(0) \right)$$

$$= q\left(D_n \frac{d\Delta n}{dx} - D_p \frac{d\Delta p}{dx} \right)\Bigg|_{x=0} \qquad (1.38)$$

$J_p(0)$ and $J_n(0)$ are the hole and electron currents at the junction respectively. Eqn. 1.38 is evaluated to give the current voltage equation for the device. The result may be expressed in the form

$$I = I_o \left[\exp \left(q V_j / kT \right) - 1 \right] - I_g \qquad (1.39)$$

where

$$I_o = q \left[\frac{p_{no} D_p}{L_p} + \frac{n_{po} D_n}{L_n} \cdot \frac{S_1 \cosh \frac{d_1}{L_n} + \frac{D_n}{L_n} \sinh \frac{d_1}{L_n}}{\frac{D_n}{L_n} \cosh \frac{d_1}{L_n} + S_1 \sinh \frac{d_1}{L_n}} \right] \qquad (1.40)$$

is a saturation current which is a function only of the dimensional and material parameters of the device, independent of the level of illumination.

$$I_g = \frac{q \alpha N_o L_p^2 e^{-\alpha d_1}}{1 - \alpha^2 L_p^2} \left(\frac{1}{L_p} - \alpha \right)$$

$$+ \frac{q \alpha N_o L_n^2}{1 - \alpha^2 L_n^2} \left\{ \frac{1}{L_n} \left[\frac{\left(S_1 \cosh \frac{d_1}{L_n} + \frac{D_n}{L_n} \sinh \frac{d}{L_n} \right) e^{-\alpha d_1} - S_1 - \alpha D_n}{\frac{D_n}{L_n} \cosh \frac{d_1}{L_n} + S_1 \sinh \frac{d_1}{L_n}} \right] + \alpha e^{-\alpha d_1} \right\} \qquad (1.41)$$

is the photogenerated current, independent of the junction voltage V_j but directly propotional to the illumination intensity as represented by N_o. I_g represents that part of the current of excess electrons and holes created by light which succeeds in diffusing to the junction. Therefore, on the average, only those electron-hole pairs will be collected which are within a diffusion length from the junction.

(a) I-V characteristics:

Solar cell current-voltage relationship is given by eqn. 1.39 which is essentially the Søhockley diode equation modified by the term I_g that takes into account the photogenerated current.

(b) Equivalent circuit:

The simplest equivalent circuit of a solar cell in the operating mode is shown in Fig. 1.3. The photocurrent is represented by a current generator I_g and is opposite in direction to the forward bias current of the diode. Shunt resistance paths are represented by R_{sh}, they can be caused by surface leakage along the edges of the cell, by diffusion spikes along dislocations or grain boundaries, or possibly by fine metallic bridges along microcracks, grain boundaries, or crystal defects. Series resistance, represented by R_s, can arise from contact resistances to the front and back (particularly for high resistivity bases, 1 to 10 ohm cm), the resistance of the base region itself, and the sheet resistance of the thin diffused or grown surface layer. More complicated equivalent circuits can be formulated to account more accurately for the distributed nature of both the series resistance and the current generator (Wolf and Rauschenbach, 1963).

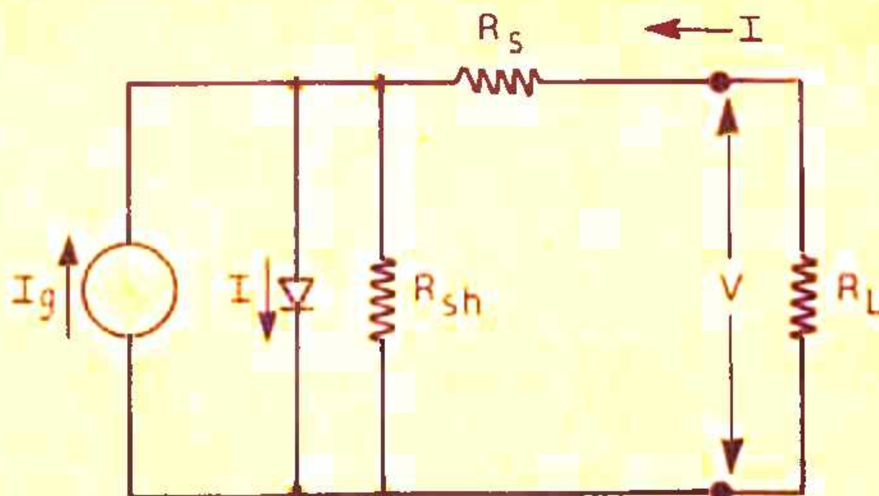

FIG. I.3 EQUIVALENT CIRCUIT OF A SOLAR CELL INCLUDING SERIES AND SHUNT RESISTANCES.

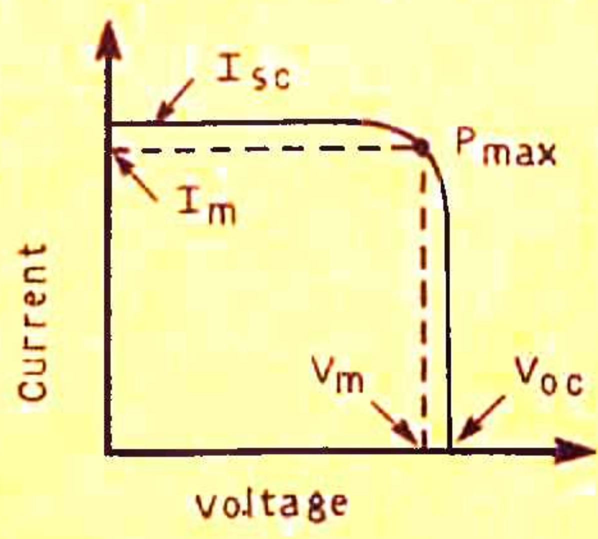

FIG. I.4 VOLTAGE AND CURRENT OUTPUT FROM AN ILLUMINATED SOLAR CELL.

(c) Relationships for negligible R_s, R_{sh} losses:

In order to use the equivalent circuit to predict solar cell output and efficiency and to make the relationships analytically manageable, the approximations are often made that series and shunt resistance effects are negligible. In such a case, eqn. 1.39 gives the relationship between the current and voltage at the terminals:

$$I_T = I_o \left[\exp(qV_T/kT) - 1 \right] - I_g \quad . \qquad (1.42)$$

Solar cell response can conveniently be examined through three main parameters (as shown in Fig. 1.4) (see P. 31) the short circuit current I_{sc}, the open circuit voltage V_{oc} and the 'fill factor', the ratio of maximum power output to the product of V_{oc} and I_{sc}.

The short circuit current I_{sc} is obtained simply by substituting $V_T = 0$ in eqn. 1.42 which gives

$$I_{sc} = - I_g \quad . \qquad (1.43)$$

The expression for open circuit voltage is obtained by substituting $I = 0$ in eqn. 1.42 as

$$V_{oc} = \left(\frac{kT}{q} \right) \ln \left(1 + \frac{I_g}{I_o} \right) \quad . \qquad (1.44)$$

Since the power output (P_{out}) is

$$P_{out} = V_T \times I_T , \qquad (1.45)$$

the maximum power output can be found by differentiating the product and setting the result equal to zero (Loferski 1963)

$$P_{out}(max) = P_{max} = I_m V_m \qquad (1.46)$$

where

$$I_m = (I_{sc} + I_o) \left[\frac{qV_m/kT}{1+(qV_m/kT)} \right] \qquad (1.47)$$

is the current output at maximum power and

$$\exp (qV_m/kT). (1 + q V_m/kT)$$

$$= (I_{sc}/I_o) + 1 \qquad (1.48a)$$

$$= \exp (q V_{oc}/kT) \qquad (1.48b)$$

allows the voltage at maximum power point to be calculated. The fill factor (FF), measures the 'squareness' of the I - V curve, and is given by

$$FF = V_m I_m / I_{sc} V_{oc} \quad . \qquad (1.49a)$$

For the low level case expression for FF is given by (Lindmayer, 1972):

$$FF = \frac{V_m}{V_{oc}} \left\{ 1 - \frac{[\exp(qV_m/kT) - 1]}{[\exp(qV_{oc}/kT) - 1]} \right\} \qquad (1.49b)$$

$$= V_m \left\{ \frac{1 - (I_o/I_{sc}) [\exp (q V_m/kT) - 1]}{(kT/q) \ln [(I_{sc}/I_o) + 1]} \right\} . \qquad (1.49c)$$

1.4.8 Efficiency :

The efficiency of a solar cell in converting light of any arbitrary spectral distribution into useful power is given by

$$\eta = V_m I_m / P_{in} \qquad (1.50)$$

where V_m, I_m are the voltage and current at the maximum power point (see Fig. 1.4). The input power is

$$P_{in} = A_t \int_0^\infty F(\lambda)(hc/\lambda)\, d\lambda \qquad (1.51)$$

where A_t is the total device area, $F(\lambda)$ is the number of photons per cm^2 per sec per unit band width incident on the device at wavelength λ and hc/λ is the energy carried by each photon.

There are various factors which limit the efficiency of solar cells and have been discussed in detail by several workers (see e.g. Wolf 1960, 1971 and Rouse 1977). Internal resistance of the solar cell is expected to play an important part in determining the cell conversion efficiency. In chapters 3, 4 and 7 we will present the results of our theoretical as well as experimental study of the series resistance and its effect on the response

of solar cells. We have neglected the effect of shunt resistance because it is not expected to be significant at high illumination intensities of our interest (Hovel 1975).

1.5 Solar cells for concentrated radiation :

In the past few years attempts to reduce the cost of solar cells have led to the design of optical concentrators to be used with solar cells, thus, making it possible to reduce the area of solar cells for collection of a given amount of solar flux. Earlier work on the use of concentrated sun light with solar cells for terrestrial applications was done by Ralph (1966) and Beckman (1966) using conical concentrators and parabolic concentration systems.

Concentrators for use with solar cells can be of fallowing types :

1. Nonstationary Concentrators:
   In these types of concentrators tracking of the sun is required. Lenses and mirrors come under this category. Fresnel lenses are widely used for concentration of sunlight. Concentration factors of more than 1000 have been achieved with the help of lenses. Spherical mirrors, parabolic mirrors, Heliostate paraboloids etc. are same examples of concentrating mirror systems.

2. Stationary concentrators or nontracking concentrators:

In these types of concentrators diurnal tracking of the sun is not required, however seasonal adjustments are necessary. Examples of such concentrators are Tabor circular cylinder and Winston compound parabolic concentrator (CPC). The maximum concentration that can be achieved using nontracking concentrators is 10 in the case of Winston's CPC.

Concentrated sunlight photovoltaic energy systems have several advantages:

1. Cost of the solar cell becomes less important relative to the cost of the system, and expensive, highly efficient cells can be used if cheap concentrators are available (Dean et al 1975).

2. It is possible to design such hybrid systems which yield both electricity as well as heat. Integration of photovaltaic and solar thermal energy conversion systems can achieve 12 % conversion efficiency when operated at 40 suns terrestrial illumination and 100°C junction temperature (Schuder et al, 1975)

The disadvantages are:-

1. Only direct sunlight can be concentrated, leading to some optical loss even on the best of days.

2. Tracking of the sun may be necessary which requires sophisticated mechanism adding to the total cost of the system. Moreover, tracking requires power and the over all efficiency of the system is reduced.

3. Another basic problem with concentration is the nonuniform intensity ditribution obtained at the surface of the solar cell. In a nontracking concentrator, solar cell may be only partially illuminated. Also, when tracking system is used e.g. with a lens, even a slight error in the adjustment will shift the solar cell away from the focus of the lens, thus making it nonuniformly illuminated.

4. Another major consideration is the heat generated as a result of the absorbed light not converted to electrical energy. As concentration ratios increase, the absorbed energy also increases, causing the cell temperature to rise. This increase in temperature results in a decrease in the cell conversion efficiency. Forced air or water cooling equipment could be used to off set this temperature rise, however, such equipment is costly, complicated, and would consume power, so there still would be a loss factor to be considered. No additional power would be required for free convective cooling, but in this

case , there would be a useful limit of concentration ratio beyond which there would be no gain in efficiency.

5. Series resistance of the cell becomes a serious problem at high intensities. Losses due to series resistance can be minimized by increasing the number of grids at the top surface of the cell at the cost of reducing the total area exposed to light.

Although several types of structures e.g. interdigited design, Vertical multijunction structure are being investigated for Silicon solar cells used with high intensity radiation, p-n homojunction structure is most widely used. In the subsequent chapters we will discuss in detail the effect of nonuniform illumination, high intensity effects, rise in temperature and internal series resistance on the response of Silicon homojunction solar cells used with concentrated light. We will also present results of an experimental study on some of these aspects.

CHAPTER- 2.

RESPONSE OF SOLAR CELLS TO NONUNIFORM ILLUMINATION

2.1 Introduction :

In general, a solar cell is nonuniformly illuminated by a concentrator. Use of lenses, for example, concentrates light at one spot of the cell. Various types of solar concentrators such as conical, parabolic and compound parabolic give different intensity distributions on the surface of the solar cell.

In cases, where a solar cell is used to measure the intensity of a laser beam or some other narrow beam, cell is only partially illuminated (Shiel and Bolmarcich 1963, Deb and Mukherjee 1965). Moreover, several experimental methods for determining physical parameters of a cell (Raynold and Meulenberg 1974, Heryer 1974) also require the use of laser. In all the above mentioned situations, cell is nonuniformly irradiated.

Rigorous theoretical calculations are available in literature on the response of a uniformly illuminated solar cell (Wolf 1960, 1963). There is, clearly a need for calculating the response of a solar cell when it is partially or nonuniformly illuminated. Physically, this represents a situation which should promote two dimensional

diffusion, and hence should, in principle, lead to a law of response that is somewhat different from that given for the case of uniform illumination. Nonuniform illumination in the conventional p-n junction solar cell corresponds to the same situation as encountered in the Vertical Multijunction cell giving rise to circulatory currents as discussed by Dhariwal et al (1975).

Some effort has already been made in this direction. Deb and Mukherjee (1966) have presented an analysis for a partially illuminated solar cell by assuming that all the light is absorbed in a thin layer at the surface of the solar cell. In doing so, they have neglected the contribution due to the base layer of the cell as well as the bulk of the diffused region which yields a major part of the photocurrent under illumination.

Seth and Dhariwal (1977) have considered the effect of absorption of light in the bulk of a partially illuminated solar cell in the case when the intensity distribution on the cell is uniform along one of the co-ordinate axis and nonuniformity is confined to only one axis on the surface of the solar cell.

Therefore, it is of interest to consider a general case of nonuniformity of illumination on the surface of the

solar cell and to derive an analytical expression for the response of the solar cell valid for any type of intensity distribution.

In this Chapter, a powerful mathematical technique is presented based on the partial fourier transform which has been used successfully in some problems in solid state theory (Tewary 1974). This technique is quite general and easily applicable to all kinds of nonuniformity or partial illumination, provided the surface recombination velocity at the surfaces normal to the junction is zero. In case, this condition is not satisfied, the technique can still be used with appropriate modifications, but then calculations become more complicated.

The mathematical technique has been described in Sec. 2.2 and a short discussion of the results is given in Sec. 2.3 . An interesting result is obtained on solving the ambipolar diffusion equation for nonuniform illumination, which shows that the nonuniformity of illumination does not effect the response of the solar cell in the case when the surface recombination velocity at the edges normal to the junction is zero. This result, however, would be modified in certain realistic situations as discussed in Sec. 2.3.

2.2 Solution of the Ambipolar Equation :

The general steady state ambipolar equation for the excess carrier concentration Δn on the p side of a p-n junction solar cell is given by (See eqn. 1.14 in Chap. 1)

$$D_n^* \nabla^2 (\Delta n_p) - \mu^* \vec{E} \cdot \nabla (\Delta n_p) - \frac{\Delta n_p}{\tau_n^*} = -g' \quad , \tag{2.1}$$

A similar equation can be written for Δp on n side.

We consider two limiting cases:

(i) $N_o \to o$ low injection case

(ii) $N_o \to \infty$ high injection case .

As discussed in Sec. 1.4.5 for both these limiting cases, the second term in Eqn. 2.1 is negligible and the coefficients D_n^* and τ_n^* become constants. However, their values are different in these two limiting cases.

Therefore, in these two limits ambipolar eqn. 2.1 has the same form and can be solved analytically. In this section solution of eqn. 2.1 is obtained in the two limiting cases for the case of nonuniform illumination.

The y-z plane is taken to be parallel to the junction and x direction is taken to be the direction of the

incident light, perpendicular to the junction (Fig. 2.1). In general, Δp, Δn and g' are functions of x, y, and z. The x dependence of the generation rate characterises the exponential absorption of light which is assumed to be monochromatic and the (y, z) dependence characterises nonuniformity of the illumination on the cell surface. In the present analysis it has been assumed that g' can be written in a separable form

$$g' = \alpha N_o f(y,z) e^{-\alpha(x+d_1)} \;;\; g_o = N_o \alpha \qquad (2.2)$$

where N_o is the number of photons falling per cm^2 per sec. on the cell surface. f(y, z) can be taken to be a gaussian, exponential or a step function according to the nature of the nonuniformity of illumination. d_1 is the width of the p region which is exposed to light. Eqn. 2.1 can now be written as

$$D_n^* \nabla^2 (\Delta n_p) - \frac{\Delta n_p}{\tau_n^*} = -\alpha N_o f(y, z) e^{-\alpha(x+d_1)} \;. \qquad (2.3)$$

A solution of the above equation for f (y,z) = 1 (uniform illumination) has been obtained in the low level limit by Wolf (1960) and in the high level limit by Dhariwal et al (1976). Eqn. 2.3 is solved under the following boundary conditions:

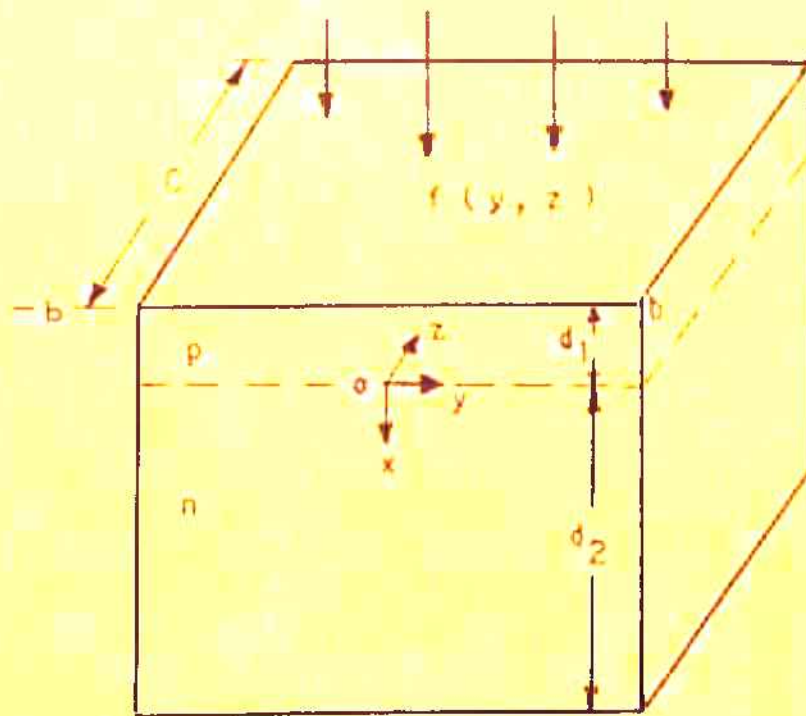

FIG. 2.1 A NONUNIFORMLY IRRADIATED p−n JUNCTION SOLAR CELL

$$\left(\frac{\partial \Delta n_p}{\partial y}\right)\Bigg|_{y\,=\,b \text{ and} -b} = 0, \qquad (2.4)$$

$$\left(\frac{\partial \Delta n_p}{\partial z}\right)\Bigg|_{z\,=\,0 \text{ and } c} = 0 \qquad (2.5)$$

and

$$\left(\frac{\partial \Delta n_p}{\partial x}\right)\Bigg|_{x\,=\,-d_1} = \frac{S_1}{D_n^*}\Delta n\Bigg|_{x\,=\,-d_1} \qquad (2.6)$$

where S_1 is the surface recombination velocity at the top surface. The thickness d_2 of the base region is assumed to be infinitely large.

In the short-circuit configuration, another boundary condition is imposed at the junction of the solar cell:

$$\Delta n\,(x,\,y,\,z)\Big|_{x\,=\,0} = 0 \quad . \qquad (2.7)$$

In view of the above described boundary conditions, we define the Partial Fourier Transform (PFT) of $\Delta n(x,y,z)$ and $f(y,z)$ over the yz plane as follows :

$$\Delta n\,(\bar{k},\,x) = \int \Delta n(\,x,\,y,\,z\,)\,e^{i(k_1 y\,+\,k_2 z)}\,dy\,dz \qquad (2.8)$$

and

$$f\,(\vec{k}) = \int f(\,y,\,z\,)\,e^{i(k_1 y\,+\,k_2 z)}\,dy.\,dz \qquad (2.9)$$

where k_1 and k_2 are the y and z components of the two-dimensional Fourier Reciprocal Vector $\vec{k}$ and the integral is over the whole y - z plane.

PFT as defined in eqns. 2.8 and 2.9, by nature of the exponential periodic function satisfies the boundary conditions given in eqns. 2.4 and 2.5 on the y and z axes respectively. The transformed boundary conditions given by eqns. 2.6 and 2.7 which $\Delta n(\vec{k}, x)$ must satisfy are the following :

$$\left. \frac{d[\Delta n(\vec{k}, x)]}{dx} \right|_{x=-d_1} = S_1 \cdot \Delta n(\vec{k}, x) \Big|_{x=-d_1} \qquad (2.10)$$

and

$$\Delta n(\vec{k}, x) \Big|_{x=0} = 0 \quad . \qquad (2.11)$$

Using eqns. 2.8 and 2.9, eqn. 2.3 can be written as :

$$-(k_1^2 + k_2^2) \int \Delta n(\vec{k}, x)\, e^{-i(k_1 y + k_2 z)}\, d\vec{k}$$

$$+ \int \frac{d^2[\Delta n(\vec{k}, x)]}{dx^2}\, e^{-i(k_1 y + k_2 z)}\, d\vec{k}$$

$$- \frac{1}{L_n^*} \int \Delta n(\vec{k}, x)\, e^{-i(k_1 y + k_2 z)}\, d\vec{k}$$

$$= - \frac{\alpha N_o}{D_n^*} \int f(\vec{k})\, e^{-i(k_1 y + k_2 z)}\, e^{-\alpha(x + d_1)}\, d\vec{k} \;, \qquad (2.12)$$

where $L_n^{*2} = D_n^* \tau_n^*$.

Substituting $k^2 = k_1^2 + k_2^2$, (2.13a)

and $\vec{k} . \vec{r} = k_1 y + k_2 z$ (2.13b)

(where $\vec{r} = (y, z)$, $d\vec{r} = dydz$)

in eqn. 2.12 and multiplying by $e^{i \vec{k}' . \vec{r}}$ on both the sides and integrating over the whole surface with respect to $\vec{r}$, the transformed equation is given by

$$\frac{d^2[\Delta n(\vec{k}, x)]}{dx^2} - (k^2 + \frac{1}{L_n^{*2}}) \Delta n (\vec{k}, x)$$

$$= \frac{-\alpha N_o}{D_n^*} f (\vec{k}) e^{-\alpha(x + d_1)} . \quad (2.14)$$

Thus, we see that the diffusion equation (eqn. 2.3) in the nonuniform case can be easily solved by reducing it to a one dimensional equation by taking its PFT. We shall give below a formal solution of the equation and use it to calculate the short circuit current.

We recall that $f (y, z)$ is a measure of nonuniformity of illumination and we choose a system of units such that $f (y, z)$ is normalised to unity as follows

$$\iint f(y,z) \, dydz = 1 \quad . \quad (2.15)$$

Thus, the total amount of light falling on the front surface of the cell is $N_o\alpha$. The solution,

$$\Delta n(\vec{k},x) = A_1\, e^{-\left(k^2 + \frac{1}{L_n^{*2}}\right)x} + A_2\, e^{\left(k^2 + \frac{1}{L_n^{*2}}\right)x}$$

$$+ \frac{\alpha\, N_o\, f(\vec{k})\, \tau_n^{*}\, e^{-\alpha(x+d_1)}}{\left[1 - L_n^{*2}(\alpha^2 - k^2)\right]} \qquad (2.16)$$

where A_1 and A_2 are constants determined by using boundary conditions given in eqns. 2.10 and 2.11.

By taking inverse PFT

$$\Delta n\,(x,y,z) = \int \Delta n\,(\vec{k}, x)\, e^{-i\,\vec{k}.\,\vec{r}}\, d\vec{k} \qquad (2.17)$$

Short circuit current :

Under short circuit conditions, current I_{sc} crossing the junction is propotional to

$$I_{sc} \propto \int \left(\frac{\partial[\Delta n\,(x,\,y,\,z)]}{\partial x} \right)\Bigg|_{x=o} .d\vec{r} \quad . \qquad (2.18)$$

A similar term on R.H.S. arises from the contribution to I_{sc} from the base region. Using eqn. 2.17, R.H.S. of eqn. 2.18 is equal to

$$\iint \frac{d[\Delta n(\vec{k}, x)]}{dx} e^{-i\vec{k}.\vec{r}} d\vec{k}\, d\vec{r} \quad . \qquad (2.19)$$

$$= \int \frac{d[\Delta n(\vec{k}, x)]}{dx} d\vec{k} \int e^{-i\vec{k}.\vec{r}} d\vec{r} \quad , \qquad (2.20)$$

$$= \int \frac{d[\Delta n(\vec{k}, x)]}{dx} \delta(\vec{k})\, d\vec{k} \qquad (2.21)$$

$$= \lim_{k \to o} \frac{d[\Delta n(\vec{k}, x)]}{dx} \quad . \qquad (2.22)$$

Thus, we see that the short circuit current depends only upon the value of $d[\Delta n(\vec{k},x)]/dx$ at $\vec{k} = 0$. From eqn. 2.16 we see that it depends upon the $k = 0$ limit of $f(\vec{k})$ and does not depend upon the detailed dependence of $f(\vec{k})$ on $\vec{k}$.

This implies that the short circuit current is independent of the nature of variation of $f(y,z)$ on yz plane and therefore is independent of the nature of nonuniformity of illumination.

To see the physical meaning of $\vec{k} = 0$ limit of $f(\vec{k})$ we consider the integral in eqn. 2.15. Writing $f(y,z)$ in terms of its PFT we get from eqn. 2.15

$$\iint f(y,z)\, dydz = \iint f(\vec{k})\, e^{-i\vec{k}.\vec{r}} d\vec{k}\, d\vec{r}$$

$$= \int f(\vec{k})\, d\vec{k} \int e^{-i\vec{k}.\vec{r}} d\vec{r}$$

$$= \int f(\vec{k})\, d\vec{k}\ \delta(\vec{k})$$

$$= \lim_{\vec{k} \to o} f(0) = 1 \quad .$$

Thus, we see that for $k' = o$, $f(o)$ gives the area of $f(y, z)$ curve on the yz plane which has been normalised to unity. Therefore we see from eqn. 2.22 that I_{sc} depends upon the total amount of light falling on the front surface and is independent of the detailed nature of nonuniformity.

In the above analysis, I_{sc} is found to be dependent only upon g_0 given. Since V_{oc} is related to I_{sc}, V_{oc} could also be considered to be independent of the nonuniformity of illumination.

2.3 Discussion :

The preceding analysis shows that the short circuit current in a nonuniformily irradiated cell does not depend on the nonuniformity of illumination. The results obtained in Sec. 2.2 will be modified when the surface recombination velocity at the edges of the cell normal to the junction is not zero. The effect of surface recombination at the edges has been considered as a perturbation by Seth and Dhariwal (1977). However, their treatment is only valied for low values of the surface recombination velocity at the edges. In the case, when it is zero, our results coincide with those obtained by Seth and Dhariwal (1977)

for a partially illuminated cell for low levels of illumination. Another point which should be noted is that the effects due to high intensity and nonuniform illumination are not linearly additive in general, become, among other reasons, the nonuniformity and high intensity of illumination will give rise to currents and fields parallel to the junction which will perturb the flow of carriers across the junction. The present analysis does not include these effects. In addition, due to the finite lateral resistance of the diffused region, the lateral flow of current is limited by this resistance, Lucovsky (1960). In a real solar cell, contact grids are present on the top surface of the solar cell for efficient collection of carriers. Nonuniform illumination will also influence the carrier collection from grids depending upon the intensity distribution on the surface of the solar cell.

CHAPTER-3.

A THEORETICAL STUDY OF THE RESPONSE OF SOLAR CELLS TO DIFFERENT ILLUMINATION LEVELS AT CONSTANT TEMPERATURE:

3.1 Introduction :

In recent years there has been a lot of effort in studying the response of solar cells at high levels of illumination (Arifov et.al.1974, James and Moon 1975, Dean et al 1975, Vasil'ev et.al.1975, Dhariwal et.al.1976, Dalal and Moore 1977, Napoli et al 1977, Fossum and Lindholm 1977, Crook and Yeargan 1977, Burgess and Fossum 1977, ~~Crook and Yeargan 1977~~, Spaderna and Navon 1978).

The interest arises :

(i) From an application point of view because solar cells are increasingly used along with concentrators which effectively reduces the cost of solar cells and

(ii) from an academic point of view because of various interesting physical processes which contribute to the response of solar cells.

As the intensity of illumination increases, the conventional Shockley theory predicts a logarithmic increase in the open circuit voltage and a linear increase in the short circuit current thus, effectively increasing

the efficiency of the p-n junction solar cells (Rappaport 1959, Wolf 1960, Sterzer 1975). However, it is observed that open circuit voltage saturates at a certain value in the limit of high intensity instead of logarithmically increasing. The saturation of open-circuit voltage has been studied by several workers (Girton 1963, Blinov et.al. 1966, Holonyak et. al. 1967, Gray 1969, Kao and Schroder 1970, Parrot 1974, Dhariwal et. al. 1976). Gray (1969) attributed it to gradients of the quasi Fermi potentials arising in the base region to satisfy the zero current condition. Parrott (1974) related V_{oc} to the product PN of the carrier densities at the junction and described a saturation of V_{oc} at high values of PN. The variation in photovoltage with light intensity cannot be calculated directly from his results. Fossum and Lindholm (1977) have derived the dependence of solar cell open circuit voltage on the illumination level, valid for high injection conditions. Their results are related to an easily measured device parameter, the uncompensated photocurrent. Girton (1963), Blinov et. al. (1966) and Holonyak et. al. (1967) have reported experimental results on the saturation of photovoltage in solar cells illuminated with intense laser beams. An useful theoretical treatment for this effect has been given by Dhariwal, Kothari and Jain (1976) (Hence forth referred as DKJ) who have developed expressions for V_{oc} and I_{sc}

as functions of uniform generation rate in the device. They have derived a boundary condition valid at all levels of illumination. This boundary condition is a modified version of the conventional Shockley boundary condition, which predicts the saturation of the open-circuit voltage in the limit of high intensity of light and reduces to the Shockley condition (see eqn. 1.37) in the limit of low levels of illumination. However, this treatment is not mathematically rigorous because of the following reasons:

(i) They have assumed uniform generation rate of carriers in the solar cell and have therefore neglected the effect of exponential absorption of light in the cell.

(ii) They have assumed the limiting form of the Ambipolar equation which may not be valid throughout the bulk of the solar cell.

(iii) They have also assumed a cell of infinite thickness which is not true in the case of a real solar cell.

The main problem in studying the response of a solar cell at high levels of illumination is the solution of the ambipolar equation which is highly nonlinear. Only in the limit of low intensities (conventional treatment) and in the limit of infinitely high intensities (DKJ treatment) the equation becomes linear and its prompt simple analytical solution is possible. The limit of infinitely

high intensities, which has been assumed by DKJ is not of course attainable in practice and it is important, therefore, that a solution of the ambipolar equation is obtained such that it is valid at all levels of illumination.

In this chapter we present a numerical solution of the ambipolar equation which does not make the three assumptions described above. It uses an iterative method which is quite simple and convenient. With the help of this solution we will discuss in detail the various aspects of the response of solar cells. We have assumed the boundary conditions derived by DKJ and with the help of the numerical techniques calculated the short circuit current, open circuit voltage, maximum power output, fill factor, I-V characteristics and the carrier concentration profile for a realistic p^+n solar cell of one ohm restivity for four different values of the absorption coefficient. We have also included the contribution of the series resistance which has the effect of saturating the short circuit current and also the effect of Dember potential. Our results are qualitatively similar to those of DKJ in the sense that they also predict a saturation of the open circuit voltage and the short circuit current. However, our treatment being more rigorous is applicable to more realistic solar cells.

In Sec. 3.2 we discuss the solution of the ambipolar equation in the different intensity regions and solve the ambipolar equation analytically in the low and high intensity limits. Sec. 3.3 describes the numerical solution of the ambipolar equation for all intensity levels. Section 3.4 deals with the electrical characteristics of solar cells. Here, we determine the solar cell current voltage relationship, short-circuit current, open-circuit voltage, fill factor and efficiency for the case of monochromatic incident radiation. Calculations of the electrical characteristics for the case of composite light are described in Sec. 3.5. Sec. 3.6 is devoted to the effect of the internal series resistance on cell response. Contribution of the Dember voltage is discussed in Sec. 3.7. Finally, in Sec. 3.8 we present the results of numerical solution of the ambipolar equation for a one ohm cm p^+n solar cell (cell parameters given in Table 3.1) to determine excess carrier density Δn, ambipolar coefficients D^*, τ^* and L^*, short-circuit current, open-circuit voltage, Dember voltage, maximum power output, fill factor, efficiency and I-V characteristics as a function of intensity. These results are compared with the results obtained by using DKJ formulation. Calculated results of the cell response for AMO spectrum are also presented.

Effects of series resistance on the short-circuit current and I-V characteristics are also discussed.

3.2 Ambipolar equation and its analytical solution:

The three dimensional ambipolar transport equation obeyed by the excess carriers in a homogeneous p-type semiconductor as given by eqn. 1.14 in Chap. 1 reduces to a one dimensional equation if we consider the case of uniform illumination on the surface of the solar cell. The resulting equation for the steady state is given by

$$D^{*} \frac{d^2(\Delta n)}{dx^2} - \mu^{*} E_{int} \frac{d(\Delta n)}{dx} + g' - \frac{\Delta n}{\tau^{*}} = 0 \qquad (3.1)$$

where Δn denotes the concentration of excess electrons. The excess carrier concentration of holes Δp, is of course, equal to Δn in accord with the charge balance assumption used in deriving eqn. 3.1 . A similar equation can be written for the N side. All the coefficients appearing in eqn. 3.1 have been discussed in Chap.1 in detail. We give below the expressions for these coefficients which we have used for our calculations (see Sec. 1.4.3 also)

$$D^{*} = \frac{(n_o + p_o + 2\Delta n)\, D_n D_p}{(n_o + \Delta n)\, D_n + (p_o + \Delta n)\, D_p} , \qquad (3.2)$$

$$\mu^{*} = \frac{(n_o - p_o)\,\mu_n \mu_p}{(n_o + \Delta n)\,\mu_n + (p_o + \Delta n)\,\mu_p} \qquad (3.3)$$

τ^{*}, the excess carrier lifetime given by the Hall-Shockley-Read theory is (See Many and Bray 1958 also)

$$\tau^{*} = \tau_{po} \frac{n_o + n_1 + \Delta n}{n_o + p_o + \Delta n} + \tau_{no} \frac{p_o + p_1 + \Delta n}{n_o + p_o + \Delta n} \qquad (3.4)$$

E_{int} is the internal Dember field arising because of the different mobilities of electrons and holes (See eqn. 1.25 in Chap. 1)

$$E_{int} = -\frac{kT}{q} \frac{b - 1}{nb + p} \frac{d(\Delta n)}{dx} \qquad (3.5)$$

where b is the ratio of electron and hole mobilities . Other symbols have their usual meanings. We see from the above expressions that coefficients in eqn. 3.1 are functions of Δn in general.

We discuss here the solution of eqn. 3.1 at different values of the generation rate g'. For the purpose of analysis we divide the whole intensity region into the following three regions and discuss the solution of eqn. 3.1 in each region:

Case 1 : Low level illumination ($\Delta p, \Delta n \ll n_o, p_o$) :

For a strongly n type semiconductor under low level illumination (see Sec. 1.4.5 also)

$$D^* = D_p$$
$$\tau^* = \tau_{po} \quad (\text{for } \Delta n \ll n_o) \qquad (3.6)$$
$$\mu^* = \mu_p \; .$$

Likewise, for a strongly extrinsic p-type crystal it is readily seen from eqns. 3.2, 3.3 and 3.4 that

$$D^* = D_n$$
$$\tau^* = \tau_{no} \quad (\text{for } \Delta p \ll p_o) \qquad (3.7)$$
$$\mu^* = \mu_n \; .$$

Electric field given by eqn. 3.5 is in general, quite small at such low intensities, and is usually neglected (Mckelvey 1966). As seen above, all the coefficients become constants at low intensities and eqn. 3.1 is readily solvable analytically.

Case 2 : High level illumination ($\Delta n, \Delta p \gg n_o, p_o$) : (see Sec. 1.4.5 also): When the density of excess carriers becomes much larger than the larger of the two quantities n_o, p_o the coefficients in eqn. 3.1 again become constants (Dhariwal et al 1976, Sabnis 1978) as given below:

$$D^* = \frac{2D_n D_p}{D_n + D_p} \quad (3.8a)$$

$$\tau^* = \tau_{no} + \tau_{po} \quad (3.8b)$$

$$\mu^* = 0 \quad (3.8c)$$

The second term in eqn. 3.1 in the high intensity limit becomes small enough to be negligible (DKJ) and we solve the eqn. 3.1 analytically in the usual approximation taking constants values of D^* and τ^* as given above and neglecting the second term in eqn. 3.1.

Case 3 : Moderate intensity illumination: In between the above two described two extreme limits we have the moderate intensity case i.e. when the excess carrier density is comparable to the larger of n_o, p_o. As is clear from expressions 3.2, 3.3 and 3.4 the ambipolar coefficients are not constants in this case but depend on the concentration of excess carriers. Therefore, for the intermediate values of Δn eqn. 3.1 has to be solved by numerical techniques.

Strictly speaking, the second term in the eqn. 3.1 is negligible only in the two limits of high and low

intensities. There is no apriori way of determining whether this term is also negligible at moderate intensities. However, following the usual practice, we obtain the solution of eqn. 3.1 neglecting the second term but obtain a separate estimate of $\bar{E}$ through the Dember effect formulation (eqn. 3.5) and add that to the expression for voltage obtained from the solution of the eqn. 3.1.

We have numerically solved the ambipolar transport equation in both the p and n regions of a p-n junction solar cell at all levels of illumination under following assumptions:

1. Generation and recombination of carriers in the space charge region is negligible.
2. Thickness of the space charge region is negligible in comparison with the diffusion length of carriers.
3. The semiconductor is nondegenerate.
4. The quasi Fermi levels for electrons and holes are constant over the space charge regions.
5. The condition of quasi neutrality holds every where.
6. The impurities are completely ionized at room temperature.

7. Reflection of light from the top surface of the cell is also not taken into account in the present analysis.

We have considered a simple p-n junction photovolatic cell made by diffusing a p type impurity into an initially n type semiconductor , so that a thin p-type surface layer is formed. The cell is illuminated by monochromatic light incident upon the p-type front surface. The physical situation may then be represented by the one dimensional model illustrated in Fig. 1.2, where uniform n and p regions are shown separated by an abrupt p-n junction at x = 0. Thicknesses of the diffused p layer and n type base are d_1 and d_2 respectively. Light is incident in the x direction.

The excess carrier generation rate $g'(x)$(Chap.1, eqn. 1.31) is given by

$$g'(x) = \alpha \, N_o \, e^{-\alpha(x+d_1)} \; . \qquad (3.9)$$

Under these circumstances, the ambipolar equation for the excess carriers on p side can be written as

$$D_n^* \; \frac{d^2(\Delta n_p)}{dx^2} - \frac{\Delta n_p}{\tau_n^*} = - \alpha \, N_o \, e^{-\alpha(x+d_1)} \; , \qquad (3.10)$$

A similar equation for the excess carriers on the n side is given by

$$D_p^* \frac{d^2(\Delta p_n)}{dx^2} - \frac{\Delta p_n}{\tau_p^*} = -\alpha N_o e^{-\alpha(x+d_1)} \qquad (3.11)$$

where Δn_p and Δp_n denote the excess electron concentration on p side and excess hole concentration on n side respectively. The general solutions of eqns. 3.10 and 3.11 for the case when D^* and τ^* are constants (e.g. in the high and low level limits)are given by:

$$\Delta n_p = A_1 e^{-x/L_n^*} + A_2 e^{x/L_n^*} + \frac{\alpha N_o \tau_n^* e^{-\alpha(x+d_1)}}{1 - \alpha^2 L_n^{*2}} \qquad (3.12)$$

and

$$\Delta p_n = B_1 e^{-x/L_p^*} + B_2 e^{x/L_p^*} + \frac{\alpha N_o \tau_p^*}{1-\alpha^2 L_p^{*2}} e^{-\alpha(x+d_1)} \qquad (3.13)$$

where $L_n^* = \sqrt{D_n^* \tau_n^*}$ (3.14a)

and $L_p^* = \sqrt{D_p^* \tau_p^*}$. (3.14b)

The coefficients A_1, A_2, B_1 and B_2 are determined from the following boundary conditions :

(i) At the front surface of the p^+n cell which is exposed to light :

$$D_n^* \left.\frac{d(\Delta n)}{dx}\right|_{x=-d_1} = S_1 \Delta n \Big|_{x=-d_1} \qquad (3.15)$$

(ii) The electron and hole concentrations at the junction are given by the following relationship (see eqns. 1.1 and 1.2 also)

$$\left(\frac{n_p}{n_n} \right)_{x=o} = \left(\frac{p_n}{p_p} \right)_{x=o} = \exp \left[-q(V_D - V_j)/kT \right] . \quad (3.16)$$

Using eqn. 3.16 and the charge neutrality condition described in Chap. 1 (eqn. 1.8) given by

$$\Delta n = n_p - n_{po} = p_p - p_{po} = \Delta p \quad (3.17)$$

DKJ have derived the following boundary conditions valid at all levels of injection for the excess carrier densities Δn and Δp at the junction ($x = o$):

$$(\Delta n_p)_o = \frac{\left\{ n_{po} + p_{no} \exp \left[-q(V_D - V_j)/kT \right] \right\} \left[\exp(qV_j/kT) - 1 \right]}{1 - \exp \left[-2q(V_D - V_j)/kT \right]} . \quad (3.18)$$

The corresponding boundary condition for Δp_n at the junction consistent with eqn. 3.13 is given by :

$$(\Delta p_n)_o = \frac{\left\{ p_{no} + n_{po} \left[\exp \left[-q(V_D - V_j)/kT \right] \right] \right\} \left[\exp(qV_j/kT) - 1 \right]}{1 - \exp \left[-2q(V_D - V_j)/kT \right]} . \quad (3.19)$$

As seen from eqns. 3.18 and 3.19, for the case of low level injection these two eqns. reduce to the conventional Shockley boundary condition used for p-n junctions.

(iii) One more boundary condition is needed for the determination of Δp_n which is provided by the eqn. :

$$D_p^* \left. \frac{d \Delta p_n}{dx} \right|_{x=d_2} = -s_2 \left(\Delta p_n \right)_{x=d_2} \tag{3.20}$$

where s_2 is the surface recombination velocity which is usually taken to be infinite for an ohmic contact covering the base of the cell.

The values of A_1, A_2, B_1 and B_2 as determined from the above described boundary conditions are given by the following expressions :

$$A_2 = \frac{(\Delta n_p)_o e^{d_1/L_n^*}\left(s_1 + \frac{D_n}{L_n^*}\right) - A\left[\left(\frac{D_n^*}{L_n^*} + s_1\right). e^{d_1\left(\frac{1}{L^*_n} - \alpha\right)} - D_n^*\alpha - s_1\right]}{e^{d_1/L_n^*}\left(\frac{D_n^*}{L_n^*} + s_1\right) + e^{-d_1/L_n^*}\left(\frac{D_n^*}{L_n^*} - s_1\right)}, \tag{3.21}$$

$$A_1 = (\Delta n_p)_o - A_2 - A\, e^{-\alpha d_1} \tag{3.22}$$

$$\text{where } A = \frac{\alpha\, N_o \tau_n^*}{(1 - \alpha^2 L_n^{*2})} . \tag{3.23}$$

and

$$B_2 = \frac{-(\Delta p_n)_o e^{-d_2/L_p^*}\left(s_2 - \frac{D_p^*}{L_p^*}\right) - A'\left[e^{-\alpha(d_2+d_1)}(s_2 - D_p^*\alpha) - e^{-\left(\frac{d_2}{L_p^*} + \alpha d_1\right)}\left(s_2 - \frac{D_p^*}{L_p^*}\right)\right]}{\left[e^{d_2/L_p^*}\left(s_2 + \frac{D_p^*}{L_p^*}\right) - \left(s_2 - \frac{D_p^*}{L_p^*}\right)e^{-d_2/L_p^*}\right]} \tag{3.24}$$

and $B_1 = (\Delta p_n)_o - B_2 - A' e^{-\alpha d_1}$. (3.25)

$$\text{where} \quad A' = \frac{\alpha N_o \tau_p^*}{(1 - \alpha^2 L_p^{*2})} \tag{3.26}$$

For $s_2 = \infty$, in the case of an ohmic back contact, B_2 reduces to a constant value which can be calculated from the above expressions. If, in addition, d_2 is infinite then $B_2 = 0$.

Now, using the above expressions excess carrier density in both the regions can be calculated at different points in the x direction which is taken to be perpendicular to the junction.

In our calculations we shall need the average value of the excess carrier density in p and n regions. The average value of excess carriers density on p side is obtained by integrating eqn. 3.12 with respect to x over the whole p region and then dividing by its thickness d_1:

$$(\Delta n)_{average} = \frac{1}{d_1}\left\{- L_n^* A_1\left(e^{-H_2/L_n^*} - e^{-H_1/L_n^*}\right) + A_2 L_n^*\left(e^{H_2/L_n^*} - e^{H_1/L_n^*}\right) - \frac{1}{\alpha} A e^{-\alpha d_1}\left(e^{-\alpha H_2} - e^{-\alpha H_1}\right)\right\} \tag{3.27}$$

where H_1 and H_2 are the limits of integration, in this case being $-d_1$ and 0 respectively. Similarly, the average excess carrier concentration $(\Delta p)_{average}$ on the n side is determined by integrating eqn. 3.13 with respect to x as x varies from 0 to d_2 and dividing it by the thickness d_2 of the n region :

$$(\Delta p)_{average} = \frac{1}{d_2} \left[-L_p^* B_1 \left(e^{-H_2/L_p} - e^{-H_1/L_p} \right) + B_2 L_p \left(e^{H_2/L_p} - e^{H_1/L_p} \right) - \frac{A' e^{-\alpha d_1}}{\alpha} \left(e^{-\alpha H_2} - e^{-\alpha H_1} \right) \right\} \quad (3.28)$$

where $H_1 = 0$ and $H_2 = d_2$.

3.3 Numerical solution of the ambipolar equation:

The conventional numerical techniques for a solution of eqn. 3.1 are rather complicated because it is a boundary value problem. A numerical solution can be obtained by using the standard Runge-Kutta or other similar methods taking an adequate number of intervals. However, the difficulty in such methods arises because one has to guess about the unknown function at one boundary such that it satisfies the prescribed condition at the other boundary. This of course is a general difficulty in the solution of the boundary value problems

using such methods. Numerical solution of the basic transport and continuity equations have been attempted by several authors over the past few years. Using the Newton-Raphson method, Graham and Hauser (1972) have solved the one dimensional time dependent nonlinear partial differential equations: (Poisson's equation, current density equation, and continuity equations) as applied to the silicon $n^{+}- n - p^{+}$ diode. The above program was modified by Dunbar and Hauser (1976) to take into account the exponential generation term for the case of solar cells. It is, of course, possible to use more sophisticated and powerful techniques like finite element method to solve such boundary value problems which are quite common in fields like stress analysis, fracture analysis etc. such a method using computer simulation has been used by Fossum (1976). He has developed a numerical analysis computer code to predict and analyse the performance of solar cells at different illumination levels. This code provides exact one dimensional numerical solutions of carrier transport in the solar cell . A transient simultaneous solution of Poisson's equation and the hole and the electron continuity equations- approximated using finite differences with variable mesh point spacings- is achieved using the impurity profile, material parameters, and the bias conditions as input.

The numerical techniques such as the one used by Fossum require substantial computational effort and are useful only when a fast computer is available. Although, the numerical results are very accurate but, quite often, the required comptational effort may not be worthwhile because of several uncertainties and physical approximations which are inherent in the equation itself. Some of these approximations arise, for example, from the facts that at any level of illumination, Diffusion coefficient, life time etc. will depend upon the doping levels and other material properties (Fossum 1976) which can not be guarranteed to be uniform through out the cell. Similarly, the absorption coefficient α is unlikely to be constant with respect to x in a realistic cell. Moreover, details of the physical processes going on in the device are not apparent from the computational process as used by Fossum. Further, qite often for the purpose of designing , analysis and testing systems for solar cells and their arrays, it is useful to have a simple computational technique yielding quick numerically approximate results. For the purpose, it is particularly convenient to have analytical/semianalytical expressions which may serve as a reasonably accurate representation for the response of a solar cell at different levels of illumination.

With the above perspective, we propose here a semianalytical numerical technique for solving the ambipolar eqns. 3.10 and 3.11 which is numerically quite accurate and yields analytical expression for a representation of the carrier profile in a solar cell at all levels of illumination. The method is similar to iteration perturbation methods used in quantum mechanics as well as several problems in material science and is simple enough to be handled on a small computer like IBM 1130 which we have used for our calculations.

This method exploits the fact that the parameters given in eqns. 3.2 and 3.4 have a slow functional dependence upon x through Δn and become constant in the two limiting cases of high and low Δn. The proposed method is described below.

We start with a value of light intensity where the coefficients in eqn. 3.1 can be taken to be reasonably constant (as for example the low level limits given in eqns. 3.6 and 3.7). When the light intensity increases, the functional dependence of these quantities on the excess carrier density will come through the unknown variables Δn, Δp. A measure of this functional dependence is provided by the derivatives as follows:

$$\frac{dD^*}{dx} = \frac{(P_1 - P_2)}{(P_3 + P_4 \Delta n)^2} \frac{d(\Delta n)}{dx} , \qquad (3.29)$$

$$\frac{d\tau^*}{dx} = \frac{(Q_1 - Q_2)}{(Q_3 + \Delta n)^2} \frac{d(\Delta n)}{dx} \qquad (3.30)$$

where P_1, P_2, P_3, P_4, Q_1, Q_2 and Q_3 are constants.

Therefore, in the case when Δn is very large ($\Delta n \rightarrow \infty$) and/or ($P-P_2$) and ($Q_1 - Q_2$) are small, dD^*/dx and $d\tau^*/dx$ become very small. This, we see that even if $d(\Delta n)/dx$ is quite large, the above derivatives dD^*/dx and $d\tau^*/dx$ are relatively small. Variation of D^* and τ^* with x in the base region is shown in Fig. 3.1 for a one ohm cm p^+ n cell (cell parameters given in Table 3.1). For these calculations values of Δn used at each point correspond to the open-circuit case. The calculated variation of D^* and τ^* with x in the diffused region is found to be rather small (less than 2 %). As a numerical approximation, therefore, it may be adequate to take an estimate of D^* and τ^* in terms of the average value of Δn in the region. The average value of Δn can itself be approximate because the resulting the error in D^*, τ^* would be small. Having obtained the first estimate of Δn we calculate D^* and τ^* by using the calculated values of Δn arising from the first estimate as:

Table-[illegible].1

CELL PARAMETERS AT T = 300°K.

Parameter		Value
Type		: $p^{+}n$
Base resistivity		: 1 ohm-cm
N_A		: 5.0×10^{17} cm^{-3}
N_D		: 5.0×10^{15} cm^{-3}
d_1		: 0.5×10^{-4} cm
d_2		: 250×10^{-4} cm
s_1		: 10^{5} cm/sec.
s_2		: 10^{15} cm/sec.
D_n	in p region*	: 9 cm^2/sec.
D_p	in p region*	: 6 cm^2/sec.
τ_{no}	in p region*	: 1.4×10^{-6} sec.
τ_{po}	in p region*	: 1.0×10^{-6} sec.
D_n	in n region*	: 28 cm^2/sec.
D_p	in n region*	: 8 cm^2/sec.
τ_{no}	in n region*	: 2.4×10^{-6} sec.
τ_{po}	in n region*	: 3.4×10^{-6} sec.
V_D		: 0.8 volts.

*Taken from the 'Silicon Semiconductor data' Wolf (1969).

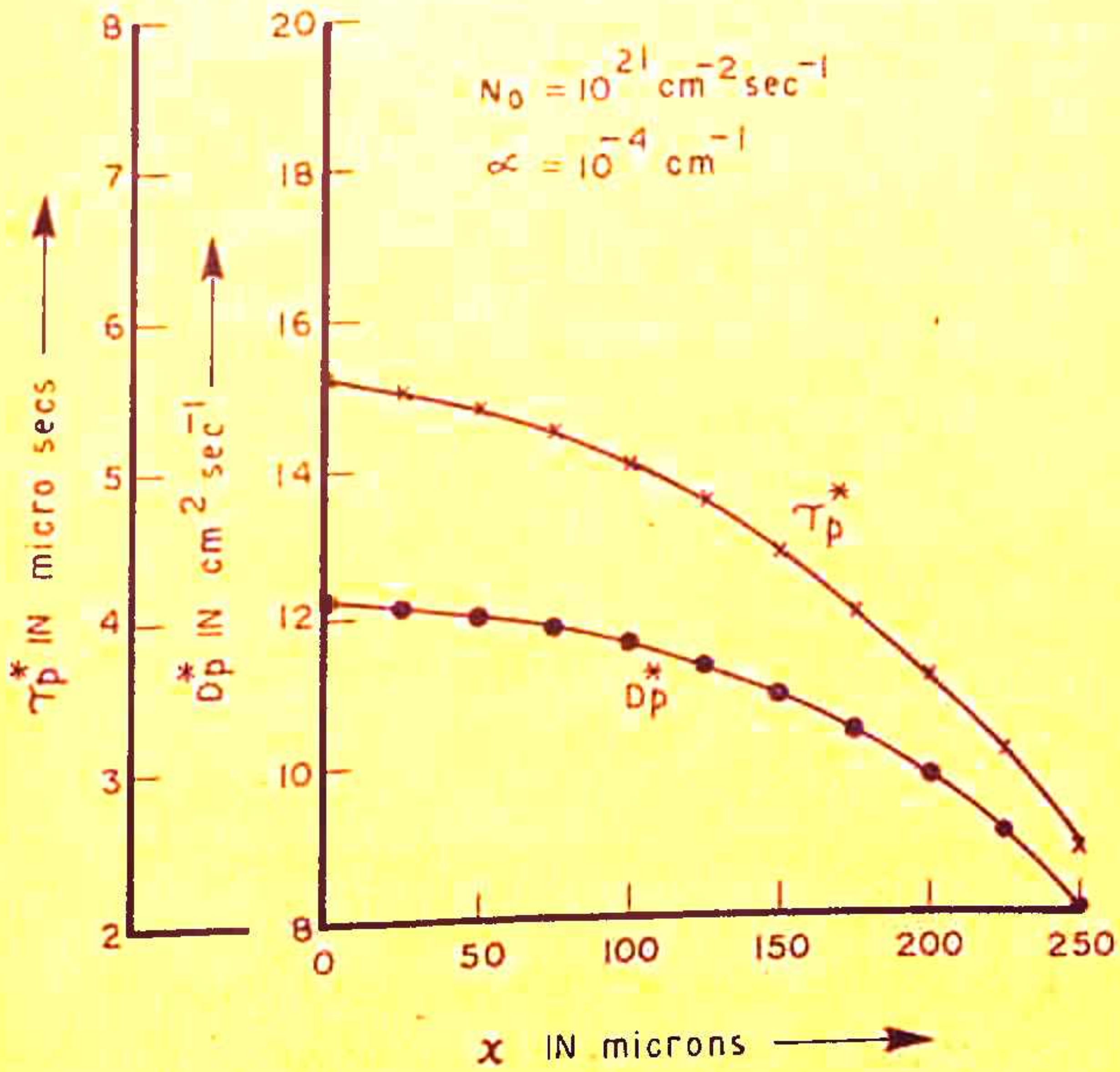

FIG.3.1 D_p^*, τ_p^* Vs x IN BASE REGION.

$$D^* = \frac{(n_o + p_o + 2\,\Delta n_{estimate})\, D_n D_p}{(n_o + \Delta n_{estimate}) D_n + (p_o + \Delta n_{estimate}) D_p} , \quad (3.31)$$

$$\tau^* = \frac{\tau_{no}(n_o + n_1 + \Delta n_{estimate}) + \tau_{po}(p_o + p_1 + \Delta n_{estimate})}{(n_o + p_o + \Delta n_{estimate})} . \quad (3.32)$$

This provides the second iteration and the iteration can be continued until the values of D^*, τ^* and the final values of Δn converges. The number of iterations required for convergence would be a measure of the efficiency and accuracy of the technique. This technique obviously cannot be applied if D^* and τ^* are sensitive to Δn and its derivatives because then the iteration would not lead to a convergent value. We find in actual practice that in most cases even the second iteration leads to a convergent value within 1 % which lends crediability to the present method of calculation. Table 3.2 gives the values of $\Delta n_{estimate}$ for five iterations calculated for $\alpha = 10^4$ cm^{-1} and $N_o = 10^{21}$ cm^{-2} sec^{-1}. As shown, the difference in the first and second iteration values is very small (less than 1 %).

As the illumination level is increased, the value of $\Delta n_{estimate}$ used for the previous illumination level is multiplied by the factor by which it is increased and is used for the first iteration.

Table-3.2

AVERAGE VALUES OF THE EXCESS CARRIER CONCENTRATION :

$N_o = 10^{21}\ cm^{-2}\ sec^{-1}$

$\alpha = 10^{4}\ cm^{-1}$

Iteration	P layer $\Delta n_{estimate}$ (cm^{-3})	N layer $\Delta p_{estimate}$ (cm^{-3})
1.	56.18×10^{13}	15.23×10^{14}
2.	56.20×10^{13}	15.11×10^{14}
3.	56.20×10^{13}	15.11×10^{14}
4.	56.20×10^{13}	15.11×10^{14}
5.	56.20×10^{13}	15.11×10^{14}

Therefore, $(\Delta n)_n = (\Delta n)_{n-1} \dfrac{N_n}{N_{n-1}}$ (3.33)

where the factor N_n/N_{n-1} gives the fractional increase in the number of photons falling per cm^2 per sec. on the cell surface.

The advantage of the present technique is its simplicity and arises from the fact that it does not require a lot of expensive computer time as compared to more sophisticated techniques and yield results which can be made as accurate as one wishes by increasing the number of iterations as mentioned before. Two or three iterations are enough to ensure approximately 1 % accuracy. In the cases where the ambipolar equation has to be solved repeatedly for different values of the light intensity and the material parameters of the cell such as where the performance analysis of solar cells is required for design purposes for different concentrations, this technique would be found more convenient, useful and economical.

3.4 Electrical Characteristics of solar cells:

3.4.1 Current voltage relationship :

The junction current I is evaluated (see eqn. 1.38 in chap. 1) for the case of constant D^* and τ^* as follows:

$$I = q\,(J_p(0) - J_n(0))$$

$$= q\left(D_n^* \frac{d(\Delta n)}{dx} - D_p^* \frac{d(\Delta p)}{dx} \right)\Bigg|_{x=0} \qquad (3.34)$$

where $d(\Delta n)/dx$ and $d(\Delta p)/dx$ are determined by differentiating eqns. 3.12 and 3.13 respectively. The result may be expressed in the form:

$$I = \frac{\left[I_o + I_o' \exp\left(-q(V_D - V_j)/kT\right) \right] \left[\exp\left(\frac{qV_j}{kT}\right) - 1 \right]}{1 - \exp\left[-2q(V_D - V_j)/kT \right]} - I_g$$

(3.35)

where

$$I_o = \frac{\left[\frac{qD_n^* n_{po}}{L_n^*} \right] \left[e^{d_1/L_n^*}\left(s_1 + \frac{D_n^*}{L_n^*}\right) - e^{-d_1/L_n^*}\left(\frac{D_n^*}{L_n^*} - s_1\right) \right]}{\left[e^{d_1/L_n^*}\left(\frac{D_n^*}{L_n^*} + s_1\right) + e^{-d_1/L_n^*}\left(\frac{D_n^*}{L_n^*} - s_1\right) \right]}$$

$$+ \frac{\left[\frac{qp_{no} D_p^*}{L_p^*} \right] \left[e^{d_2/L_p^*}\left(s_2 + \frac{D_p^*}{L_p^*}\right) - e^{-d_2/L_p^*}\left(\frac{D_p^*}{L_p^*} - s_2\right) \right]}{\left[e^{d_2/L_p^*}\left(s_2 + \frac{D_p^*}{L_p^*}\right) + e^{-d_2/L_p^*}\left(\frac{D_p^*}{L_p^*} - s_2\right) \right]}$$

(3.36)

and

$$I'_o = \frac{\dfrac{qD_n^* p_{no}}{L_n^*}\left[e^{d_1/L_n^*}\left(s_1 + \dfrac{D_n^*}{L_n^*} \right) - e^{-d_1/L_n^*}\left(\dfrac{D_n^*}{L_n^*} - s_1 \right) \right]}{\left[e^{d_1/L_n^*}\left(\dfrac{D_n^*}{L_n^*} + s_1 \right) + e^{-d_1/L_n^*}\left(\dfrac{D_n^*}{L_n^*} - s_1 \right) \right]}$$

$$+ \frac{\dfrac{q D_p^* n_{po}}{L_p^*}\left[e^{d_2/L_p^*}\left(s_2 + \dfrac{D_p^*}{L_p^*} \right) - e^{-d_2/L_p^*}\left(\dfrac{D_p^*}{L_p^*} - s_2 \right) \right]}{\left[e^{d_2/L_p^*}\left(s_2 + \dfrac{D_p^*}{L_p^*} \right) + e^{-d_2/L_p^*}\left(\dfrac{D_p^*}{L_p^*} - s_2 \right) \right]} . \qquad (3.37)$$

I_g is the photogenerated current independent of the junction voltage V_j and is given by the expression:

$$I_g = B \frac{\dfrac{1}{L_n^*}\left[\left(\dfrac{D_n^*}{L_n^*} + s_1 \right) e^{d_1\left(\frac{1}{L_n^*} - \alpha \right)} - 2(D_n^*\alpha + s_1) - \left(\dfrac{D_n^*}{L_n^*} - s_1 \right) e^{-d_1\left(\frac{1}{L_n^*} + \alpha \right)} \right]}{\left[e^{d_1/L_n^*}\left(\dfrac{D_n^*}{L_n^*} + s_1 \right) + e^{-d_1/L_n^*}\left(\dfrac{D_n^*}{L_n^*} - s_1 \right) \right]} + B\alpha\, e^{-\alpha d_1}$$

$$+B' \frac{\dfrac{1}{L_p^*}\left[e^{\left(-\alpha d_1 + \frac{d_2}{L_p^*}\right)}\left(s_2 + \dfrac{D_p^*}{L_p^*} \right) + e^{\left(-\alpha d_1 - \frac{d_2}{L_p^*}\right)}\left(s_2 - \dfrac{D_p^*}{L_p^*} \right) - 2e^{-\alpha(d_1+d_2)}(s_2 - D_p^*\alpha) \right]}{\left[e^{d_2/L_p^*}\left(s_2 + \dfrac{D_p^*}{L_p^*} \right) - \left(s_2 - \dfrac{D_p^*}{L_p^*} \right) e^{-d_2/L_p^*} \right]}$$

$$- B'\alpha\, e^{-\alpha d_1} \qquad (3.38)$$

$$\text{where } B = \frac{q\,\alpha\,N_o\,L_n^{*2}}{(1 - \alpha^2 L_n^{*2})} \tag{3.38a}$$

$$\text{and} \quad B' = \frac{q\,\alpha\,N_o\,L_p^{*2}}{(1 - \alpha^2 L_p^{*2})} \tag{3.38b}$$

The plot of I V_s.V(eqn. 3.35) gives the I-V characteristics of the solar cell. In the low injection limit (V_j << V_D) eqn. 3.35 reduces to eqn. 1.39 derived in Chap.1.

3.4.2 Maximum Power output :

Maximum power point (P_{max}) in the I - V curve is obtained by calculating the product IV at each point on the I-V curve. The current and voltage at the maximum power point are denoted by I_m and V_m respectively. Therefore (see eqn. 1.46 also),

$$P_{max} = I_m V_m \tag{3.39}$$

3.4.3 Short-circuit current :

Under short-circuit configuration eqn. 3.35 gives for $V_j = 0$,

$$I_{sc} = - I_g \tag{3.40}$$

i.e. the short circuit current flows in the direction opposite to that of the photo generated current, the magnitude of both being the same if the circuit resistance (including the internal resistance of the device it self) is zero.

3.4.4 Open circuit voltage :

Under open-circuit configuration; $(I=0, V_j=V_{oc})$, we obtain from eqn. 3.35

$$I_g = \frac{\left[I_o + I_o' \exp\left(-\frac{q(V_D - V_{oc})}{kT}\right)\right]\left[\exp\left(\frac{q\,V_{oc}}{kT}\right) - 1\right]}{1 - \exp\left[-2q\,(V_D - V_{oc})/kT\right]} \qquad (3.41)$$

Above equation is quadratic in exp (qV_{oc}/kT) and when solved gives two values of V_{oc}. One of the roots is negative and is therefore, discarded from physical considerations. It is clear from eqn. 3.41 that the maximum value that V_{oc} can attain is V_D corresponding to the limiting case of infinitely high intensities. This result is in agreement with that predicted by DKJ . For low level injections, eqn. 3.41 reduces to eqn. 1.44:

$$V_{oc} = \frac{kT}{q} \ln\left(1 + \frac{I_g}{I_o}\right) .$$

Contribution of the Dember effect to the open-circuit voltage will be discussed in Sec. 3.7.

3.4.5 Fill factor:

Fill factor (FF) is calculated using the expression (see eqn. 1.49a also):

$$FF = \frac{P_{max}}{I_{sc} \times V_{oc}} \qquad (3.41a)$$

where I_{sc} and V_{oc} are determined from eqns. 3.40 and 3.41 respectively. P_{max} is determined from the plot of I-V characteristics.

3.4.6 Efficiency :

As defined in Chap. 1 efficiency (η) of the solar cell is determined by using (see eqn. 1.50 also):

$$\eta = \frac{P_{max}}{P_{in}} \qquad (3.41b)$$

where P_{in} is the incident power on the solar cell, as given by eqn. 1.51 in Chap. 1.

3.5 Determination of the cell response for continuous spectrum :

All the preceding analysis has been based upon a

situation in which the photovoltaic cell is illuminated with monochromatic radiation. In most of the actual applications to which such devices are put, the illumination source is sunlight, which, of course, has a broad continuous spectrum of wavelengths. In this case, it is necessary to calculate the actual spatial distribution of excess carrier generation. The generation rate $g'(x)$ is no longer the simple exponential function shown in eqn. 3.9 but a superposition of many such exponential functions representing many wavelengths, each with a characteristic absorption coefficient $\alpha(\lambda)$ as obtained from the observed optical absorption spectrum of the semiconductor crystal and each with a characteristic intensity factor $N_o(\lambda)$ according to the spectral intensity of sunlight at each wavelength. $g'(x)$ is then represented by

$$g'(x) = \sum_{\lambda} \alpha(\lambda)\, N_o(\lambda)\, e^{-\alpha(x+d_1)}$$

$$= \int_{\lambda_1}^{\lambda_2} \alpha(\lambda)\, N_o(\lambda)\, e^{-\alpha(x+d_1)} \qquad (3.42)$$

in the wavelength interval λ_1 to λ_2. Therefore, in this case the ambipolar eqns. 3.10 and 3.11 become integral eqns. which are not solvable analytically. We have therefore,

solved them numerically for fifteen values of wavelengths in the interval 0.4 to 1.1 microns to obtain the short-circuit current in each case. The absorption coefficient for each wavelength was determined using the analytical expression given by Shumka (1970) based upon the experimental data of Dash and Newman (1955). This value of I_{sc} obtained for each wavelength was multiplied by the factor $N_o(\lambda)$ corresponding to AMO spectrum given by Johnson (1954) and then added to give the total short-circuit current under AMO spectrum (see Wolf 1963 also). V_{oc}, IV characteristics, P_{max}, FF and efficiency are calculated in the same manner as described in sec. 3.4.

3.6 Effect of the internal series resistance:

In this section we discuss the effect of the internal series resistance on the cell response.

3.6.1 I-V characteristics :

A finite internal series resistance R_s of the cell gives rise to a voltage drop IR_s across the cell. Therefore, voltage measured at the terminals V_T will be less than the junction voltage V_j by the amount :

$$V_T = V_j - IR_s \, . \qquad (3.43)$$

This causes a reduction in the current flowing across the solar cell and the I-V relationship given by eqn. 3.35 for an ideal cell of zero internal resistance is modified to :

$$I = \frac{\left\{\left[I_o + I_o' \exp\left[-\frac{q(V_D-(V_T+IR_s))}{kT}\right]\right]\right\}\left[\exp\left(\frac{q(V_T+IR_s)}{kT}\right)-1\right]}{1 - \exp\left[\frac{-2q(V_D-(V_T+IR_s))}{kT}\right]} - I_g. \quad (3.44)$$

For the low injection case, eqn. 3.44 reduces to

$$I = I_o \left[\exp \frac{q(V_T+IR_s)}{kT} - 1\right] - I_g \cdot \quad (3.44a)$$

3.6.2 <u>Short circuit current</u> :

For the short-circuit configuration, on substituting $I = I_{sc}$ and $V_T = 0$, eqn. 3.44 becomes:

$$I_{sc} = \frac{\left\{I_o + I_o' \exp\left[\frac{-q(V_D - I_{sc} R_s)}{kT}\right]\right\}\left[\exp\left(\frac{q\, I_{sc} R_s}{kT}\right)-1\right]}{1 - \exp\left[\frac{-2q\,(V_D - I_{sc} R_s)}{kT}\right]} - I_g. \quad (3.45)$$

Therefore, for a finite internal resistance, I_{sc} is not equal to I_g but is smaller by the quantity given in

the first term of eqn. 3.45. Limiting form of the eqn. 3.45 shows that the resistive drop limits I_{sc} to an upper value given by

$$(I_{sc})_{max} = V_D/R_s \quad . \qquad (3.46)$$

We have neglected here the contribution of the Dember effect in calculating the current. However, it is expected to be of second order only. For the low level limit ($V_j << V_D$), eqn. 3.45 can be written as

$$I_{sc} = I_o \left[\exp\left(\frac{q\, I_{sc} R_s}{kT} \right) - 1\right] - I_g . \qquad (3.46a)$$

3.6.3 Open circuit voltage (V_{oc}) :

In the open-circuit configuration, the junction potential is obtained by putting I = 0 in eqn. 3.44 and V_{oc} is therefore, independent of R_s.

3.6.4 Maximum power output and fill factor:

Because of the change in I-V characteristics due to the presence of a finite series resistance (eqn. 3.44), P_{max} and FF are also expected to change. P_{max} and FF are calculated in the same manner as described in Sec. 3.4.

3.7 Contribution of Dember effect :

Strictly speaking, if the charge neutrality condition is assumed as is implicit in eqn. 3.1, the internal field due to Dember effect cannot arise. The calculation of Dember effect in this model is therefore, an approximation which is however quite standard and conventional (Mckelvey (1966)).

Dember voltage contribution to the total open-circuit voltage of a solar cell has been calculated by DKJ under the three assumptions as described in Sec. 3.1. Using the same treatment, we have calculated the Dember voltage in both the n and p regions in the present formulation as given by the following expressions :

$$V_p = -\frac{kT}{q} \frac{(b-1)}{(b+1)} \ln \left[\frac{p_o + (b+1)(\Delta n_p)_o}{p_o + (b+1)(\Delta n_p)_{-d_1}} \right] \qquad (3.47)$$

is the voltage drop in the p region and

$$V_n = \frac{kT}{q} \frac{(b'-1)}{(b'+1)} \ln \frac{n_o b' + (b'+1)(\Delta p_n)_o}{n_o b'} \qquad (3.48)$$

is the voltage drop in the n region. These expressions have been derived by integrating eqn. 3.5 for the internal electric field with respect to the excess carrier density

Δn. Integration limits are obtained by substituting the value of Δn at the junction and at the front and back surfaces of the solar cell under open circuit conditions. In eqns. 3.47 and 3.48 $(\Delta n_p)_o$ and $(\Delta p_n)_o$ are the excess carrier values at the junction, and are calculated using eqns. 3.18 and 3.19. $(\Delta n_p)_{-d_1}$ is the excess carrier concentration at the front surface. Δn at the back surface of the cell is taken to be zero because of the presence of an ohmic contact. b and b' are the electron to hole mobility ratios in the p and n regions respectively.

The total voltage drop V_B due to Dember effect is given by the sum of eqns. 3.47 and 3.48. as

$$V_B = V_n + V_p \qquad (3.49)$$

Therefore, under open circuit conditions, the total open-circuit voltage of the p-n junction is

$$V_{oc} = V_{joc} + V_B \qquad (3.50)$$

where V_{joc} is the open circuit voltage at the junction and V_B is the voltage drop in the n and p regions under open circuit conditions.

We have calculated V_n and V_p by using the numerical technique described in Sec. 3.3. The results

depend upon the values of $(\Delta p_n)_o$, $(\Delta n_p)_o$ and $(\Delta n_p)_{-d_1}$ and are therefore, sensitive to the generation rate of carriers which in our case is exponential.

In the limiting case of infinite p and n regions, the expressions for V_n and V_p (eqns. 3.47 and 3.48) reduce to eqns. (11) and (12) obtained by DKJ in their paper (for I = 0) :

$$V_n = \frac{kT}{q} \frac{(b-1)}{(b+1)} \ln \left[1 + \frac{b+1}{b} \frac{(\Delta p_n)_o}{N_D} \right], \qquad (3.51)$$

$$V_p = - \frac{kT}{q} \left(\frac{b'-1}{b'+1} \right) \ln \left[1 + \frac{(b'+1)(\Delta n_p)_o}{N_A} \right]. \qquad (3.52)$$

For b = b',

$$V_B = \frac{mkT}{q} \left[\ln \left(1 + \frac{2(\Delta p_n)_o}{(1+m) N_D} \right) - \ln \left(1 + \frac{2(\Delta n_p)_o}{(1-m) N_A} \right) \right]. \qquad (3.53)$$

$$\text{with } m = \frac{(b-1)}{(b+1)} . \qquad (3.53a)$$

In the high illumination level limit ($g' \to \infty$), eqn. 3.53 reduces to eqn. 17 derived by DKJ in their paper for this limit as :

$$V_B = \frac{mkT}{q} \ln \frac{N_A}{b N_D} . \qquad (3.54)$$

3.8 Results and Discussions:

In this section we present the results of our calculations obtained by numerically solving the non-linear ambipolar transport equation in the p and n regions (see eqns. 2.10 and 3.11) of a typical p^+n solar cell (cell parameter given in Table 3.1) using the technique described in Sec. 3.3. The ambipolar coefficients D^*, τ^* and L^* in the base region calculated for different values of N_o (number of photons falling per cm^{-2} sec^{-1} on the cell surface) are shown in Fig. 3.2. It shows the variation of D^*, τ^* and L^* as a function of N_o for $\alpha = 10^4$ cm^{-1} starting from the low level limit to the high level limit when these coefficients become constant. In the diffused region, variation of the ambipolar coefficients with N_o is not appreciable (less than 1 %) in the range of N_o considered by us. Using these values of the ambipolar coefficients and the excess carrier density Δn calculated as a function of N_o, short-circuit current open-circuit voltage, fill factor and I-V characteristics of the solar cell are determined and discussed below. These results are compared with the results obtained by using DKJ formulation. G_o corresponds to the generation rate of excess carriers in DKJ formulation. N_o determines the illumination level in the present formulation,

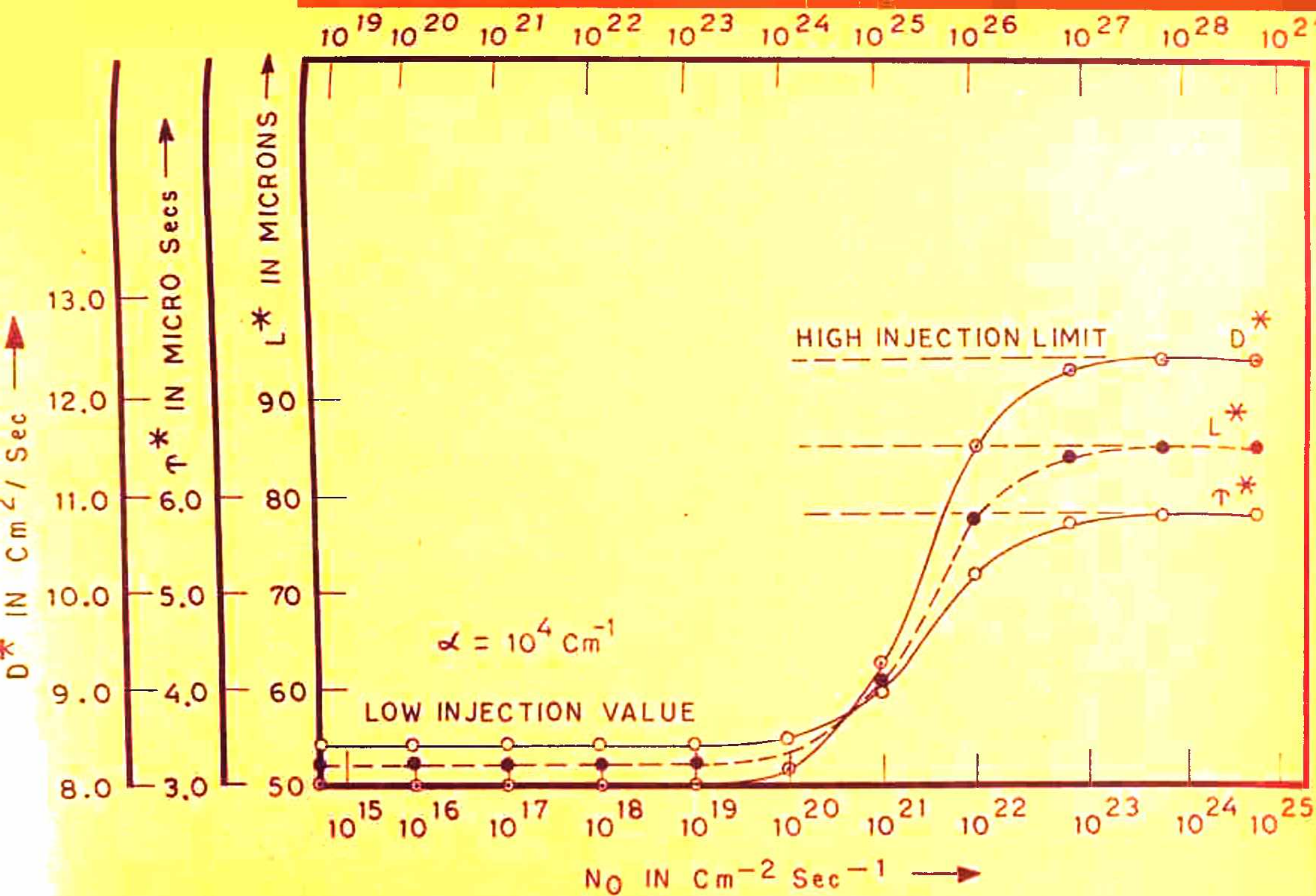

FIG.3.2 VARIATION OF D^*, τ^* AND L^* WITH N_0 IN THE BASE REGION.

generation rate of carriers at the top surface of the cell being $N_o \alpha$. In Secs. 3.8.1 to 3.8.5 we describe the calculated cell response as a function of illumination level obtained by neglecting the effect of the internal resistance of the cell. Effect of the internal series resistance of the cell on its response is discussed separately in Sec. 3.8.6.

3.8.1 Short circuit current :

I_{sc} increases linearly with light intensity as predicted by DKJ formulation for constant D^* and τ^*. Table 3.3 gives I_{sc} for different values of N_o calculated in the present formulation. It shows a small nonlinearity in the increase of I_{sc} with N_o for high values of N_o of the orders of 10^{21} cm^{-2} sec^{-1}. This superlinear variation of I_{sc} with N_o is appreciable only for $\alpha = 10^{-2}$ cm^{-1} and is attributed to the increase in D^* and τ^* (Fig. 3.2) with N_o (see eqns. 3.38 and 3.40 also) in the base region.

3.8.2 Open-circuit voltage :

V_{oc} is shown to increase logarithmically with N_o in both the formulations in Fig. 3.3a. As predicted in Sec. 3.4.4, V_{oc} saturates to V_D in both the formulations, as the high injection limit being reached earlier in DKJ formulation due to the uniform generation rate considered by

Table-3.3

CALCULATED VALUES OF CELL RESPONSE PARAMETERS FOR DIFFERENT VALUES OF N_o AND α (CELL PARAMETERS GIVEN IN TABLE 3.1)

N_o	$\alpha = 10^2\ cm^{-1}$			$\alpha = 10^3\ cm^{-1}$			$\alpha = 10^4\ cm^{-1}$		
$cm^{-2}sec^{-1}$	I_{sc} Amps	V_{oc} Volts	FF	I_{sc} Amps	V_{oc} Volts	FF	I_{sc} Amps	V_{oc} Volts	FF
10^{17}	$5.51x10^{-3}$	0.532	0.81	$1.34x10^{-2}$	0.555	0.81	$1.45x10^{-2}$	0.557	0.82
10^{18}	$5.54x10^{-2}$	0.592	0.82	$1.34x10^{-1}$	0.615	0.82	$1.45x10^{-1}$	0.617	0.83
10^{19}	$5.79x10^{-1}$	0.651	0.83	1.34	0.671	0.84	1.46	0.673	0.84
10^{20}	6.68	0.705	0.85	13.7	0.718	0.87	14.6	0.719	0.86
10^{21}	71.5	0.744	0.88	$1.41x10^{2}$	0.754	0.89	$1.46x10^{2}$	0.754	0.89
10^{22}	$7.21x10^{2}$	0.775	0.90	$1.42x10^{3}$	0.783	0.91	$1.46x10^{3}$	0.784	0.91

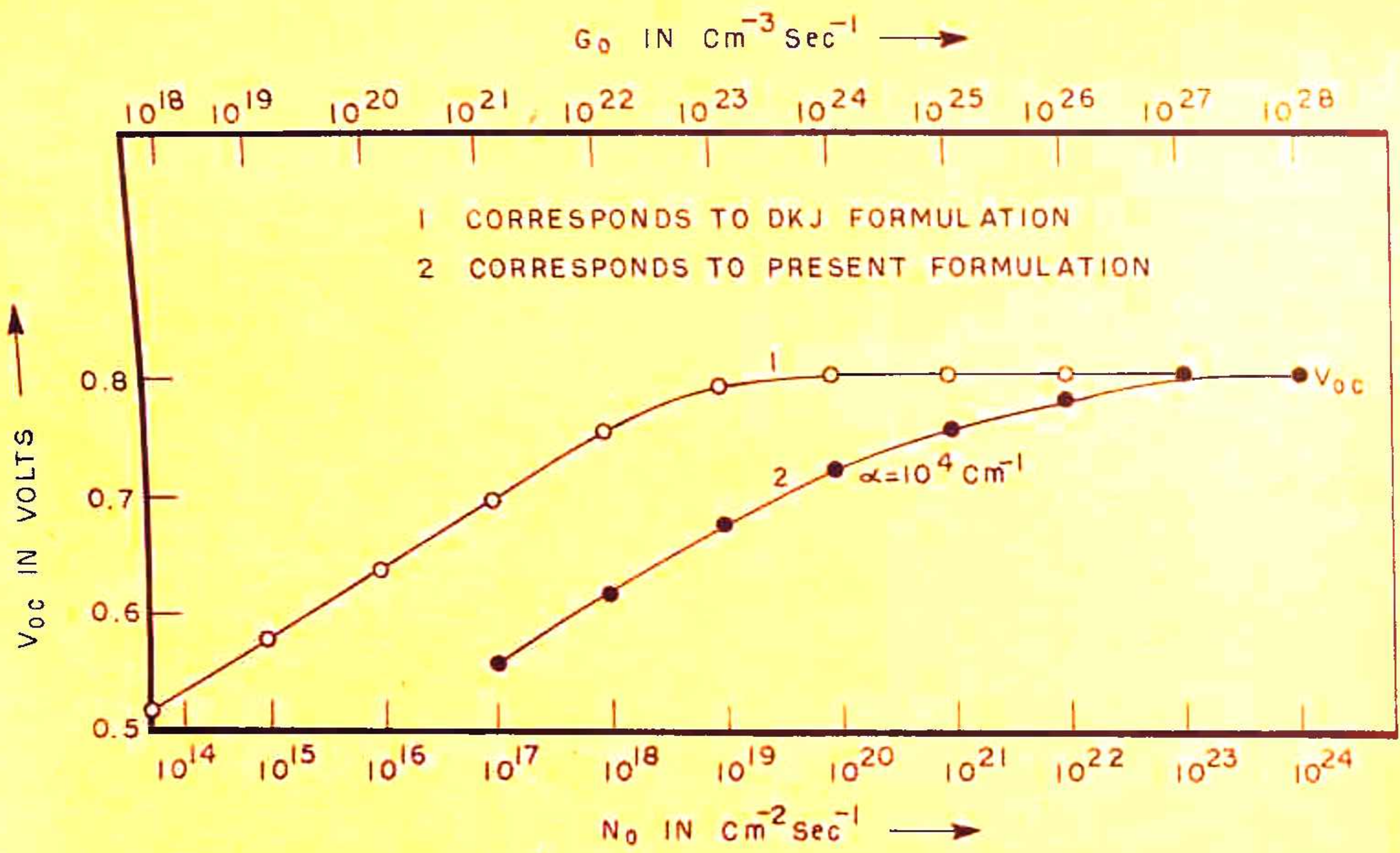

FIG. 3.3a V_{oc} Vs N_0.

them.

Dember voltage (V_B) in the open-circuit configuration is plotted as a function of N_o in Fig.3.3b. The difference in the values of V_B calculated in the two formulations primarily arises because of the exponential absorption of light considered by us instead of the uniform generation rate of carriers assumed by DKJ which gives larger values of $(\Delta n)_o$ and $(\Delta p)_o$ at the junction (see eqns. 3.47 and 3.48) for a particular illumination level.

3.8.3 I-V characteristics :

I-V characteristics generated for both the formulations are shown in Fig. 3.4. Fill factor as a function of N_o is plotted in Fig. 3.5. FF increases with N_o in both the formulations as expected.

3.8.4 Calculated cell response for different wavelengths:

The response of the solar cell was calculated for four values of $\alpha = 10^2$, 10^3, 10^4 and 10^5 cm^{-1} which correspond to wavelengths of 1.0, 0.8, 0.5 and 0.39 micron respectively. Due to the exponential absorption of light carriers are created at different depths in the solar cell corresponding to different values of α, resulting in a change in the current collected by the junction for each

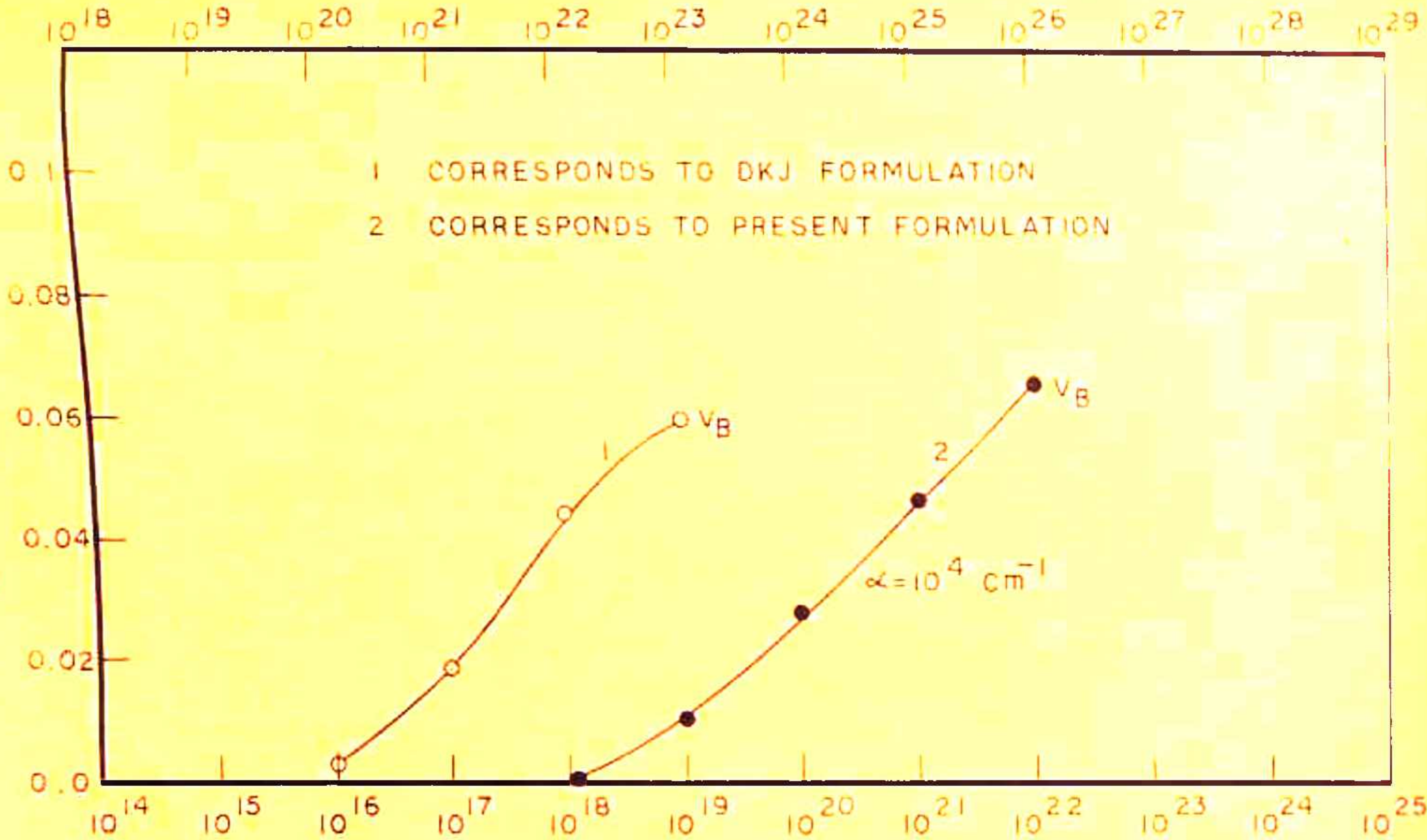

FIG 3.3b V_B Vs N_0

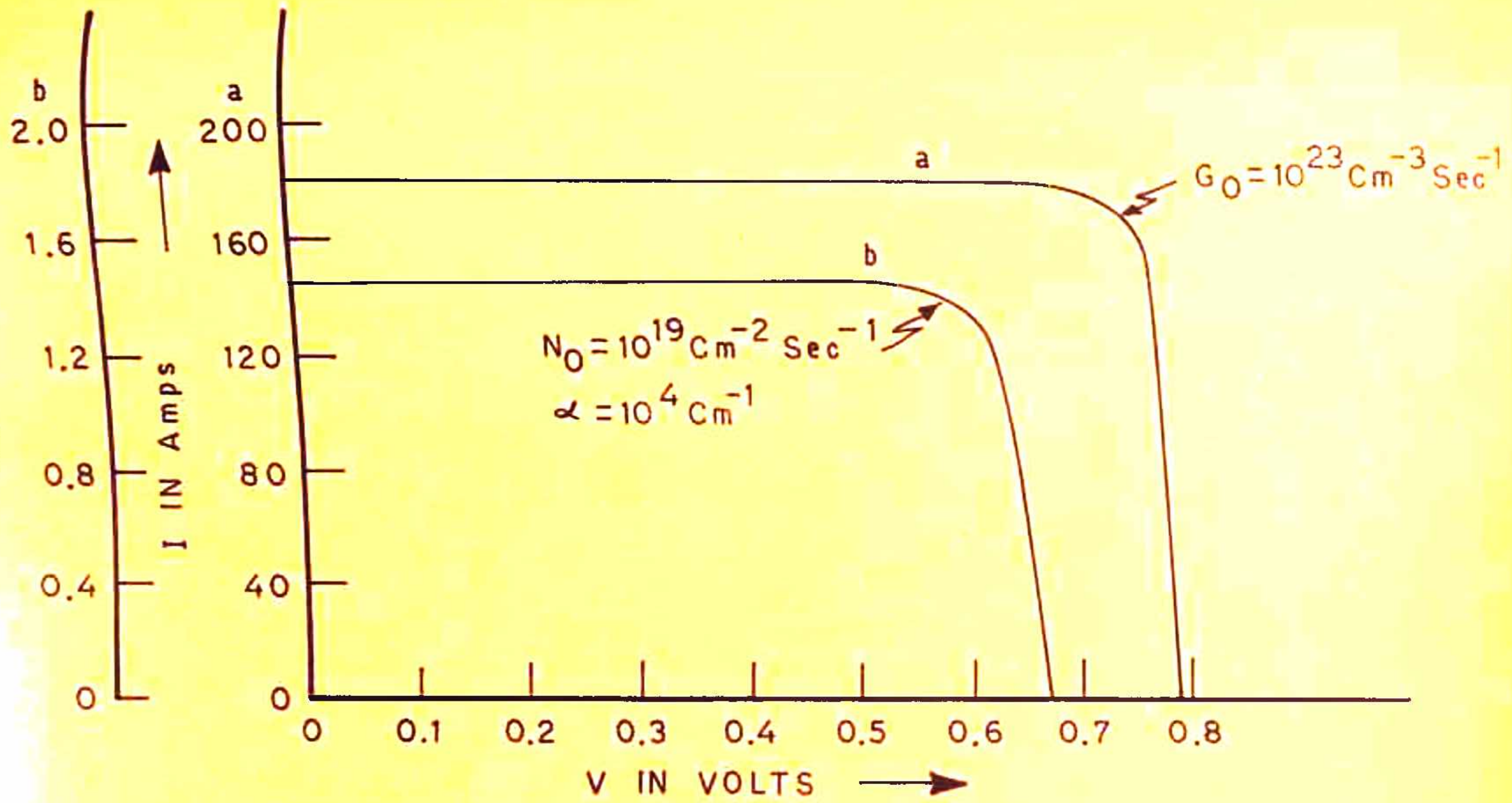

FIG.3.4 I V CHARACTERISTICS
CURVE a CORRESPONDS TO THE FORMULATION OF DKJ
CURVE b CORRESPONDS TO PRESENT FORMULATION

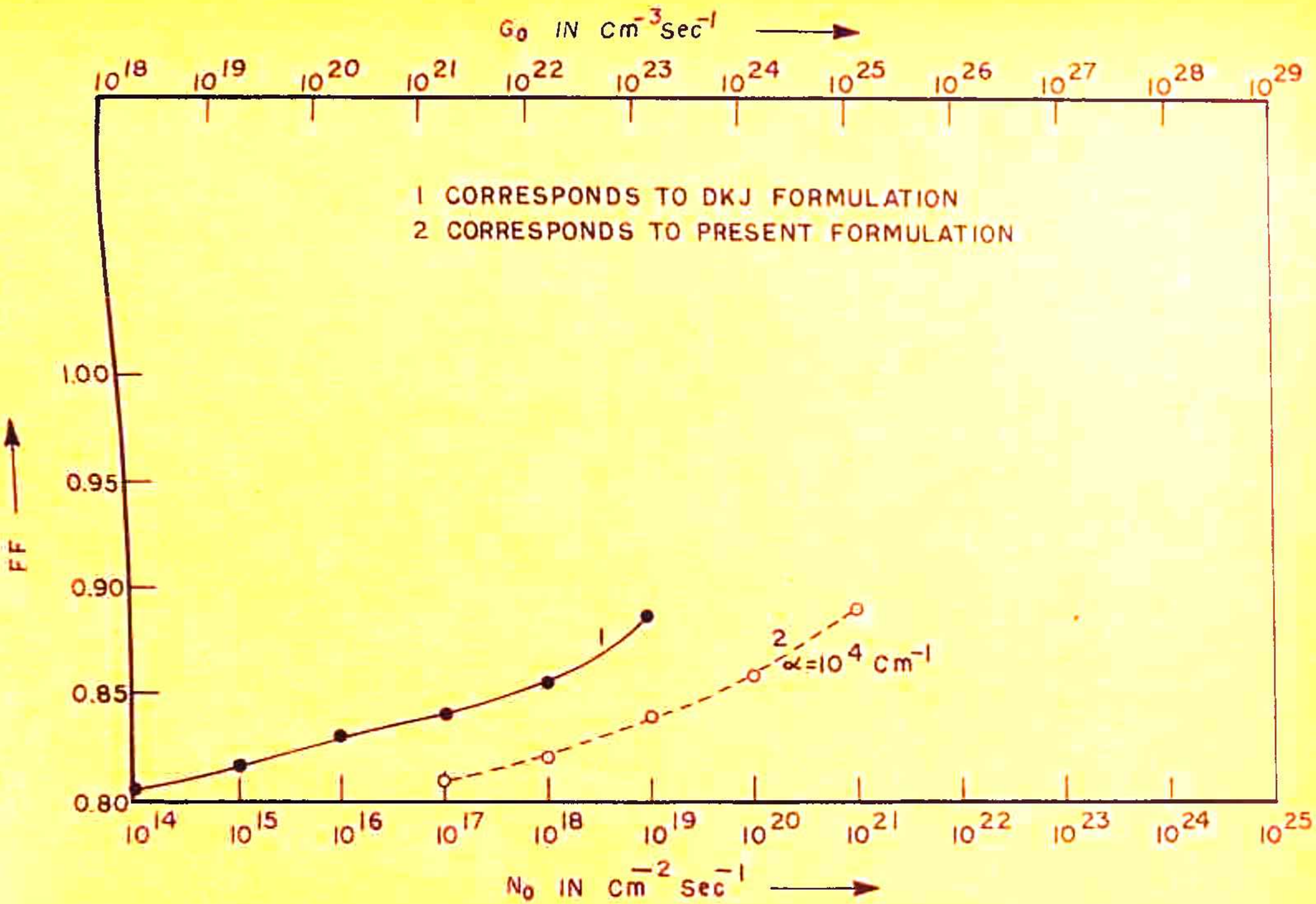

FIG. 3.5 FILL FACTOR Vs N_0.

value of α. Carrier profiles for $\alpha = 10^2$ and 10^4 cm^{-1} for the open circuit as well as short circuit configuration are shown in Figs. 3.6a and 3.6b in the diffused and base regions respectively. These curves correspond to $N_o = 10^{21}$ cm^{-2} sec^{-1}. As shown in Fig. 3.6b excess carrier density (Δp) in the base region decreases rapidly as the distance from the junction increase for $\alpha = 10^4$ cm^{-1} whereas for $\alpha = 10^2$ cm^{-1}, Δp Vs x curve peaks at x = 75 microns. For larger values of α most of the absorption of light is near the surface only, therefore Δp decreases monotonically with α in the base region. For $\alpha = 10^2$ cm^{-1}, larger number of photons are absorbed in the base region giving rise to a different profile of excess carriers as shown in Fig. 3.6b. Different boundary conditions imposed at the junction (see eqns. 3.18 and 3.19) corresponding to short-circuit configuration ($V_j = 0$) and open-circuit configuration ($V_j = V_{oc}$) give rise to different carrier profiles in the two configurations as shown in Figs. 3.6a and 3.6b.

Table 3.3 gives the values of I_{sc}, V_{oc} and FF for different N_o calculated for three value of α as described in Sec. 3.4. Same trend is obtained in the variation of each of the above mentioned parameters with increase in N_o for different values of α as expected. Fig. 3.7 presents the I-V characteristics for $N_o = 10^{17}$ cm^{-2} sec^{-1} and 10^{21} cm^{-2} sec^{-1} for $\alpha = 10^2$ cm^{-1}.

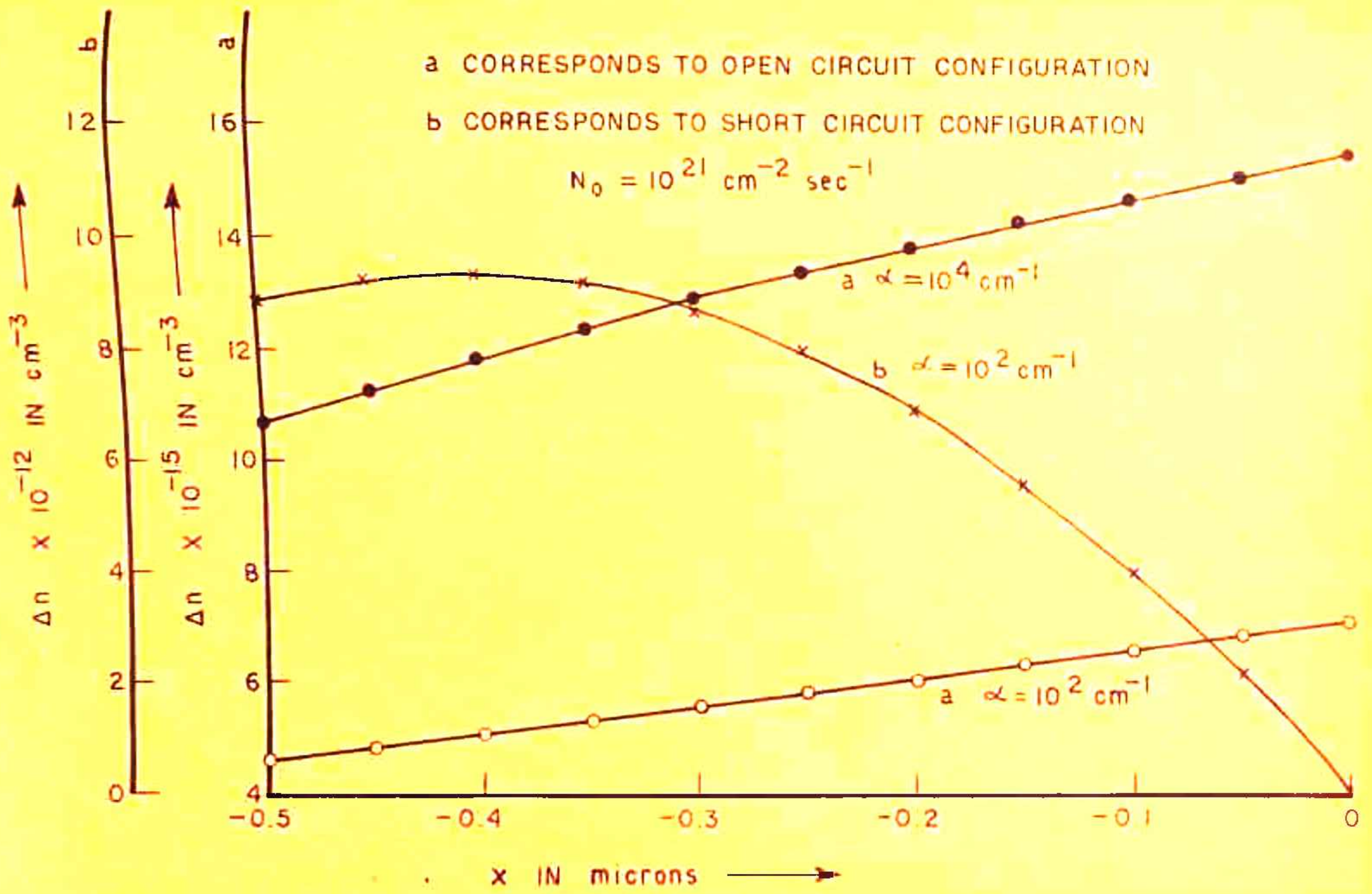

FIG.3.6a EXCESS CARRIER DENISTY (Δn) Vs x IN THE DIFFUSED REGION.

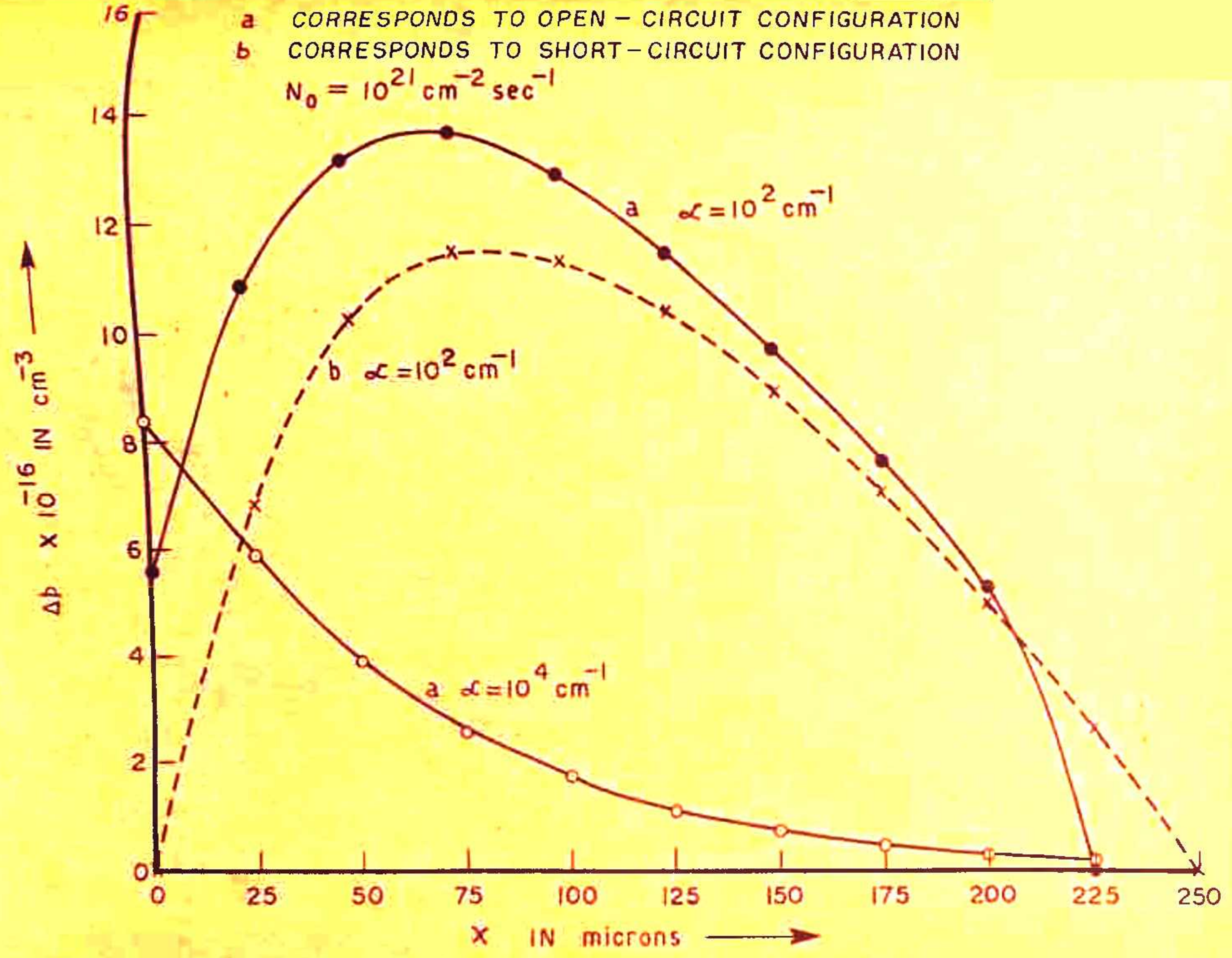

FIG.3.6b EXCESS CARRIER DENSITY (Δp) Vs x IN THE BASE REGION.

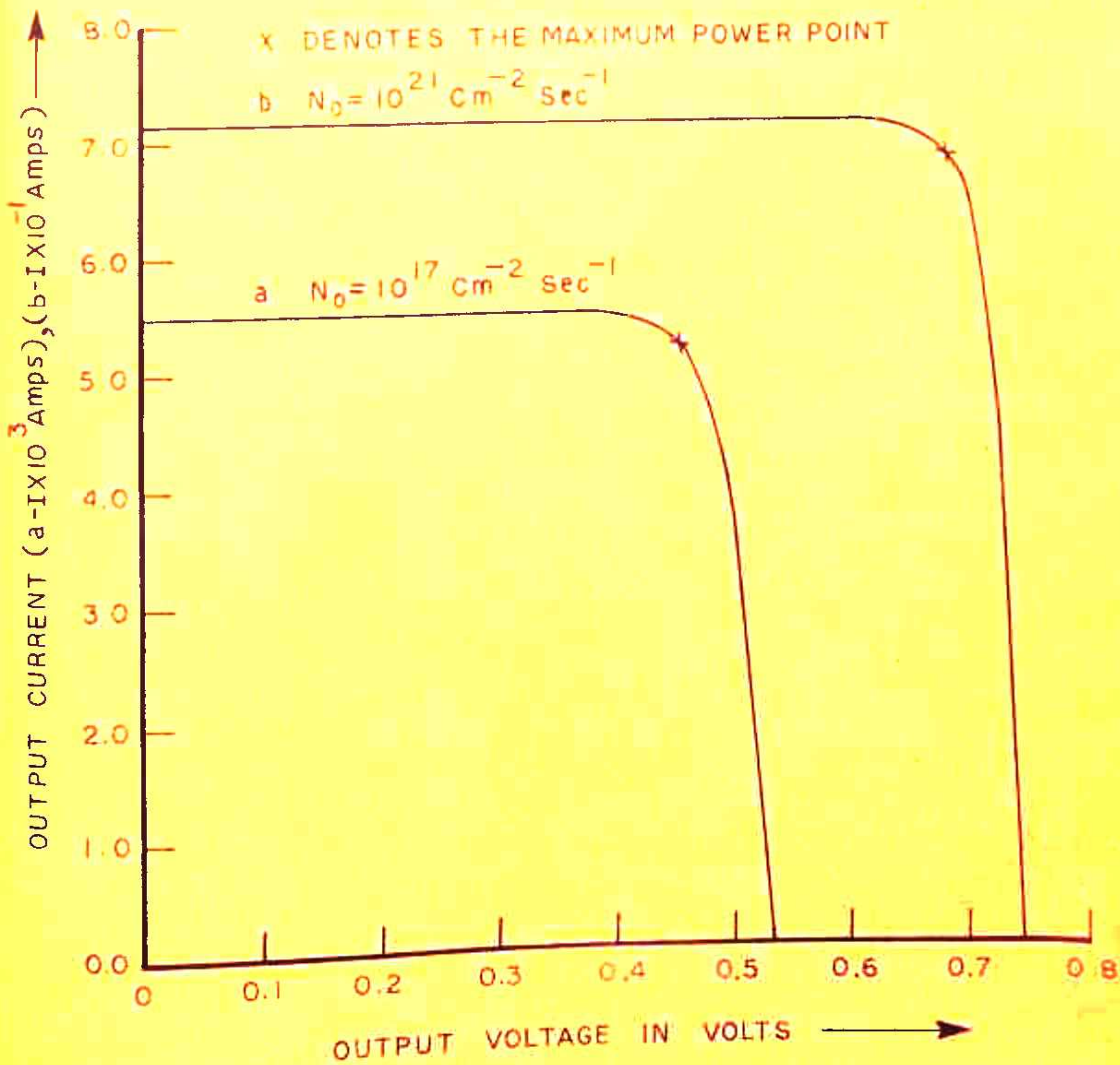

FIG.3.7 I – V CHARACTERISTICS CORRESPONDING TO $\alpha = 10^2$ cm^{-1}.

3.8.5 Calculated cell response for AMO spectrum :

Response of the cell for AMO spectrum was calculated as described in Sec. 3.5 for different values of the concentration factor C. Fig. 3.8 gives the I-V characteristics corresponding to C = 1* and 1000. Increase in concentration gives rise to more rectangular characteristics as shown in Fig. 3.8. I_{sc} increases from 3.89×10^{-2} Amps at C = 1 to 39.9 Amps at C = 1000. Increase in V_{oc}, FF and efficiency (η) as a function of C is shown in Fig. 3.9 calculated for AMO spectrum.

I_{sc} calculated as a function of wavelength (λ) in the wavelength range 0.4 to 1.1 μm (which is the corresponding range used in calculating cell response for AMO spectrum) is shown in Fig. 3.10 for $N_o = 10^{17}$ cm^{-2} sec^{-1} . Fig. 3.10 also shows I_{sc} calculated for two values of the junction depth equal to 0.5 micron and 2.0 microns respectively (all other cell parameters being same). As shown, the peak of the curve shifts towards longer wavelengths for the larger value of the junction depth (d_1 = 2.0 μm). This can be attributed to the effect of increased lifetimes and therefore, longer diffusion lengths of carriers in the lightly doped base region as compared to the heavily doped diffused region. Moreover, for wavelengths below 0.8 micron

---

*Here C = 1 corresponds to one sun which is defined to be an illumination of 98 mW/cm^2 with an AMO spectrum.

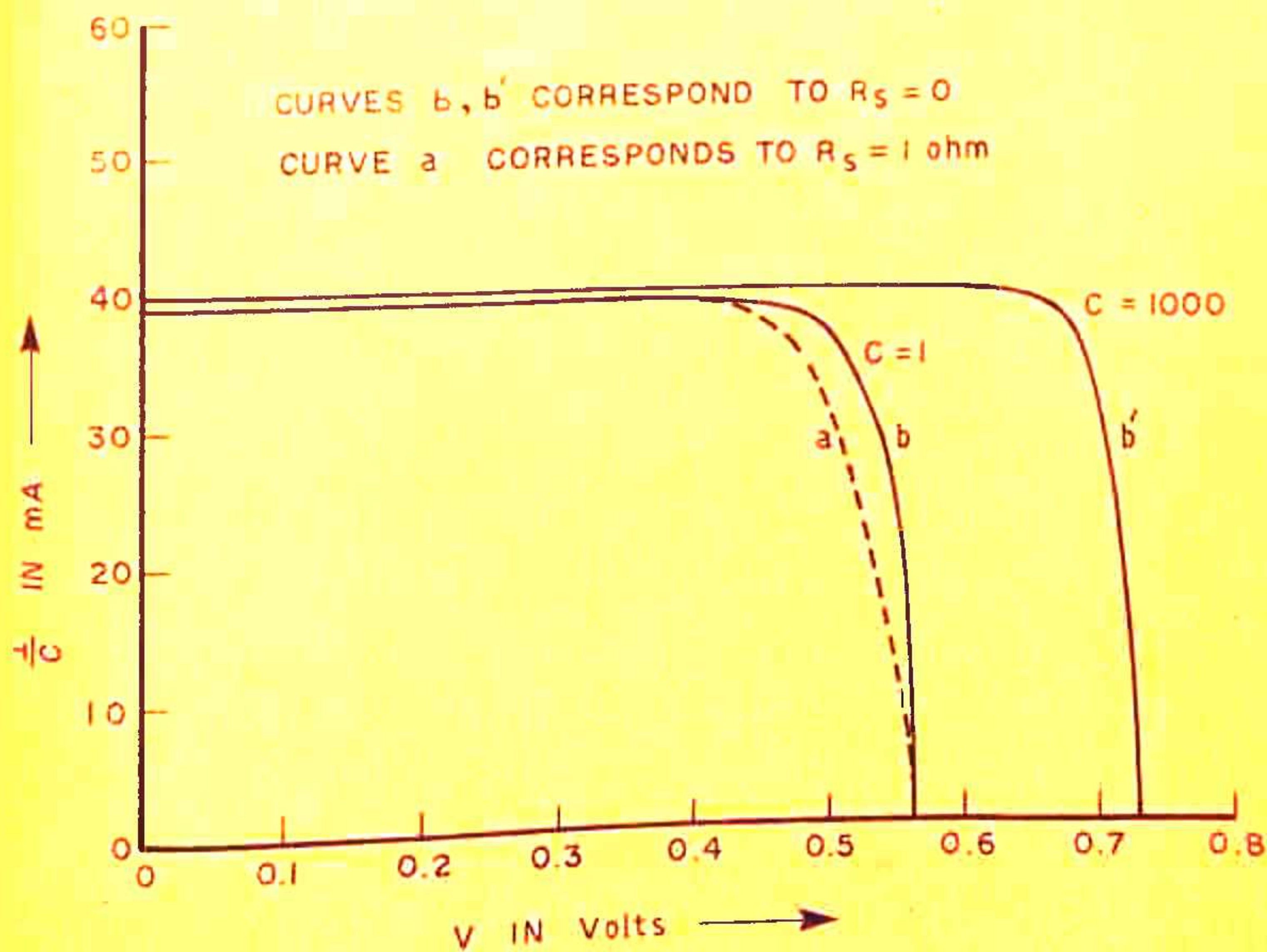

FIG.3.8 CALCULATED I - V CHARACTERISTICS FOR AMO SPECTRUM.

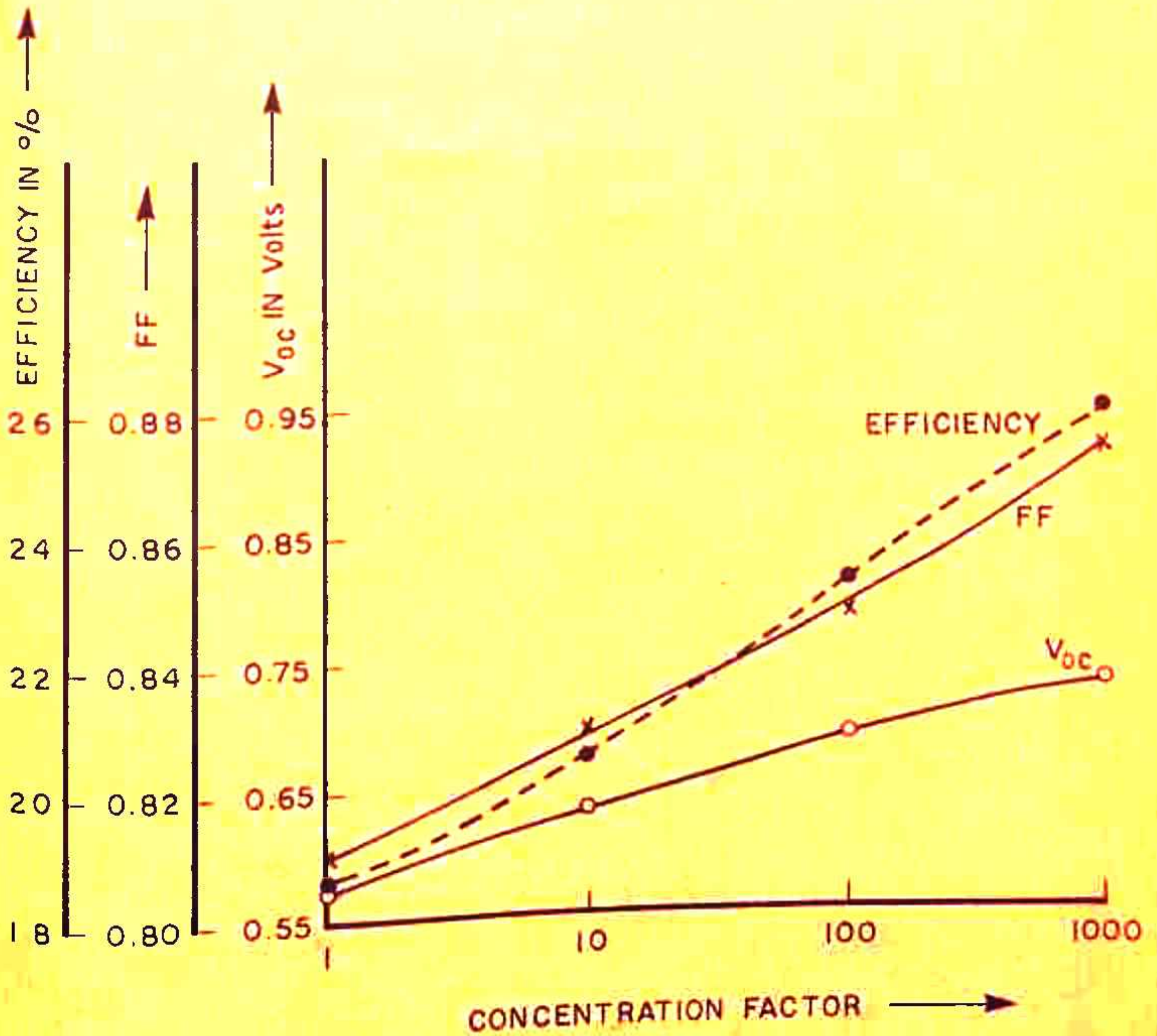

FIG. 3.9 V_{oc}, FF AND CELL EFFICIENCY AS A FUNCTION OF CONCENTRATION FACTOR IN AMO SPECTRUM.

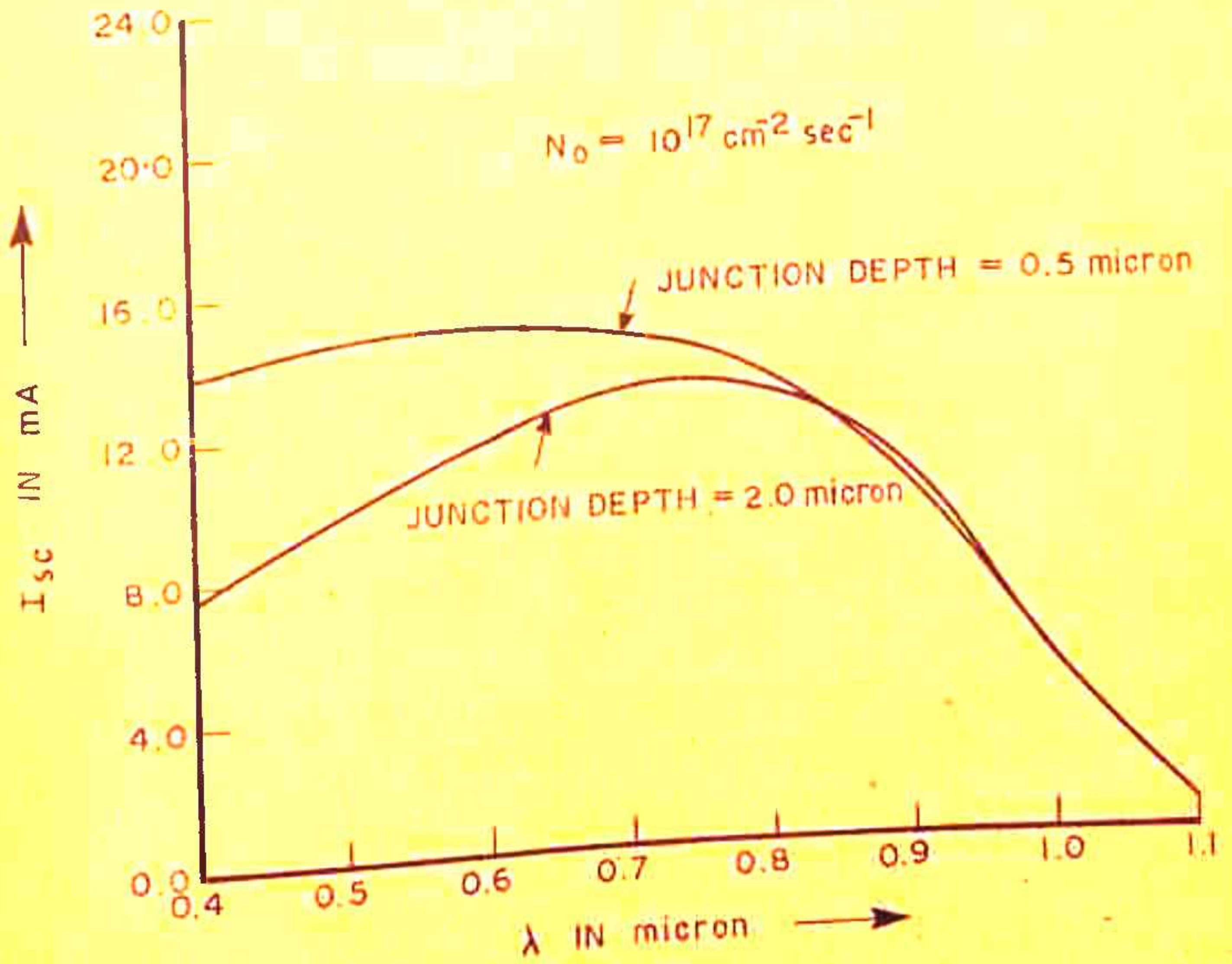

FIG.3.10 I_{sc} Vs λ

there is a large reduction in I_{sc} corresponding to the junction depth of 2.0 micron. This is expected because for a larger value of the junction depth, more carriers are absorbed in the diffused region resulting in the increase in the loss of carriers due to low lifetimes and surface recombination in the diffused region.

3.8.6 Effect of series resistance :

In the calculations described earlier in Secs. 3.8.1 to 3.8.5, effect of the internal series resistance on the cell response is not considered. It is important to consider the effect of R_s for high intensity illumination (see Chap. 1). In this section we present the calculated I-V characteristics (Sec. 3.6) for different levels of illumination taking into account the effect of series resistance. Fig. 3.8 (see P. 103) shows the cell I-V characteristics under AMO spectrum (C = 1) for R_s = 0 and R_s = 1 ohm. The degradation in the I-V characteristics is clear from curves a and b in Fig. 3.8. P_{max} decreases from 18.2 mw to 16.8 mw. The resulting decrease in FF is from 0.81 for R_s = 0 to 0.75 for R_s = 1 ohm. I-V characteristics for C = 10 are plotted in Fig. 3.11 corresponding to R_s = 0, 0.5 and 1.0 ohm. For higher

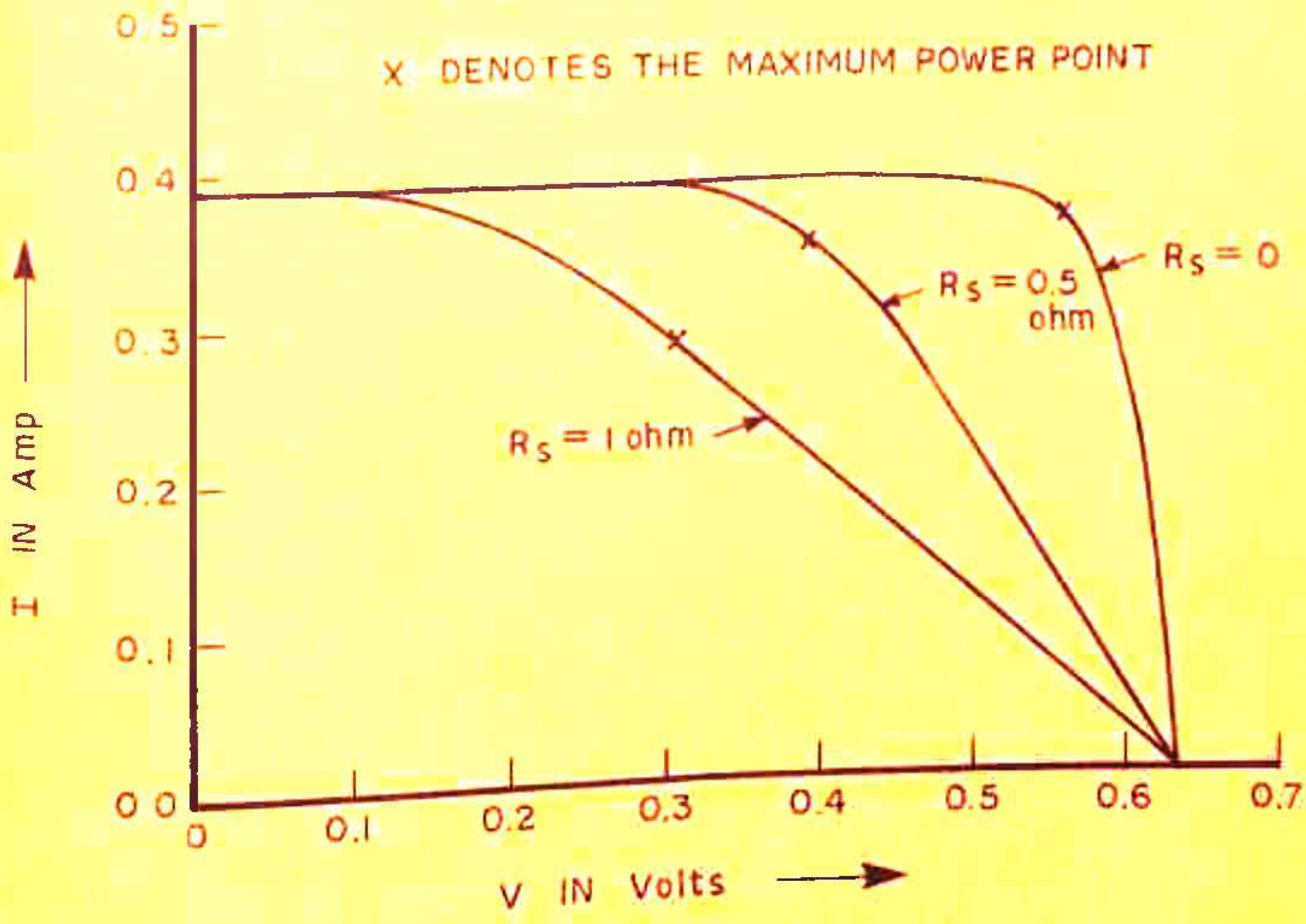

FIG. 3.11 I - V CHARACTERISTICS UNDER AMO SPECTRUM (C=10).

concentration factors, effect of R_s on the cell characteristics appears to be more drastic resulting in a large decrease in the FF and maximum power output of the cell. Table 3.4 gives the calculated values of η, V_m, P_{max} and FF for the above mentioned three values of the series resistance.

The short-circuit current was calculated for different values of I_g (see eqn. 3.45) and is shown in Fig. 3.12 as a function of I_g for R_s = 1 ohm. As is clear from the graph, I_{sc} saturates to the value V_D/R_s = 0.8 Amp in the present case as predicted in Sec. 3.6.2. In chap. 4 we will present the results of an experimental study on the response of solar cells as a function of illumination intensity at constant temperature. A detailed study of the effect of series resistance and its determination will be presented in Chap. 7.

3.8.7 Infinitely high intensities:

In the present analysis of the response of solar cells to high levels of illumination described in this chapter, we have not considered some of the additional effects which might be coming into the picture at infinitely high intensities. At intensities of the order of

Table-3.4

CALCULATIONS FOR FINITE SERIES RESISTANCE OF THE CELL

R_s ohm	Concentration factor (C)*	P_{max} Watts	FF	V_m Volts	η %
0	1	18.2×10^{-3}	0.81	0.494	18.6
1	1	16.8×10^{-3}	0.75	0.456	17.1
0	10	20.4×10^{-2}	0.83	0.557	20.8
0.5	10	13.9×10^{-2}	0.56	0.393	14.2
1.0	10	8.8×10^{-2}	0.36	0.304	9.0

* C = 1 corresponds to one sun which is defined to be an illumination of 98 mW/cm^2 with an AMO spectrum.

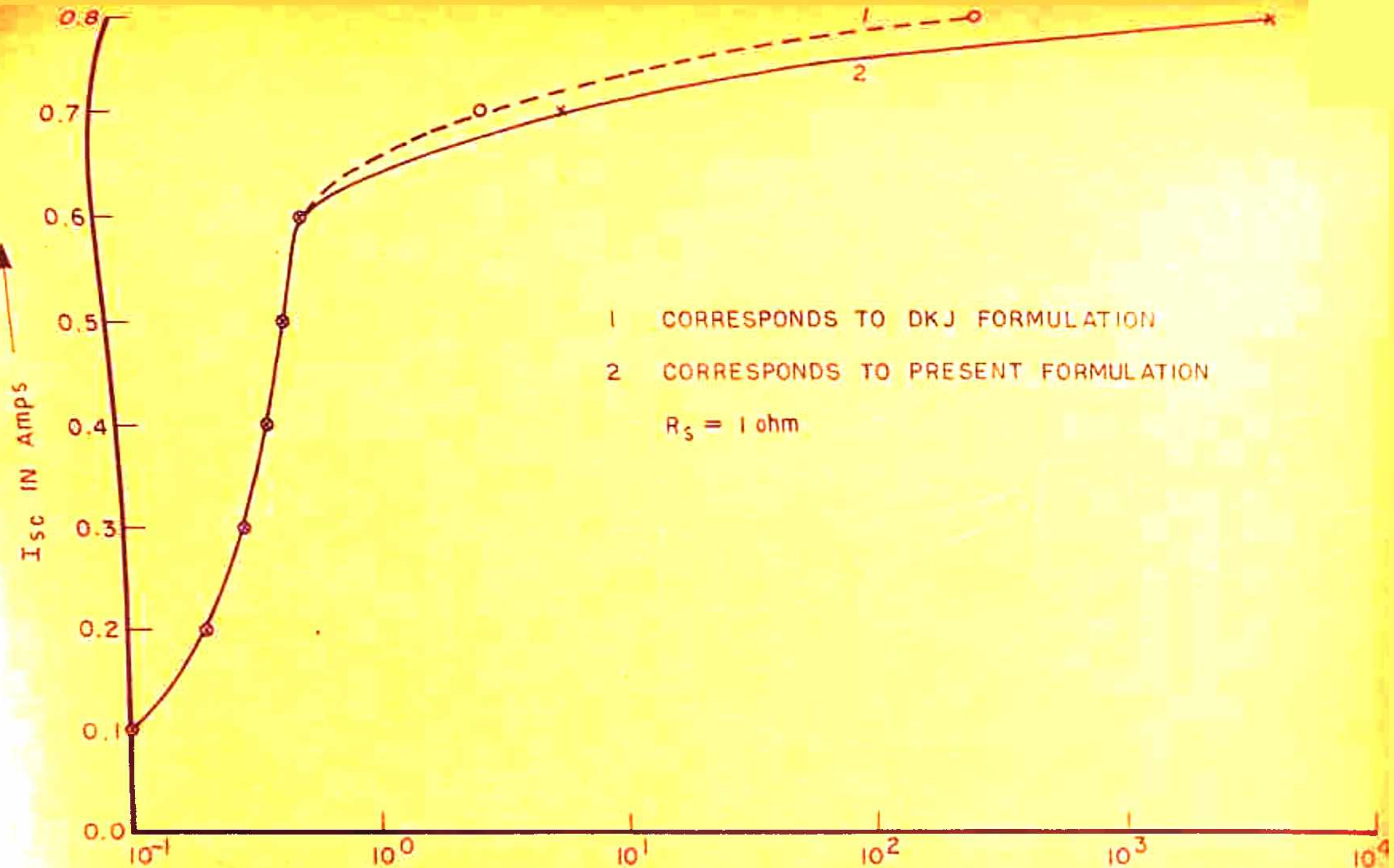

FIG.3.12 I_{sc} Vs I_g.

$10^{[illegible]}$/watt/cm^2 or more, several other effects e.g. Auger recombination, exciton generation, plasma reflection may become important. Moreover, at high illumination intensities a change in the life time of excess carriers is expected because of the saturation of trap levels (Dhariwal et al 1978). Since details of the whole process are not very clear at the moment, we have confined ourselves to the change in life time with the illumination intensity arising due to the increase in the value of excess carrier density Δn (see eqn. 3.4) as predicted by the conventional theory.

Blinov et. al. (1966) have reported a decrease in the open circuit voltage of a p-n junction cell at the illumination intensity of the order of 10^5 watts/cm^2, using an intense laser beam. This result comes as a surprise because all the theoretical calculations predict a saturation of the open circuit voltage beyond a certain value of the illumination intensity. A plausible explaination of this observed effect comes from plasma reflection due to which the incident light is totally reflected out of the medium at intensities of this order (Agarwala et. al. 1978).

CHAPTER-4.

AN EXPERIMENTAL STUDY OF THE RESPONSE OF SOLAR CELLS TO DIFFERENT ILLUMINATION LEVELS. AT CONSTANT TEMPERATURE

4.1 Introduction :

In Chapter 3, we presented a detailed study of the solar cell response as predicted from theoretical considerations. In this chapter, we present the results of some of the experiments done to study the response of solar cells as a function of illumination intensity. The temperature of these cells was maintained constant during these measurements. We have measured the I-V characteristics of 10 ohm cm, n^+p space qualty solar cells at different light intensities using 1000 watt Xenon Arc lamp and AMO simulator as light sources. The resulting changes in the I-V characteristics, short-circuit current, open-circuit voltage, Fill factor, maximum power output and efficiency of the cells are qualitatively discussed. Sec. 4.2 deals with the description of the experimental set up used for the measurement of I-V characteristics. In Sec. 4.3 results of these measurements are presented and discussed. Sec. 4.4 gives some conclusions drawn from this study.

4.2 Experimental set up :

Photovoltaic I-V characteristics of solar cells were measured using the circuit shown in Fig. 4.1. Details of the equipment used are given in Table 4.1a. A 1000 watt Xenon Arc lamp powered by a stablised power supply was used as a light source. The typical output spectrum of the Xenon Arc lamp (as given by Oriel Corporation) is shown in Fig. 4.2. An AMO spectrum solar simulator was used to calibrate the experimental solar cells and also for taking I-V characteristics under AMO spectrum. The solar cell was mounted on a rectangular brass mount as shown in Fig. 4.3a. This mount had the provision for circulating water to keep the temperature of the cell constant. A calibrated copper-constantan thermocouple soldered to the top surface of the mount near the cell was used to monitor the temperature of the solar cells. The front of the mount was covered with a glass plate to reduce the direct heating of the cell under illumination.

An Ultracryostat (MK 70) was used to control the temperature of the solar cell at 28°C. Digital multimeters of 4 $\frac{1}{2}$ digit were used to measure the current in the circuit and voltage across the load.

Table 4.1a

DETAILS OF THE EQUIPMENT USED

Xenon Arc Lamp	: Oriel Corporation, LE-29177, C-60-51 powered by a stablised power supply, 8550-7.
AMO Spectrum solar simulator	: Schoffel Instrument Corporation, LH151N.
Ultra Cryostat	: MK 70, Temperature Control accuracy: ± 0.5 degree
Thermopile	: Kipp and Zonen, CAI- 754286
X-Y Recorder	: Hewlett Packard, 7035B, Accuracy at full scale: 0.2 %.
Digital Multimeters	: 1) Aplab, 1005, 4 $\frac{1}{2}$ digits, Accuracy in the measurement of voltage: ± 0.2 % of the range ± 1 digit. 2) Yamuna, 1012, 4 $\frac{1}{2}$ digits, Accuracy in the measurement of current : ±0.1 % of range ± 1 digi[t]

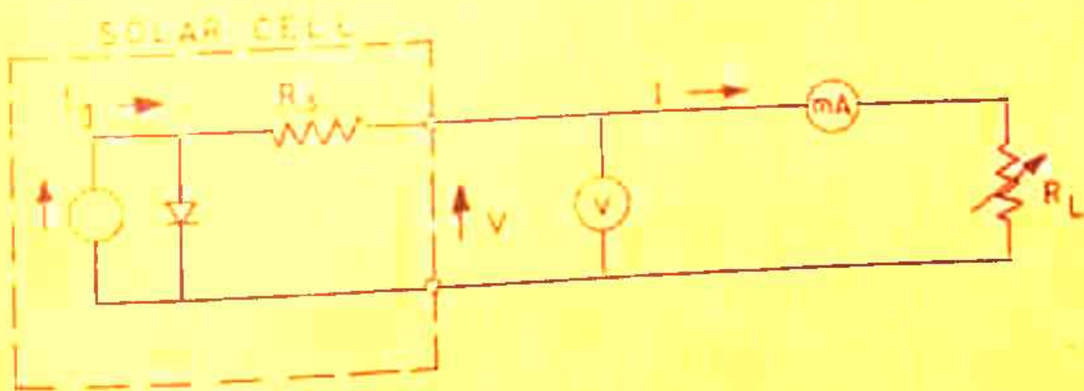

$$I = I_0 \left\{ \mathrm{EXP} \left[\frac{q(V + IR_s)}{AkT} \right] - 1 \right\} - I_g ; \; I \leq 0 \quad V \geq 0$$

FIG. 4.1 CIRCUIT DIAGRAM FOR MEASURING PHOTOVOLTAIC CHARACTERISTICS (CONSTANT ILLUMINATION)

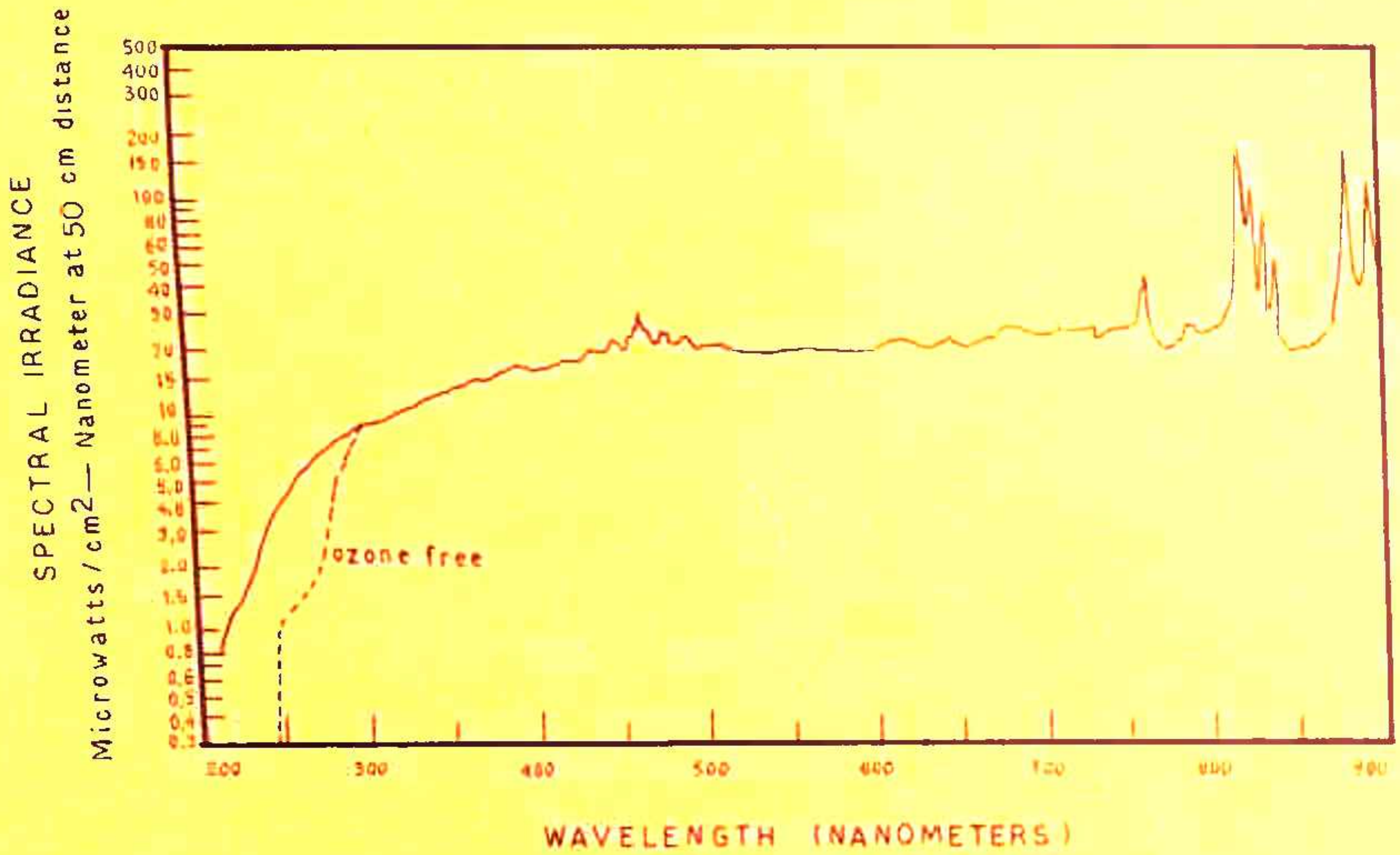

FIG. 4.2 TYPICAL OUTPUT SPECTRUM OF 1000 WATT XENON ARC LAMP.

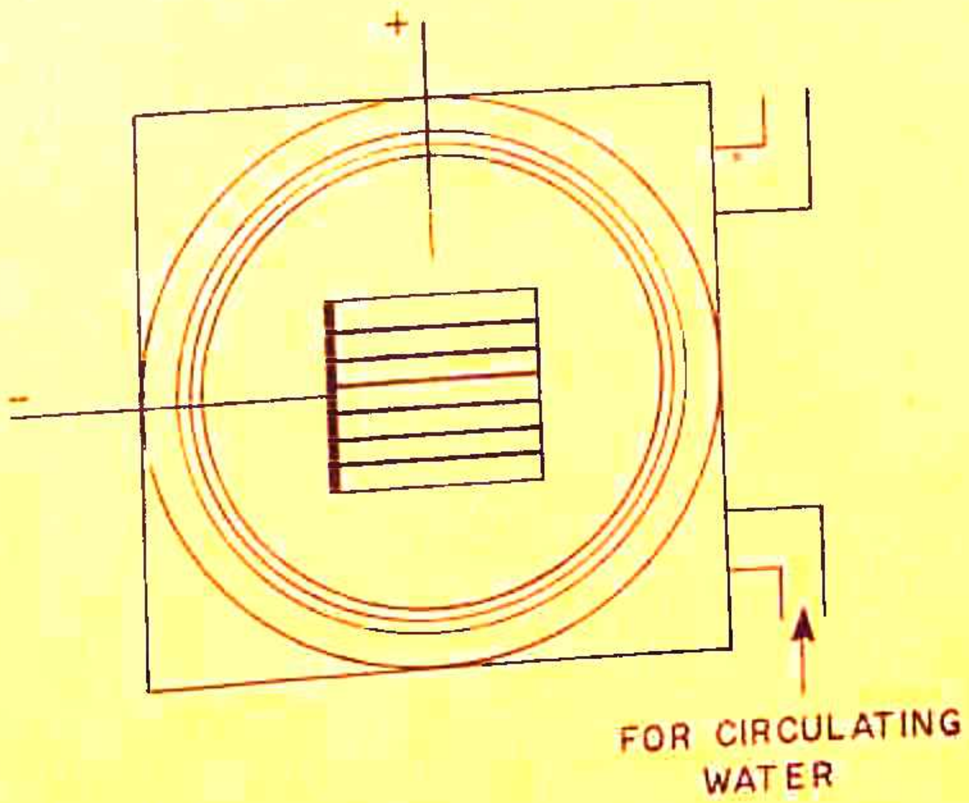

FIG. 4.3a SOLAR CELL MOUNT. (TOP VIEW)

Load (R_L) in the circuit was varied with the help of 1 K potentiometer. For some of the measurements an X-Y Recorder was used to trace the current voltage characteristics. The curve end points were verified with digital multimeter readings.

Intensity of illumination falling on the solar cell was varied by changing the distance of the cell from the lamp. Light intensity was measured with the help of a calibrated thermopile. The output of the thermopile was quoted to be linear with incident energy from the lower (measuring limit) up to 0.1 watt/cm^2 with only 2 % decrease in the sensitivity above the intensity of 50 mw/cm^2. E.M.F. for 0.1 mw/cm^2 intensity was quoted to be equal to 9.58×10^{-6} volts for the 8 m.m. slit which was used for our experiments. For measurement of illumination intensities above 0.1 watt/ cm^2, neutral density filters of known optical density (NPL, Delhi) were used to reduce the intensity of illumination falling on the thermopile. The thermopile sensitivity was quoted to be constant within 1 % over a wide range of wavelengths from approximately 1500 °A up to atleast 15 microns.

Standard solar cells No. 3000 and 3001 (Spectrolab, Heliotak, U.S.A.) were used to calibrate the experimental solar cells under AMO spectrum.

Experimental solar cells were 2 x 2 cms n on p space quality solar cells fabircated by the solar cell group at SSPL, Delhi. These solar cells have a finger grid pattern on the top surface consisting of six equally spaced grids and an ohmic bar. Electrical contacts on the n and p regions are made using metals Ti, Pd and Ag. Total exposed area of these cells is 90 % of the total cell area. The starting material of the cell is a p-type Boron-doped 10 ohm- cm Silicon of thickness about 300 microns. Phosphorous is diffused into it to form a n-type layer at the top of the slice. The thickness of the n layer is 0.4 micron approximately. An antireflection coating of TiO_2 , 650 Å thick is used to reduce the losses due to reflection at the surface. To protect the cell from intense radiation in outer space, a coverslip of Ce-doped glass is fixed on the top surface with a special adhesive. Table 4.1b gives the parameters of the experimental cells. Fig. 4.3b shows the I-V characteristics of a typical experimental cell under AMO illumination.

Table-4.1b

PARAMETERS OF EXPERIMENTAL SOLAR CELLS

Type	: n^+p
Base Resistivity	: 10 ohm cm
Cell dimensions	: 2 cm x 2 cm
Starting material	: p-type Boron doped silicon
Thickness of p region	: 300 microns approximately
Junction depth	: 0.4 micron approximately
Total exposed area	: 90 %
Thickness of TiO_2 antirefl-ection coating	: 650°A
Number of finger grids	: 6
Width of finger grids	: 200 microns each
Width of the ohmic bar	: 600 microns
Material of coverslip	: Ce-doped glass
Series resistance	: 0.4 ohm approximately (as measured by us)

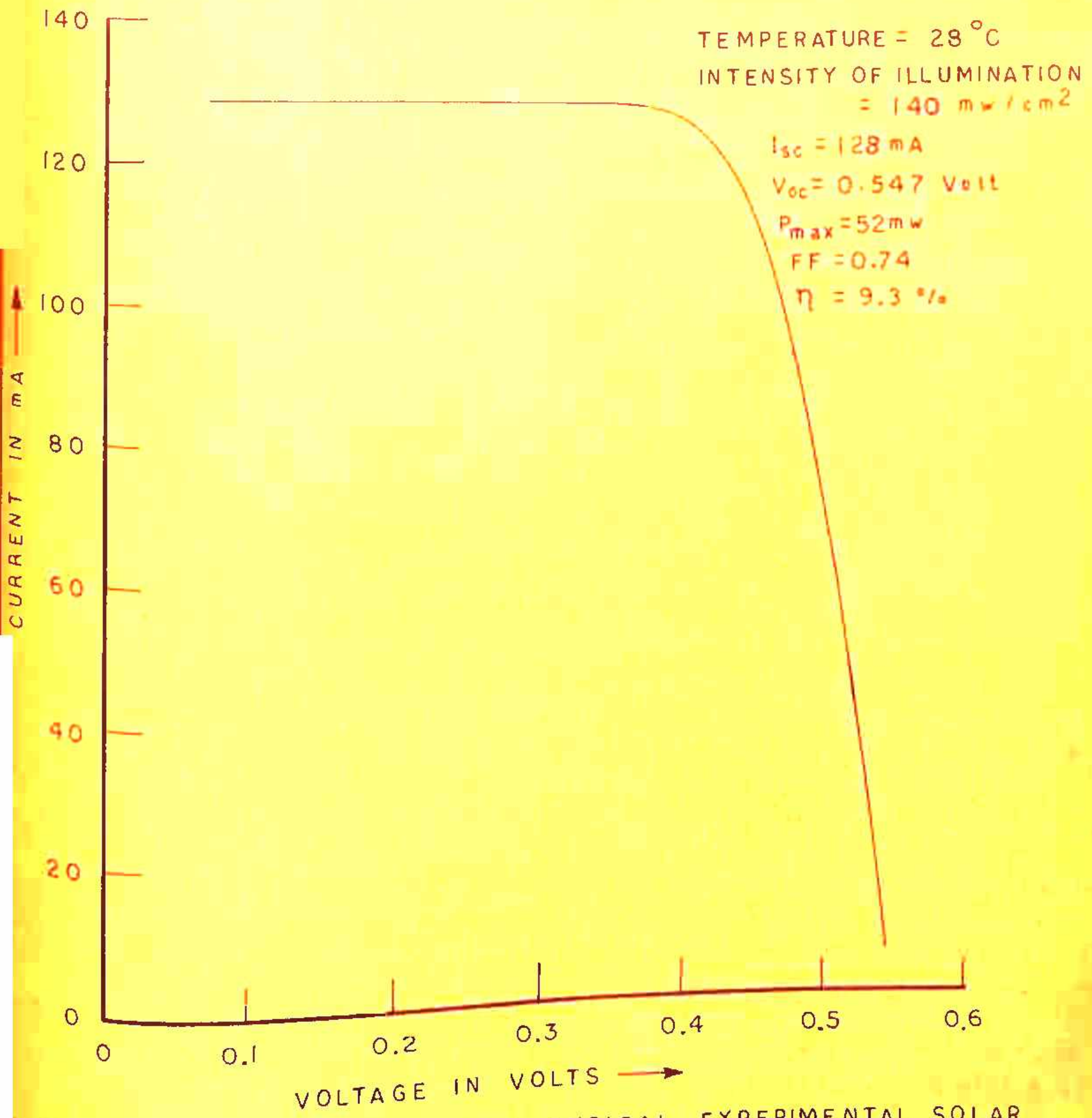

4.3b OUTPUT IV CURVE OF A TYPICAL EXPERIMENTAL SOLAR CELL UNDER AMO SOLAR SPECTRUM AT CONSTANT TEMPERATURE.

4.3 Experimental results and discussions:

In this section we will present the results of measurement of cell I-V characteristics, short-circuit current (I_{sc}), open circuit voltage (V_{oc}) at different illumination levels of known intensity. We will also discuss the variation of cell response parameters e.g. I_{sc}, V_{oc} and FF with the increase in light intensity. Resulting change in the cell efficiency is also discussed.

4.3.1 Photovoltaic I-V characteristics :

Photovoltaic I-V characteristics of several solar cells were measured at different intensities and a constant temperature of 28°C. Since, similar results were observed in each case, the I-V characteristics of only one cell under different illumination intensities are presented here. Figs. 4.4a, 4.4b and 4.4c show the photovoltaic characteristics at nine values of the intensity in the range 62.8 mw/cm^2 to 1.35 watt/cm^2 measured under the Xenon Arc lamp described in Sec. 4.2. The drastic change in the cell characteristics as the illumination is increased in quite apparent from these curves. The rapid degradation in these characteristics

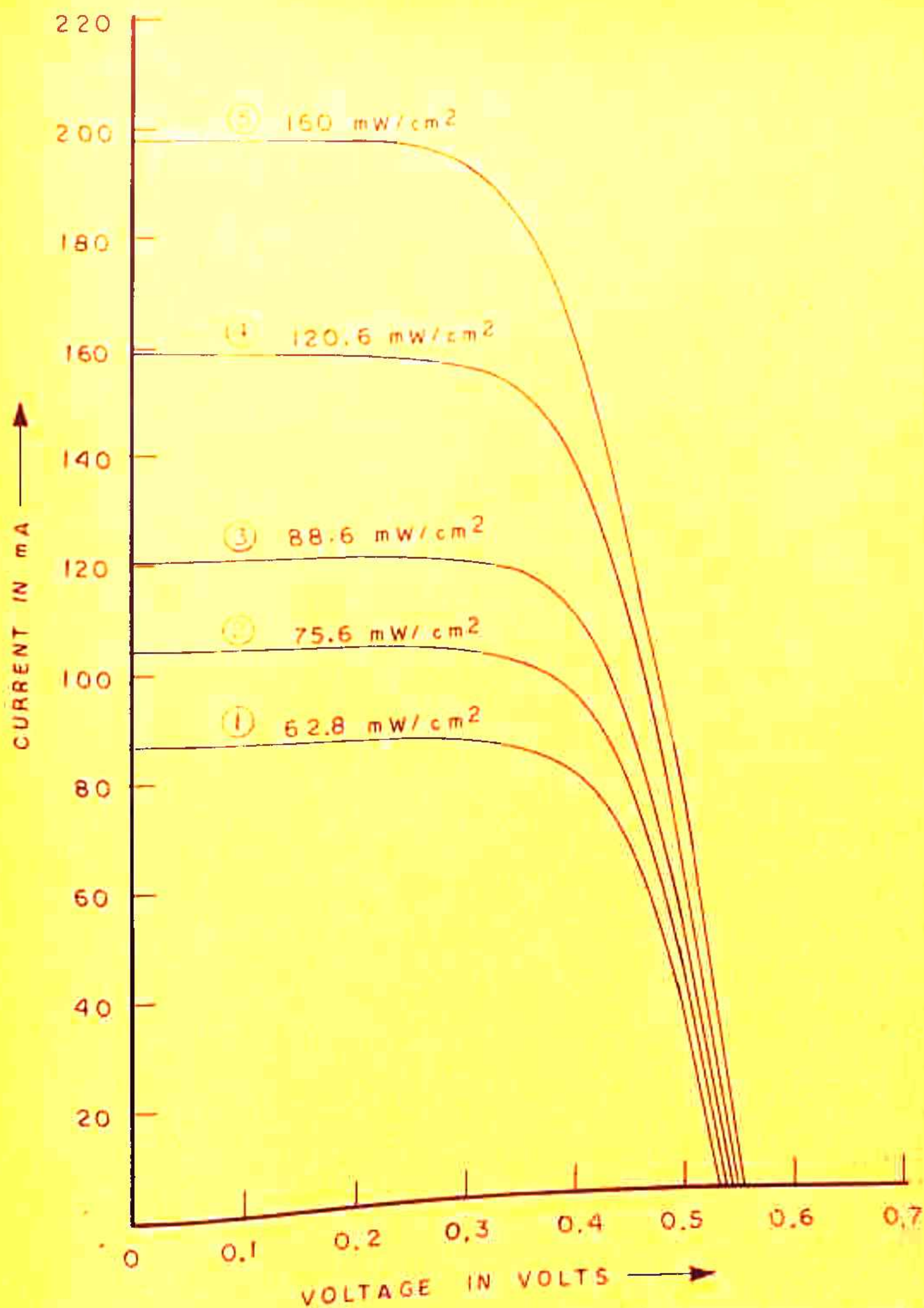

G.4.4a CELL P : I – V CHARACTERISTICS AT DIFFERENT ILLUMINATION LEVELS AND CONSTANT TEMPERATURE (28 °C)

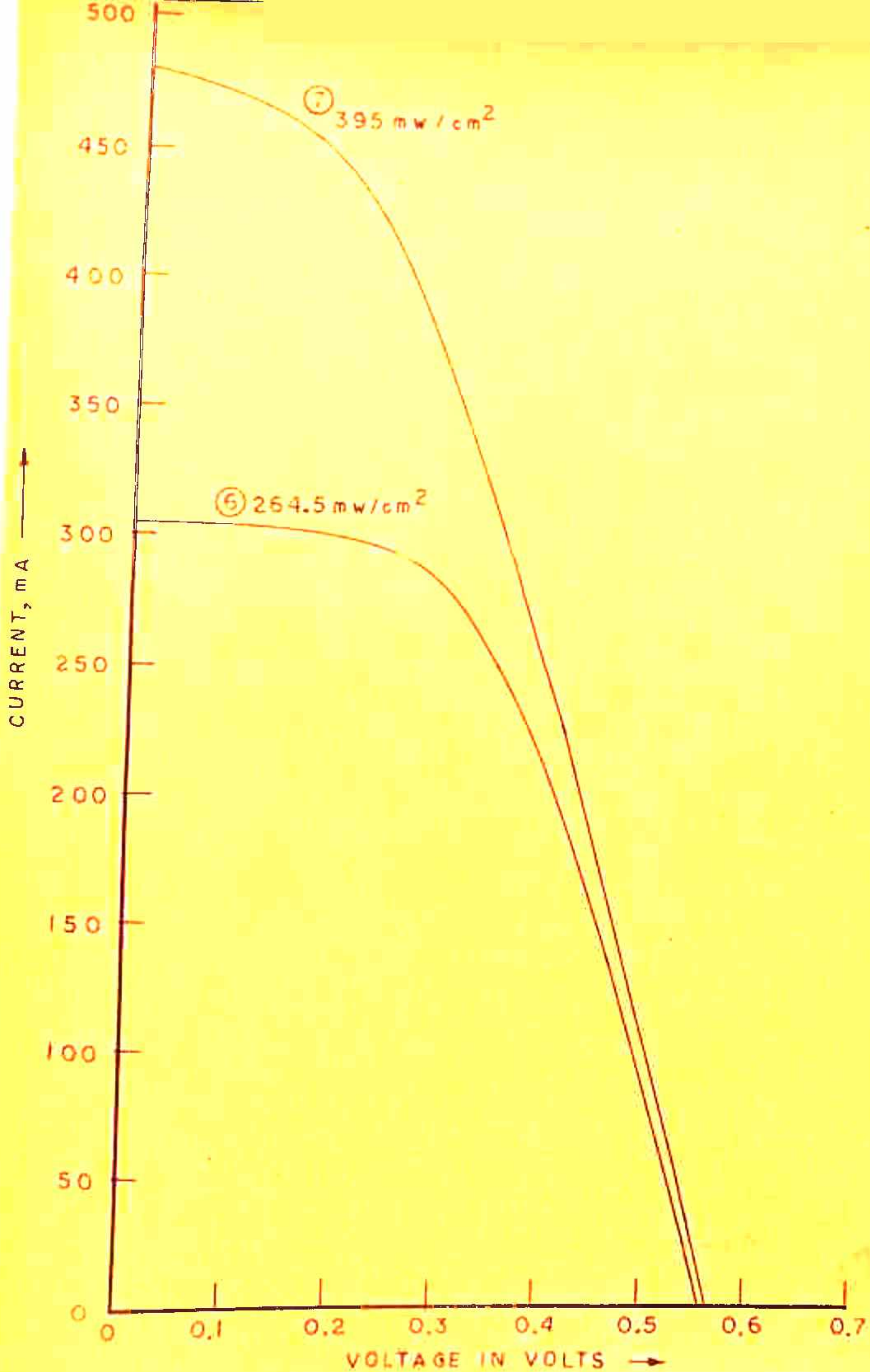

G.4.4b CELL P: I–V CHARACTERISTICS AT DIFFERENT ILLUMINATION LEVELS AND CONSTANT TEMPERATURE (28 °C)

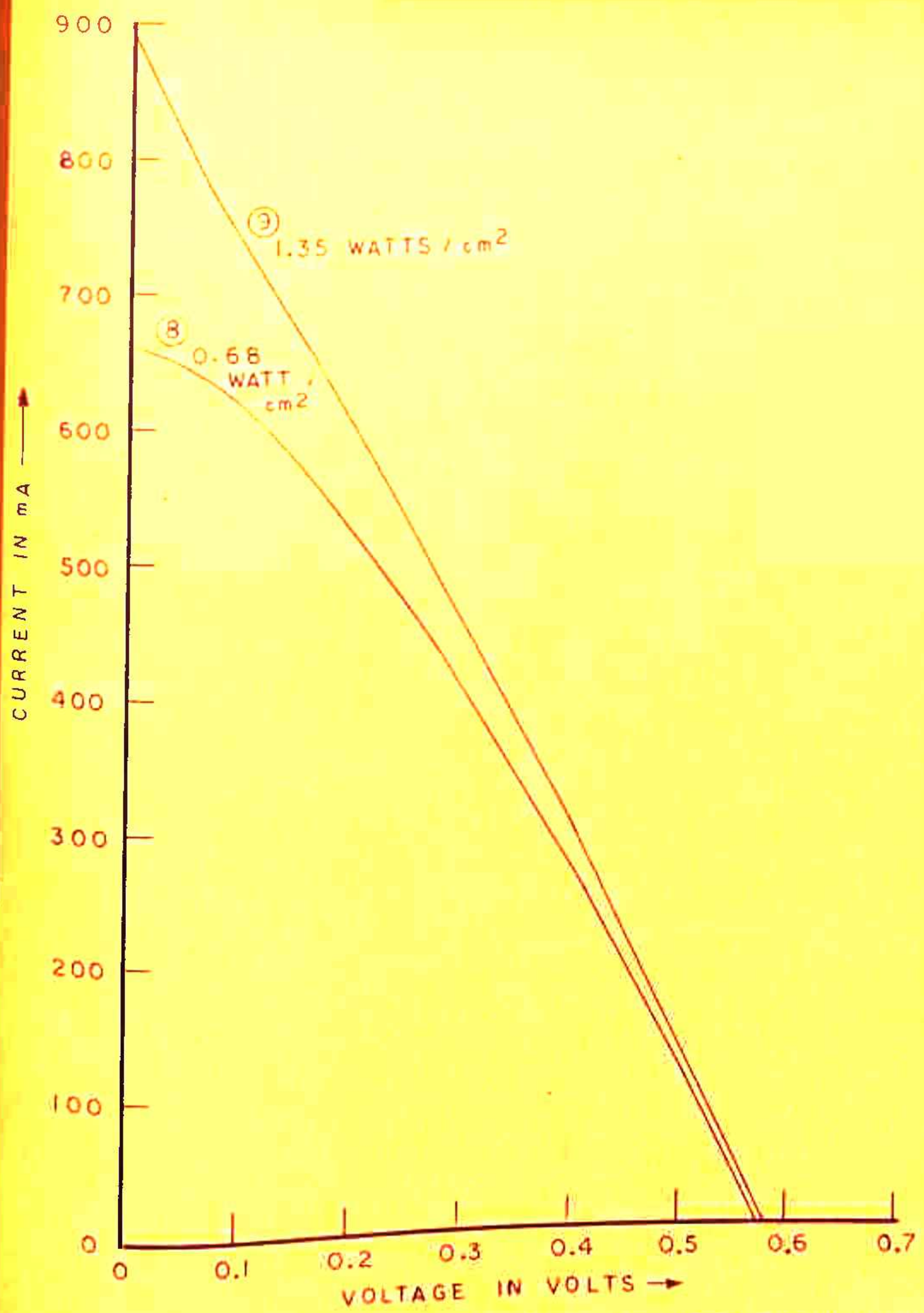

FIG.4.4C CELL P : I – V CHARACTERISTICS AT DIFFERENT ILLUMINATION LEVELS AND CONSTANT TEMPERATURE (28 °C)

with the increase in light intensity observed by us is similar to that observed by other workers (Wolf and Rauschenbach 1963, Castle 1976, Napoli et al 1977). The main reason for this degradation was found to be the high series resistance of the cells. At low intensities fairly good rectangular characteristics are obtained (4.4a) for intensities in the range 62.8 to 160 mw/cm^2. But, above this range of intensity, the effect of series resistance starts dominating (Fig. 4,4b) and at the intensity of 1.35 watts/cm^2, the characteristics become almost triangular (Fig. 4.4c) due to the severe effect of R_s. This observed trend in the characteristics at high intensities is as theoretically predicted in Chap. 3 (see secs. 3.6.1 and 3.8.6 and Fig. 3.11 also) for the finite series resistance of solar cells.

4.3.2 <u>Open-circuit voltage</u> :

The increase in V_{oc} with intensity is shown in Fig. 4.5. As predicted theoretically (see secs. 3.6.3 and 3.8.2), V_{oc} increases logarithmically as a function of intensity at low intensities (see Figs. 3.3 and 3.9 also). Above 160 mw/cm^2 intensity, the rate of increase of V_{oc} was found to be less than logarithmic. This could be explained as caused by the voltage

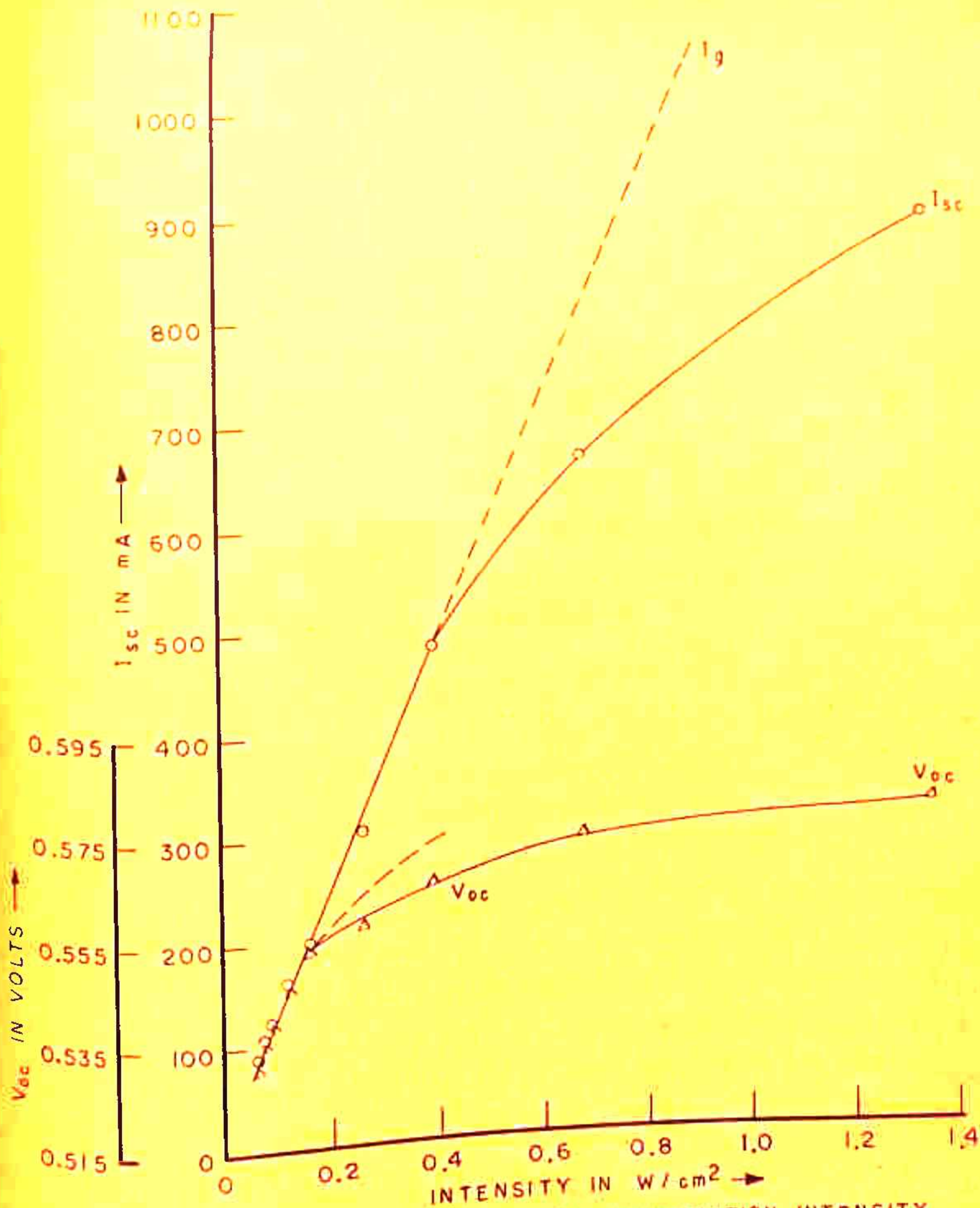

CELL P: I_{sc}, V_{oc} Vs ILLUMINATION INTENSITY

FIG. 4.5

drop V_p in the base region which will be subtracted from the open-circuit voltage at the junction of a n^+p cell (see sec. 3.7), thus causing the open circuit voltage to rise more slowly than predicted by theory. Moreover, the voltage drop in the base region is expected to saturate V_{oc} to a value much below the diffusion potential for a n^+p cell (Dhariwal et al 1976). For our experimental cell, V_{oc} tends to saturate at the value of about 0.58 volts in the illumination intensity range we have considered (Fig. 4.5).

4.3.3 Short-circuit current :

The short circuit current Fig. 4.5 increases linearly up to the intensity of the order of 400 mw/cm^2. Above this value of intensity there is a departure from linearity. Nonlinear variation of I_{sc} with the increase in light intensity has also been reported by Wolf and Rauschenbach (1963) for a cell of 3.5 ohms internal resistance. The dotted line in Fig. 4.5 represents the photogenerated current I_g which increases linearly with light intensity. The saturation of I_{sc} with the increase in intensity for a cell of finite series resistance has been discussed in Chap. 3 (see Fig. 3.12). We will show in Chap. 7 how a measure of

nonlinearity in I_{sc} Vs light intensity curve can be used to estimate the series resistance of solar cells.

4.3.4 Maximum power output (P_{max}) :

The voltage and current at the maximum power point are plotted in Fig. 4.6 as a function of light intensity. Initially V_m decreases rapidly with intensity then the rate of decrease becomes somewhat slower above the intensity of 400 mw/cm^2. Increase in I_m is almost linear up to 400 mw/cm^2 light intensity. Above this, I_m tends to saturate because of the effect of series resistance.

P_{max} as a function of light intensity is shown in Fig. 4.7. Initially P_{max} increases rapidly with the increase in light intensity. Above the intensity value of 0.7 watt/cm^2 it tends to become constant. Fig. 4.8 shows the shift in the maximum power point to lower voltages with the increase in intensity, caused by the increasing voltage drop IR_s in the solar cell which is directly subtracted from the junction voltage. This result is in agreement with that obtained theoretically considering the effect of series resistance in Chapter 3 (see Table 3.4).

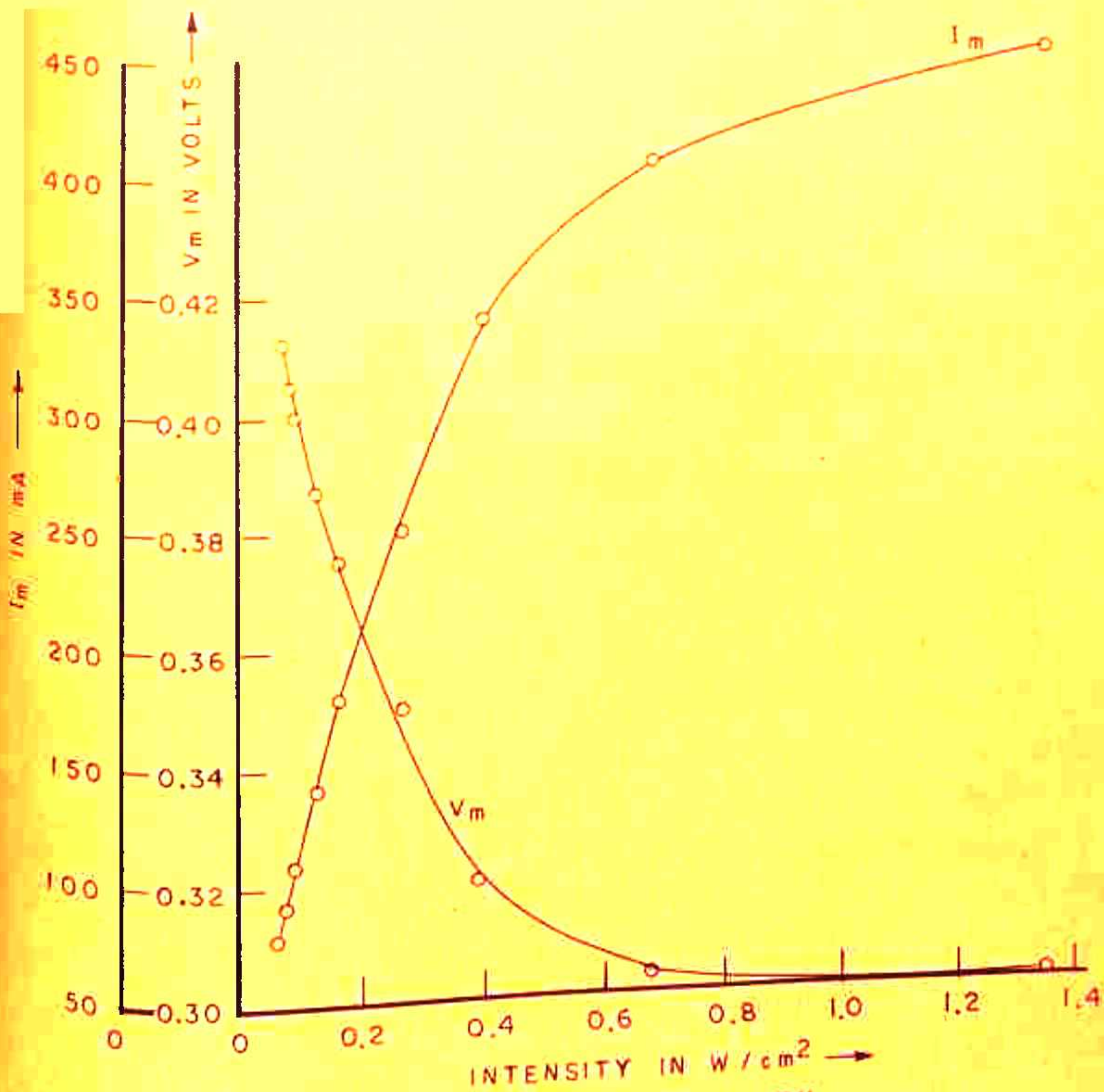

FIG.4.6 I_m, V_m Vs ILLUMINATION INTENSITY.

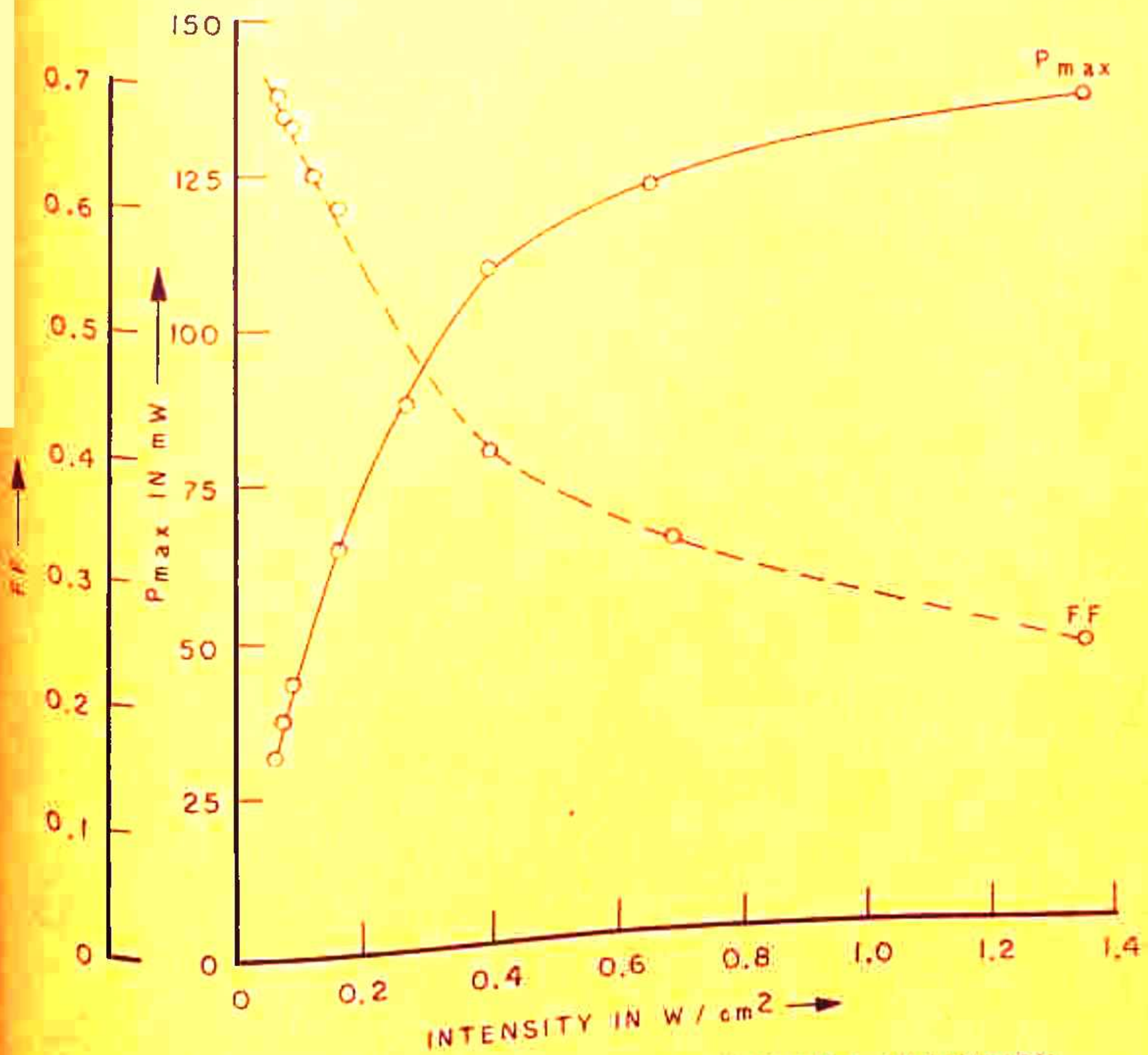

FIG. 4.7 CELL P : Pmax, FF Vs ILLUMINATION INTENSITY

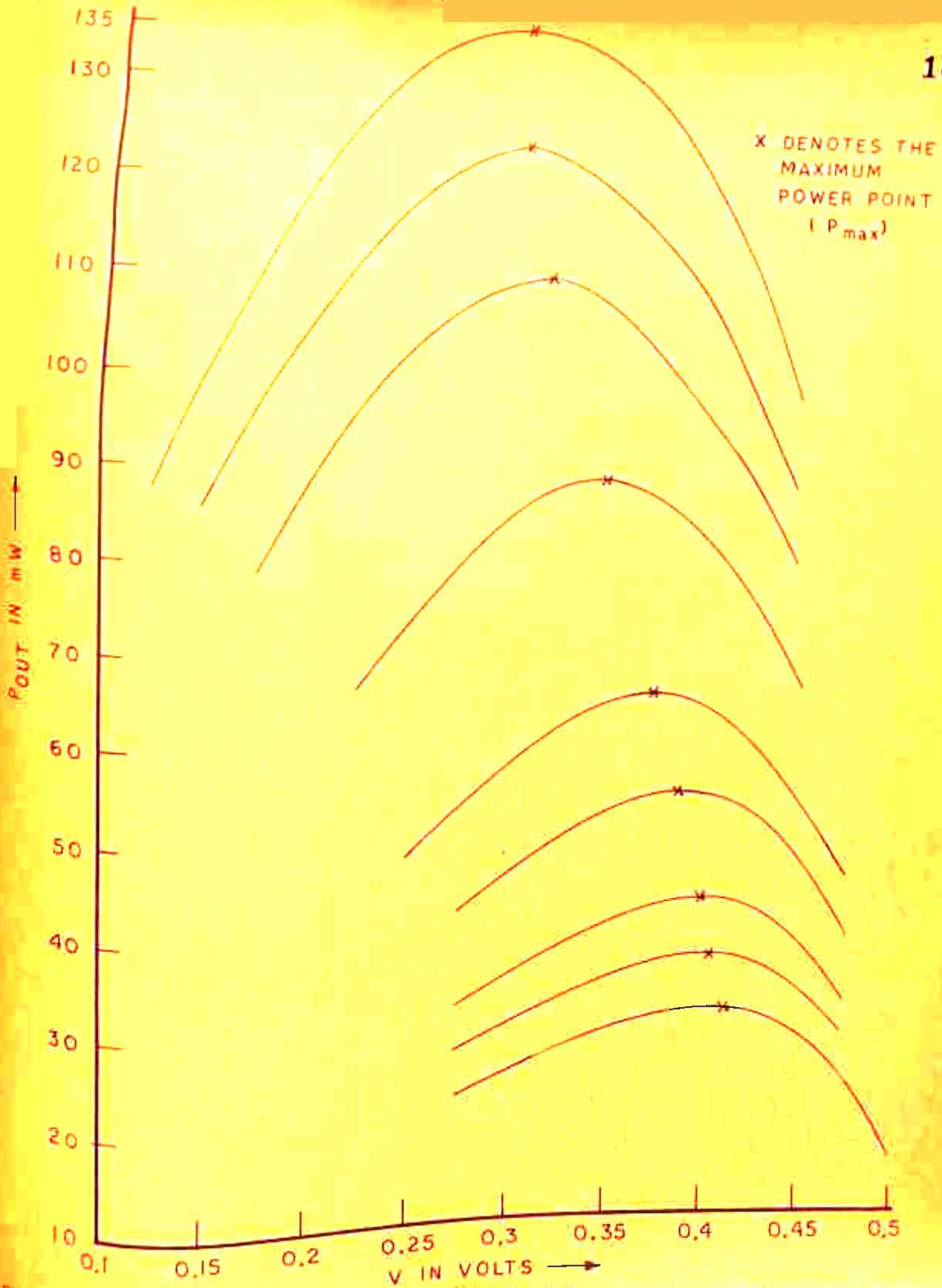

FIG. 4.8 CELL P: OUTPUT POWER (P_{OUT}) Vs VOLTAGE (V)

4.3.5 Cell efficiency (η) and fill factor(FF):

Efficiency of the experimental solar cell (Fig. 4.9) decreases rapidly as the light intensity is increased. It reduces from 12.6 % to 2.5 % as the light intensity is increased from 0.062 watt/cm^2 to 1.35 watt/cm^2. This decrease in efficiency is caused by the degradation in the fill factor as shown in Fig. 4.7. At a constant temperature, fill factor should increase with intensity provided the series resistance has a negligible effect (Hovel 1975 and Sterzer 1975). In our experimental cells, the decrease in FF with the increase in intensity seems to be caused by the high series resistance of the cells (See Table 3.4 also) .

4.4 Conclusions :

We see from the experimental results described in Sec. 4.3 that they confirm our theoretical predictions given in Chap. 3. These results can be summarized as follows :

(1) The effect of the series resistance in our experimental solar cells start dominating even at lower intensities in the intensity range considered by us. The continuous degradation

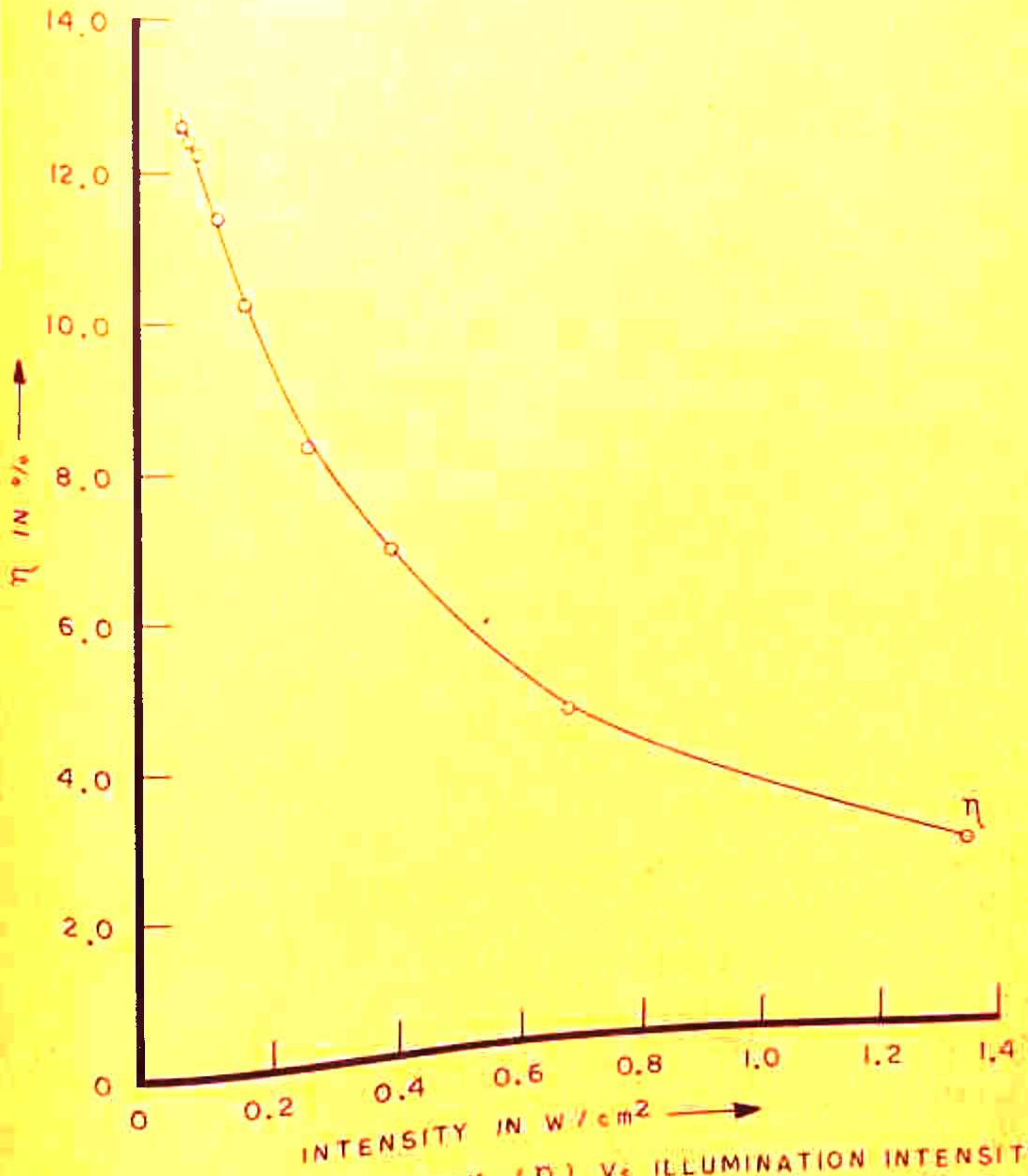

FIG. 4.9 CELL P: EFFICIENCY (η) Vs ILLUMINATION INTENSITY

in the I-V characteristics and the shift of P_{max} towards lower voltages with the increase in intensity is attributed to the strong effect of series resistance as discussed in Chap.3.

(2) The logarithmic variation of V_{oc} with the increase in intensity for low values of intensity and its tendency to saturate to a constant value at higher intensities is in qualitative agreement with the theoretically predicted results in Chap. 3.

(3) The observed linear increase in I_{sc} with intensity for low values of intensity and its departure from linearity at high intensities of illumination is also in accord with the theory given in Chap. 3 (see Fig. 3.12) for a finite resistance of the solar cell.

(4) The intensity of light at which the series resistance effects start dominating in a solar cell depends on the magnitude of its internal series resistance. The observed monotomic decrease in cell efficiency and fill factor

with increasing illumination level in the intensity range considered by us is a special feature of these types of cells and could be due to the high series resistance of these cells because of their high base resistivities (10 ohm-cm). The measured series resistance of these cells was found to be 0.4 ohm approximately. A more detailed study of the series resistance is given in Chap. 7. Because of the above mentioned high value of R_s, the degradation in the I-V characteristics, FF and efficiency with increasing intensity is as expected. Since, our experimental solar cells were designed for space applications, therefore, the base resistivity was chosen to be high so as to reduce the effect of radiation damage encountered in such situations. However, for terrestrial applications, it has been demonstrated by Burgess and Fossum (1977) that low base resistivity cells (0.3 ohm cm) give optimum performance for the illumination levels much higher than 1 sun. Their 0.3 ohm cm n^+/p silicon solar cells have exhibited conversion efficiencies above 11.8 % up to 90 suns. The

efficiency versus illumination level curve for these cells have been reported to peak at about 30 suns with a peak efficiency of 14 percent.

CHAPTER-5.

EFFECT OF TEMPERATURE ON THE RESPONSE OF SOLAR CELLS AT DIFFERENT LEVELS OF ILLUMINATION

5.1 Introduction :

In chapters 3 and 4 we discussed the response of solar cells to high intensity illumination assuming temperature of the cell to remain constant. In real situations, for space as well as terrestrial applications, particularly when concentrators are used, the actual temperature at which the solar cell operates does not remain constant. Thus, a knowledge of the temperature dependence of the response of solar cells is vital for design purposes and for the selection of proper materials for solar cells.

It is, therefore, important that the temperature dependence of the response of solar cells is properly studied and analysed. Various attempts on this problem (referred below) have already been made, but most of them have considered only certain limited aspects. There is, clearly a need for a detailed comprehensive study and analysis of the response of a solar cell in which the temperature dependence of all the important parameters such as α, E_g, n_i , V_D, D^*, τ^* and the photogenerated

carrier density Δn is taken into account. The objective of this chapter is to present such a comprehensive analysis by solving the actual steady state ambipolar transport eqn. 3.1 at different temperatures with the help of the numerical technique described in Sec. 3.3.

In space applications, the temperature of the solar cell can vary from 133°K to about 573°K (Yasui and Schmidt, 1970). For energy conversion on earth, the operational temperature of the solar cell depends, among other factors such as system geometry etc., on the concentration factor (Pfeiffer et al 1962, Savchenko and Tarnizhevskii 1969, Schueler et al 1975, Dean et al 1975, Fossum and Burgess 1976, Napoli et al 1977, Dalal and Moore 1977, Spaderna and Navon 1978) and in practical cases may vary from 300°K to 400°K. Design considerations of concentrator systems employing single-crystal silicon solar cells suggest that solar illumination levels between 50 and 100 suns are most cost effective (Fossum and Schueler, 1976) . If only passive cooling of the cell is used, or if the system is used in a combined photovoltaic-solar thermal total energy mode (Schueler et al 1975), the cells must operate at elevated temperatures (up to 400°K).

The early studies of temperature effects on the output characteristics of solar cells were made by Wysocki and Rappaport (1960), Pfeiffer et al (1962), Broder et al (1964), Walkden (1967), Jain et al (1968), Savchenko et al (1969), Shumka (1970), Yasui and Schmidt (1970), Lewise and Kirkpatrick (1970), Brandhorst and Hart (1970) and others. Decrease in V_{oc} and change in I_{sc} with temperature has been studied in detail both experimentally as well as theoretically. Shumka (1970) and Bhaumik and Sharon (1976) have discussed theoretically the increase in short-circuit current with temperature. Their results, however, do not predict the observed different behaviour in dfferent spectral regions.

More recently, Dean et al (1975), Napoli et al (1977) and Dalal and Moore (1977) have calculated the rise in temperature of the cell at different concentrations in actual operational conditions by setting up the heat balance equations for a particular system geometry. Their results are useful for design purposes.

Spaderna and Navon (1978) have analyzed a conventional n^+-p-p^+ solar cell structure for operation under highly concentrated sunlight and various levels of heat sinking. They have solved the two dimensional

temperature-dependent ambipolar carrier flow equations numerically to obtain the I-V characteristics of the device. The thermal problem is solved taking into account Joule heating and cooling as well as thermal effects due to minority carrier generation and recombination and the excess energy of photons. However, the variation of D^*, τ^*, V_D, n_i, E_g, V_{oc}, I_{sc} and the excess carrier density at different temperatures is not shown explicitly. Moreover, the change in the spectral response with temperature is not discussed at all.

Here, our aim is to discuss the temperature dependence of the various solar cell material parameters, and to use it to calculate the temperature dependence of the response of the solar cell under illumination. Results of some of the experiments done on the temperature dependence of cell response will be presented in Chap.6.

In this chapter, we present our calculations on short-circuit current, open-circuit voltage, I-V characteristics, fill factor, efficiency and spectral response as a function of temperature. Numerical results are reported in the temperature range 300 - 400°K, obtained by solving the one-dimensional temperature dependent ambipolar eqn. 3.1 for a p^+n, 1 ohm cm solar cell (cell parameters like d_1, d_2, s_1, s_2, N_A and N_D are same as

given in Table 3.1), using the numerical technique described in Sec. 3.3. All the assumptions made in Chap. 3 regarding the solar cell model are assumed to be valid here also. Calculations are done for AM 0 spectrum as well as for a monochromatic light of wavelength 0.6 micron for different levels of illumination. A short discussion of these results is given in Sec. 5.3, where the relevent published experimental work of other people is reported. In Sec. 5.2 we will discuss the temperature dependence of the various cell parameters e.g. absorption coefficient α and band gap E_g (Sec. 5.2.1) diffusion length L^* (Sec. 5.2.2), generation rate g' (Sec.5.2.3), intrinsic carrier concentration n_i (Sec. 5.2.4), diffusion potential V_D (Sec. 5.2.5), reverse saturation current I_o (Sec. 5.2.6) responsible for the change in I_{sc}, V_{oc}, P_{max}, FF, efficiency, I-V characteristics and spectral response of the solar cell with temperature as discussed in Sec. 5.3.

5.2 Temperature dependence of the various cell parameters:

In this section, we discuss the temperature dependence of each of the cell parameters separately.

5.2.1 Photon absorption coefficient:

The most important fundamental electron transition by photon absorption in silicon solar cells is indirect in nature. Direct transitions (Moss 1959) also occur for photons of energy greater than 2.5 eV, but at these energies most of the absorption is at the surface only.

According to Macfarlane et al (1958), four phonons with energies corresponding to the temperatures 212°K, 670°K, 1050°K and 1420°K participate in the indirect transitions. But, only phonons corresponding to θ_1=212°K and θ_2= 670°K are considered usually, since the other phonons are expected to be less effective (Mclean 1960). Then the total photon absorption coefficient α is generally expressed as

$$\alpha (\nu , T) = A(T) (h\nu - \bar{E}_g)^2 \qquad (5.1)$$

where

$$A(T) = a_1 \coth \frac{\theta_1}{2T} + a_2 \coth \frac{\theta_2}{2T} . \qquad (5.2)$$

$\bar{E}_g(T)$ is the optical band-gap and is less than the energy band gap by the exciton binding energy which is approximately equal to 0.01 eV for silicon. ν is the frequency of light .

The temperature dependence of $\alpha(\nu, T)$ arises from the temperature dependence of A(T) and $\bar{E}_g(T)$. Thus,

$$\frac{d\alpha(\nu,T)}{dT} = \frac{\partial\alpha(\nu,T)}{\partial A}\frac{dA}{dT} + \frac{\partial\alpha(\nu,T)}{\partial\bar{E}_g}\frac{d\bar{E}_g}{dT}. \qquad (5.3)$$

The values of constants a_1 and a_2 are obtained by comparing eqn. 5.1 with the measured data of Dash and Newman (1955). Numerical values of a_1 and a_2 in eqn. 5.2 as determined by Shumka (1970) are

$$a_1 = 1.28 \times 10^3/(eV)^2 \text{ cm},$$

and $$a_2 = 1.13 \times 10^3/(eV)^2 \text{ cm}.$$

The analytical expression for the experimental $\alpha(\nu,T)$ in cm^{-1} is :

$$\alpha(\nu,T) = \left[1.28 \times 10^3 \coth\frac{212}{2T} + 1.13 \times 10^3 \coth\frac{670}{2T}\right] \times (h\nu - \bar{E}_g)^2. \qquad (5.4)$$

The above analytical expression represents a good fit to the data for $h\nu < 2.35$ eV at 300°K and $h\nu < 2.25$ eV at 77°K. For higher energies the analysis predicts lower

values than observed because additional absorption is expected from direct transitions as well as indirect transitions to other minima in the conduction band. The photon absorption spectrum for $h\nu > 2.5$ is not expected to make any significant contribution to the photogenerated current and therefore, we have used the analytical expression given in eqn. 5.4 without any modification. More recently, experimentally measured values of the absorption coefficient for silicon are given by Runyan (1967). But in the absence of values of α in the whole wavelength range of interest and an experimental fit to this data, we have used eqn. 5.4 for our calculations. Moreover, since no measurements of absorption coefficient above room temperature are available to our knowledge, we have used the values of a_1 and a_2 given in eqn. 5.4 for calculating the absorption coefficient at higher temperatures also.

Optical band gap:

Optical band gap $\bar{E}_g(T)$ is given by

$$\bar{E}_g(T) = E_g(T) - E_{ex}, \tag{5.5}$$

where $E_g(T)$ is the energy band gap and E_{ex} is the exciton binding energy approximately equal to 0.01 eV for silicon. The temperature dependence of $\bar{E}_g(T)$ arises from the temperature dependence of $E_g(T)$. $\bar{E}_g(T)$ varies almost quadrati-

cally with temperature as follows:

$$\bar{E}_g(T) = (1.156 - 5.025 \times 10^{-7}\, T^2) \text{ eV} \quad . \qquad (5.6)$$

Above expression is based on the experimental data of Macfarlane et al (1958).

The absorption coefficients are calculated in this manner in the wavelength range 0.4 -1.1 microns and the temperature range 300 - 400°K, which is the range used in the calculation of the response of the solar cell. Fig. 5.1 shows the calculated values of α as a function of temperature(T) for three wavelengths in the range mentioned earlier. As is clear from the graph, increase in α with T is much more for longer wavelength (λ=1.0 μm) as compared to short wavelengths (λ = 0.4 μm). Fig. 5.2 gives the plot of α Vs λ at 300°K and 400°K in the whole wavelength interval 0.4 - 1.1 micron. α is shown to increase with T for all wavelengths. We have taken into account the variation of band gap with temperature while calculating the absorption coefficients at different temperatures. However, while evaluating the integral in the whole wavelength range the band gap variation will enter again in the limits of integration λ_1 to λ_2 (see eq n. 3.42). Variation of $\bar{E}_g$ determined by using eqn. 5.6

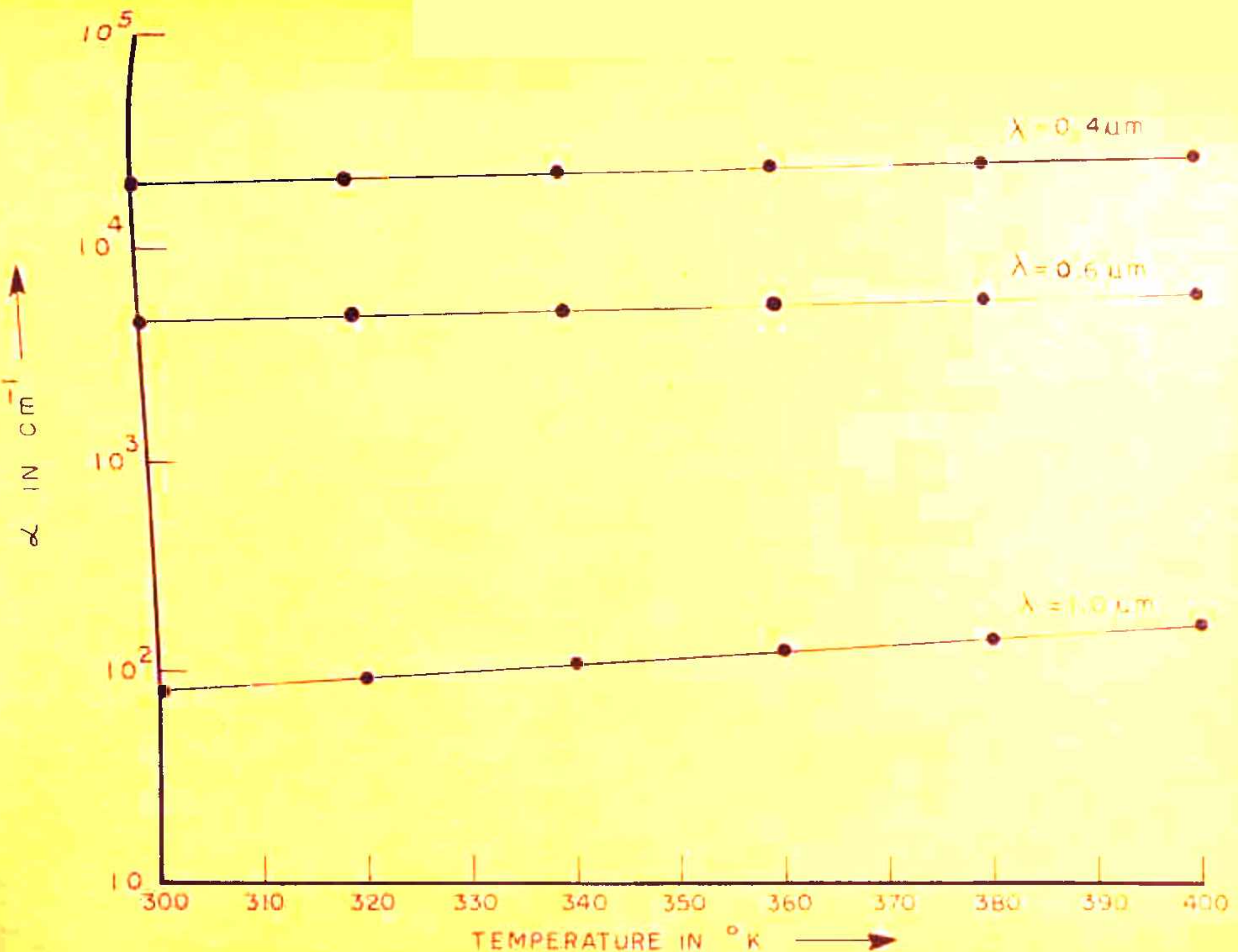

FIG. 5.1 CALCULATED α AS A FUNCTION OF TEMPERATURE FOR DIFFERENT WAVELENGTHS

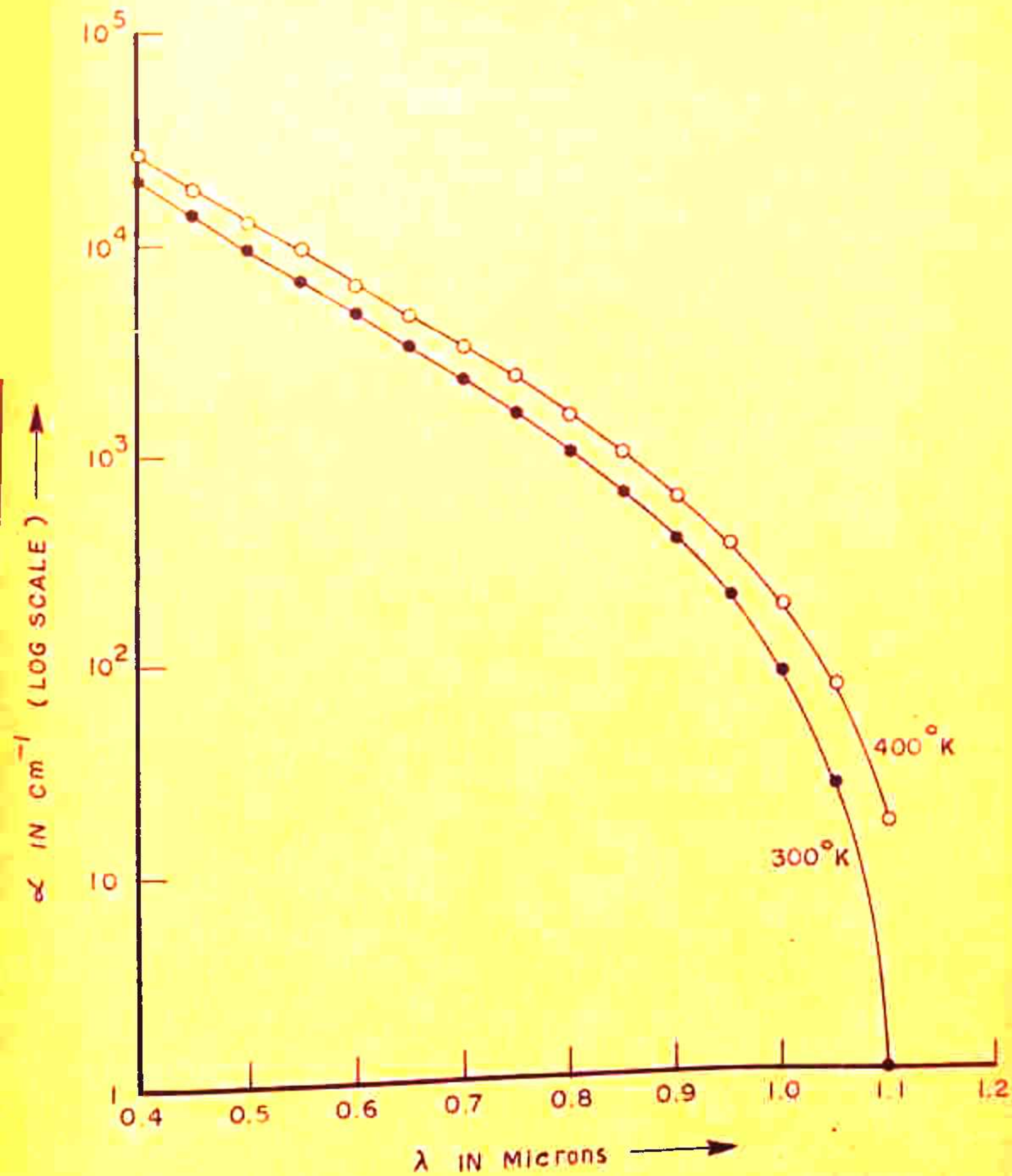

FIG. 5.2 α Vs λ AT DIFFERENT TEMPERATURES.

is shown in Fig. 5.3 as a function of temperature which shows a decrease in $\bar{E}_g$ with temperature.

5.2.2 Diffusion length :

The ambipolar diffusion length L^* of the excess carriers in the p and n regions of the solar cell depends on their diffusion coefficients and lifetimes. Therefore, to calculate the temperature dependence of the diffusion length we have to study the temperature variation of D^* and τ^* separately. First we discuss the change in τ^* with temperature.

If we assume that the temperature dependence of the lifetime is determined by the single level recombination statistics of [illegible], Shockley and Read (1952) and Hall (1952) (see eqn. 1.18 also), the life time in the n type region is given by (for low level injection)

$$\tau_p^* = \tau_{po}\left(1 + \exp\left(\frac{E_T - E_F}{kT} \right)\right) \tag{5.7}$$

Similarly, for p type region eqn. 1.18 reduces to

$$\tau_n^* = \tau_{no} + \tau_{po} \exp\left(\frac{E_T + E_F - 2E_i}{kT} \right) \tag{5.8}$$

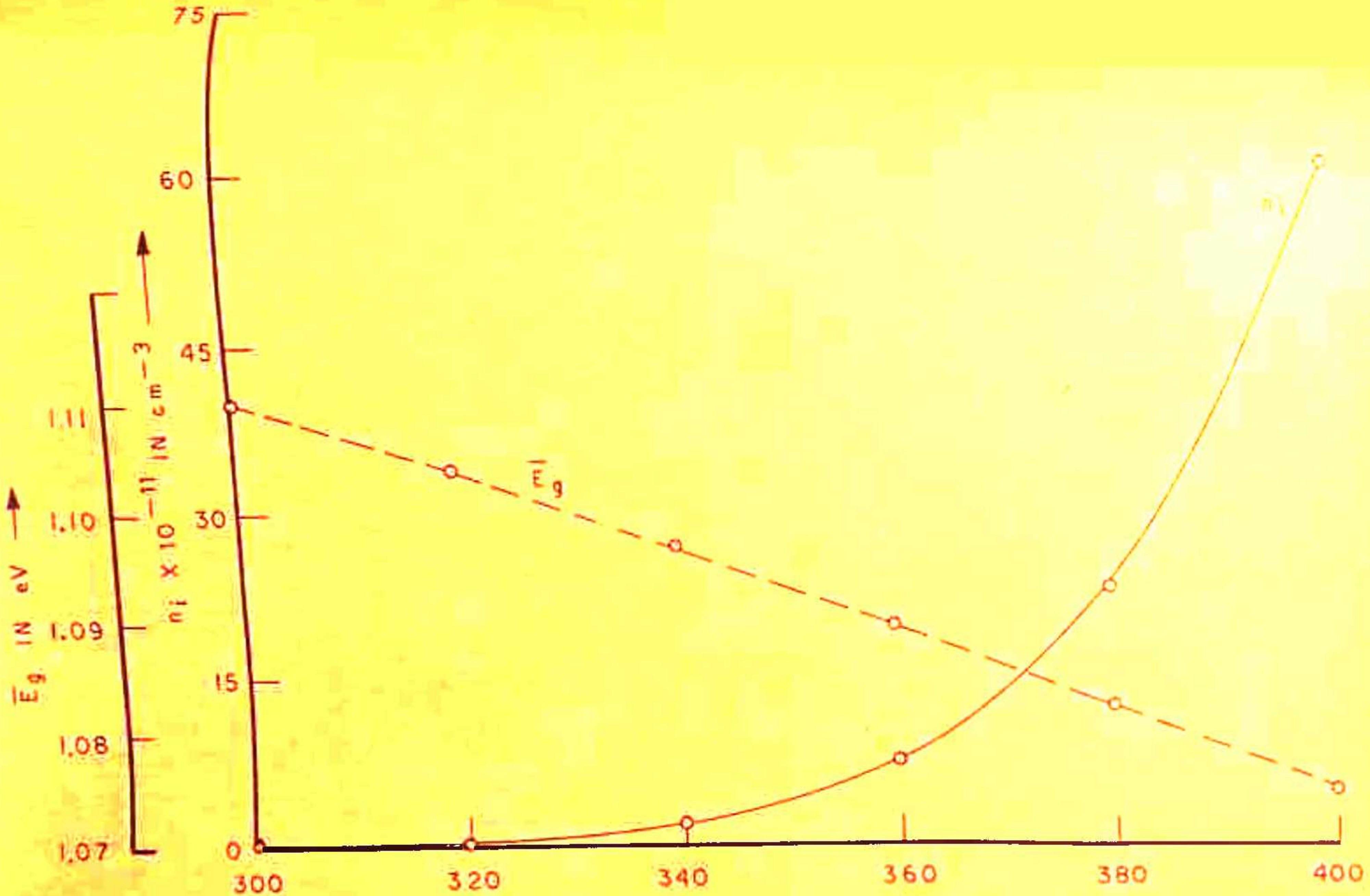

FIG.5.3 $\overline{E}_g$ AND n_i V_s T

The temperature dependence of the lifetime arises from the exponential terms in the foregoing equations. If the difference between E_F and E_T is large compared to kT, the exponential terms in eqns. 5.7 and 5.8 are negligible and they remain negligible as the temperature is increased until E_F is within a few kT of E_T. The temperature at which the lifetime increases depends upon the doping level and the trap level. For our analysis, we have assumed the trap level to be 0.05 eV below the intrinsic Fermi level E_i. In this case the variation of τ^* with temerature is found to be very small (less than 2 %) in the temperature range considered, and is therefore negligible. The effects of Auger recombination are not taken into account.

The variation of D^* with temperature depends on the temperature dependence of the excess carrier density Δn and the hole and electron diffusion coefficients D_n , D_p (see eqn. 3.2). For low intesnsities D^* reduces to the minority carrier value (see Sec. 3.2). Diffusion coefficient of minority carriers is related to that of the carrier drift mobility μ by the Einstein's relation (see eqns. 1.5 and 1.6)

$$D = (kT/q) \mu \quad (5.8a)$$

The magnitude of μ and its temperature variation are dependent on Scattering mechanisms in the semiconductor. Lattice and impurity ion scattering are most dominant. We give below the empirical expressions for the mobilities due to both types of scattering (Conwell, 1952, 1964). Impurity scattering mobility has been calculated by using the following empirical expression given in terms of the background concentration C_B:

$$\mu_I = 4.7 \times 10^{17} \left(\frac{m_o}{m_{eff}} \right)^{1/2} \frac{T^{3/2}}{C_B \ ln(1+4.5x10^8 \ T^2 C_B^{\ 2/3})} . \qquad (5.9)$$

For our calculations we have assumed free carrier mass m_o to be equal to the effective mass m_{eff}. Lattice (thermal) scattering mobility is calculated by using the following empirical expressions :

$$\mu_{L_n} = 2.1 \times 10^9 \ T^{-2.5} \ cm^2/V \ sec \text{ for electrons} \qquad (5.10)$$

and $$\mu_{L_p} = 2.3 \times 10^9 \ T^{-2.7} \ cm^2/V \ sec \text{ for holes}. \qquad (5.11)$$

Total carrier mobility μ is determined by impurity mibility μ_I and the lattice mobility μ_L:

$$\frac{1}{\mu} = \frac{1}{\mu_I} + \frac{1}{\mu_L} \qquad (5.12)$$

from which the temperature dependence of μ can be derived. As seen from eqn. 5.9 the mobility μ_I is, to a first approximation, inversely propotional to impurity-ion density and thus μ_I will be strongly dependent on the doping density and on the type of dopant present.

In our discussion we have assumed the absence of traps. Traps may play a dominant role in determining the magnitude and temperature dependence of mobility. There-fore, experimental data on the temperature variation of mobility is expected to give more reliable information. The minority carrier diffusion coefficient values can be determined from the mobility value using eqn. 5.8a. In the n region D^* is found to decrease with T whereas in the p region it is found to increase with T. This is due to the fact that diffusion coefficient is a strong function of doping density through mobility.

Using the relation, $L^* = \sqrt{D^* \tau^*}$ (5.12a) diffusion length can be calculated at a particular tem-erature. For low level limit L^* is simply the minority carrier diffusion length.

For Higher illumination intensities both D^* and τ^* become functions of Δn, Δp also (see Sec. 3.2) and

therefore, it is necessary to calculate the excess carrier densities to estimate D^* and τ^*. We have calculated the average values of Δn, Δp for different light levels by solving the ambipolar eqns. 3.10 and 3.11 numerically in the p and n regions of the solar cell. $\Delta n_{average}$ and $\Delta p_{average}$ are shown as a function of temperature in Figs. 5.4 and 5.5 respectively. As is clear from the graph that $\Delta n_{average}$, $\Delta p_{average}$ decrease with the increase in temperature. Fig. 5.6 shows the variation in L_n^* and L_p^* with temperature in the p and n regions respectively for two values of $N_o = 10^{17}$ and 10^{21} $cm^{-2}sec^{-1}$. In p region L_n^* increases slowly (its value being same for the two values of N_o) with T due to the increase in D_n^* with T. L_p^* decreases linearly with the increase in T.

5.2.3 <u>Generation rate:</u>

Generation rate g' is given by (see eqn. 3.9 also)

$$g' = N_o \alpha e^{-\alpha(x + d_1)}$$

We see from the above expression that the generation rate depends upon the temperature through the absorption coefficient α. The temperature dependence of α has been discussed in Sec. 5.2.1. In addition, the generation rate has also an indirect and implicit dependence on the temperature

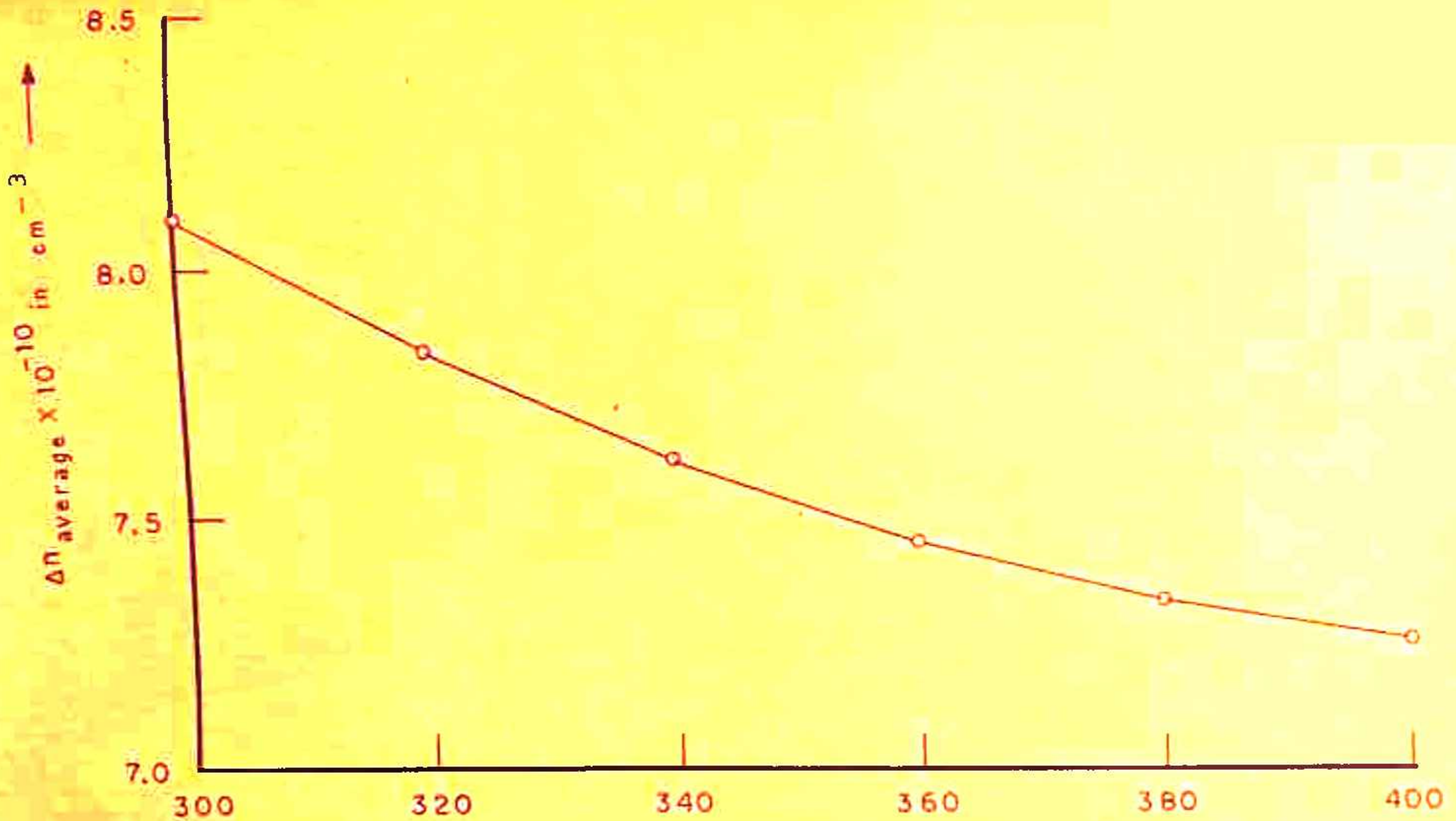

FIG. 5.4 EXCESS CARRIER DENSITY ($\Delta n_{average}$) Vs T IN p REGION FOR $\lambda = 0.6$ μm.

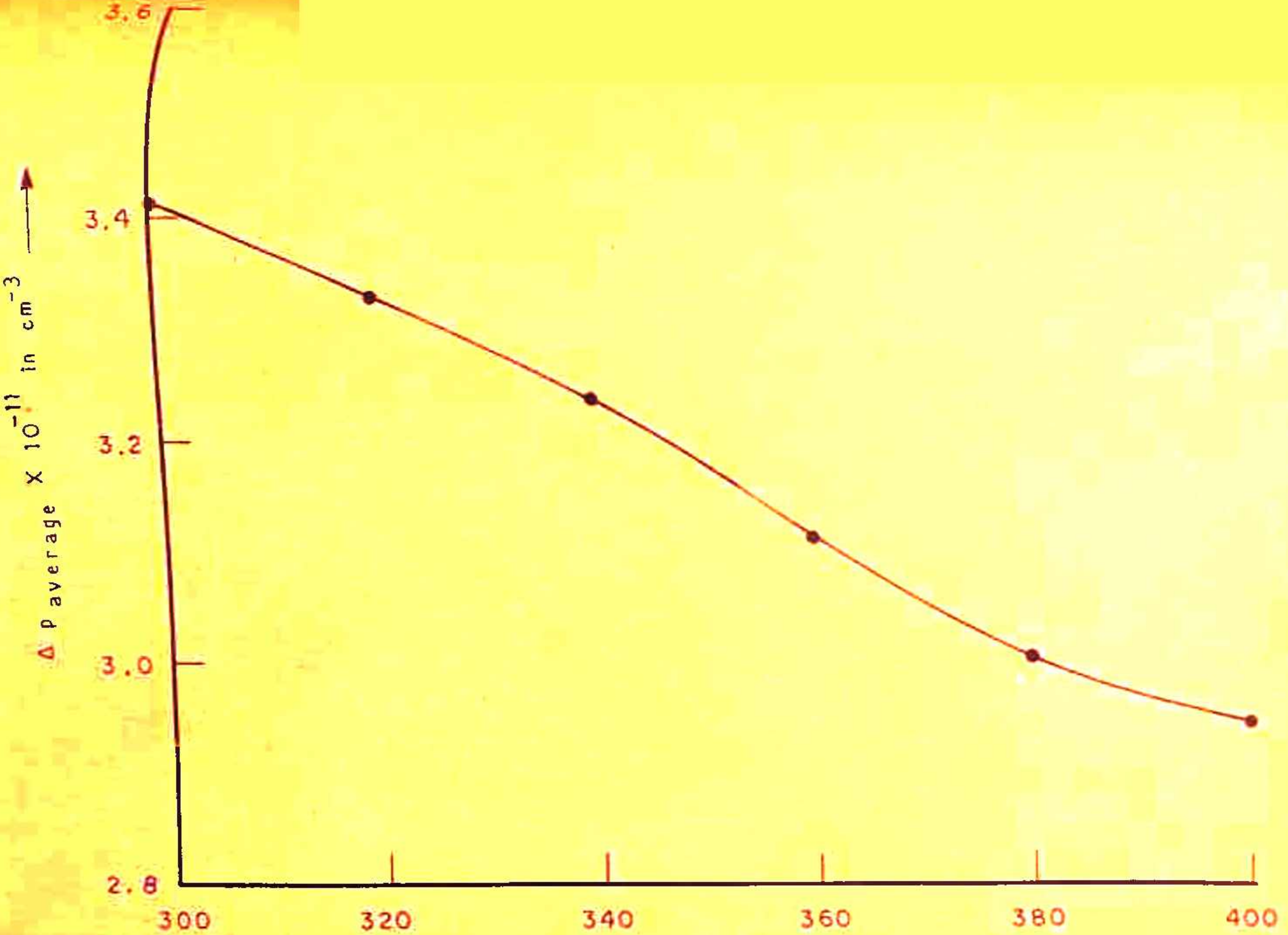

FIG.5.5 EXCESS CARRIER DENSITY ($\Delta p_{average}$) Vs T IN n REGION FOR $\lambda = 0.6\ \mu m$.

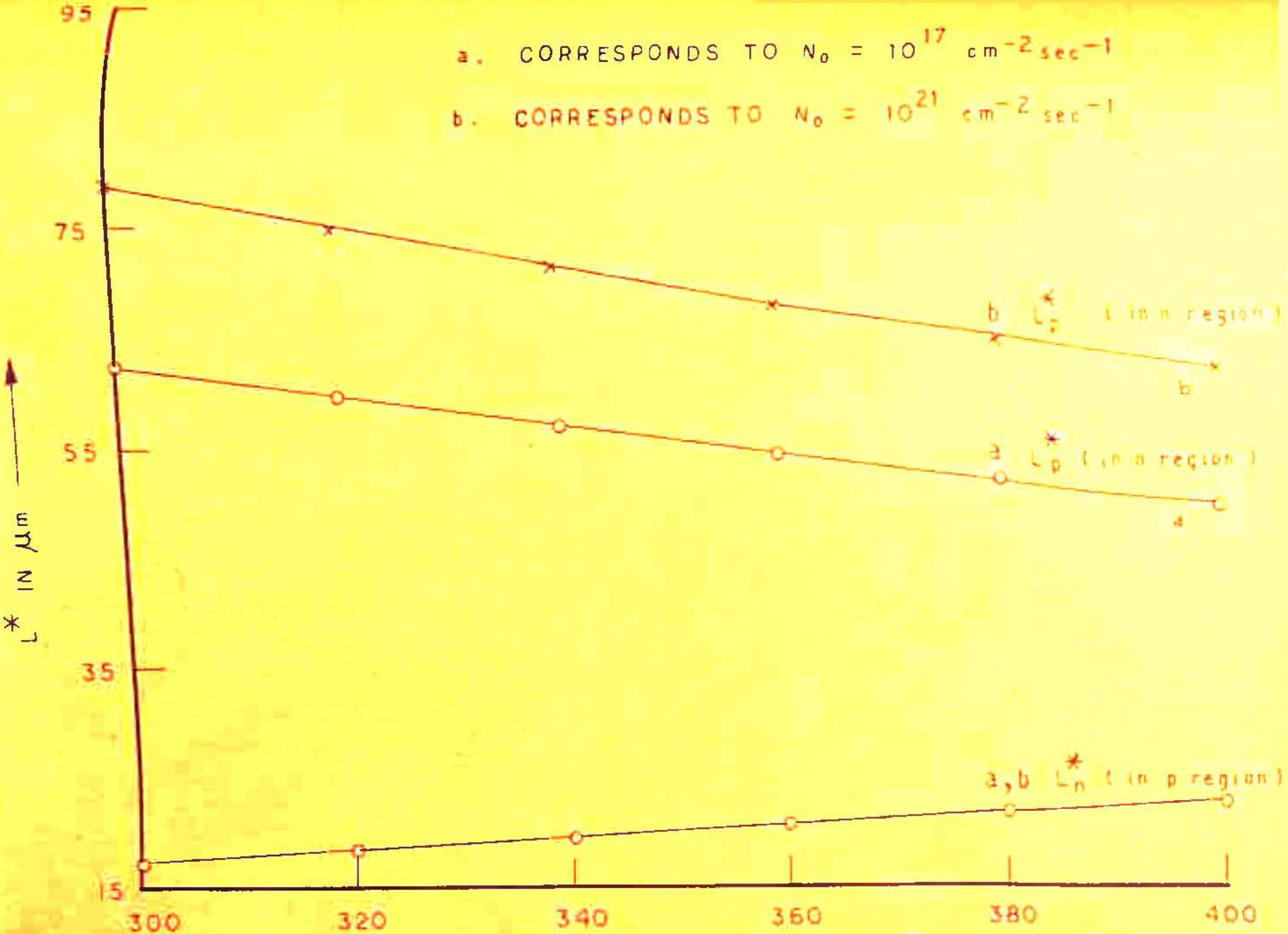

FIG.5.6 AMBIPOLAR DIFFUSION LENGTH (L^*) Vs TEMPERATURE .

through the band gap, in case of the composite light. This arises because band gap is a function of temperature as discussed in Sec. 5.2.1. Due to the decrease in the band gap with temperature, there is a consequent increase in the number of photons which are effective in creating electron hole pairs resulting in an increase in the generation rate. This, indirect temperature dependence of the generation rate is, however, quite small and is usually neglected in the range of temperature in which we are presently interested. We shall also neglect this dependence and consider only the dependence of the generation rate which arises through the absorption coefficient α .

5.2.4 Intrinsic carrier concentration :

The intrinsic carrier concentration n_i is a rapidly varying function of temperature as is clear from the well known expression (see e.g. Mckelvey, 1966):

$$n_i(T) = 2 \left(\frac{2\pi (m_p m_n)^{1/2} kT}{h^2} \right)^{3/2} \exp(-E_g(T)/2kT) \qquad (5.13)$$

Fig. 5.3 shows the increase of n_i with T.

5.2.5 Diffusion potential:

Temperature dependence of the diffusion potential (V_D) is given by

$$V_D = \frac{kT}{q} \ln \frac{N_D N_A}{n_i^2(T)}$$

Fig. 5.7 shows that V_D decreases almost linearly with the rise in temperature.

5.2.6 Reverse saturation current :

In eqn. 3.35 both I_o and I_o' correspond to the reverse saturation current I_o in eqn. 1.39. The temperature dependence of I_o and I_o' (see eqns. 3.36 and 3.37) arises because of the variation in L^*, D^* and n_i^2 as discussed in Secs. 5.3 and 5.5. Rapid increase in I_o and I_o' with T is presented in Fig. 5.8.

5.3 Results and Discussions :

We have solved the ambipolar diffusion equations 3.10 and 3.11 for different values of temperature taking into account the temperature dependence of the various cell parameters as discussed in Sec. 5.2. The temperature dependence of the cell response thus determined is presented in this section in the temperature range 300^oK to 400^oK (in steps of 20^oK) for a $p^+ n$ si solar cell (cell parameters d_1, d_2 s_1, s_2, N_A, N_D same given in Table 3.1)

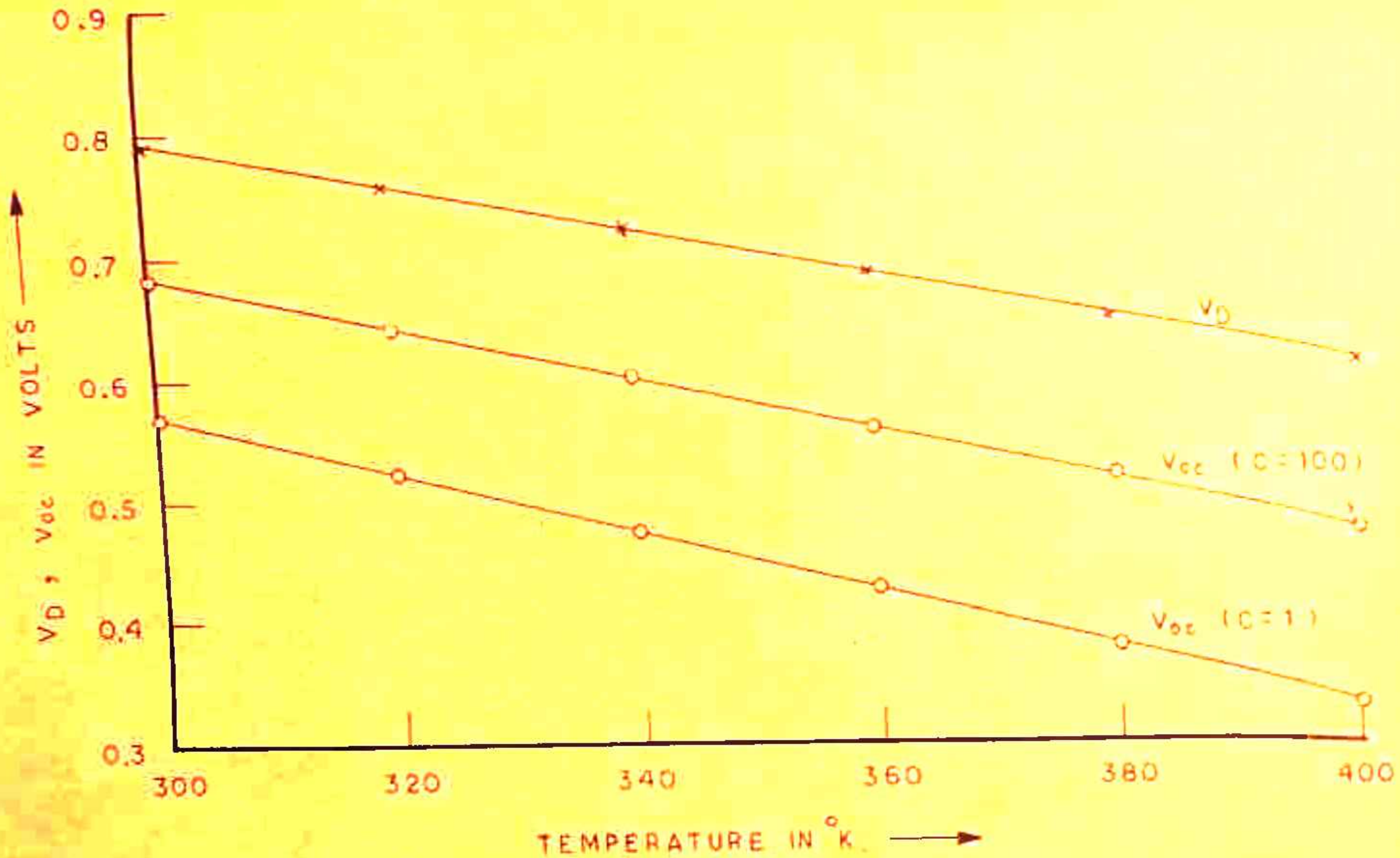

FIG. 5.7 V_D , V_{oc} Vs T

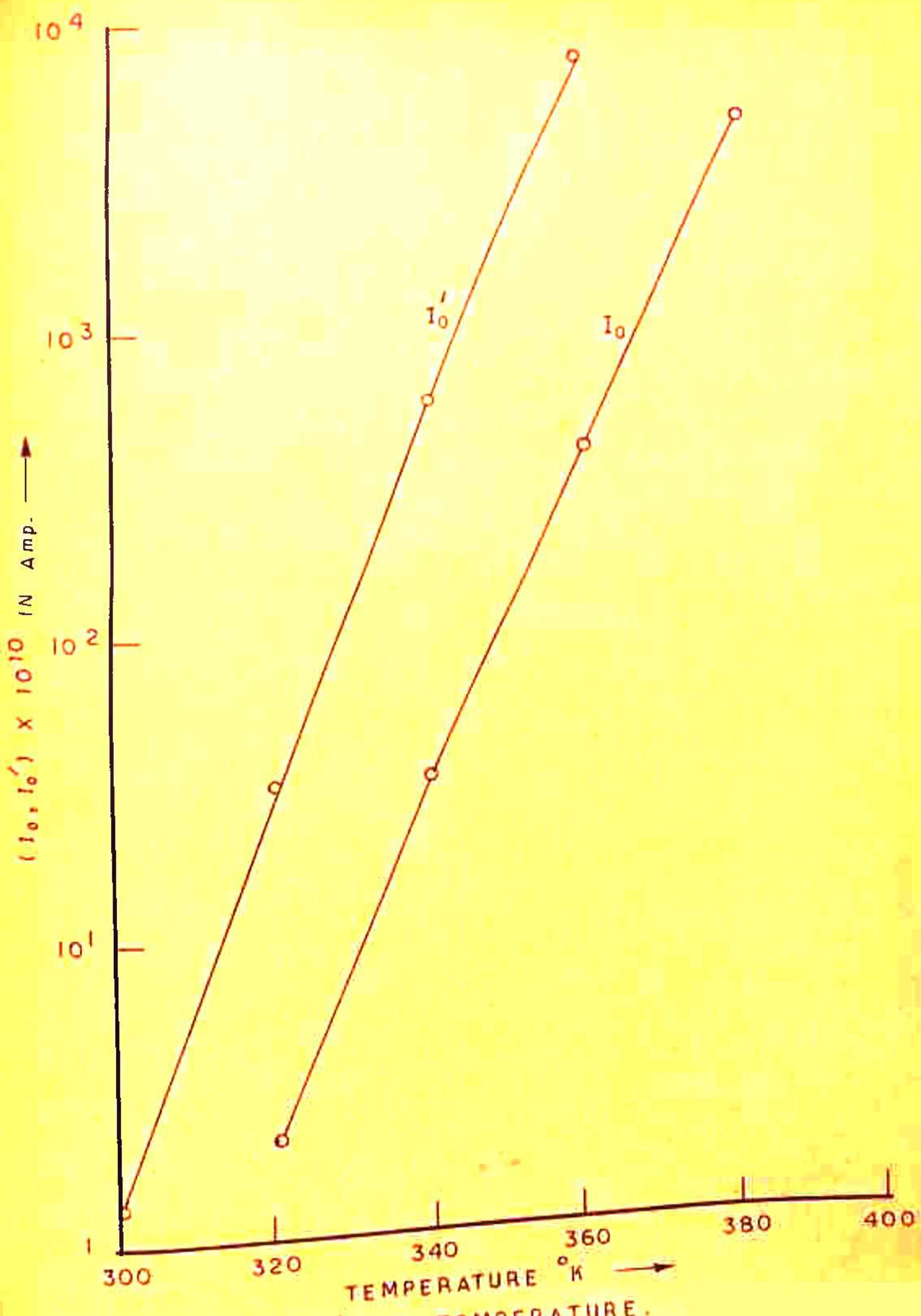

FIG. 5.8 (I_0, I_0') Vs TEMPERATURE.

Effect of internal resistance of the cell is not taken into account.

Short circuit current:

The temperature dependent parameters responsible for the change in I_{sc} with T are absorption coefficient, band gap, and the diffusion length (eqns. 3.38 and 3.40). Variation of I_{sc} with temperature for AMO spectrum is shown in Fig. 5.9 for concentration values of 1 and 100. There is a linear increase in I_{sc} (about 4 %) for 100°K rise in temperature for C = 1 and 4.4 % for C= 100. Increase in I_{sc} with temperature have also been experimentally observed by several outhers. The variation in I_{sc} with T for 1 ohm cm p/n and 2 ohm cm n/p si cells at several intensities are reported by Yasui and Schmidt (1970). They also found that I_{sc} increases at a slower rate for lower light intensities.

Spectral response :

Increase in the short circuit current for fifteen values of wavelength in the interval 0.4-1.1 μm were calculated as a function of temperature. As is clear from Fig. 5.10, there is a red shift of the spectral response of the cell as temperature is increased from 300°K to 400°K.

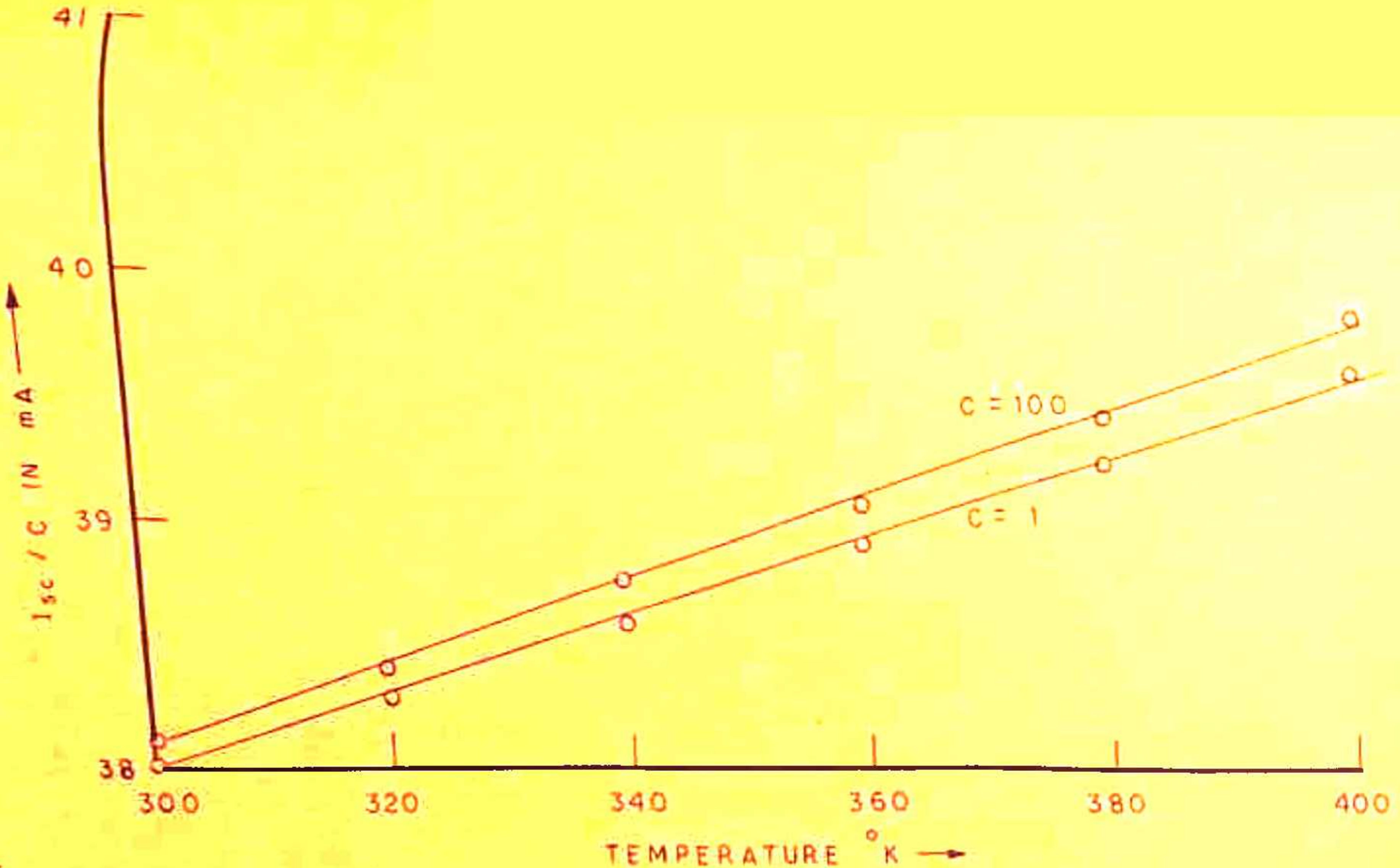

FIG. 5.9 I_{sc}/C Vs TEMPERATURE.

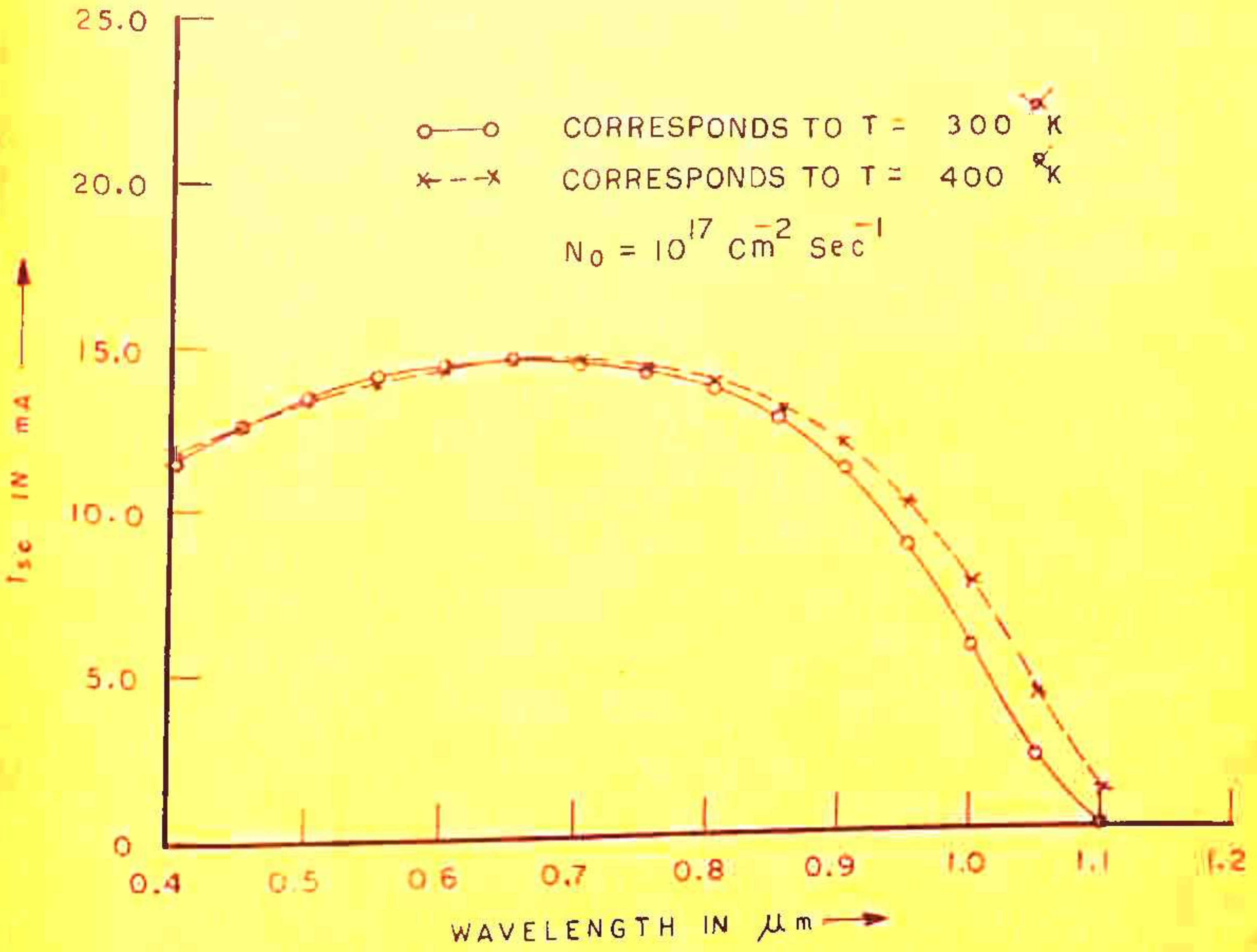

FIG. 5.10 SPECTRAL RESPONSE AT DIFFERENT TEMPERATURES

We have also tested these theoretical predictions regarding the variation in the spectral response with T experimentally. Results will be presented in Chap. 6.

Open circuit voltage:

V_{oc} dependence on temperature arises primarily through n_i. Increase in n_i with temperature gives rise to large values of I_o and I'_o resulting in a rapid fall in V_{oc}. Temperature dependence of I_{sc} (eqn. 3.41) also contribute to the variation of V_{oc} with temperature.

It is interesting to note the effect of the decrease in diffusion potential with T on the value of V_{oc}. Fig.5.7 (P.160) gives a plot of V_{oc} Vs T for two values of concentration factor (C = 1, 100) under AMO spectrum. Since V_D determines the saturation value of V_{oc} (see. 3.41) , fall in V_{oc} with T is more rapid for lower concentration values (2.39 mV/^oK) for C = 1 , 2.05 mV/^oK for C = 100). Measured open-circuit voltages under low level illumination decrease with temperature at a rate of about 2.5 mv/^oC for 10 ohm-cm Si cells and 2.2 mV/^oC for 2 ohm-cm Si devices (Yasui and Schmidt 1970, , Luft 1971).

The value of V_{oc} which we have plotted in Fig. 5.7 is the open-circuit voltage at the junction. Total open-

circuit voltage is the sum of V_{oc} at the junction and the Dember voltage. Dember voltage (V_B) is also expected to change with temperature as is clear from eqns. 3.47 and 3.48. The temperature dependent perameters in V_n and V_p are the mobility ratios b and b' and the excess carrier densities Δp, Δn. Since the contribution of the Dember voltage itself is expected to be small as compared to the junction voltage, we have neglected it.

I-V characteristics :

The current voltage characteristics of solar cells (eqn. 3.35) are modified with the increase in T. Fig. 5.11 shows the I-V characteristics under AMO spectrum (C = 1) at temperatures 300°K and 400°K generated by considering the change in I_{sc}, V_{oc}, V_D, I_o, I_o' with temperature. Fig. 5.11 shows these curves for concentration factors 1 and 100. The degradation in I-V characteristics with T is more drastic at lower concentrations. Modification of these characteristics with T changes P_{max}, FF and efficiency of the cell with the rise in temperature. The degradation in the cell characteristics with the rise in temperature is in agreement with the experimentally observed results of other authors (see e.g. Lewis and Kirkpatrick 1970).

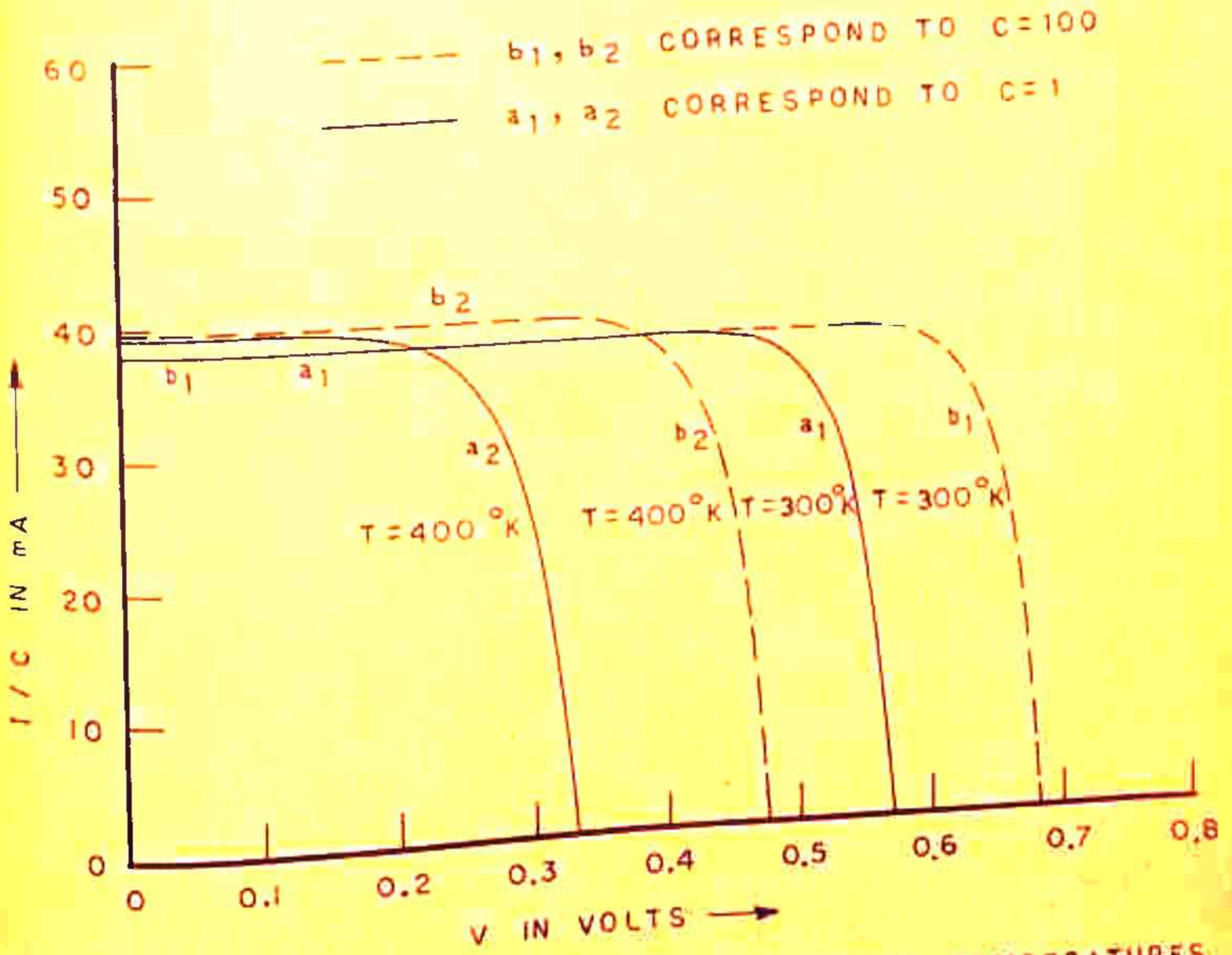

FIG.5.11 I – V CHARACTERISTICS AT DIFFERENT TEMPERATURES AND ILLUMINATION LEVELS.

Maximum power :

Maximum power decreases with T because of the drastic reduction in V_{oc}. Fig. 5.12 shows the calculated decrease of P_{max} with T for C = 1 ,100 under AMO spectrum. The decrease in P_{max} is found to be 8.78×10^{-2} mw/^{o}K for C=1 and 7.47 mw/^{o}K for C=100. The decrease in P_{max} with temperature has also been reported by Yasui and Schmidt (1970) in their experiments.

Fill factor :

Decrease in FF with T is presented in Fig. 5.13 for C = 1 and 100. This decrease arises due to the degradation in the cell characteristics from the ideal rectangular shape as the temperature increases. Part of this decrease is due to the lower open-circuit voltages and part to the increasing softness (roundness) in the knee of the I-V curve as temperature increases in the exp (qV_j/kT) term in eqn. (3.35) . The calculated value of FF(Fig. 5.13) decreases by 16.4 % for C = 1 and 9 % for C = 100 in the temperature range considered. Calculated decrease in FF with T is in agreement with the observed decrease in FF with T above 200°K by Yasui and Schmidt (1970).

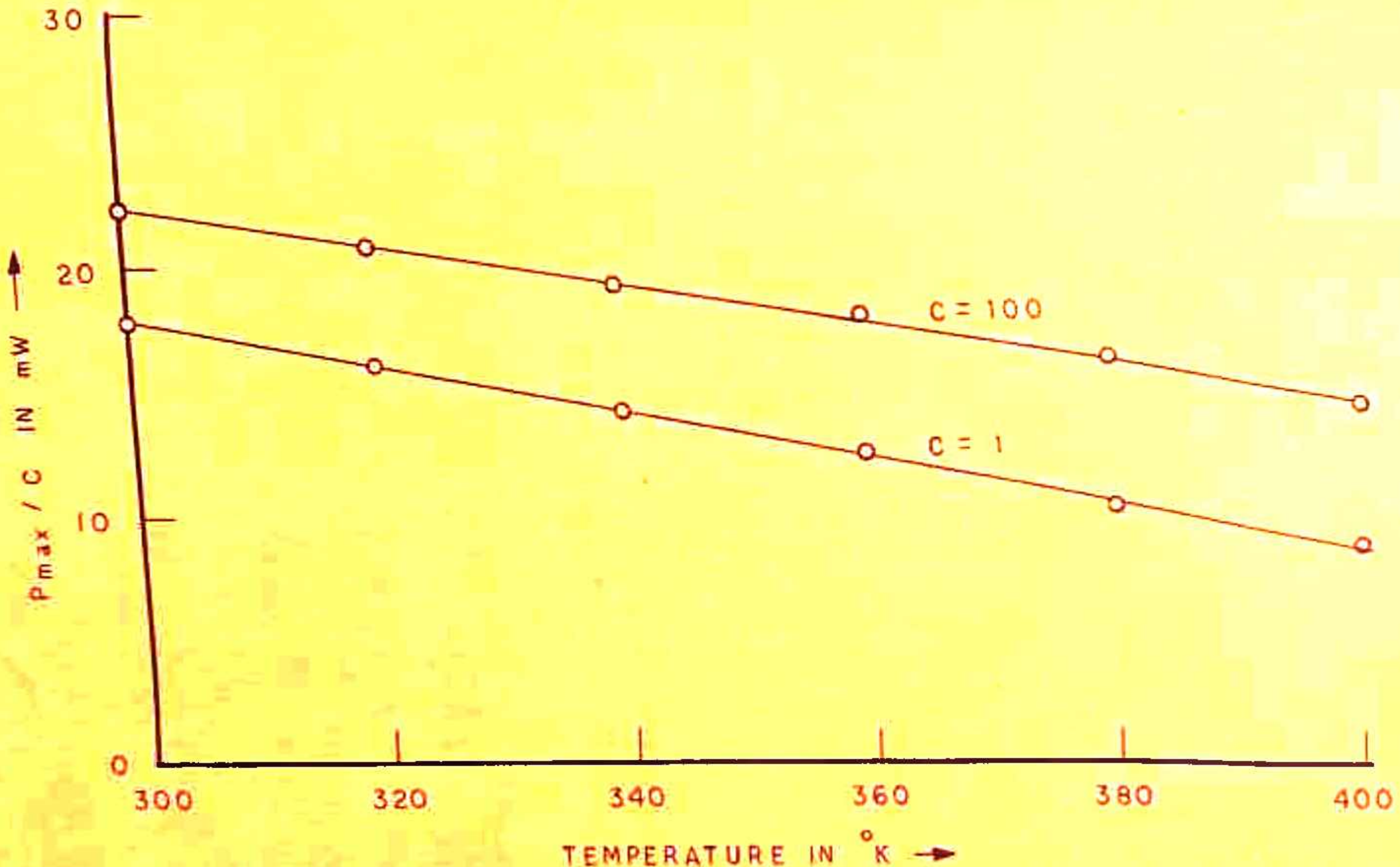

FIG. 5.12 P_{max} / C Vs TEMPERATURE.

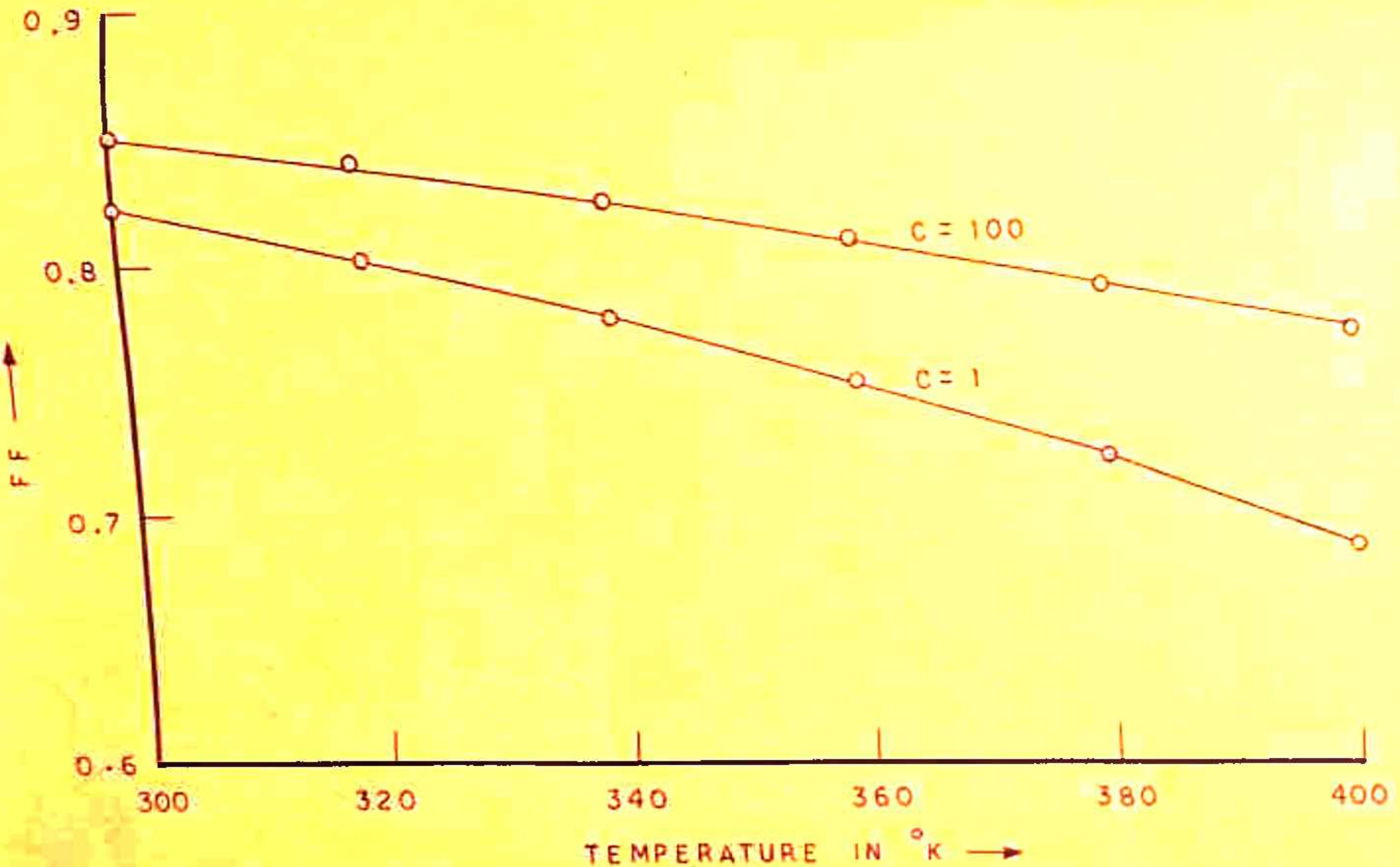

FIG. 5.13 FILL FACTOR (FF) Vs TEMPERATURE

Efficiency (η):

As a result of the decrease in V_{oc} and FF with increasing temperature, partly offset by the improvement in I_{sc}, the efficiency normally decreases with increasing temperature as shown in Fig. 5.14. The calculated value of η decreases at the rate of about 0.09 % per ^{o}K for C = 1 and 0.076 % per ^{o}K for C = 100. Rappaport and Wysocki (1961), Gobat et. al. (1962) have observed that the rate of change in efficiency with temperature near room temperature is 0.04-0.06 % per ^{o}K approximately for conventional Si cells having 1 - 10 ohm-cm resistivities. Experimental studies of Lewis and Kirkpatrick (1970) on several Si solar cells over a temperature range from $20^{o}C$- $200^{o}C$ with incident radiation from 1 to 25 solar constant also show the decrease in efficiency with temperature.

Thus, we see that our theoretical predictions on the variation in the response of solar cells with the rise in temperature taking into account the temperature dependence of various cell parameters confirm the experimental results of other workers. In addition our calculations also show that the effect of temperature on the cell response at higher concentration factors is less severe than at lower levels of illumination. We will discuss the variation of spectral response of solar cells with temperature in detail in Chap. 6 and present some experimental results also.

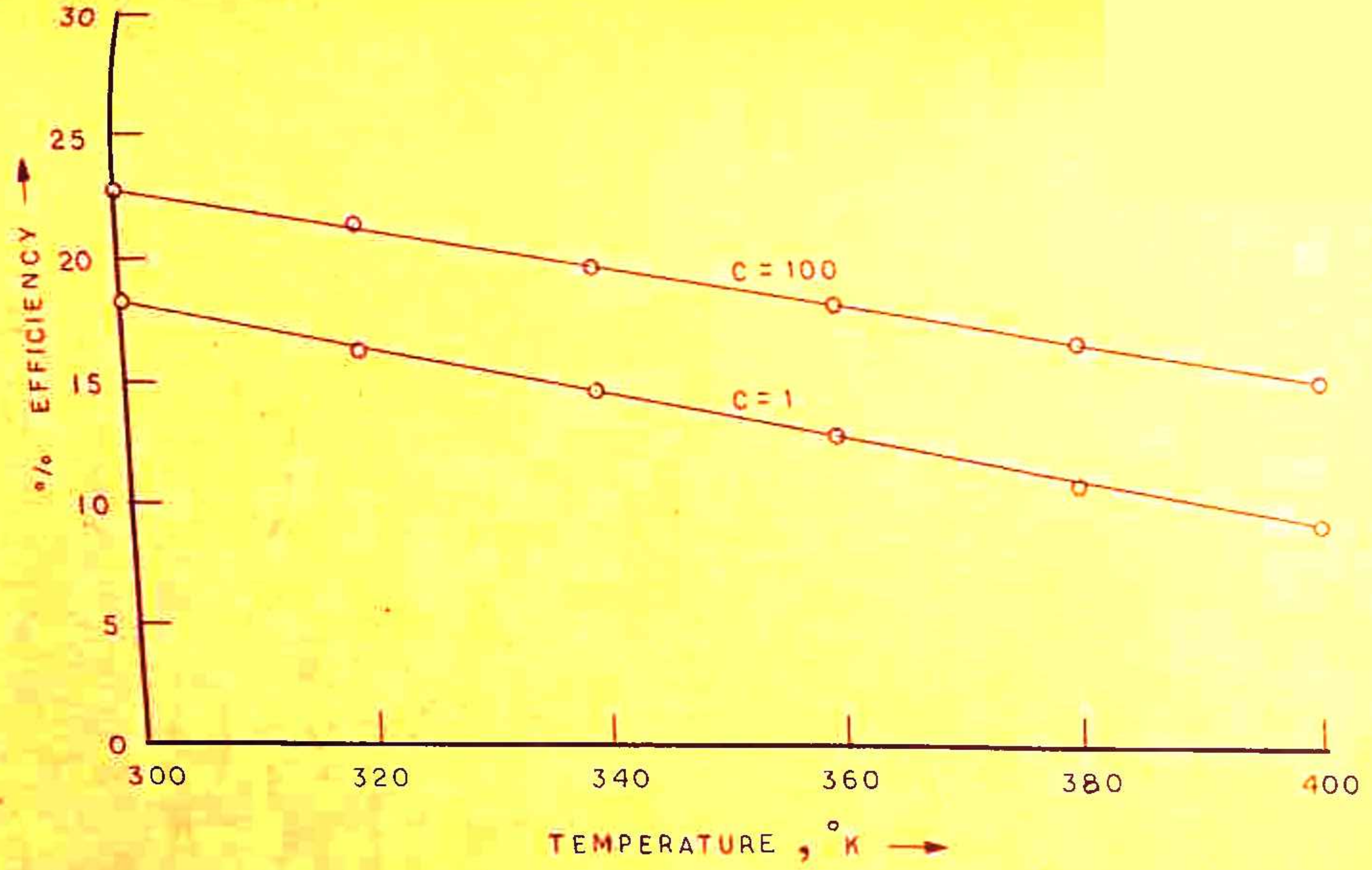

FIG.5.14 EFFICIENCY Vs TEMPERATURE.

CHAPTER-6.

AN ANALYSIS OF THE VARIATION OF SPECTRAL RESPONSE OF SOLAR CELLS WITH TEMPERATURE

6.1 Introduction :

The response of the solar cell as a function of wavelength of the incident light is known as the spectral response of the cell. It is determined from the photocurrent collected at each wavelength relative to the number of photons incident on the surface at that wavelength. Therefore, measurement of the short circuit current (I_{sc}) at different wavelengths is generally used to give the spectral response of the cell.

In general, the minority carrier diffusion length and life time in a solar cell are influenced not only by the quality of the starting material but also by changes induced by processing, so it is important to be able to measure this parameter not only on the raw material, but probably even more importantly on the finished solar cell. Measurement of the spectral response of a solar cell can be used to determine the minority carrier diffusion length in the base region (Loferski and Wysocki 1961, Stokes and Chu 1977, Bell and Freedman 1978). Other cell parameters

like junction depth and surface recombination velocity can also be estimated from the spectral response of solar cells. A study of the spectral response with temperature is, therefore, important for design purposes as well as for the determination of cell parameters like diffusion length at different temperatures.

The change in the short circuit current with temperature for different spectral regions have been observed by very few authors. Experimental results on the change in spectral response with temperature are reported by Walkden (1967), Brandhorst and Hart (1970), Fischer-Colbrie et al (1976) and Chappell (1976) in different ranges of temperatures Though all these authors have found an increase in the relative spectral response in the infra-red region, the magnitude of the increase reported by different authors is not the same. The results in the ultraviolet region also show a discrepancy. Moreover, the peak wavelength appears to shift with temperature by different amounts in these papers. These results are not well understood at present, and therefore, a satisfactory explaination is needed. In chapter 5, we have shown the change in the spectral response of a solar cell with temperature as expected from theory. In this chapter, we present an experimental study of the

change in spectral response of Silicon solar cells with
temperature in the wavelength interval 0.4- 1.1 micron.
We have made measurements of the spectral response of
10 ohm- cm $n^{+}p$ space quality solar cells in the tempera-
ture range 304.5^{o}K to 366.5^{o}K. Since the experimental
measurement of the absolute spectral response of the solar
cell is quite difficult for the kind of accuracy required
for determination of cell parameters, we have used normalised
spectral response curves to extract information about the
diffusion length in the base region. I_{sc} is determined
for a constant intensity of light at each wavelength which
is defined as the energy falling on the cell per cm^{2} per
second for each value of wavelength. We have also experi-
mentally observed the change in short circuit current with
temperature under two different spectra AMO and AM1. The
observed results will be discussed in the following sections.
Section 6.2 describes the experimental arrangement. Experi-
mental results are described in Sec. 6.3. In Sec. 6.4 the
temperature dependence of various parameters responsible
for the change in spectral response with temperature are
described. Also, relative contribution of the base and
the diffused region to the total spectral response of the
cell is determined. Sec. 6.5 deals with the discussion of
experimental results and the determination of diffusion

length at different temperatures from the spectral response. Finally Sec. 6.6 presents various conclusions drawn from this study.

6.2 Experimental arrangements :

A Carl Zeiss Quartz prism Monochromator (Model No. SPM2) was used with a 1000 watt Oriel Xenon Arc Lamp as the light source. A calibrated thermopile (Kipp and Zonen, CA-1, 754286) was used to measure the intensity of light falling on the cell at each wavelength (for details see Sec. 4.2 in Chap. 4), the slit-width of the monochromator being fixed at 0.9 m.m. The spectral band width (defined as the width at half maximum intensity of the spectral range covered by the exit slit) as a function of wavelength is shown in Fig. 6.1. A schematic diagram of the experimental set up is shown in Fig. 6.2. Voltage developed across the solar cell was measured across a one ohm standard resistance from OSAW using a Keithley nanovoltmeter model No. 148. Meter accuracy was 2 % of full scale on all the ranges. The relative intensity was measured at each wavelength using the thermopile described earlier and the relative spectral response of the cell normalized with respect to the peak value was determined.

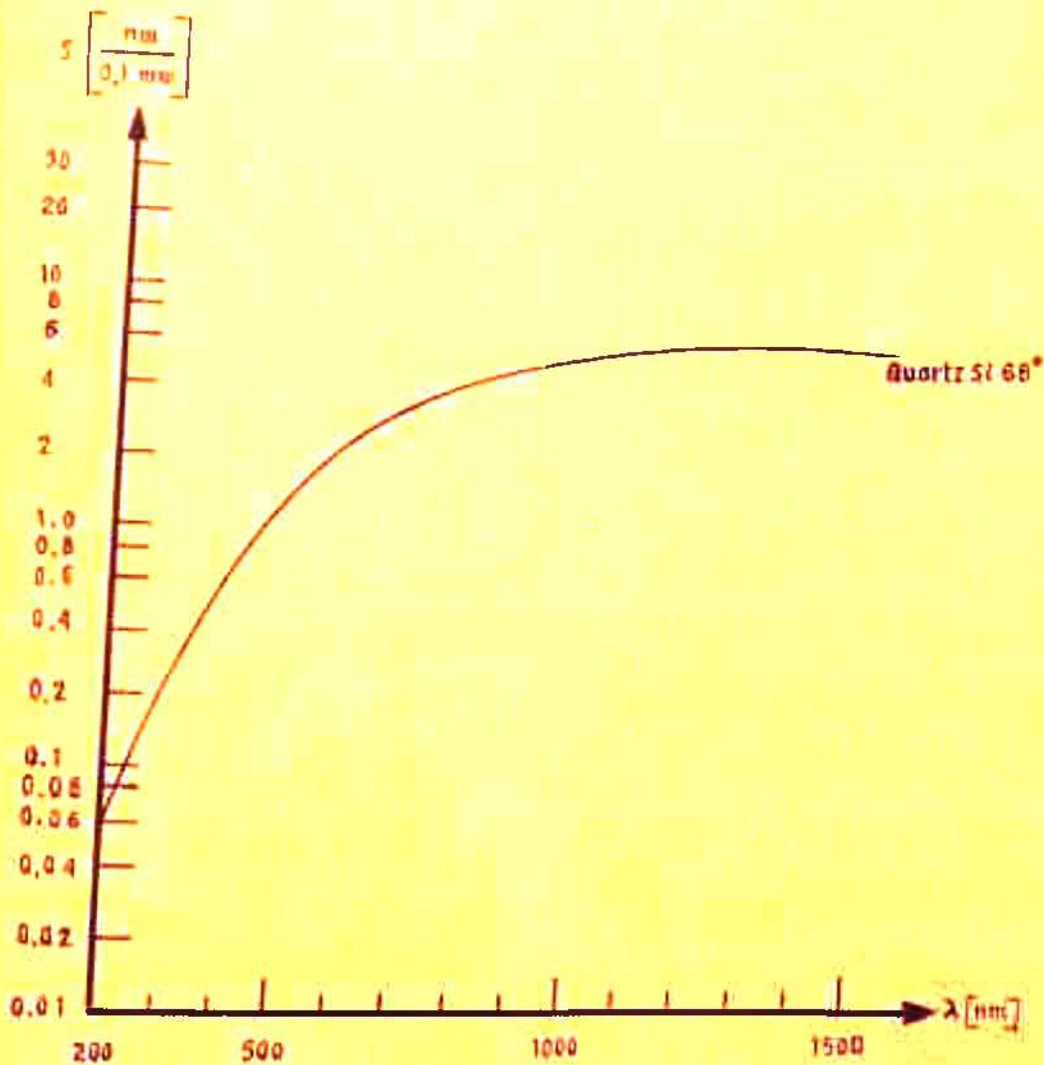

FIG. 6.1 SPECTRAL BAND – WIDTH S IN TERMS OF nm AT 0.1 mm SLIT – WIDTH IN THE WAVELENGTH REGION FROM 200..1500 nm.

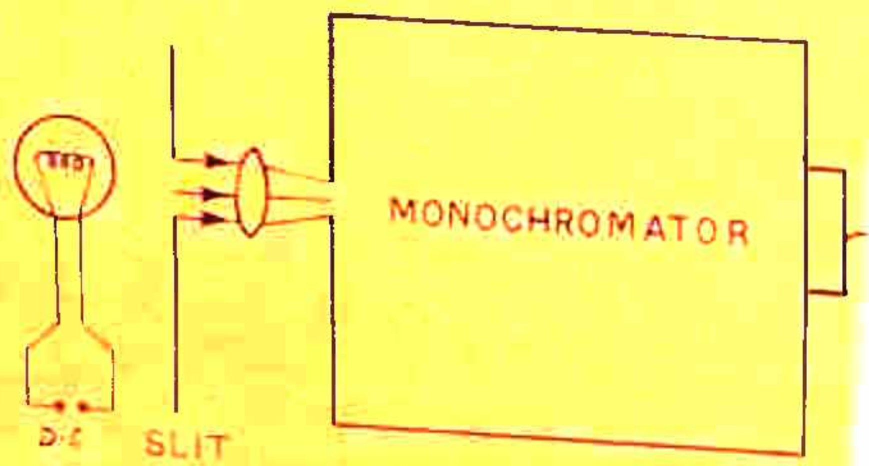

FIG. 6.2 SETUP FOR SPECTRA

AL RESPONSE MEASUREMENT.

An improvised heating unit was used to heat the cells up to 100°C. The hot bit of a 60 watt soldering iron was removed and a copper plate of 2.5 x 2.5 cms in size soldered to a copper rod was fixed to the soldering iron. A copper constantan thermocouple was attached to the copper plate and the experimental cell was fixed on the plate.

An experiment was conducted to determine the temperature difference, if any, between the cell and the copper plate. In this experiment a thermocouple was attached on the top of the cell and comparison of the reading of this thermocouple was made with that of the thermocouple attached to the plate. The difference in the two readings was less than 1° below 50°C and less than 2° at 100°C.

Short circuit current and open circuit voltage of the solar cells was measured in the temperature range 300°K to 368°K under AMO simulator and 1000 watts, Philips Quartz Halogen lamp using digital multimeters described in Sec. 4.2. The output spectrum of the Quartz Halogen lamp is similar to the AM1 spectrum shown in Fig. 1.1.

6.3 Experimental results :

The relative spectral response (RSR) measured at room temperature (304.5°K) and at 366.5°K is shown

in Fig. 6.3 a, corresponding to a constant value of the
intensity of light falling on the cell at each wavelength.
The results at the intermediate temperatures being similar
in nature are not shown for the sake of clarity. The major
feature of these results is a red shift of the whole RSR
at high temperatures. RSR in the long wavelength region
increases whereas below about 0.85 micron it decreases as
the temperature rises. There is a shift in the peak posi-
tion towards longer wavelengths from about 0.85 micron to
0.89 micron in the present range of temperature. RSR deter-
mined for constant value of $N_o(\lambda)$ (number of photons falling
per cm^2 per sec at each wavelength) is plotted in Fig. 6.3b.
The change in the short circuit current with temperature
under AMO and AM1 spectra are shown in Fig. 6.4. The rate
of increase in I_{sc} with temperature is more in the AM1
spectrum as compared to AMO spectrum. Fig. 6.5 shows the
increase in I_{sc} and decrease in V_{oc} with temperature under
AMO spectrum for the experimental cell. In the next section
we will discuss the effect of various cell parameters
responsible for the change in RSR with temperature.

6.4 The role of various cell parameters in the temperature dependence of RSR :

Here, we discuss the various factors which are

1 T = 304.5 °K (PT)
2 T = 366.5 °K

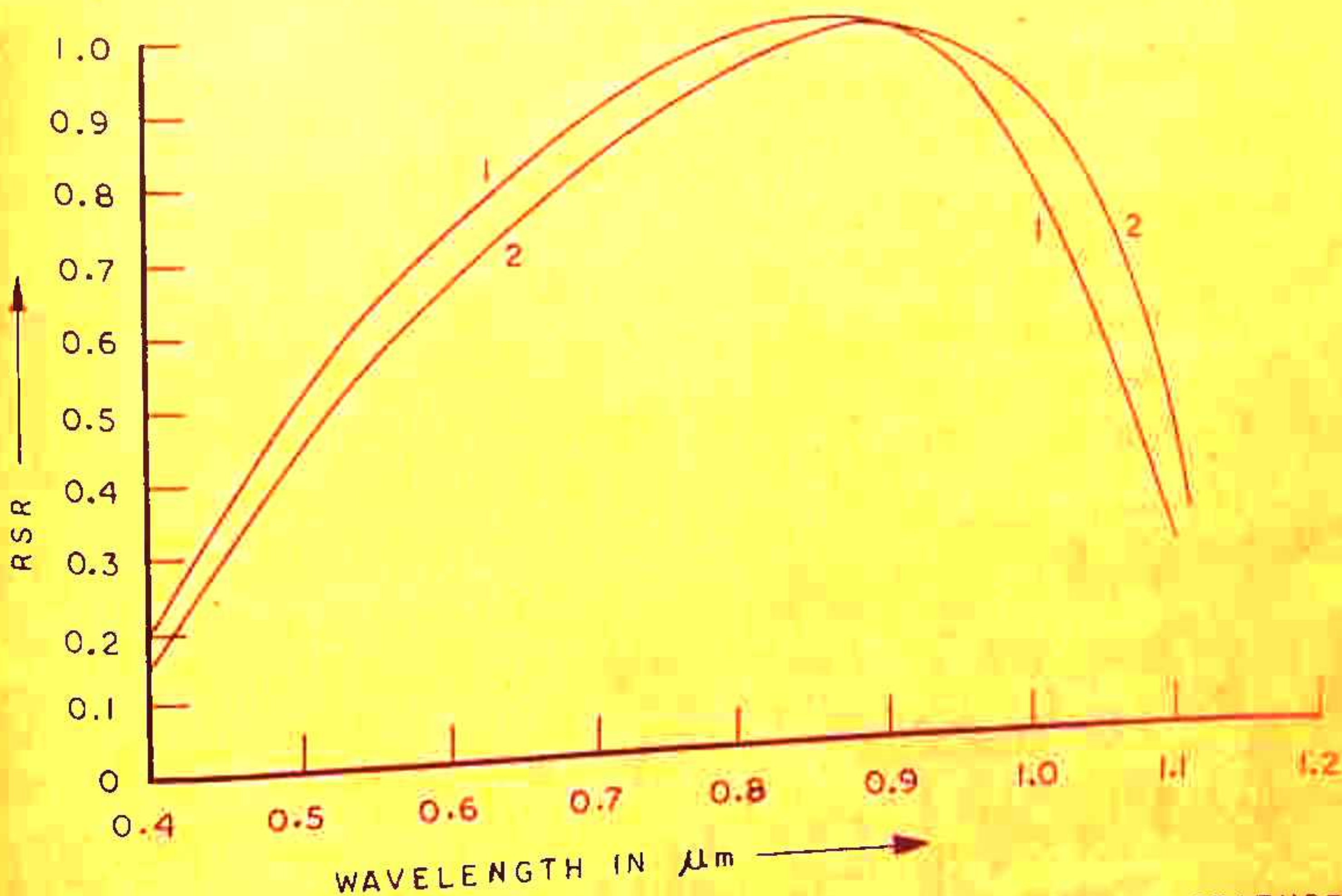

FIG. 6.3a CELL Q : OBSERVED RSR AT DIFFERENT TEMPERATURES FOR CONSTANT ILLUMINATION INTENSITY.

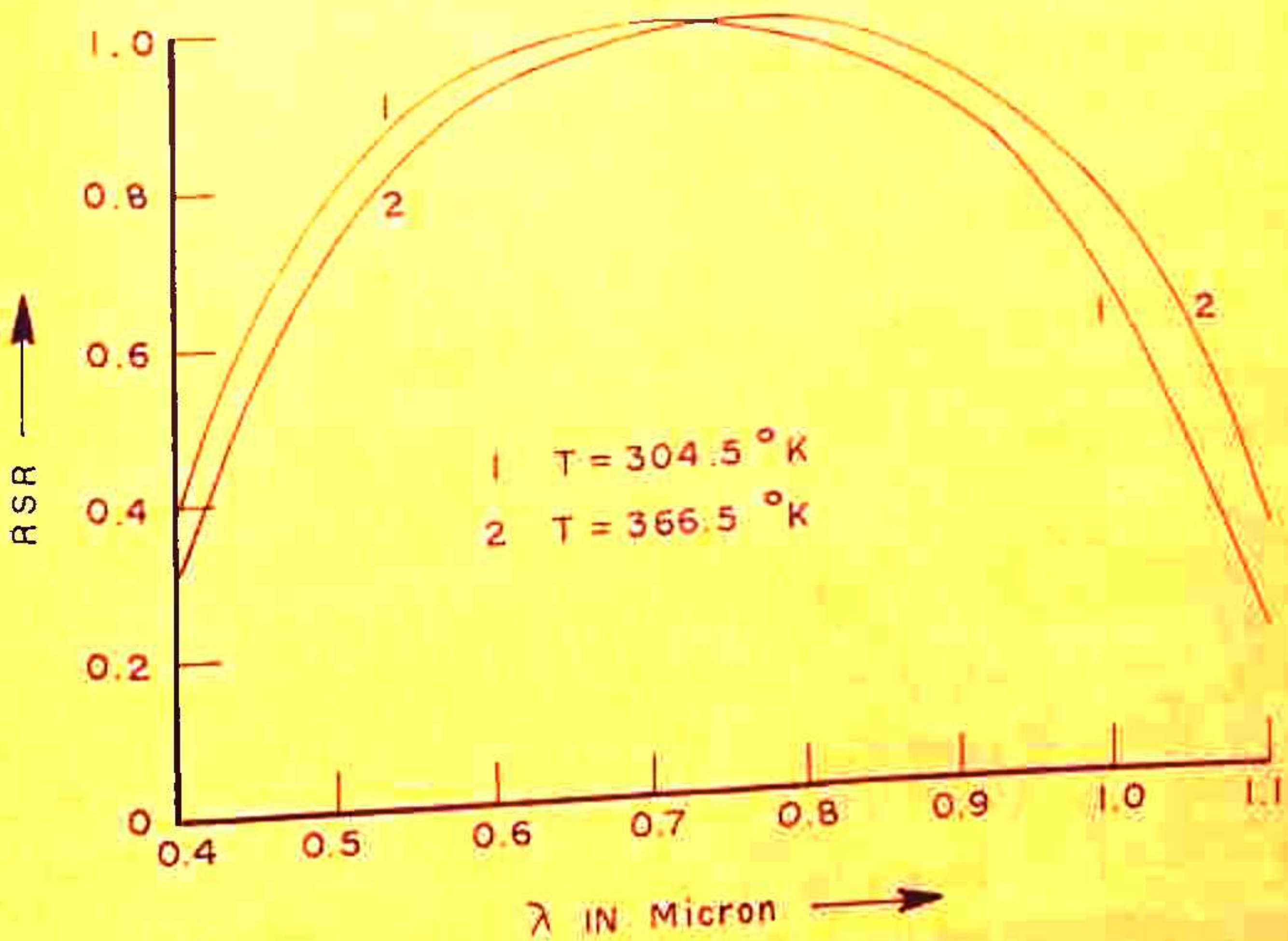

FIG. 6.3b CELL Q: OBSERVED RSR AT DIFFERENT TEMPERATURES CONSTANT No.

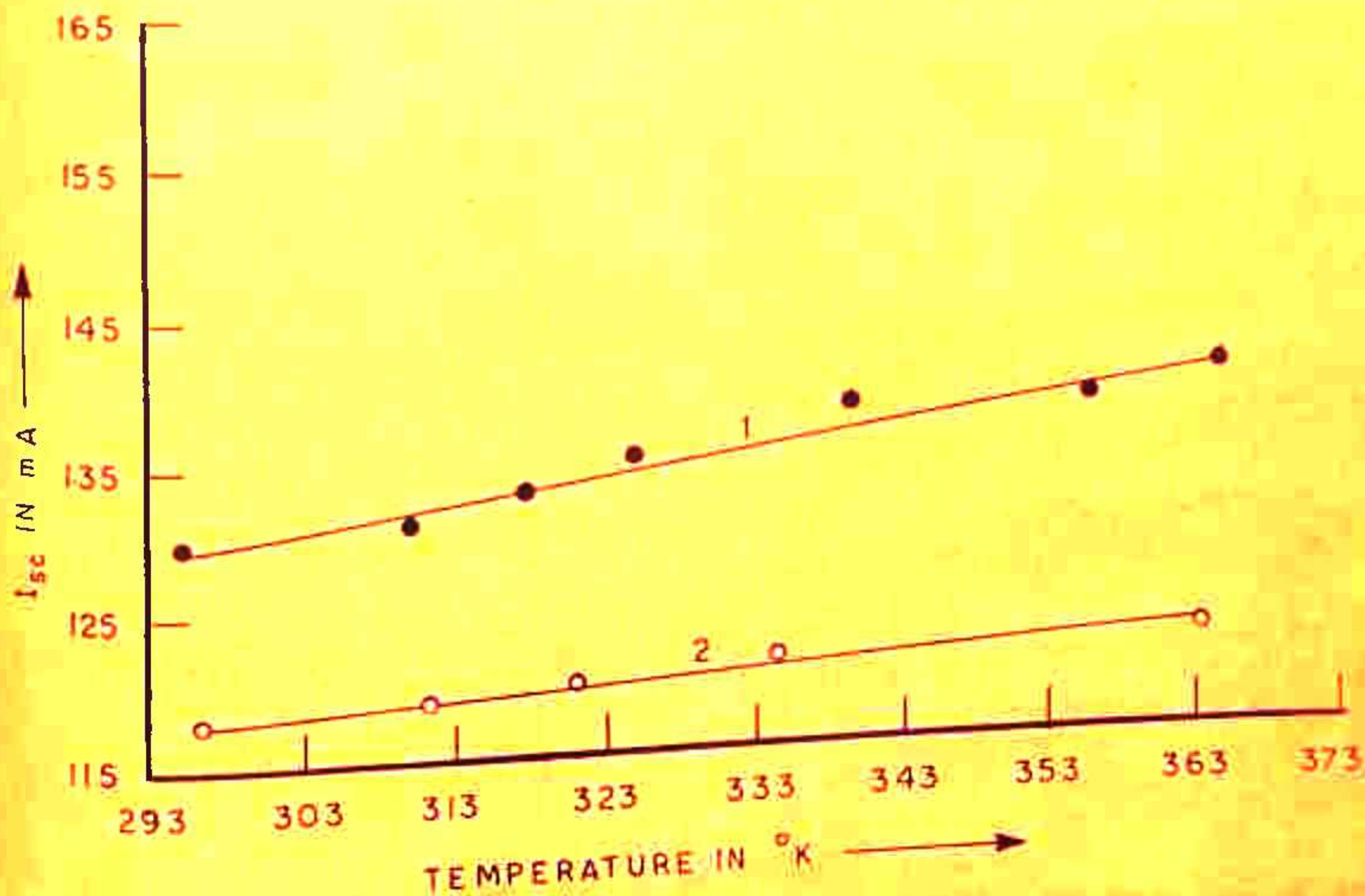

FIG. 6.4 CELL Q : I_{sc} Vs TEMPERATURE

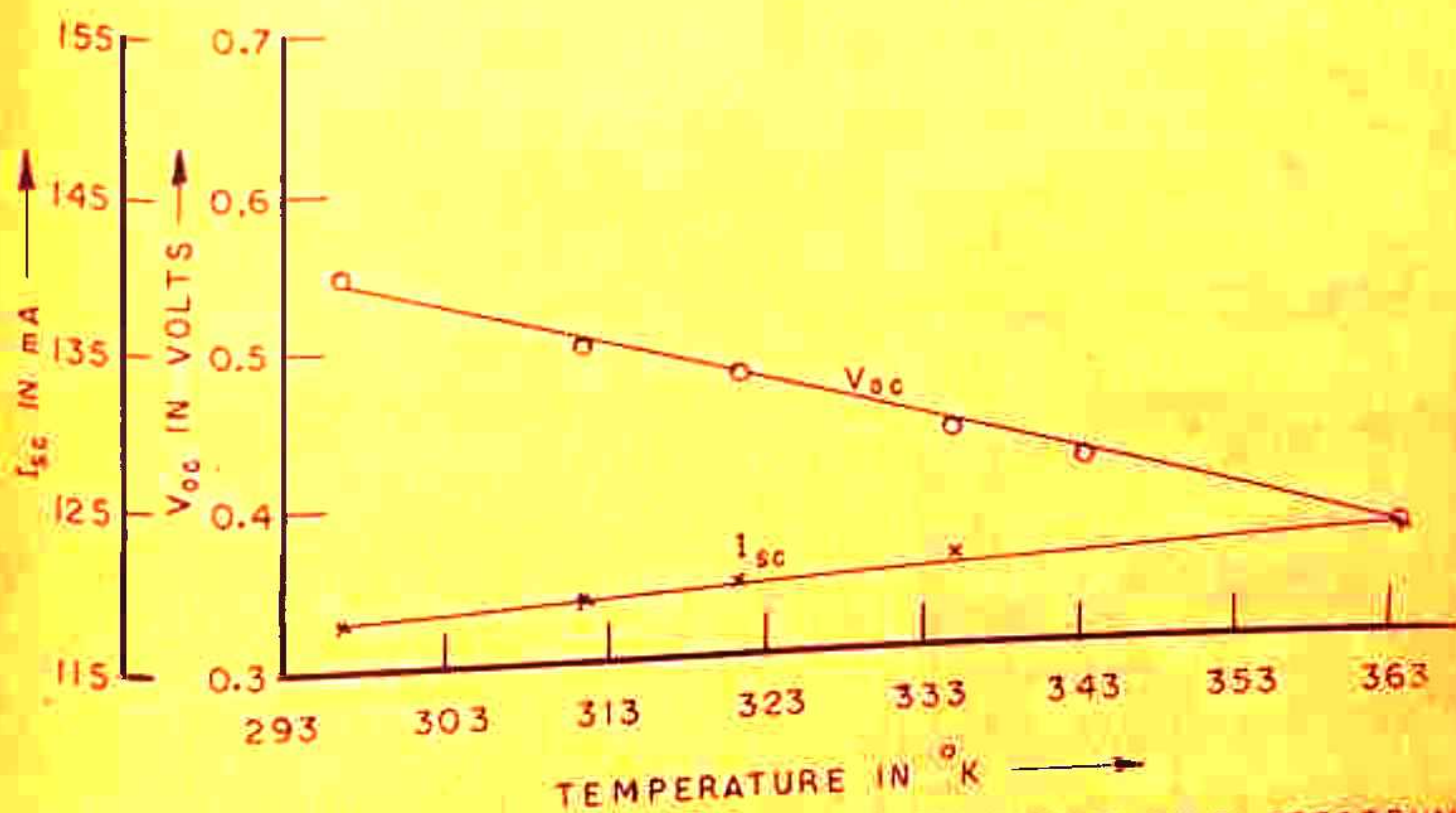

FIG.6.5 CELL Q : I_{sc}, V_{oc} Vs TEMPERATURE UNDER AMO SPECTRUM

responsible for the change in spectral response of the solar cell with temperature. Short circuit current for a monochromatic light of wavelength λ incident on the cell is calculated by summing the current from the n-layer and the p-layer. The contribution from the p-type base layer with an ohmic contact at the back surface is given by: for low level injection (Stokes and Chu 1977)

$$J_B = \frac{q\, N_o \alpha\, L_n}{1-\alpha^2 L_n^2}\, e^{-\alpha d_1} \left[(1-\alpha L_n) + \left(\frac{e^{-\frac{d_2}{L_n}} - e^{-\alpha d_2}}{\sinh \frac{d_2}{L_n}} \right) \right] \tag{6.1}$$

where L_n denotes the diffusion length of minority carriers in the p type base layer and d_1, d_2 are the thicknesses of the diffused and base layers respectively. All other symbols have their usual meaning. For $d_2 \gg L_n$, the second term in brackets is negligible and eqn. 6.1 reduces to

$$J_B = q\, N_o \frac{\alpha\, L_n}{(1 + \alpha\, L_n)}\, e^{-\alpha d_1}. \tag{6.2}$$

Expression for current collected from the top n-layer is given by (Bell and Freedman 1978)

$$J_s = \frac{q N_o \alpha L_p}{\alpha^2 L_p^2 - 1} \left[\alpha L_p e^{-\alpha d_1} - \frac{\alpha L_p - e^{\alpha d_1} \sinh d_1/L_p + s_1 \tau_p/L_p (1 - e^{-\alpha d_1} \cosh d_1/L_p)}{s_1 \tau_p/L_p \sinh d_1/L_p + \cosh d_1/L_p} \right] \quad (6.3)$$

where s_1 is the surface recombination velocity at the top surface and L_p is the minority carrier diffusion length in the n-region. Other symbols have their usual meaning.

If the recombination at the surface is quite high (of the order of 10^6 cm/sec) and the minority carrier diffusion length is small (of the order of 0.1 μm which is generally the case in the diffused region), it is a good approximation to take

$$s_1 \tau_p / L_p^2 \gg \alpha \text{ and } s_p/L_p \gg 1.$$

Under these approximations eqn. 6.3 reduces to (Bell and Freedman 1978):

$$J_s = q N_o \frac{\alpha L_p}{1 - \alpha^2 L_p^2} \left[(1 - \alpha L_p) e^{-\alpha d_1} + \frac{1 - e^{(d_1/L_p - \alpha d_1)}}{\mathrm{Sin\,h}\ d_1/L_p} \right]. \quad (6.4)$$

The total short circuit current is given by

$$I_{sc} = J_B + J_S \quad . \tag{6.5}$$

The absorption of light in the depletion layer of the cell is also expected to contribute to RSR (Bell and Freedman 1978). Since a correct estimate of the depletion layer width is hard to determine, we have not included its effect separately in our calculations. However, it is expected to have a small contribution only, in a practical solar cell (Hovel 1975).

The important parameters in the expressions for J_S and J_B are the junction depth d_1, the diffusion length of minority carriers (L_n, L_p) and the absorption coefficient. The variation of spectral response and short circuit current with temperature will naturally depend on these parameters. We discuss below the effect of change of these parameters with temperature on the temperature dependence of the spectral response.

6.4.1 Absorption coefficient :

Using the expression 5.4 we have calculated α at temperatures 304.5°K and 366.5°K in the wavelength range 0.4 - 1.1 micron. Wavelengths shorter than 0.4 micron get

absorbed at the surface and therefore do not contribute to the short circuit current because of high surface recombination velocity. Wavelengths larger than 1.1 micron are incapable of producing electron hole pairs and therefore are not of any interest. The computed absorption coefficients are given in Table 6.1 . Variation of band gap $\bar{E}_g$ (eqn. 5.6) is taken into account while calculating the absorption coefficients at different temperatures. However, in the temperature range considered, variation in $\bar{E}_g$ is not appreciable, being less than 2 % .

We see from the Table 6.1 that the increase in absorption coefficient is quite large as the temperature is increased from 304.5°K to 366.5°K. The increase in α is larger at longer wavelengths.

In general, since the absorption coefficient increases for all wavelengths, the rays of light will be absorbed at shorter depths in the Si solar cells as a result of the increase of temperature. It is now easy to see how the spectral response is going to be affected due to the increase in temperature because of the increase in the absorption coefficient. In general, the electron hole pairs created by the red and infrared rays will now be created closer to the junction. This will give rise to an

TABLE-6.1

CALCULATED VALUES OF THE ABSORPTION COEFFICIENT AT DIFFERENT TEMPERATURES

S.No.	Wavelength (λ) μm	Absorption coefficient (α) cm^{-1}	
		$T = 304.5^{o}K$	$T = 366.5^{o}K$
1	0.4	20538	24483
2	0.45	14057	16831
3	0.50	9749	11732
4	0.55	6799	8231
5	0.60	4747	5787
6	0.65	3298	4054
7	0.70	2264	2813
8	0.75	1524	1920
9	0.80	998	1279
10	0.85	625	821
11	0.90	366	498
12	0.95	194	278
13	1.00	85.7	135
14	1.05	24.9	49.5
15	1.10	1.18	7.92

increase in the short circuit current at these wavelengths and a consequent increase in the spectral response. In the blue and violet regions, a larger number of electron hole pairs are now created closer to the surface on increasing the temperature. If surface recombination velocity is negligible and if the diffusion length in the diffused layer is more than the thickness of the diffused layer, it is not likely to have any effect on the short circuit current and the observed spectral response will remain practically unchanged. On the other hand, if the surface recombination velocity is large or if there is a dead layer near the surface or/and if the diffusion length is smaller than the thickness of the layer, then this shift in the position of creation of electron hole pairs for short wavelengths will result in a suppression of the spectral response.

The shift in the peak position of the spectral response curve with increasing temperature can also be explained from general physical considerations. Using eqn. 6.2 we have derived the following relation between diffusion length and absorption coefficient at the peak of the spectral response;

$$d_1 = \frac{1}{\alpha (1 + \alpha L_n)} \qquad (6.6)$$

where d_1 is the junction depth. eqn. 6.6 is derived by differentiating eqn. 6.2 for the base contribution with respect to α at the peak of RSR since diffused layer contribution is expected to be negligible near the peak. Since α determines the wavelength on which the peak occurs and since at higher temperatures the wavelength for the same value of α will be longer, it is expected that the peak will shift towards longer wavelengths even if the diffusion length remains unchanged.

6.4.2 Diffusion length :

Life time of excess carriers in the experimental solar cell was measured in the temperature range 303°K to 366.5°K by open circuit voltage decay (OCVD) method (Agarwal 1979). The results are shown in Fig. 6.6. Life time is shown to increase from 3.9 μ secs to 7 μ secs as temperature increases from 304.5°K to 366.5°K.

Diffusion coefficient in the base region was calculated at temperatures 304.5°K, 327°K and 366.5°K using the expressions given in Sec. 5.2.2. Diffusion length was calculated using these values of life time and diffusion coefficient and its values are given in Table 6.2. We find that the diffusion length increases for 304.5°K to 366.5°K temperature rise by 17 % approximately. Increase in the

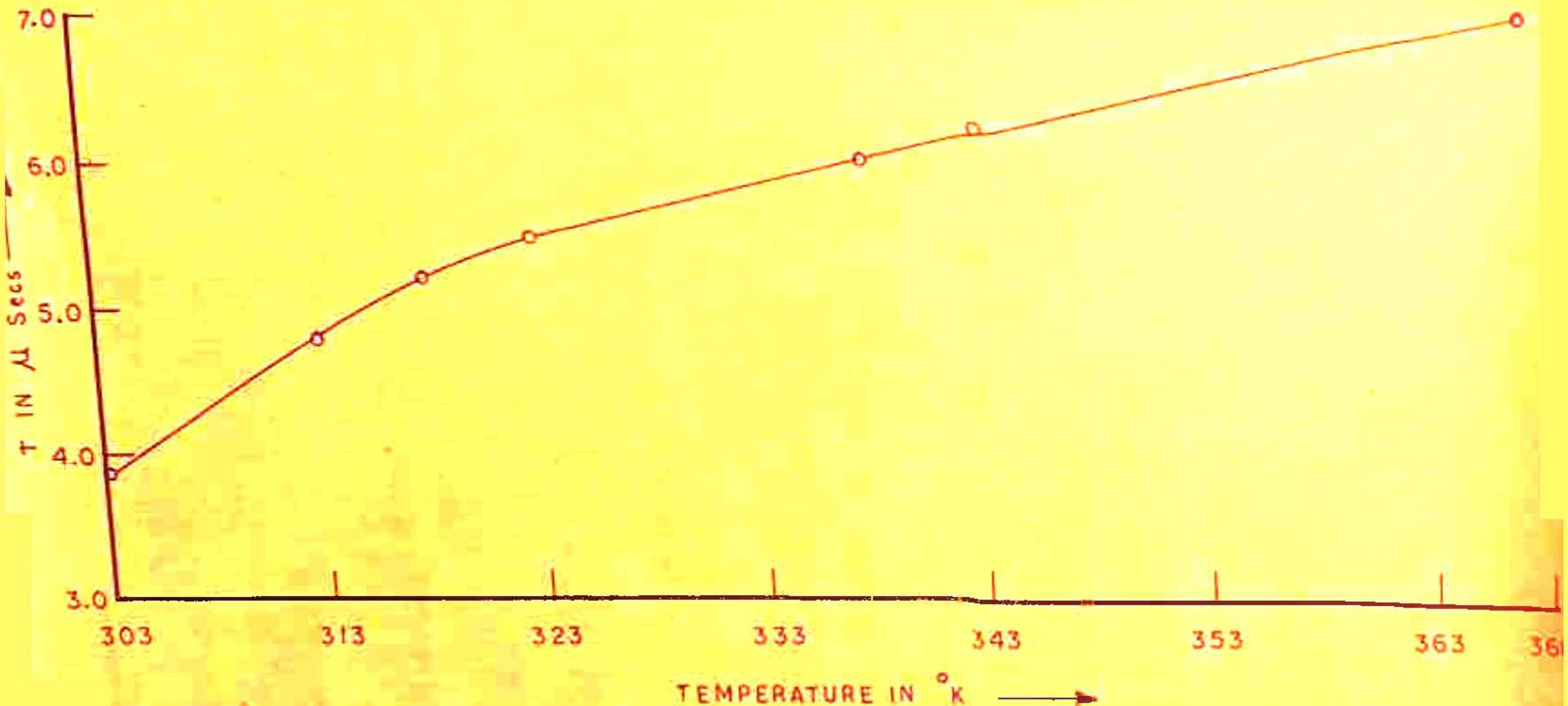

FIG. 6.6 LIFE TIME (τ) AS A FUNCTION OF TEMPERATURE AS DETERMINED BY OCVD METHOD.

TABLE-6.2

DIFFUSION LENGTH AT DIFFERENT TEMPERATURES

Temperature ^{o}K	D_n cm^2/sec	τ_n (OCVD method) μ secs.	L_n μm
304.5	33	3.9	114
327	30	5.2	125
366.5	25	7	134

diffusion length is expected to increase the short circuit current.

6.4.3 Band gap :

The expression for band gap variation with temperature is given in Chap. 5 (eqn. 5.6) Using this expression the value of E_g at 304.5°K and 366.5°K were found to be 1.109 eV and 1.086 eV respectively. Since the decrease in band gap in this temperature range is very small (less than 2 %), we don't expect it to play a significant part in the temperature dependence of the spectral response and I_{sc} under AMO and AM1 spectra.

6.5 Discussion of the experimental results and their theoretical interpretation :

Results of the observed variation in RSR and I_{sc} at different temperatures are discussed below:

6.5.1 Variation of short circuit current with temperature under AMO and AM1 spectra:

We first discuss the increase of short circuit current with temperature as shown in Fig. 6.4 for AMO and AM1 spectra. In each case, the intensity was measured with

a standard solar cell and was adjusted to correspond to that of one sun. It is seen that the increase in short circuit current with temperature is much more rapid in the case of AM1 spectrum as compared to that with AMO spectrum. This is the first time that the effect of spectral composition of incident light on the temperature increase of short circuit current has been studied and reported. This result can be understood with the help of the observed relative spectral response at two different temperatures 304.5°K and 366.5°K respectively (Fig. 6.3a). It is clearly seen, that the response is adversely affected in the ultraviolet region but increases appreciably in the infrared region. Since AMO has large content of blue and violet light (Fig. 1.1) and since the current in this region is suppressed with the increase of temperature, the temperature increase in the short circuit current is smaller in the AMO spectrum as compared to that in the AM1 spectrum.

We study now, in detail the observed spectral response at different temperatures. The main features which we have to explain are following:

(a) Increase in the relative spectral response for longer wavelengths above 0.85 micron.

(b) Suppression of the RSR in the short wavelength region.

(c) Shift in the peak position towards longer wavelengths with the rise in temperature. We now discuss these three factors one by one.

6.5.2 Spectral Response in the long wavelength region :

The well known expression for spectral response in the red and infra-red region is (Stokes 1977, Bordina & Golovner 1977)

$$I_{sc} = \frac{q\, F_o\, L_n \exp(-\alpha d_1)}{(\alpha^{-1} + L_n)} \quad \text{for cell thickness } d_2 >> L_n \text{ and } \alpha d_2 > 1 \tag{6.7}$$

where $F = F_o \exp(-\alpha d_1)$ is the light intensity incident on the base region. L_n is the diffusion length in the base. Eqn. 6.7 is valid even if the diffusion length is of the order of cell thickness d_2. (Error being less than 3 % for $L_n \sim d_2$). Stokes (1977) has suggested that if the intensity of light is adjusted to maintain a given I_{sc} for all wavelengths then the above equation is reduced to

$$F = K(\alpha^{-1} + L_n), \tag{6.8}$$

where K is a constant depending only on the cell parameters and the value of I_{sc} selected. This makes the application of the above equation convenient for the determination of

diffusion length. However, the same purpose can be served by writing the above equation in a different form

$$I_{sc} = \frac{K_1}{(\alpha^{-1} + L_n)} \quad . \tag{6.9}$$

Therefore, if we plot $1/I_{sc}$ as a function of $1/\alpha$ from the longer wavelength part of Fig. 6.3 and extrapolate it, the negative intercept on the axis $1/I_{sc} = 0$ gives the value of L_n. The value of $1/I_{sc}$ and $1/\alpha$ derived from these plots are shown in Figs. 6.7a and 6.7b where λ/I_{sc} is plotted as a function of $1/\alpha$ for constant illumination intensity at each wavelength. The values of diffusion lengths in the base obtained in this manner are 175 microns at 304.5^{o}K and 206 microns at 366.5^{o}K. The values of diffusion length calculated as described in Sec. 6.4.2 (Table 6.2) are considerably smaller than the values determined from RSR.

It is well known that the value of life time determined by different methods are not the same. More importantly Neugroschel et al (1977) have recently pointed out that the life time determined by any of the open circuit voltage decay (OCVD) or Junction current recovery (JCR) methods is not the life time in the base region but some effective life time which appears in the diffused layer also.

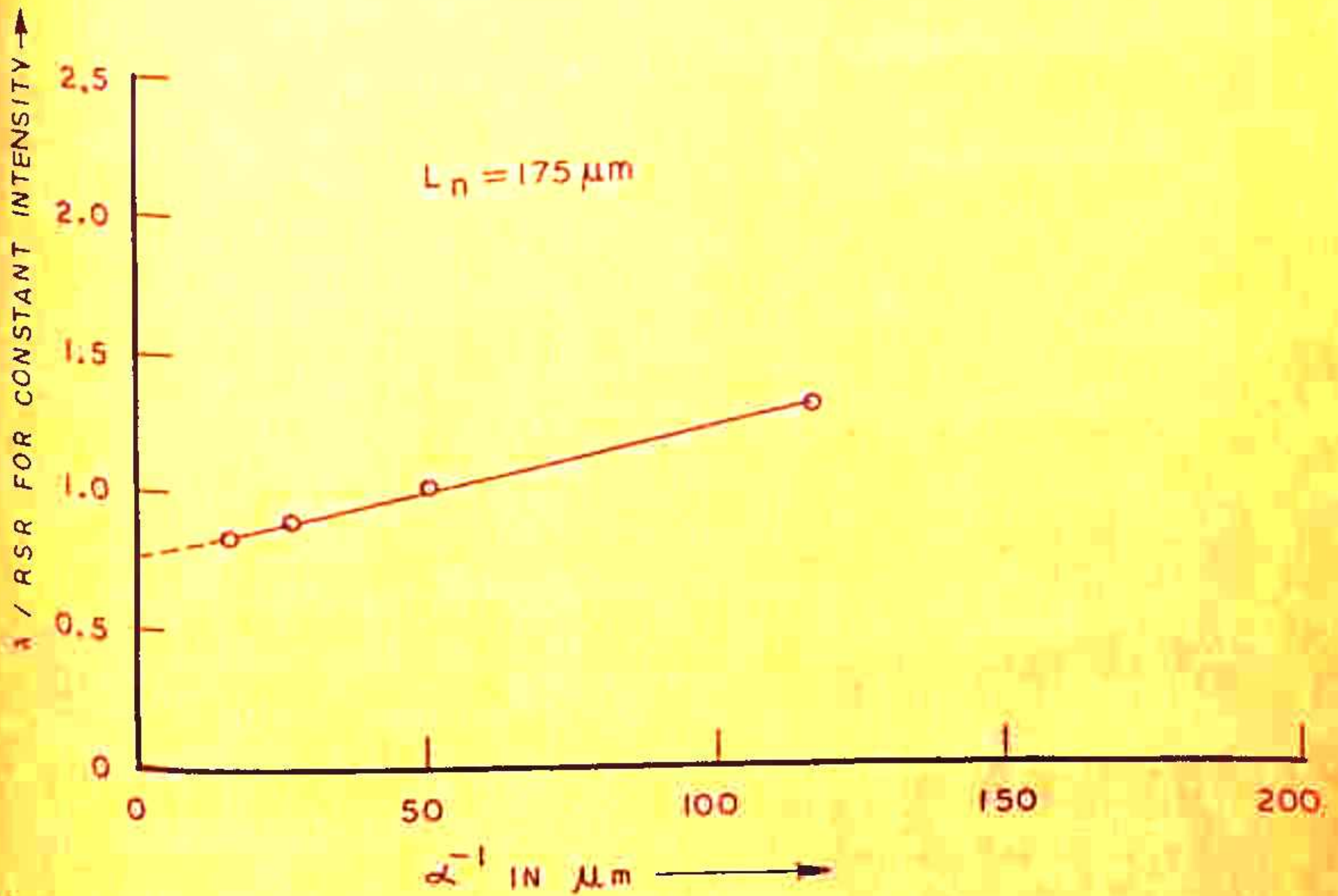

FIG.6.7a CELL Q : DETERMINATION OF DIFFUSION LENGTH IN THE BASE REGION FROM RSR (T = 304.5 °K) MEASURED FOR CONSTANT ILLUMINATION INTENSITY.

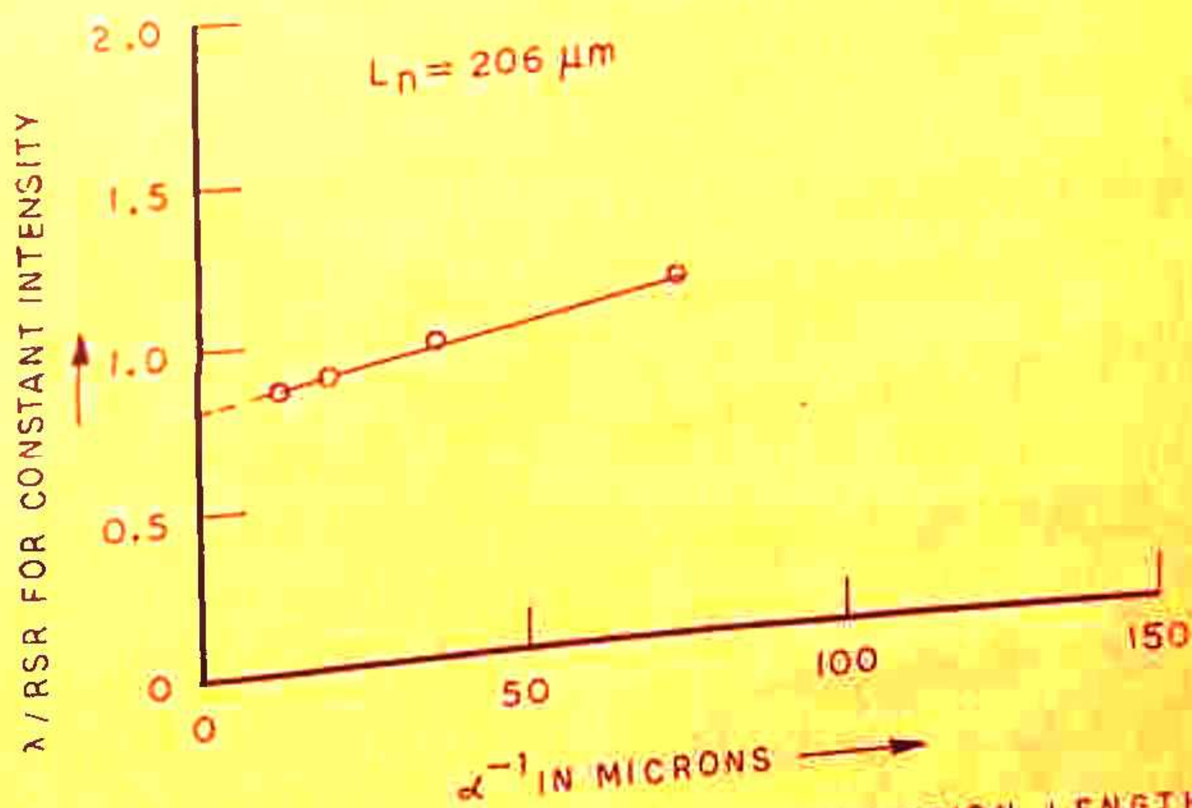

FIG. 6.7b CELL Q : DETERMINATION OF DIFFUSION LENGTH IN THE BASE REGION FROM RSR (T = 366.5°K) MEASURED FOR CONSTANT ILLUMINATION INTENSITY.

The life time in the base derived from the observed life time by these methods is found to be considerably larger (Neugroschel et al 1977) in some cases. We therefore, accept the values of diffusion lengths determined from the spectral response as the correct ones. Using these values of L_n and the values of α from Table 6.1 correspon- ding to the two temperatures, current from the base layer was calculated using eqn. 6.2 at temperaturer $304.5^{o}K$ and $366.5^{o}K$ in the wavelength interval 0.4 - 1.1 micron (see Table 4.1b for parameters of the experimental cell) eqn. 6.4 was used to calculate the contribution from the diffused n-type layer . Note that these eqns. give the current corresponding to constant number of photons. Experimen- tally observed RSR for constant N_o is plotted in Fig. 6.3b. Since in the diffused region life time of excess carrier is usually very short, of the order of 10^{-9} secs (Wolf 1971) because of the heavy doping, the diffusion length L_p in the diffused layer was assumed to be 0.1 micron. Taking this value of L_p and the values of α corresponding to 304.5 and $366.5^{o}K$ temperatures, the spectral response expected theo- retically from the diffused layer was computed for the junction depth of 0.4 micron (Table 4.1b). The total Relative spectral response (RSR) taking into account the contribution from the base as well as the diffused region is

shown in Fig. 6.8 for the two temperatures. Fig. 6.8 also shows the relative contribution from the base and the diffused layers at above mentioned temperatures. As is clear from Fig. 6.8, contribution from the diffused region is appreciable only in the short wavelength side i.e. 0.4 -0.8 micron. At higher temperatures (366.5^{o}K), contribution from the base region increases for wavelengths larger than 0.8 microns (Fig. 6.8). This accounts for the increase in the spectral response at higher wavelengths. Theoretically calculated RSR is shown to be in good agreement with the experimentally determined points in the RSR versus wavelength plot in the longer wavelength region above 0.8 micron as shown in Figs. 6.9a and 6.9b for the temperature values of 304.5^{o}K and 366.5^{o}K respectively.

6.5.3 Spectral response in the short wavelength region :

For shorter wavelengths, the situation is different. There is a slight increase in the current from the diffused layer because of increase in the absorption coefficient α. But, the decrease in the contribution from the base layer of the cell is much more (Fig. 6.8) resulting in a decrease in the spectral response at wavelengths shorter than 0.7 micron. Figs. 6.9a and 6.9b show the change in spectral response

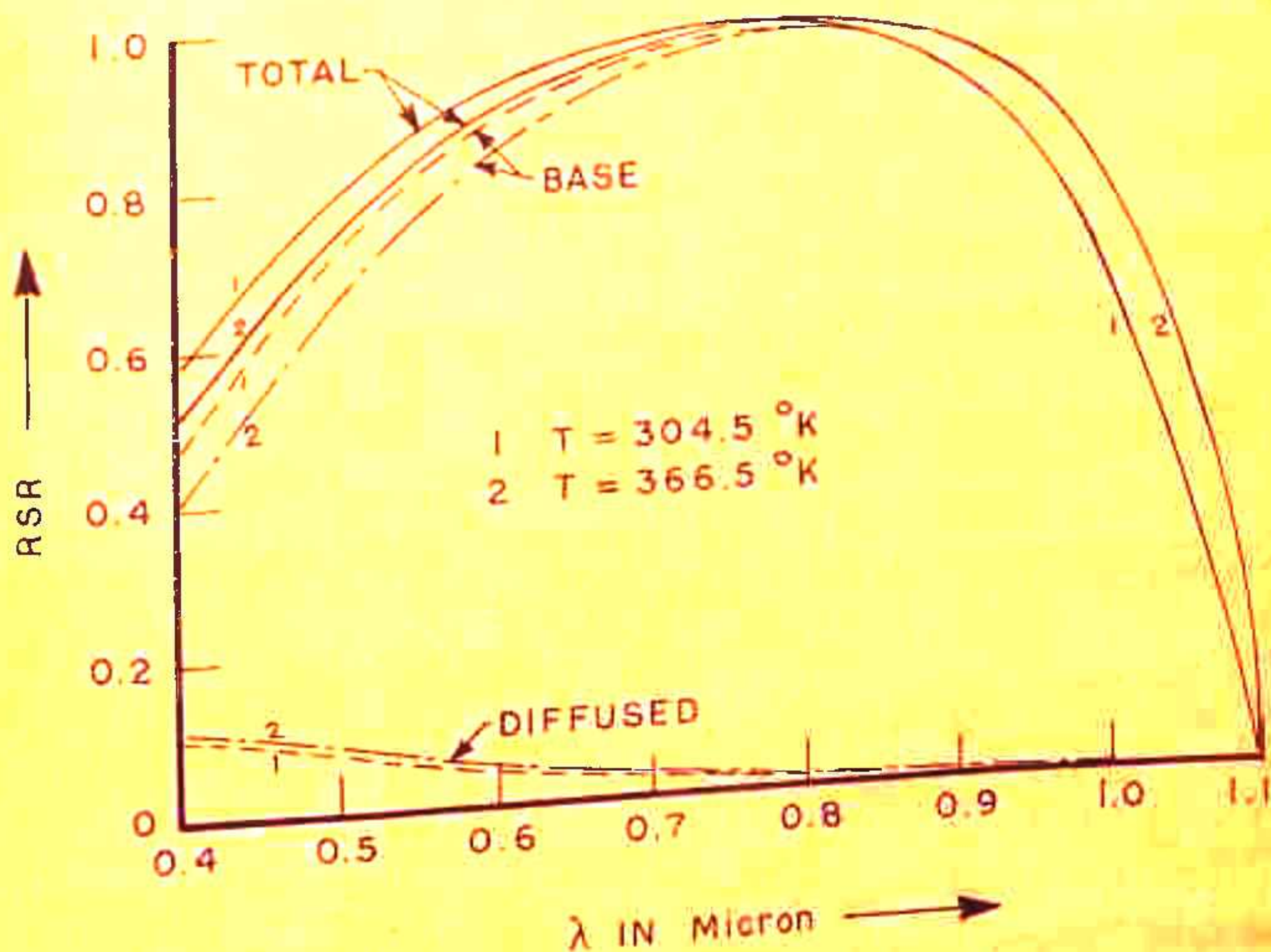

FIG. 6.8 RELATIVE CONTRIBUTION OF THE BASE AND DIFFUSED REGIONS TO THE TOTAL RSR CALCULATED FOR TWO TEMPERATURES.

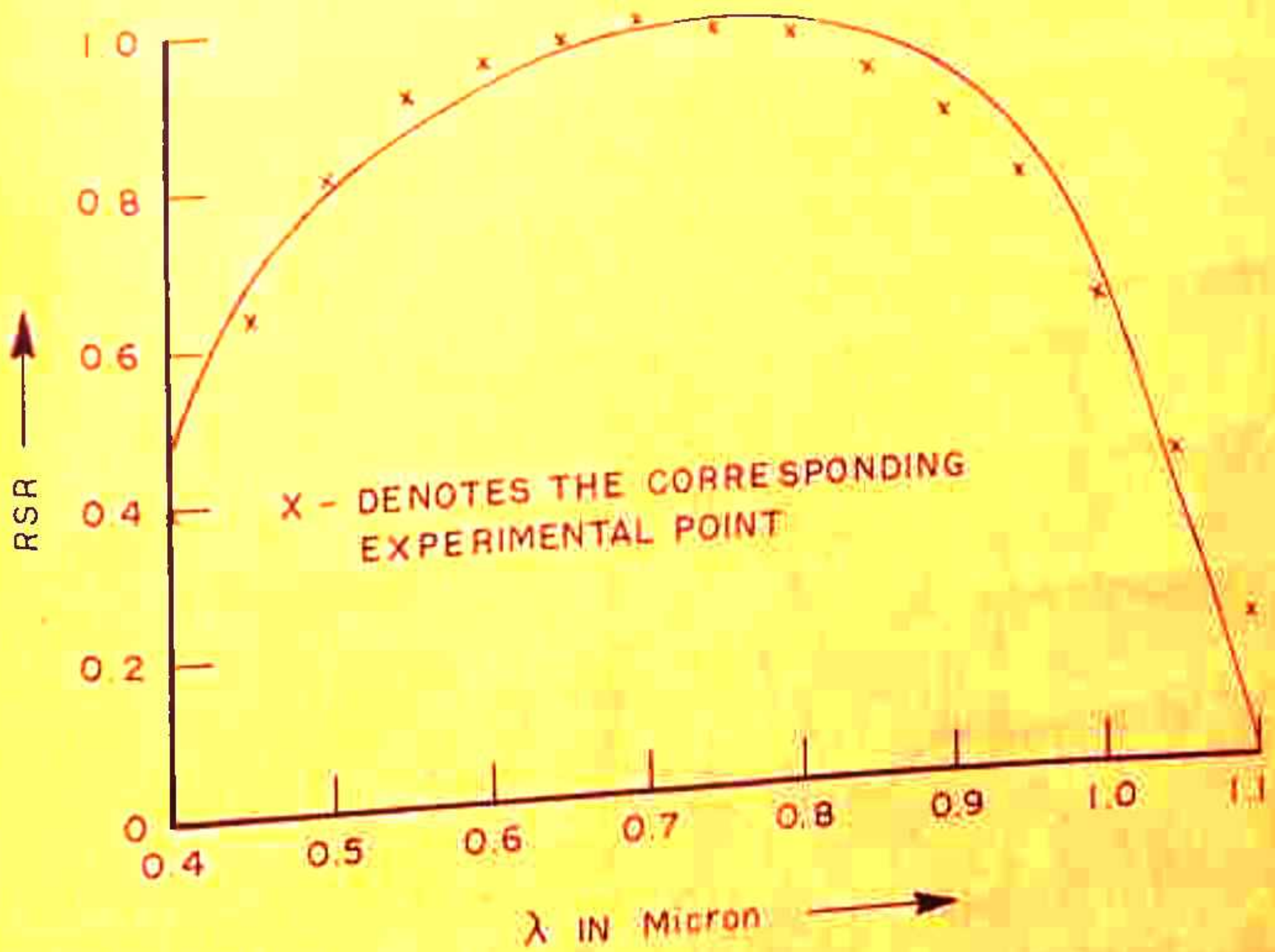

FIG.6.9a CALCULATED RSR AT 304.5°K(ROOM TEMPERATURE).

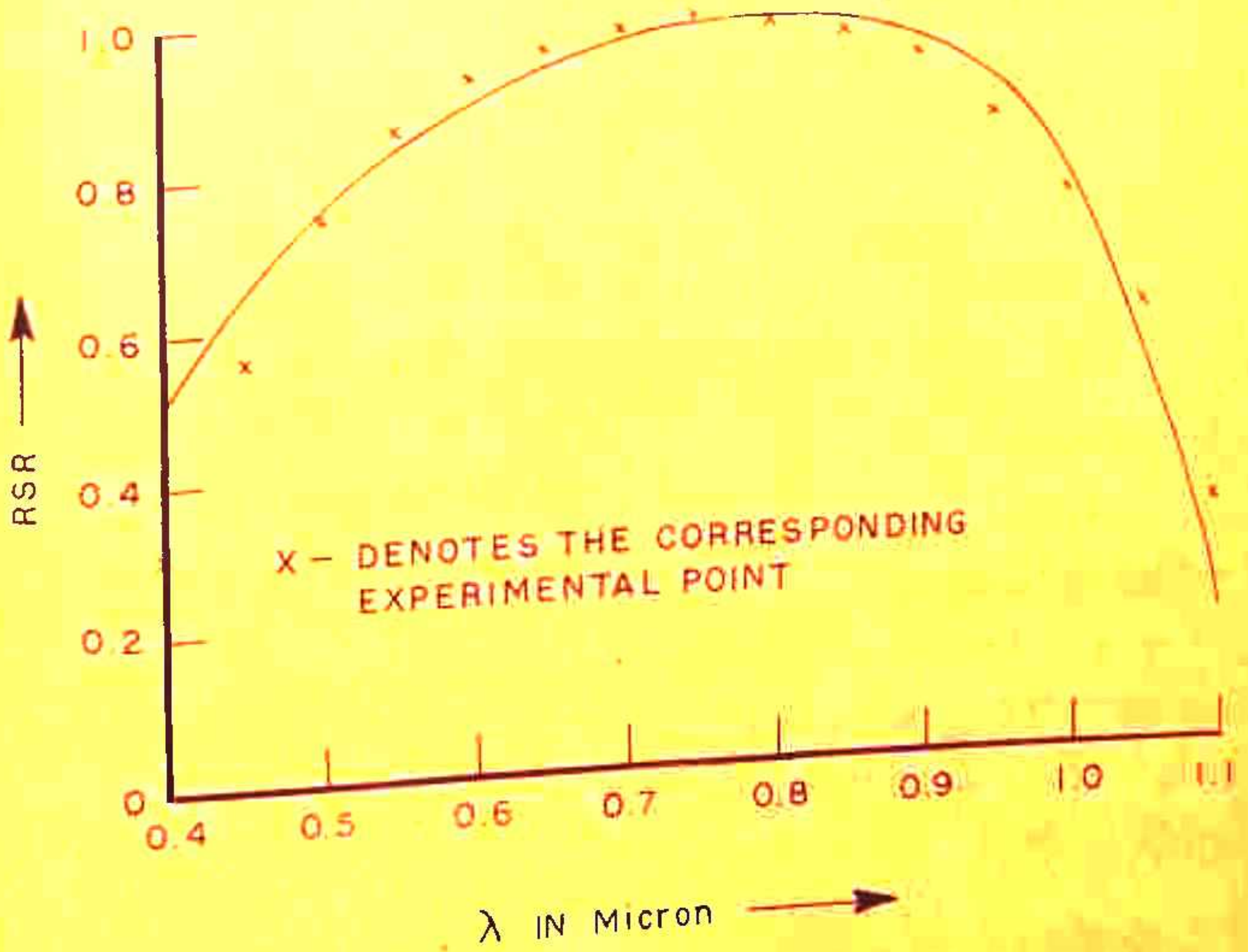

FIG. 6.9b CALCULATED RSR AT 366.5 °K TEMPERATURE.

at two temperatures as predicted theoretically. Experimental points are also shown on these curves for comparison. At shorter wavelengths of 0.4 and 0.45 micron, the discrepancy in the calculated and experimental points could arise due to the reflection from the antireflection coating which is found to be pronounced at these wavelengths (Agarwal 1979). A good agreement is obtained in the wavelength range 0.5 - 0.8 μm.

6.5.4 Peak position :

Since contribution from the diffused region is negligible near the peak region, eqn. 6.6 derived from eqn. 6.2 for current from the base can be used for determining the shift in the peak with temperature. Using the diffusion length values of 175 microns and 206 microns at 304.5°K and 366.5°K respectively and junction depth of 0.4 micron, α at the peak position was calculated using eqn. 6.6. The values of α at the peak corresponding to the two temperatures are found to be 1165 cm^{-1} and 1075 cm^{-1}. The corresponding values of λ are 0.78 micron and 0.82 micron respectively. The calculated shift in the peak position is 0.04 micron. The observed shift in peak (0.05 micron) is also towards longer wavelengths from 0.71 to 0.76 micron

(see Fig. 6.3b) as predicted theoretically. From Figs. 6.9a and 6.9b, it is clear that there is a good agreement between the experimentally observed and calculated RSR in the region near the peak at both the temperatures.

6.5.5 Relative contribution of diffusion length and absorption coefficient at different temperatures :

If we assume the diffusion length to remain constant and only consider the increase in value of α, the increase in spectral response with temperature on the long wavelength side (0.9 μm) is about 34 % less than the otherwise calculated value taking into account the increase in L_n. For longer wavelength this difference is found to be even smaller. We, therefore, attribute more than 66 % of the increase in I_{sc} at longer wavelengths to the rapid change in the absorption coefficient. This is expected from general considerations because if the diffusion length is not increased due to the increase in temperature, the rapid increase in the absorption coefficient with temperature will give rise to the absorption of longer wavelength photons closer to the junction and therefore, carriers will be collected more efficiently . Increase in the diffusion length is an additional effect in the same direction.

Situation in the short wavelength side is somewhat more complicated. As the absorption coefficient increases, a larger fraction of the electron hole pairs which were previously produced in the bulk closer to the junction will now be generated in the diffused layer. Because of the high surface recombination velocity and low life time in this region, these carriers have a poor chance of collection. Therefore, for short wavelengths, spectral response is suppressed. A quantitative estimate of the relative contribution of increase in L_n and α is not possible in this case.

6.6 Conclusions :

The study of spectral response with temperature has revealed the following new features:

(a) Increase of short circuit current with the temperature of the cell is dependent on the composition of the spectrum.

(b) The difference in the increase of short circuit current for a given temperature rise is sensitive to the junction depth and quality of material in the diffused layer.

(c) The diffusion length determined from the long wave-length side of the spectral response shows the expected increase in temperature. The diffusion length determined in this manner is more than that determined from the measured life time and the estimated diffusion coefficient. The difference is attributed to the fact that the observed life time is not the lifetime in the base but is an effective life time, influenced by the life time in the diffused layer.

(d) The relation derived between the absorption coefficient at the peak, junction depth and the diffusion length in the base region (eqn. 6.6) can be used to determine the junction depth in a solar cell if the diffusion length and the peak position of the spectral response are known.

CHAPTER-7.

MEASUREMENT OF SERIES RESISTANCE OF SOLAR CELLS

7.1 Introduction :

The internal series resistance of a solar cell is a parameter which seriously degrades its maximum conversion efficiency. We have noted in Chapters 3 and 4, how strongly the series resistance affects the response of solar cells. Two types of effects occur because of the finite series resistance (R_s) of a solar cell:

(i) $I^2 R_s$ loss:: The resistive components in solar cells cause power dissipation. This becomes especially large at high illumination levels.

(ii) Due to the finite internal resistance of the cell a voltage drop appears across the junction of the cell in such a manner that the available voltage and load current are reduced. This results in a drastic reduction of the power output of solar cells. At high intensities, this effect becomes more severe.

Therefore, for design purposes to optimize the performance of solar cells especially for high intensity and temperature conditions, an accurate knowledge of the

value of series resistance is necessary. It is also helpful in predicting the output characteristics at various light intensity levels. Several authors have discussed the determination of the series resistance and its effect on the characteristics of solar cells (Wolf 1960, Wysocki 1961, Pfeiffer et al 1962, Schoffer and Pfeiffer 1963, Handy 1967, Jain and Stubar 1967, Call and Kerwin 1976, Bobbio and Califano 1976, Napoli et al 1977, Bordina et al 1977, Boone and Van Doren 1978, Spaderna and Navon 1978). In the cases where the cell is nonuniformly illuminationed , the effect of internal resistance of the cell is very important (Lucovsky 1960).

Wolf's analysis (1960) makes it possible to express the 'unit cell' resistance as a lumped element in series with an ideal diode. This treatment is based on the assumption that the unit cell is essentially one dimensional and that the current is uniformly distributed over the active surface.

Effect of the series resistance on the I-V characteristics and the short-circuit current has been discussed in Chapter 3. These calculations were based on the assumption that R_s can be represented as a lumped element as shown in Fig. 1.3.

Wolf and Rauschenbach (1963) pointed out that the series resistance of the diffused layer being a distributed resistance, the effective resistance of the cell becomes a function of current and voltage at which the cell is operated. In several of the cases investigated by them, however, the authors found that lumped resistance model was quite adequate. A more detailed experimental investigation of R_s was presented by Imamura and Portscheller in 1970 by using the following three methods :

a) p-n junction and dark forward characteristics method.

b) Dark curve method.

c) Illuminated curve method using the I-V characteristics at different illumination levels.

They found that each of these methods gives different value of the series resistance. Imamura and Portscheller (1976) also observed that the series resistance determined by all these methods decreases at high current levels. In addition they observed that the resistance determined by the p-n junction and dark forward characteristics method increases with the rise in temperature.

Evdokinov (1972) suggested another method for determining the series resistance at the cell operating point using a single photovoltaic I-V characteristics of

the solar cell. This technique requires a very accurate reproduction of the I-V curve segment near the open-circuit point and also involves rather cumbersome calculations. Therefore, the above mentioned three methods a, b and c are generally used for the measurement of series resistance.

Therefore, considering the importance of this parameter, it appears that sufficient experimental work on the determination of the series resistance of variety of solar cells have not been done. In this Chapter, a study of the measurement of series resistance of solar cells by above mentioned three different methods a,b and c is presented. A new method for measuring the series resistance is also proposed. Experimental results on the determination of series resistance by the new method as well as by the other two conventional methods (a and c) are reported and discussed.

Sec. 7.2 contains a brief description of the theory of above mentioned three conventional methods of determining the series resistance of the solar cell using various types of cell I-V characteristics. Sec. 7.3 deals with the description of the experimental set up In Sec. 7.4 a comparison of the three methods is given and a new method of determining the series resistance is described. In Sec. 7.5 experimental results are reported

and discussed. Sec. 7.6 gives some conclusions drawn from this study.

7.2 Theory of the different methods used for determing the series resistance:

The three types of current voltage characteristics of solar cells used in the determination of the series resistance are (i) Photovoltaic characteristics (ii) Dark forward characteristics and (iii) P-N junction characteristics. A detailed description of these is given below.

7.2.1 Description of the various I-V characteristics of solar cells :

(i) Photovoltaic (PV) characteristics:

These are obtained under fixed illumination, usually of known intensity. A resistive load is varied between short-circuit and open-circuit conditions, while measuring the voltage across the solar cell terminals and the current out of these terminals. The experimental set-up used in the measurement of PV characteristics is described in Sec. 7.3.

Since, we are interested in the applications of solar cells at relatively high current densities, effects of shunt resistance are neglected (Hovel 1975). Under illumination, the theoretical solar cell equation based on a lumped parameter version has the following form:

$$I=I_o\left(e^{\frac{q}{AkT}(V_T+ I R_s)}-1\right) -I_g \qquad (7.1)$$

where A is a dimensionless constant between 1 and 5 known as the diode quality factor. The junction voltage V_j and the terminal voltage V_T are related by (see eqn. 3.43 also)

$$V_j = V_T + I R_s \; ,$$

In this case, voltage measured at the terminals V_T is smaller than the junction voltage because of the voltage drop IR_s across the cell. Eqn. 7.1 reproduces the obtained characteristics sufficiently well for most of the cases. However, for high level injection eqn. 3.44 gives the correct relationship.

(ii) Dark forward (DF) characteristics:

These characteristics are obtained when the solar cell is used as a diode without application of any illumination, but by supplying d.c. power from an external bias supply. The experimental arrangement for measuring these characteristics is described in Sec. 7.3 Under dark conditions, the forward bias current flows through the

p-n junction and the junction voltage is smaller than the terminal voltage by the voltage drop across the lumped series resistance.

i.e. $V_j = V_T - I_T R_s$,

$$\text{Thus, } I_T = I_o \left(e^{\frac{q}{AkT}(V_T - I_T R_s)} - 1 \right) . \qquad (7.2)$$

I_T and V_T are the terminal current and voltage under forward biasing. For large forward bias voltage (usually > 0.4V), A is taken to be equal to one in accord with the predictions of Schockley's diffusion theory. For lower voltages A is expected to be > 1, because the recombination current in the space charge region dominates the forward current in this case (Wolf et al 1977).

(iii) P-N junction characteristics:

In this case, the solar cell is illuminated, but with variable light intensity. The intensity of illumination need not be known, if the value of the light generated current I_g, can be determined. For the low series resistance solar cells, I_g can be taken to be equal to I_{sc}, the short circuit current. This condition is fulfilled when the cell resistance is sufficiently small so that the output current I of the device, when measured by the photovaltaic output method is constant for all

terminal voltages between 0 and 0.1 volts (see e.g. Wolf and Rauschenbach 1963). The measurement consists of determining the short circuit current I_{sc}, which under the present conditions equals the light generated current I_g, and the opencircuit voltage V_{oc} for every light intensity setting. Each pair of corresponding short-circuit current and open-circuit voltage values is plotted as one point in the first quadrant of the current-voltage plane. Through the variation of the illumination level, a succession of such points is obtained which presents the desired current-voltage characteristics. If at higher light intensities the condition of flatness of the photovoltaic output characteristics under zero voltage is not satisfied, then the measurement of light intensity is reqired. I_g can be determined independently from this. The current -voltage relationship obtained in this way is called the p-n junction characteristics. These characteristics are independent of the effect of series resistance when I_{sc} can be taken to be equal to I_g. In such a case, p-n junction characteristics are described by the equation

$$I_{sc} = I_o \left(\exp \left(qV_{oc}/AkT \right) - 1 \right) \quad . \qquad (7.3)$$

Eqn. 7.3 gives a relationship between the short-circuit current and the open-circuit voltage of a solar cell and

is derived from eqn. 7.1 by substituting $I= 0, V=V_{oc}$ corresponding to the open-circuit configuration and writing I_{sc} in place of I_g when they are equal.

Using these three types of I-V characteristics R_s is determined using the methods described below.

7.2.2 <u>Various methods for determination of the cell internal series resistance:</u>

(a) <u>P-N junction and dark forward characteristics method:</u>

In this method dark forward characteristics is plotted alongwith the p-n junction characteristics for a given cell. (Fig. 7.1a). If V_1 and V_2 are the voltage on the two curves corresponding to the same value of current I, the series resistance is given by

$$R_s = \frac{V_2 - V_1}{I} = \frac{\Delta V}{I} \quad (7.4)$$

(b) <u>Dark curve method</u> :

In this method dark forward I-V characteristics and photovoltaic characteristics of the same cell are used to estimate the series resistance (Fig. 7.1b). Two points P and Q are located on the dark and illuminated characteristics, such that their co-ordinates are $(V_1, \Delta I_{sc})$ and $(V_2, I_{sc} - \Delta I_{sc})$, respectively.

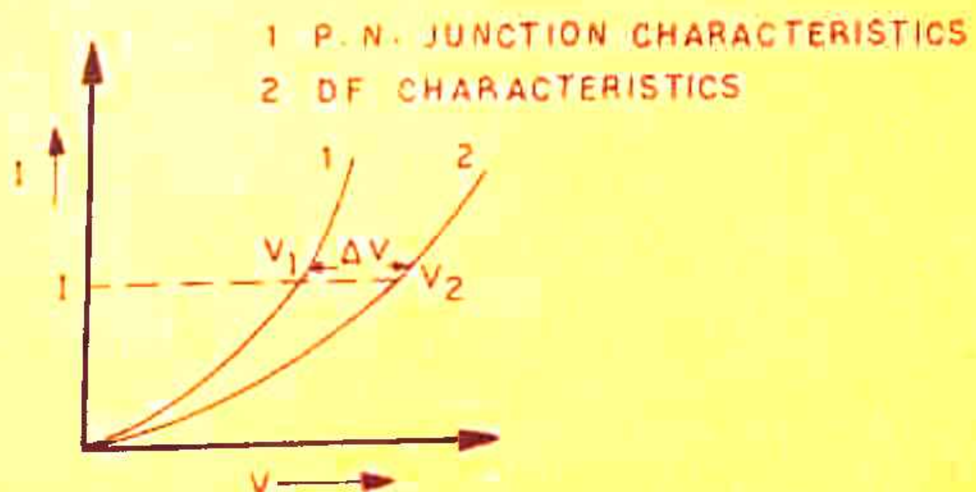

FIG.7.1a P. N. JUNCTION AND DARK FORWARD CHARACTERISTICS

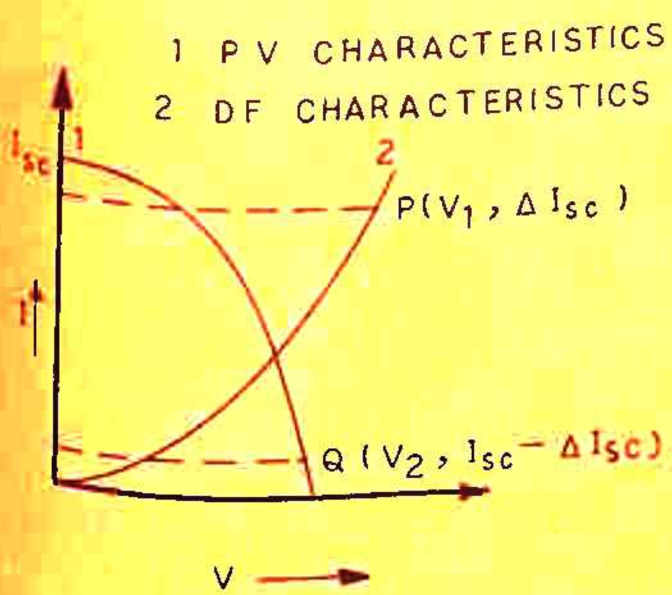

FIG.7.1b DARK CURVE METHOD

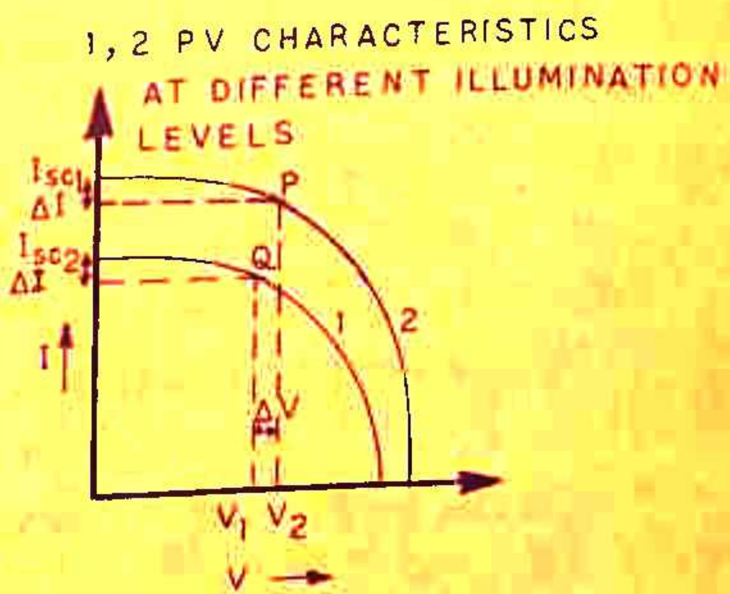

FIG.7.1c ILLUMINATED CURVE METHOD

Then R_s is given by

$$R_s = \frac{V_1 - V_2}{I_{sc}} \qquad (7.5)$$

(c) Illuminated curve method :

This uses two I-V characteristics of the cell in the photovoltaic mode at different levels of illumination, as shown in Fig. 7.1c. Suppose the values of the short-circuit currents for the two intensities are I_{sc1} and I_{sc2} respectively. Two points P and Q are located on the two curves such that their co-ordinates are (V_1, I_{sc1} - ΔI) and (V_2, I_{sc2} - ΔI), respectively. The series resistance R_s, is given by

$$R_s = \frac{V_2 - V_1}{I_{sc1} - I_{sc2}} \qquad (7.6)$$

I is refereed to as the correlation current difference. Generally, the points P and Q are chosen near the maximum power point.

7.3 Experimental set up :

I-V characteristics of the 2 x 2 cms, $n^+ p$ solar cells (cell parameters given in Table 4.1b) were measured to determine the series resistance. The

experimental set up used for different I-V characteristics is described below:

7.3.1 Photovoltaic characteristics:

These characteristics were measured at constant temperature under 1000 watt Oriel Xenon Arc lamp and an AMO simulator. Details of the set up are described in Chapter 4 (see 4.2). Circuit diagram is shown in Fig. 4.1.

7.3.2 P-N junction characteristics:

P-N junction characteristics were measured under 1000watts Philips Quartz Halogen lamp, AMO simulator and Xenon Arc lamp. Circuit used is shown in Fig. 7.2a. Short circuit current and open circuit voltage of the solar cell was measured using 4 1/2 digit, digital multimeters described in Sec. 4.2. Intensity of the light falling on the cell was varied by changing the distance of the cell from the lamp. Temperature of the cell was kept constant by circulating water through the brass mount on which the cell was mounted. For this purpose, an ultracrystal Model MK 70 was used. The accuracy in the temperature control was ± 0.5 degree. Intensity of light was measured using a calibrated Thermopile Model No. CA1, 754286 (Kipp and Zonen) and standard solar cells (No. 3000 and 3001 from spectralab, USA) as described in Sec. 4.2.

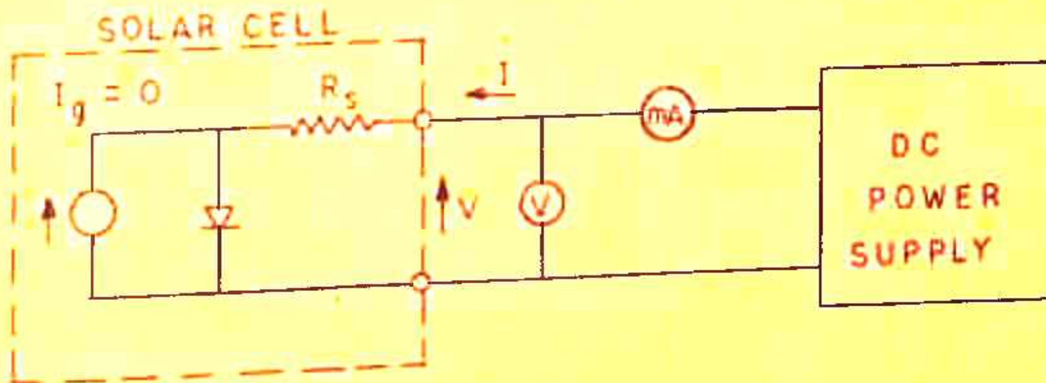

$$I = I_0 \left\{ EXP \left[\frac{q(V - IR_s)}{AkT} \right] - 1 \right\} ; I \geq 0 \; V \geq 0$$

FIG. 7.2a CIRCUIT DIAGRAM FOR MEASURING DARK – FORWARD CHARCTERISTICS (WITH OUT ILLUMINATION)

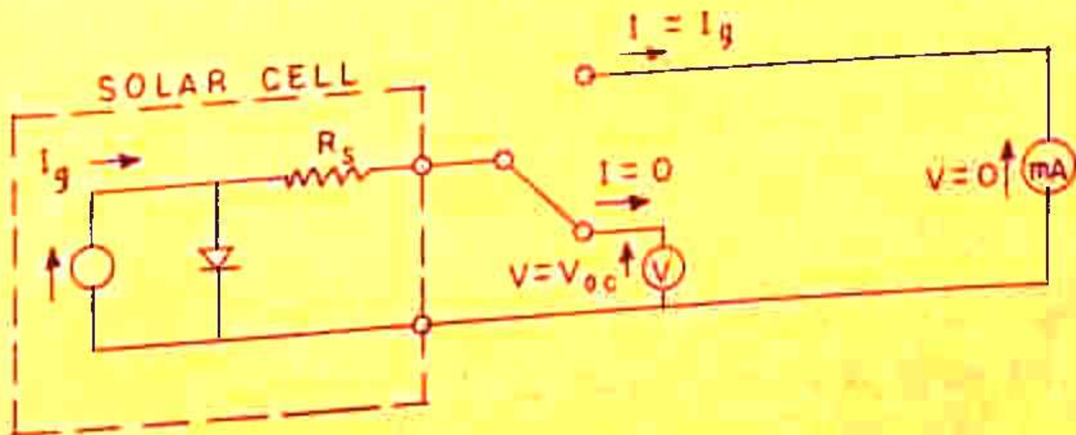

$$I_g = I_0 \left[EXP \left(\frac{q V_{oc}}{AkT} \right) - 1 \right]$$

FIG. 7.2b CIRCUIT DIAGRAM FOR MEASURING P – N JUNCTION CHARCTERISTICS (VARIABLE ILLUMINATION)

7.3.3 Dark forward characteristics :

Dark forward characteristics of the solar cells were measured using the circuit shown in Fig. 7.2b.

A Systronix Transistor Power supply Type 611 was used to provide forward bias to the solar cell. For different values of the forward voltage applied to the solar cell, corresponding current flow was measured.

7.4 Comparison of different methods of measuring the series resistance :

In this section, a comparison of different conventional methods of measuring the series resistance is persented. A new method of measuring R_s is also described.

7.4.1 Comparison of the three conventional methods of meas-uring R_s:

(a) In p-n junction and dark forward cheracteristics method, it is assumed that the p-n junction characteristics is free from resistance effects. At light intensities high enough so that the product of internal series resistance and terminal current exceeds 250 mV, the short-circuit current can no longer be considered identical to the light generated current (Wolf and Rauschenbach 1963). Therefore, if one does not exceed

the intensity level beyond which R_s affects I_{sc}, the resistance to be measured enters in the plot of dark forward characteristics. Since the resistance is not a lumped resistance, in the dark forward mode, the applied voltage which is the maximum value of the voltage exists across the grid and the base and it decreases in regions away from the grids. On the other hand, in the illuminated mode the maximum voltage exists away from the grids if the cell is operated in the short-circuit configuration. It should, therefore, be remember that the value of internal resistance obtained by this method carresponds with the dark forward characteristics and is different at different current levels.

(b) In the dark curve technique also the effect of R_s on I_{sc} becomes significant at high intensities and thus, this method is applicable only when I_{sc} can be taken to be equal to I_g. Also, the value of series resistance at the open circuit point using this method would be same as that determined from the p-n junction and dark forward technique. At all other points R_s will enter both in the photovoltaic as well as dark forward I-V characteristics.

(c) The illuminated curve method of measuring R_s using two I-V characteristics at different intensity levels is somewhat better in the sense that both the plots correspond to illuminated mode of operation and the resistance values therefore correspond to the actual working conditions of the solar cell. The deficiency in this method arises because of the current dependence of R_s and therefore, the use of different sets of PV characteristics at different intensities may not give a unique value of R_s.

7.4.2 Description of the new method for measuring R_s:

In this section we will describe a new method for determination of the series resistance of solar cells. Wolf and Rauschenbach (1963) have shown (see Fig. 3, page 152 of their paper) that the plot of short-circuit current versus intensity deviates from linearity at high intensities. This deviation is given by the following equation derived from eqn. 7.1 for the short circuit configuration (V=0):

$$\ln \frac{(I_g + I_{sc})}{I_o} = \frac{q\, I_{sc} R_s}{AkT} \qquad (7.7)$$

where I_g is the light generated current which is equal

to the short-circuit current at low intensity values where the effect of series resistance is not significant and I_{sc} versus intensity graph is linear. It is obvious that a plot of this deviation from linearity given by $\ln (I_g - I_{sc})$ (since I_{sc} is negative) versus short circuit current will have a slope given by

$$s = \frac{qR_s}{AkT} , \qquad (7.7a)$$

A is taken to be a variable parameter since an accurate determination of A is not possible. We expect A to be greater than one because of the small voltage drop occuring at the junction in the short-circuit condition. We have taken A to be equal to 2 for calculating R_s from eqn. 7.7a because this gives a good agreement with the resistance values determined by other methods. Thus, R_s can be determined from the slope of $\ln (I_g - I_{sc})$ versus I_{sc} curve. This is proposed as a new method for measuring the series resistance of a solar cell. We have measured the series resistance of solar cells using this method. We will show in Sec. 7.5 that results obtained by this method agree well with the results obtained by other methods. As compared to other methods this seems to be the simplest way of determining the series resistance of solar cells. It requires the measurement of only short-

circuit current as a function of known intensity values and therefore, R_s can be estimated in different intensity regions. Values of R_s measured by using this method as well as other methods are given in Sec. 7.5.

7.5 Experimental results and discussions :

In this section results obtained by using the two conventional methods (a) and (c) described in Sec. 7.2 as well as the new method of measuring R_s are presented. Results of the measurement of R_s at different temperatures are also described. Some interesting results observed on the specially designed solar cells with different exposed areas are also reported.

7.5.1 Series Resistance as measured by different methods:

Series resistance of 2 x 2 cm, 10 ohm -cm n^+p solar cells (cell parameters given in table 4.1) was measured using the dark forward p-n junction characteristics method, illuminated curve method and by the new method discussed in the last section. Temperature of the cell was maintained constant during these measurements.

(a) The p-n junction and D.F. characteristics of cell P at room temperature are shown in Fig. 7.3. The R_s values calculated using the difference in voltage between the two points at the same current level on the two characteristics are given in Table 7.1 for different values of the current level. As seen from Table 7.1 the series resistance thus determined appears to decrease with the increase in the current level, a result in agreement with that observed by Imamura and Portscheller (1970). The range of decrease in R_s in the case of the experimental solar cell P is from 0.4 ohm to 0.36 ohm as the current level is increased from 90 to 240 mA.

(b) Fig. 7.4 gives the measured photovoltaic characteristics of cell P at three different values of illumination intensity. Table 7.2 contains the values of R_s obtained at different points on the I-V curve by using 3 sets of characteristics (1) - (2), (1) - (3) and (2) - (3) as shown in Fig. 7.4. The value of R_s obtained in all the three cases seems to decrease at points away from the short-circuit configuration and nearer to the open-circuit configuration i.e. R_s decreases rapidly as the junction voltage increases,

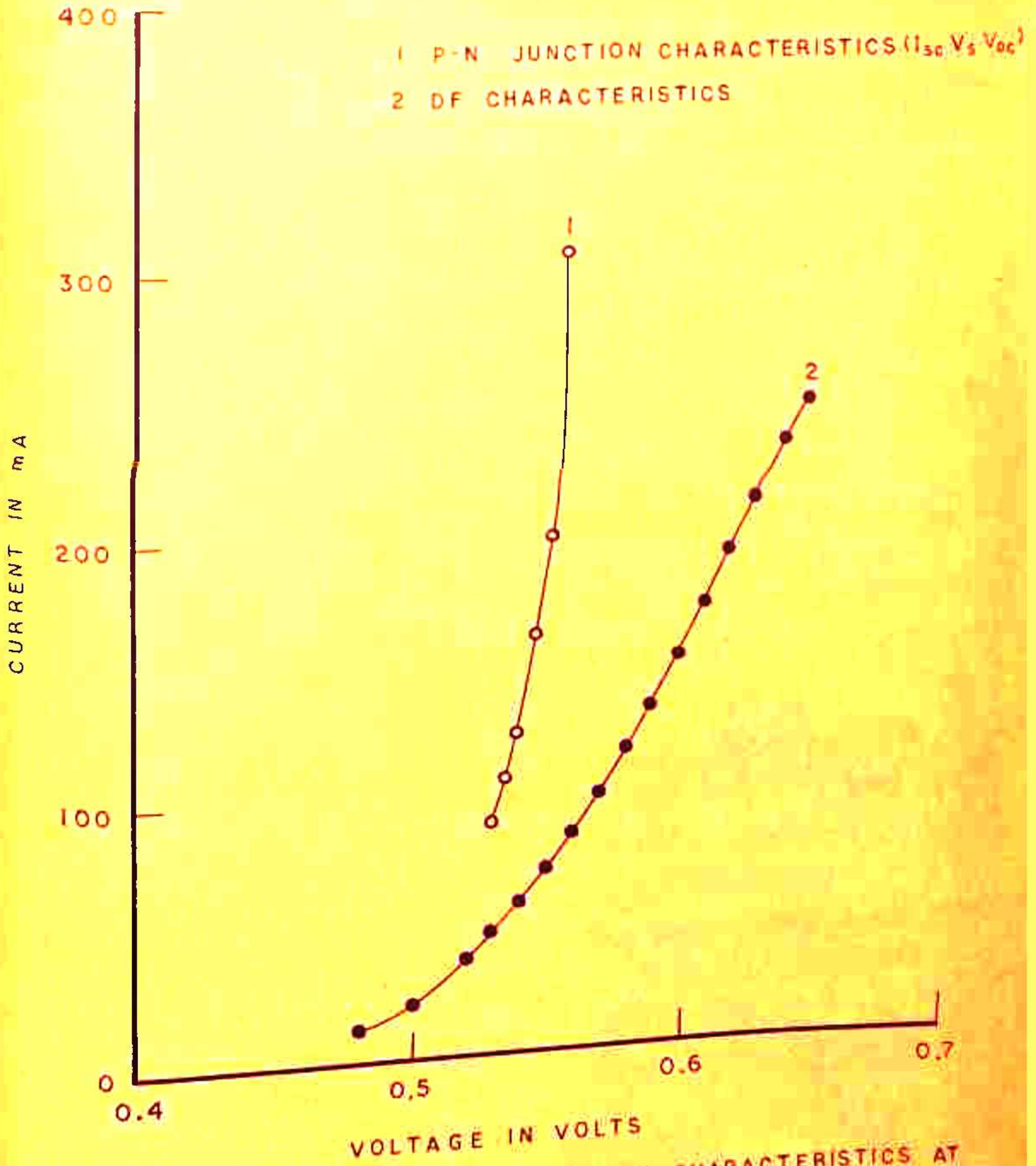

FIG.7.3 CELL P : DF AND P-N JUNCTION CHARACTERISTICS AT ROOM TEMPERATURE.

Table-7.1

CELL P: MEASURED VALUES OF R_s AT DIFFERENT CURRENT LEVELS USING D-F AND PN JUNCTION CHARACTERISTICS

Current level I (mA)	ΔV (Volts)	R_s (Ohm)
90	0.036	0.4
100	0.038	0.38
120	0.046	0.38
140	0.052	0.37
160	0.06	0.37
180	0.066	0.36
200	0.073	0.36
240	0.088	0.36

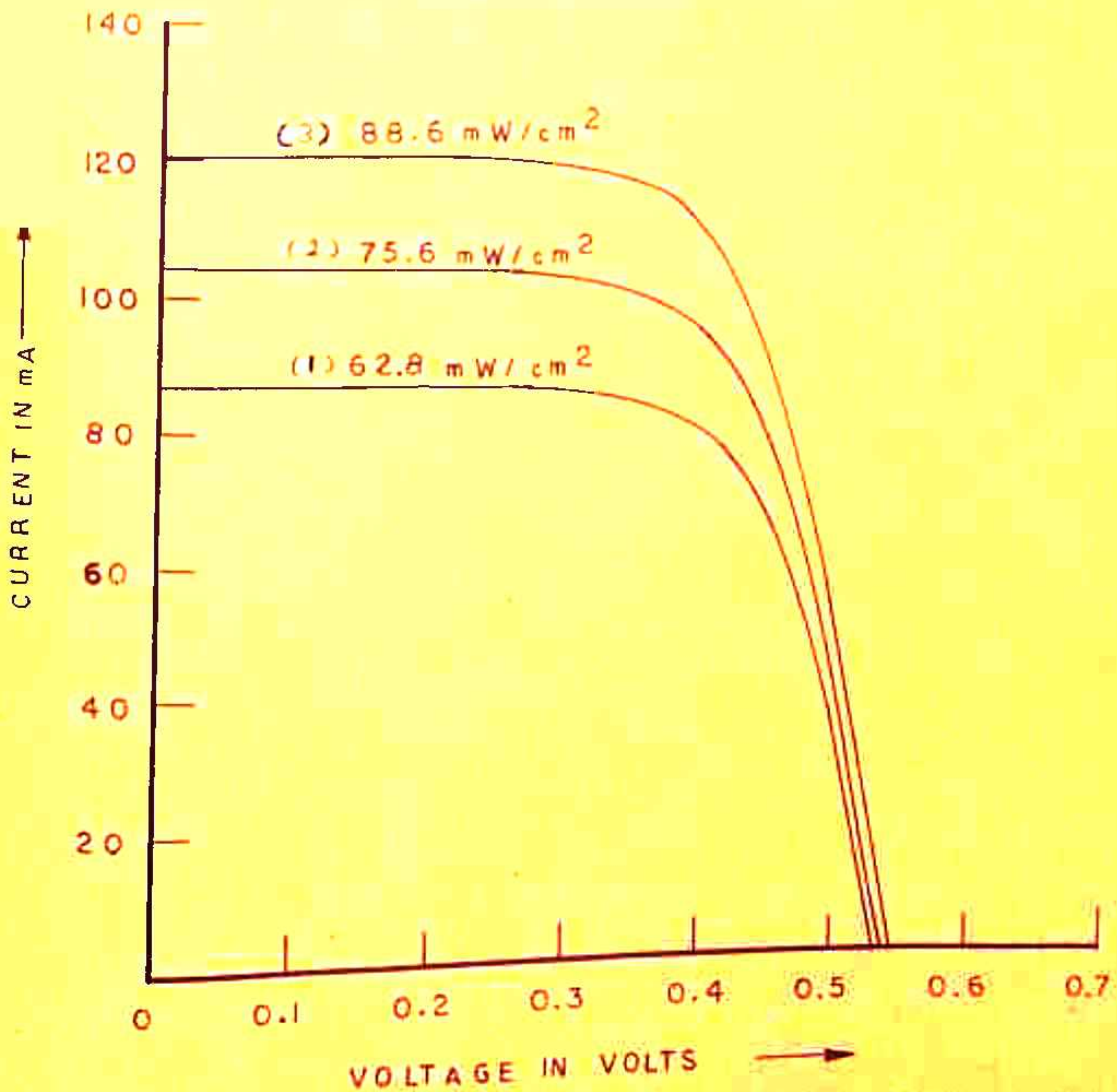

FIG. 7.4 CELL P : I - V CHARACTERISTICS AT DIFFERENT ILLUMINATION LEVELS AND CONSTANT TEMPERATURE (28 °C)

Table-7.2

CELL P: SERIES RESISTANCE VALUES AT DIFFERENT CORRELATION POINTS AND LIGHT INTENSITIES: (SEE FIG.7.

	Initial Intensity ($mW\ cm^{-2}$)	Initial light generated current (I_{sc1}) (mA)	Final Intensity ($mW\ cm^{-2}$)	Final light generated current(I_{sc2}) (mA)	Light generated current difference (I_{sc}) (mA)	Correlation current difference(I) (mA)	Measured R_s (Ohm)
(1)-(2)	62.8	87	75.6	104	17	7	2.85
						17	0.88
						27	0.37
						37	0.27
						47	0.21
						57	0.175
						67	0.15
(2)-(3)	75.6	104	88.6	121	17	7	—
						17	0.29
						27	0.37
						37	0.27
						47	0.21
						57	0.22
(1)-(3)	62.8	87	88.6	121	34	7	2.85
						17	1.17
						27	0.74
						34	0.66
						37	0.54
						47	0.42
						57	0.39
						67	0.37

taking its minimum value near $V = V_{oc}$ and maximum value near $I = I_{sc}$. These results are similar to those observed by Wolf and Rauschenbach (1963). Moreover, there is a discrepancy in the values of series resistance measured from the three different sets of curves, corresponding to different intensity levels. R_s values determined by using the set of curves 2-3 which corresponds to higher intensity values are found to be smaller than those obtained by other sets. All these results clearly point out the dependence of R_s on the current level.

(c) The I_{sc} Vs intensity of illumination curve given by Wolf and Rauschenbach (1963) is shown in Fig. 7.5a. From this graph the deviation of I_{sc} from linearity $\ln(I_g - I_{sc})$ is calculated and plotted as a function of I_{sc} in Fig. 7.5b (see P 235). The slope of this plot at low illumination intensities (below 250 mW/cm^2) corresponds to an internal resistance of 3.6 ohms provided A is taken to be equal to 2. This value of the series resistance, thus obtained is in good agreement with the value 3.5 ohms as given by Wolf and Rauschenbach. However, slope of the graph between $\ln(I_g - I_{sc})$ and I_{sc} is found to decrease for higher illumination

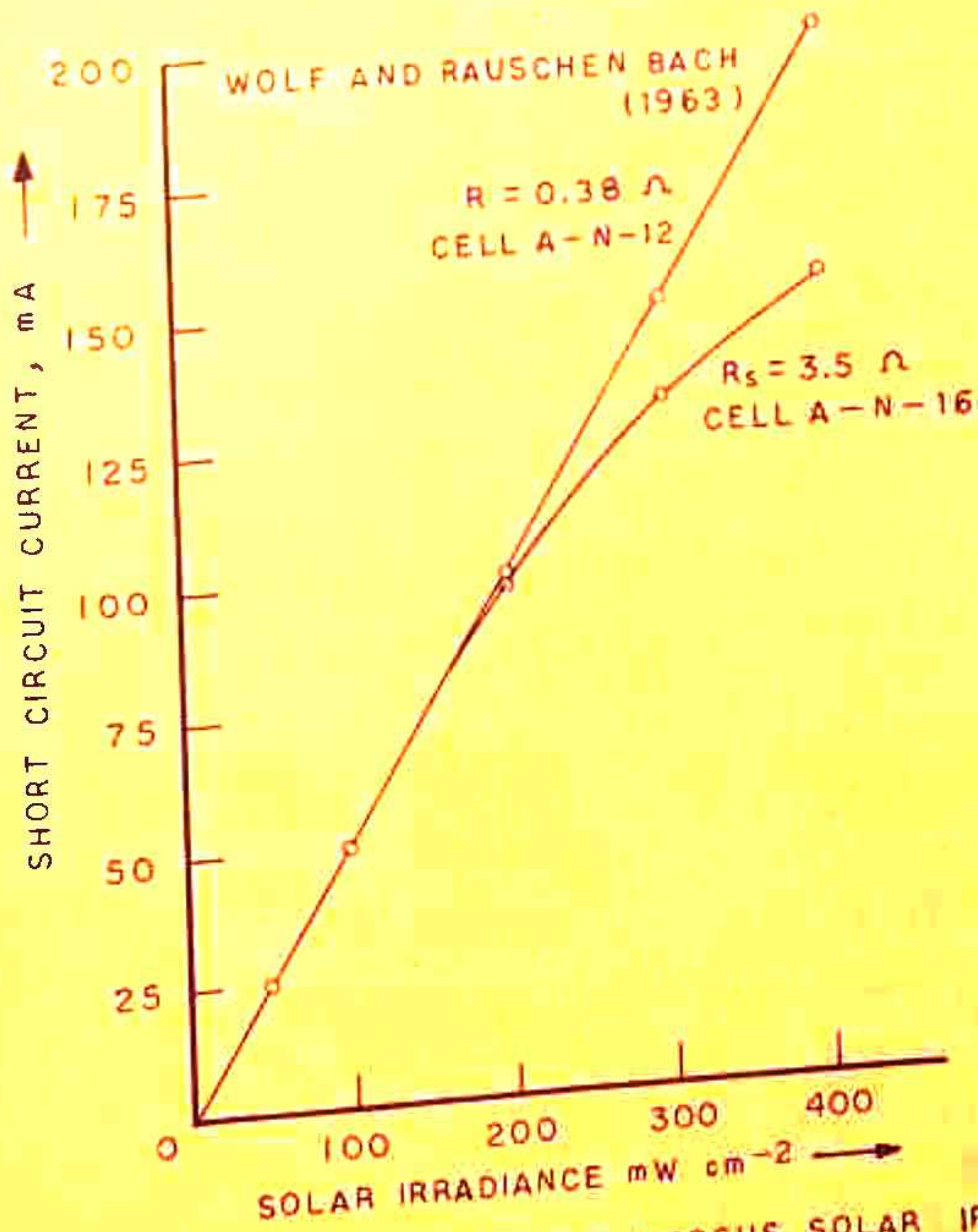

FIG. 7.5a SHORT CIRCUIT CURRENT VERSUS SOLAR IRRADIANCE AT DIFFERENT INTERNAL SERIES RESISTANCE VALUES.

levels (Fig. 7.5b). Values of R_s corresponding to the different slopes in the intensity regions (a), (b) and (c) are given in Table 7.3. These results indicate that the series resistance begins to fall above the intensity value of 250 mW/cm^2.

For the experimental cell P, I_{sc} was measured as a function of illumination intensity and the graph of I_{sc} V_s intensity of illumination is shown in Fig. 7.6. The nonlinearity in the increase in I_{sc} with intensity in this graph begins above the value of intensity equal to 400 mW/cm^2 indicating that below this intensity level, effect of R_s on I_{sc} is not significant. From this graph $\ln(I_g - I_{sc})$ is measured and plotted as a function of I_{sc} as shown in Fig. 7.7. This comes out to be a straight line, and the value of R_s as determined from its slope comes out to be 0.46 ohm if A is taken to be equal to 2. This value of series resistance of cell P is in good agreement with the value 0.4 ohm as measured by p-n junction D.F. characteristics method.

7.5.2 Measurement of series resistance at high temperatures:

Series resistance of experimental cells was measured at different temperatures using the p-n junction

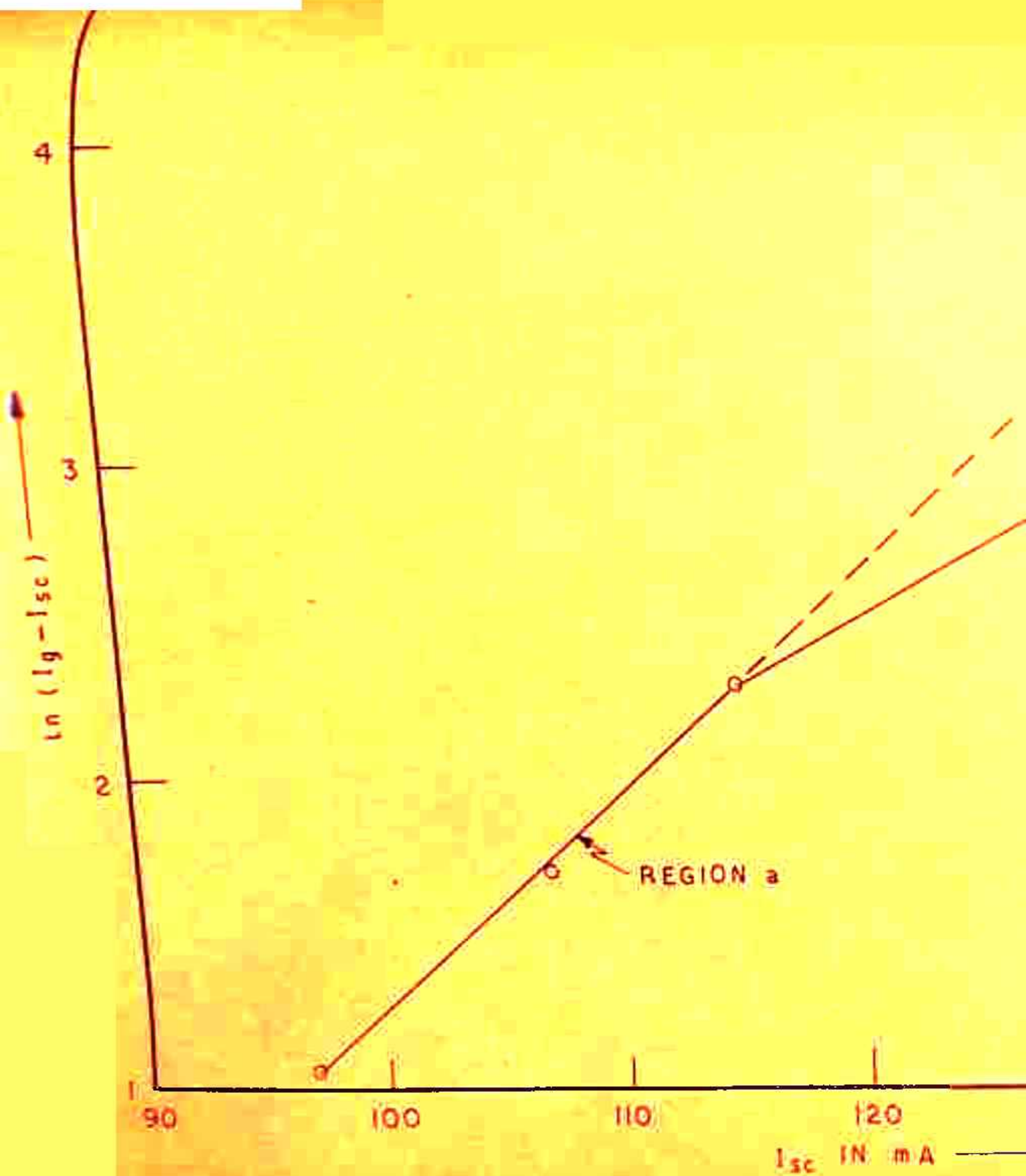

FIG. 7.5b ln (Ig — Isc) Vs Isc

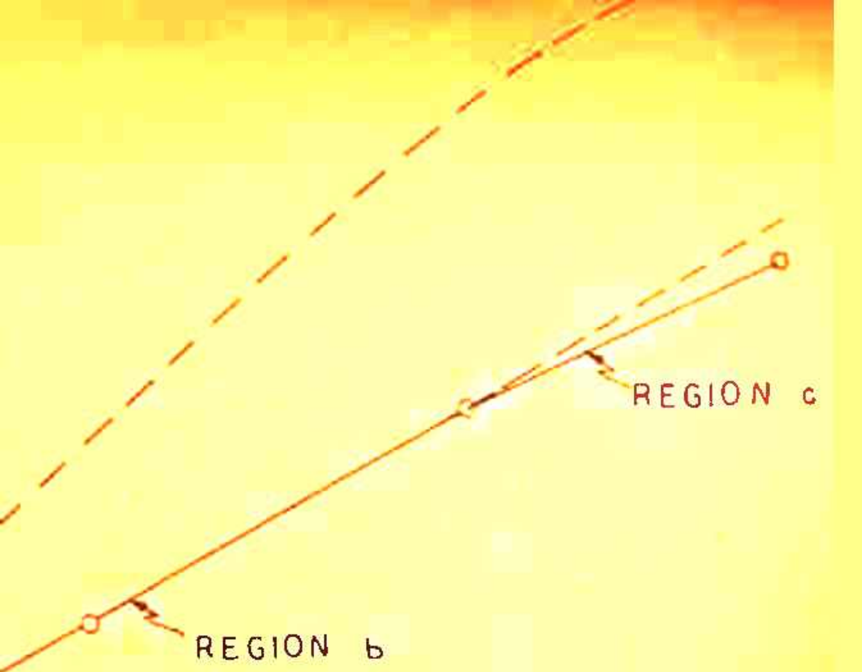

130 140 145 150 152.5

Table-7.3

CELL P : R_s VALUES AS DETERMINED BY THE NEW METHOD

Intensity Region	Intensity of illumination (mW/cm^2)	R_s (Ohm)
a	Below 250	3.6
b	250 -350	2.2
c	350 -400	1.9

Table-7.4

SERIES RESISTANCE OF CELL Q AT DIFFERENT TEMPERATURES AS MEASURED FROM P-N JUNCTION AND D F CHARACTERISTICS METHOD:

I (mA)	R_s in ohm at different Temperatures		
	303^oK	315.5^oK	333^oK
100	0.44	0.50	0.56
150	0.44	0.47	0.53
200	0.45	0.46	0.53

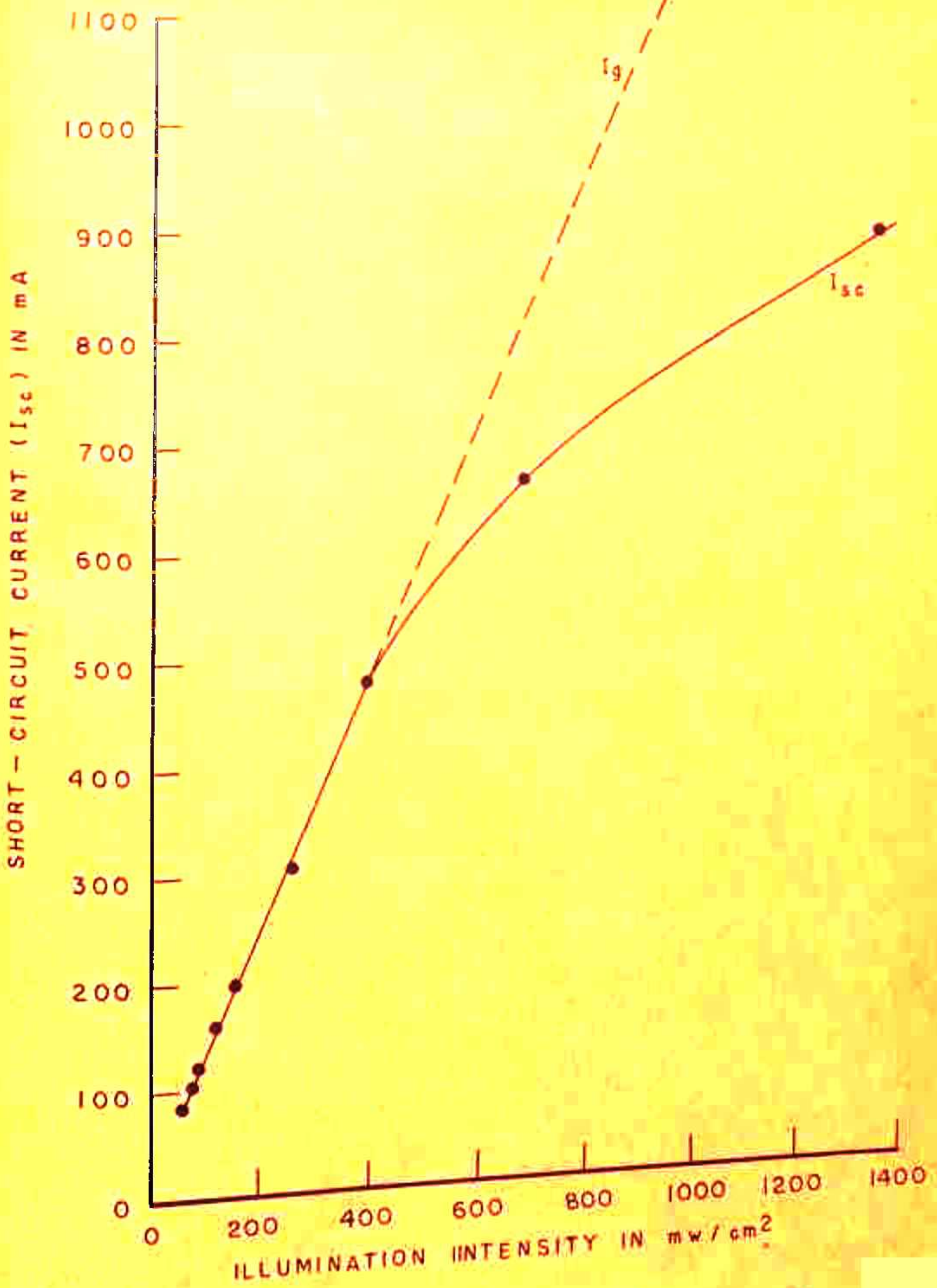

FIG. 7.6 CELL P : I_{sc} Vs INTENSITY OF ILLUMINATION

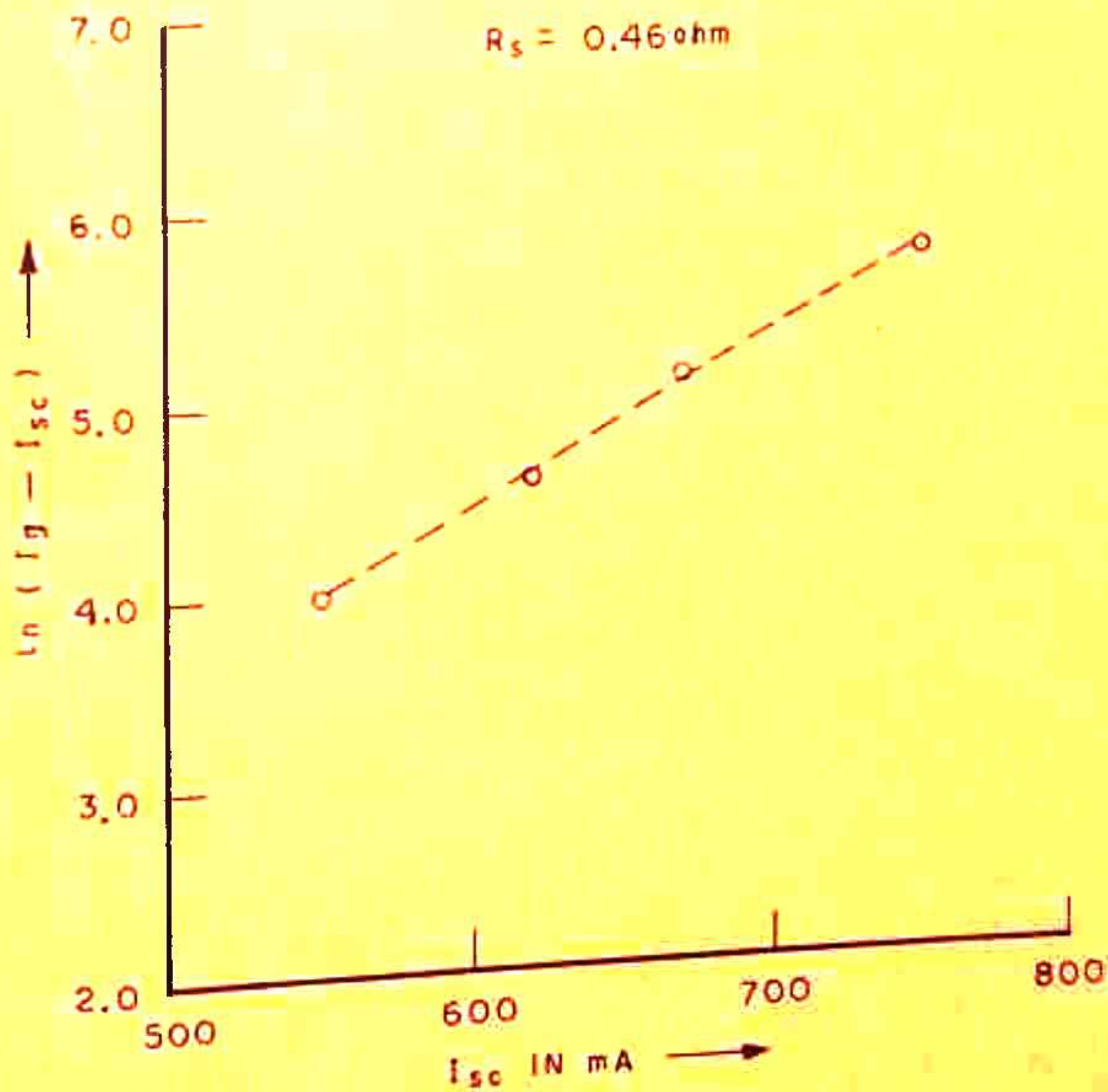

FIG. 7.7 CELL P : ln (Ig − Isc) Vs Isc

DF characteristics method. The temperature of the solar cell was raised using the heating arrangement described in Sec. 6.2. The p-n junction characteristics and DF characterstics of cell Q were measured at temperatures 303°K, 315.5°K and 333°K. These characteristics are shown in Fig. 7.8. As is clear from the graph, DF as well as p-n junction characteristics shift towards lower voltages as the temperature is increased. This is expected because the increase in I_o with temperature (see Sec. 5.2.6) results in the increase of dark current for the same value of junction voltage, hence there is a shift in the DF characteristics towards lower voltages. Increase in temperature also results in a rapid decrease in V_{oc} and a slight increase in I_{sc} (see Chap. 5) which causes the shift in the p-n junction characteristics towards lower voltages. The values of R_s measured at different current levels for the above mentioned three temperature values are given in Table 7.4 (see P. 236). The increase in the value of R_s with the increase in temperature obtained in this case is found to be in agreement with the results of Imamura and Portscheller (1970).

7.5.3 Series resistance of specially designed cells:

An experimental investigation of the series resistance of cells having different exposed areas and

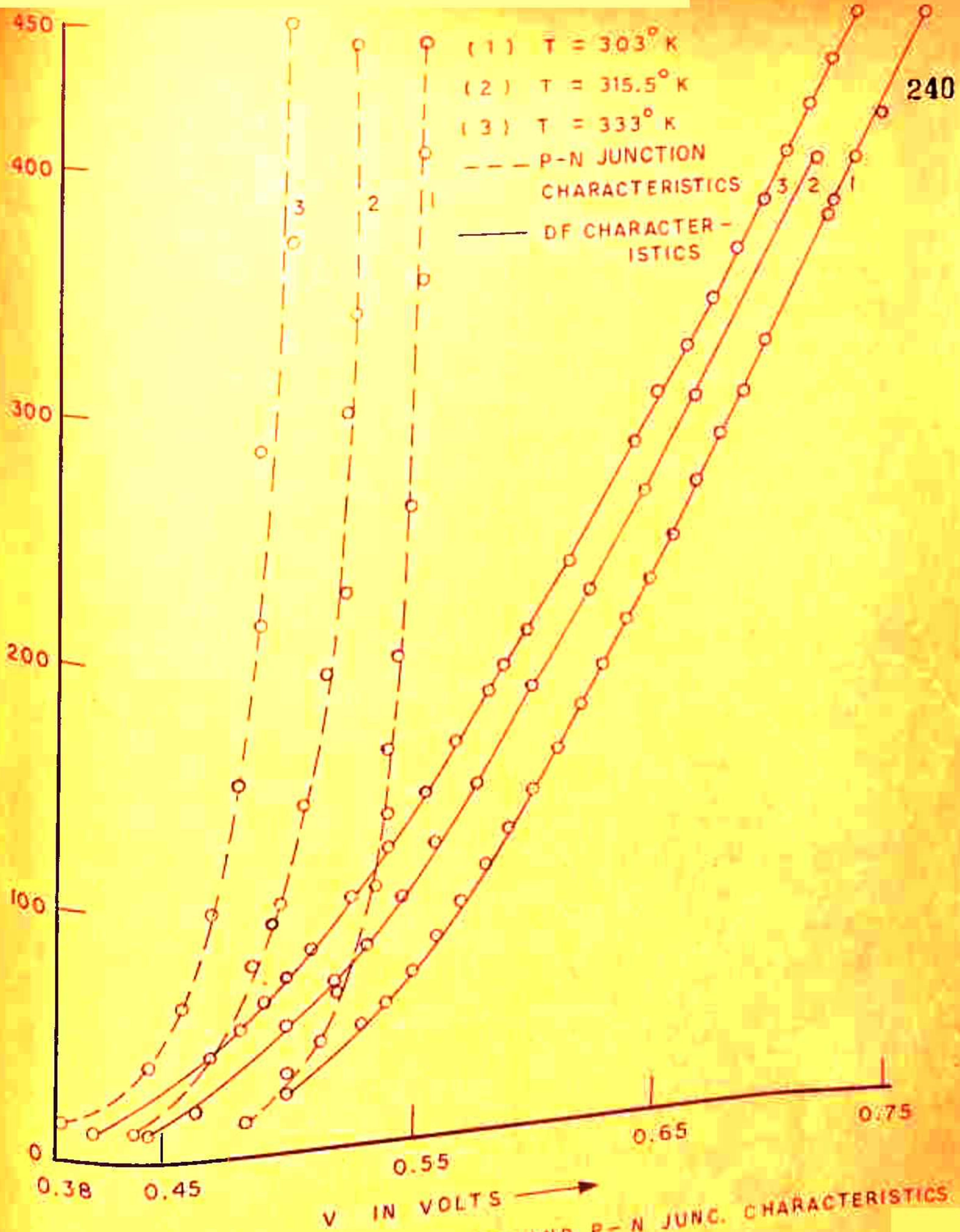

FIG.7.8 CELL Q : DARK — FORWARD AND P-N JUNC. CHARACTERISTICS AT DIFFERENT TEMPERATURES

grid configuration is important for the purpose of optimization of the grid width and spacing. Variation in the number of grids on the cell surface, grid width and spacing esentially implies a change in the resistance of the diffused layer which is a distributed resistance. Therefore, a study of the characteristics of such cells and their series resistance is not only of interest from the design point of view but is also useful in studying the effect of the distributed nature of the series resistance of solar cell . Since sufficient experimental data on solar cells having different exposed areas is not available in literature to our knowledge, an attempt was made to investigate the characteristics of such solar cells.

To study the effect of grid width and grid configuration on the series resistance, four solar cells were specially fabricated. A large circular slice was diffused and four 1 cm x 1 cm cells were cut from this. These cells designated as A_1 A_2, A_3 and A_4 having different grid configurations are shown in Fig. 7.9. The grid width and spacing is given in Table 7.5. Cell A_4 was fully covered by metal at the top surface. DF and p-n junction characteristics of these four cells are shown in Fig. 7.10. Series

Table-7.5

DIMENSIONS OF SPECIALLY DESIGNED SOLAR CELLS HAVING DIFFERENT EXPOSED AREAS

Cell type: $n^+ p$ Base resitivity: 10 ohm cm

Area : 1x1 cm Width of the ohmic bar: 600 μm

Cell No.	No. of Grids	Grid width (μm)	Grid spacing (μm)
A_1	6	140	1300
A_2	3	230	1330

Table-7.6

R_s VALUES OF A_1, A_2, A_3 CELLS AS DETERMINED FROM P-N JUNCTION D-F CHARACTERISTICS METHOD

A_1			A_2			A_3		
I (mA)	ΔV (Volt)	R_s (ohm)	I (mA)	ΔV (Volt)	R_s (ohm)	I (mA)	ΔV (Volt)	R_s (ohm)
25	0.010	0.4	25	0.012	0.48	25	0.666	2.64
50	0.017	0.34	50	0.024	0.48	40	0.080	2.00
60	0.018	0.3	60	0.028	0.47	50	0.088	1.76
75	0.018	0.24	75	0.029	0.38	60	0.093	1.55
85	0.020	0.23	85	0.33	0.4	75	0.102	1.36
						85	0.108	1.27

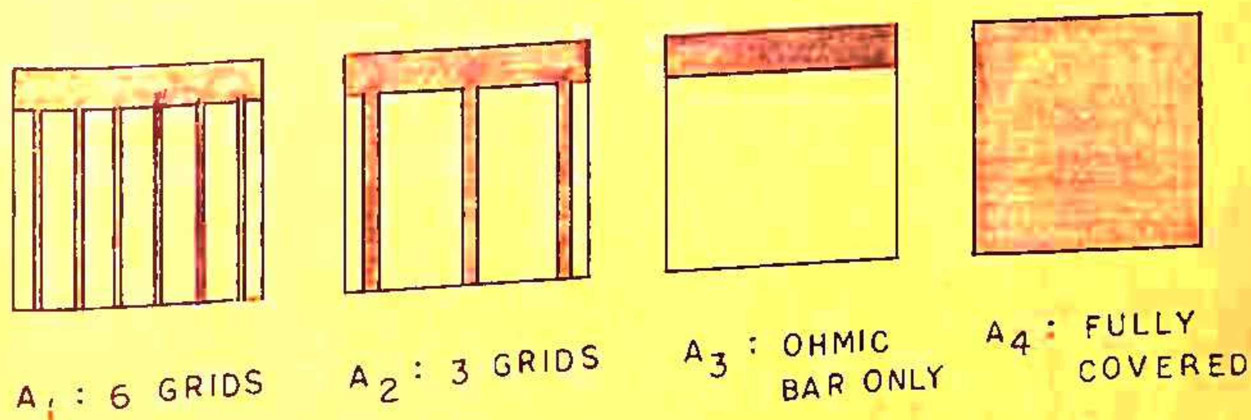

FIG.7.9 TOP SURFACE OF 1X1 Cms SOLAR CELLS HAVING DIFFERENT EXPOSED AREAS.
(NOT TO THE SCALE)

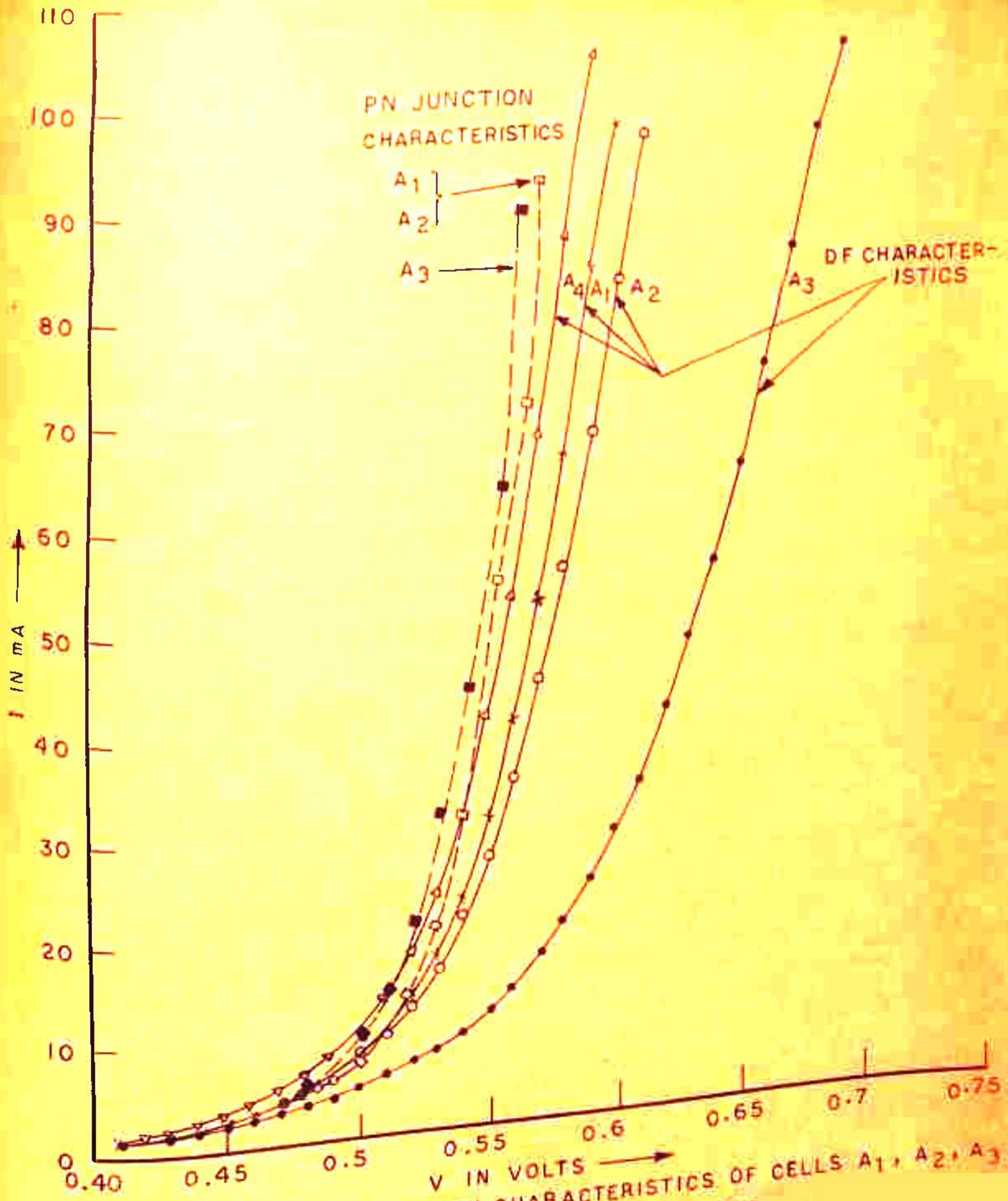

FIG.7.10 DF AND P-N JUNCTION CHARACTERISTICS OF CELLS A_1, A_2, A_3 AND A_4 HAVING DIFFERENT EXPOSED AREAS.

resistance values for the three cells A_1, A_2, A_3 as calculated by the conventional method using these characteristics are given in Table 7.6. Fig. 7.11 shows the decrease in the series resistance of cells A_1, A_2 and A_3 with the increase in the current level. Following are the noteworthy points in the characteristics of these solar cells.

(i) P-N junction characteristics of all cells except the cell having only an ohmic bar coincide. This result was not fully understood because p-n junction characteristics is expected to be free from resistance effects as discussed in Sec. 7.2.1 for low intensities.

(ii) DF characteristics shift to right towards higher voltages as the number of grids decreases, This result is expected from general physical considerations because a decrease in the number of metallic grid strips on the cell surface results in an increase in the diffused layer resistance causing a larger voltage drop at a particular current level as compared to cells having more number of grids.

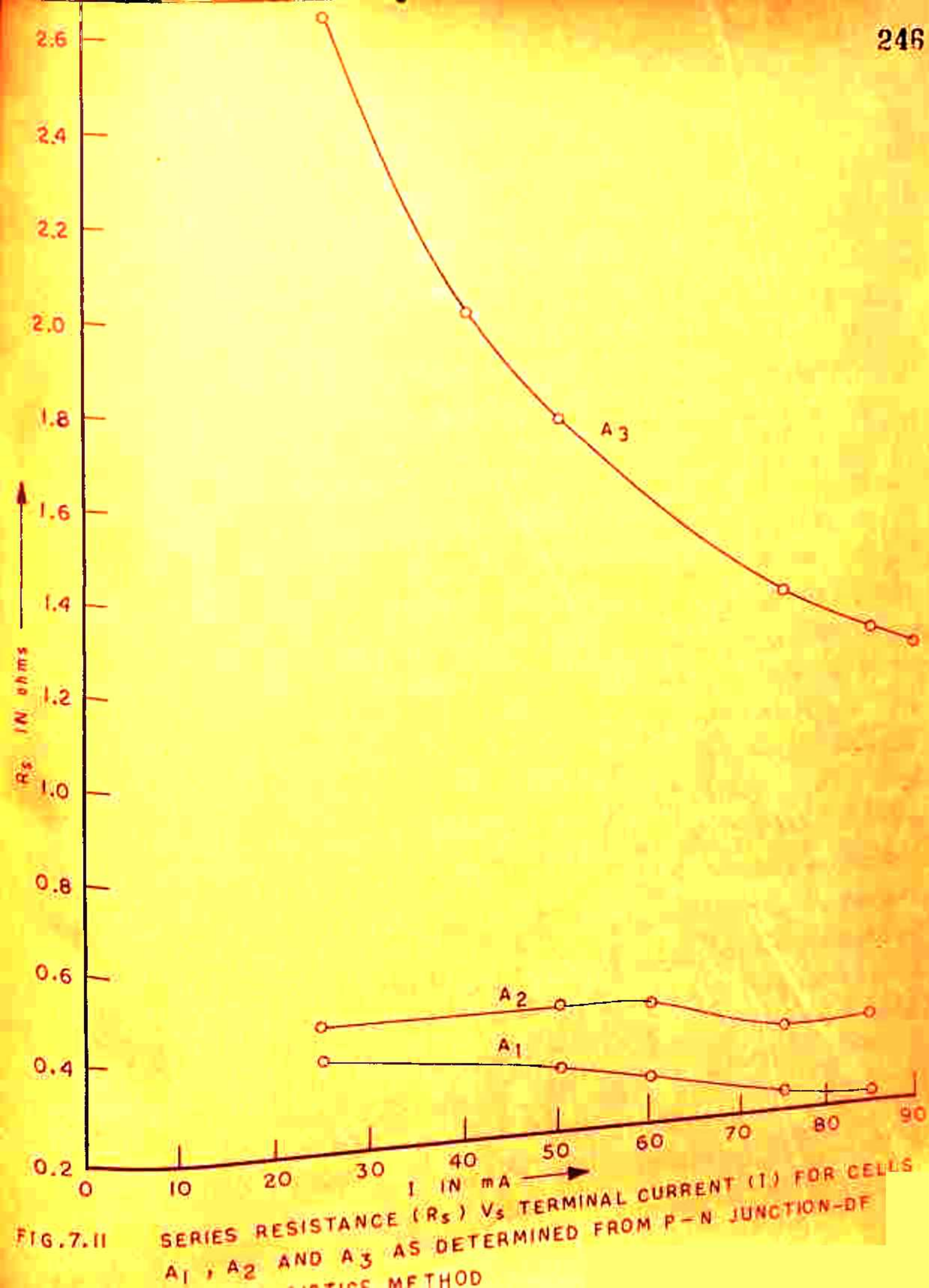

FIG.7.11 SERIES RESISTANCE (R_s) Vs TERMINAL CURRENT (I) FOR CELLS A_1, A_2 AND A_3 AS DETERMINED FROM P-N JUNCTION-DF ...ISTICS METHOD

(iii) In general, it was observed that the measured series resistance was larger for cells having smaller number of grids a result in agreement with observation (ii). Moreover, R_s determined in this way seems to decrease rapidly with the terminal current and this decrease was found to be much pronounced in the case of cell A_3 having only the ohmic bar (see Fig. 7.11).

(iv). The D F characteristics of the completely covered cell lies higher than the p-n junction characteristics at lower currents and voltages. This is the result one would expect theoretically since the resistance of the fully covered cell is expected to be smallest. However, at higher voltages the p-n junction characteristics lies higher than the D F characteristics of fully covered cell. Unfortunately, these experimental results could not be explained by theories available in this area and it is felt that a detailed two-dimensional analysis of the solar cell taking into account its grid structure is needed to explain these results.

7.6 Conclusions :

A study of the experimental methods for the measurement of series resistance of solar cells investigated in this chapter reveals the following interesting features:

(1) The experimental I-V characteristics are not accurately described by the lumped parameter equivalent model of Fig. 1.3. This is because a constant value of R_s is not obtained at different portions of the I-V curve. These results are in agreement with those reported by other workers in this area. However, series resistance measured by these methods can be regarded as an 'effective' resistance which is a function of the terminal current, light intensity and temperature.

(2) In this chapter, a new method for determining the series resistance is proposed which appears to be useful for predicting the value of series resistance at different illumination intensities provided a correct estimate of the parameter A can be made.

(3) Finally, results of an experimental study of the I-V characteristics and series resistance of solar cells having different grid configurations and exposed areas give certain interesting features of the effect of series resistance on the characteristics of such cells which could not be explained by the existing theories.

REFERENCES

Agarwala A., Madan M.K. and Tewary V.K. (1978) Proceedings of the International Solar Energy Society Congress, New Delhi, India 2 , 734.

Agarwal S.K. (1979) Private communication.

Arifov U.A. et. al. (1974) Geliotekhnika 10, 3.

Beckman W.A. et.al. (1966) Solar Energy 10, 132.

Bell R.O. and Freedman G.M. (1978) The conference record of the thirteenth IEEE Photovoltaic Specialists Conference, 89.

Bhaumik B. and Sharon R. (1976) Applied Physics Letters 29, 257.

Blinov J.M. et. al. (1966) JETP Letters 3, 234.

Bobbio S. and Califano F.P. (1976) The conference record of the twelfth IEEE Photovoltaic Specialists Conference, 71.

Boone J.L. and Van Doren T.P. (1977) IEEE Transactions on Electron Devices ED-25, 767.

Bordina N.M. and Golovner T.M. (1977) Geliotekhnika 13, 11.

Bordina N.M., Zaitseva A.K. and Strel'tsova V.I. (1977) Geliotekhnika 13, 17.

Brandhorst H.W. and Hart R.E., Jr. (1970) The conference record of the eighth IEEE Photovoltaic specialists conference, 142.

Broder J.D. et.al.(1964) presented at 4th Annual Photovoltaic Specialists Conference, Cleveland, Ohio, June, 2-3.

Burgess E.L. and Fossum J.G. (1977) IEEE Transactions on Electron Devices ED-24, 433.

Call R.L. and Korvin W.J. (1976) The conference record of twelfth IEEE Photovoltaic Specialists Conference, 721.

Castle J.A. (1976) The conference record of twelfth IEEE Photovoltaic Specialists Conference, 751.

Chapin D.M., Fuller C.S. and Pearson G.L. (1954) Journal of Applied Physics 25, 676.

Chappell T.I. (1976) The conference record of twelfth IEEE Photovoltaic Specialists Conference, 760.

Conwell E.M. (1952) Proceedings of the IRE 40, 1327.

Conwell E.M. (1964) RTI Report ASD-TDR-63-316 V.

Crook D.L. and Yeargan J.R. (1977) IEEE Transactions on Electron Devices ED-24, 330.

Cummerow R.L. (1954) Physical Review 95, 16; 561.

Dalal V.L. and Moore A.R. (1977) Journal of Applied Physics 48, 1244.

Dash W.C. and Newman R. (1955) Physical Review 99, 1151.

Dean R.H., Napoli L.S. and Lin S.S. (1975) RCA Review 36, 324.

Deb S. and Mukherjee M.K. (1965) IEEE Journal of Quantum Electronics QE-1, 219.

Deb S. and Mukherjee M.K. (1966) International Journal of Electronics 21, 89.

Dhariwal S.R., Kothari L.S. and Jain S.C. (1975) Journal of Physics D 8 , 1321.

Dhariwal S.R., Kothari L.S. and Jain S.C. (1976) IEEE Transactions on Electron Devices ED-23, 504.

Dhariwal S.R., Kothari L.S. and Jain S.C. (1978) Proceedings of the International Solar Energy Society Congress, New Delhi, India 2 , 714.

Dunbar P.M. and Hauser J.R. (1976) Solid State Electronics 19, 95.

Evdokimov V.M. (1972) Geliotekhnika 8, 16.

Fischer Colbrie E. et. al. (1976) The conference record of the twelfth IEEE Photovoltaic Specialists Conference, 40.

Fossum J.G. (1976) Solid State Electronics 19, 269.

Fossum J.G. and Schueler D.G. (1976) International Electron Devices Meeting, Washington, D.C.

Fossum J.G. and Burgess E.L. (1976) The conference record of twelfth IEEE Photovoltaic Specialists Conference, 737.

Fossum J! G. and Lindholm F.A. (1977) IEEE Transactions on Electron Devices ED-24, 325.

Girton D. (1963) Proceedings of the IEEE (Letters) 51, 938.

Gobat A.R., Lamorte M.F. and McIver G.W. (1962) IRE Transactions Military Electron, 6, 20.

Graham E.D. and Hauser J.R. (1972) Solid State Electronics 15, 303.

Gray P.E. (1969) IEEE Transactions on Electron Devices ED-16, 424.

Hall R. (1952) Physical Review 87, 387.

Handy R.J. (1967) Solid State Electronics, 10, 765.

Heryer J.C. (1974) Journal of Applied Physics 45, 224.

Holonyak N. et.al. (1967) Journal of Applied Physics 38, 5422.

Hovel H.J. (1975) 'Solar Cells', Semiconductors and Semimetals 11, Academic Press, New York.

Imamura M.S. and Portscheller J.I. (1970) The conference record of the eighth IEEE Photovoltaic Specialists Conference, 102.

Jain S.C., Sehgal H.K. and Gangadhar R.B. (1968) Journal of Scientific and Industrial Research 27, 295.

J[illegible]in [illegible].G. and Stub[illegible]r F.[illegible] (1967) Advanced Energy Conversion 7, 167.

J[illegible]es [illegible] and [illegible]oon R.L. (1975) Applied Physics Letters, 26, 467.

Jonscher A.K. (1960) 'Principles of Semiconductor Device Operation', John Wiley and Sons, New York.

Johnson F.S. (1954) Journal of Meteorology 11, 431.

KaO Y.C. and Schroder D.K. (1970) IEEE Transactions on Electron Devices ED-17, 384.

Lewis C.A. and Kirkpatrick J.P. (1970) The conference record of eighth Photovoltaic Specialists Conference, 123.

Lindmayer J. (1972) Comsat Technical Review 2, 105.

Loferski J.J. (1956) Journal of Applied Physics 27, 777.

Loferski J.J. (1963) Proceedings of IEEE 51, 667.

Loferski J.J. and Wysocki J.J. (1961) RCA Review 22, 38.

Lucovsky G. (1960) Journal of Applied Physics 31, 1088.

Luft W. (1971) IEEE Transactions on Aerospace Electronics Systems AES-6, 332.

Macfarlane G.G. et.al. (1958) Physical Review 111, 1245.

Many A. and Bray R. (1958) Progress in Semiconductors 3, 117 (Heywood, London).

McKelvey J.P. (1966) 'Solid State and Semiconductor Physics', Harper and Row, New York.

Mclean T.P. (1960) Progress in Semiconductors 5, 94 (Heywood, London).

Meinel A.B. and Meinel M.P. (1976) Applied Solar Energy, Addison-Wesley Publishing Company, Inc. Philippines.

Moss T.S. (1959) 'Optical properties of Semiconductors', Academic Press Inc., 117.

Napoli L.S. et.al. (1977) RCA Review 38, 76.

Neugroschel A., Lindholm F.A. and Sah C.T. (1977), IEEE Transactions on Electron Devices ED-24, 662.

Parrott J.E. (1974) IEEE Transactions on Electron Devices, ED-21, 89.

Pfeiffer C. et al. (1962) Journal of Engineering for Power, Trans. ASME 84, Series A, 33.

Prince M.B. (1955) Journal of Applied Physics 26, 534.

Ralph E.L. (1966) Solar Energy 10, 67.

Rappaport P. (1954) Physical Review 93, 246.

Rappaport P. (1959) RCA Review 20, 373.

Rappaport P., Loferski J.J. and Linder E.G. (1956) RCA Review XVII, 100.

Rappaport P. and Wysocki J.J. (1961) Acta Electron. 5, 364.

Rayhold J.H. and Meulenberg A. (1974) Journal of Applied Physics 12, 2582.

Rittner E.S. (1954) Physical Review 96, 1708.

Rothwarf A. and Boer K.W. (1975) Progress in Solid State Chemistry 10, 71.

Rouse L.M. (1977) Journal of Materials Science 12, 602.

Runyan W.R. (1967) Southern Methodist University Report SMU, 83 (unpublished).

Sabnis A.G. (1978) Solid State Electronics 21, 581.

Savchenko, I.G. and Tarnizhevskii B.V. (1969) Geliotekhnika 5, 23.

Schiel E.J. and Bolmarcich J. (1963) Proceedings of the IEEE 51, 1780.

Schoffer P. and Pfeiffer C. (1963) Journal of Engineering for Power, Trans. ASME 85, Series A, 208.

Schueler D.G. et.al. (1975) the conference record of eleventh IEEE Photovoltaic Specialists Conference, 327.

Seth B.M. and Dhariwal S.R. (1977) International Journal of Electronics 42, 41.

Shockley W. (1949) Bell System Technical Journal 28, 435.

[illegible] and Read W.T. (1952) Physical Review 87, 835.

Shumka A. (1970) The conference record of eighth IEEE Photovoltaic Specialists Conference, 96.

Spaderna D.W. and Navon D.H. (1978) IEEE Transactions on Electron Devices ED-25, 1291.

Sterzer F. (1975) RCA Review 36, 316.

Stokes E.D. and Chu. T.L. (1977) Applied Physics Letters 30, [illegible].

[illegible] (1974) Journal of Physics C 1, 261.

Vasil'ev A.M.. et.al. (1975) Geliotekhnika 11, 18, (English translation: (1975) Applied Solar Energy 11, 72).

Walkden M.W. (1967) Royal Aircraft establishment Technical Report 67091.

Wallmark T. (1957) Proceedings of the I.R.E. 45, 474.

Wolf H.F. (1969) 'Silicon Semiconductor Data' International Series of Monographs on Semiconductors 9, Pergaman Press, London.

Wolf M. (1960) Proceedings of the I.R.E. 48, 1246.

Wolf M. (1963) Proceedings of the I.E.E.E. 51, 674.

Wolf M. and Rauschenback H. (1963) Advanced Energy Conversion 3, 455.

Wolf [illegible]. (1971) Energy Conversion 11, 63.

[illegible]., Hoel [illegible]. and Stirn R.J. (1977) IEEE Transactions on Electron Devices ED-24, 419.

[illegible]i J.J. and Rappaport P. (1960) Journal of Applied Physics 31, 571.

Wysocki J.J. (1961) RCA Review 22, 57.

Yasui R.K. and Schmidt L.W. (1970) The conference record of eighth IEEE Photovoltaic Specialists Conference, 110.